Understanding the function of the Rtt101 E3 ubiquitin ligase in response to replication stress

Dissertation

zur Erlangung des Grades

Doktor der Naturwissenschaften

Am Fachbereich Biologie

der Johannes Gutenberg-Universität Mainz

vorgelegt von

Vanessa Kellner

geboren am 23.09.1988

in Mannheim, Germany

Mainz, 2018

Tag der mündlichen Prüfung: 18. Mai 2018

Table of Contents

List of Publications

Graf, M.*, Bonetti, D.*, Lockhart, A.*****, Serhal, K., **Kellner, V**., Maicher, A., Jolivet, P., Teixeira, M.T., and Luke, B. (2017). Telomere Length Determines TERRA and R-Loop Regulation through the Cell Cycle. *Cell 170*, 72-85 e14.

Buser R.*, **Kellner V.***, Melnik A., Wilson-Zbinden C., Schellhaas R., Kastner L., Piwko, W., Dees, M., Picotti, P., Maric, M., Labib, K., Luke, B., and Peter, M. (2016). The Replisome-Coupled E3 Ubiquitin Ligase Rtt101^{Mms22} Counteracts Mrc1 Function to Tolerate Genotoxic Stress. *PLoS Genetics* 12(2): e1005843.

*: shared first-authorship

Summary

The duplication of the cellular genetic material has to be precisely regulated to maintain genome integrity. Damage caused by a wide range of exogenous factors, commonly summarized as replication stress, interferes with DNA replication. Genome integrity is further threatened by endogenously arising structures such as ribonucleotide monophosphates (rNMP) that are frequently misincorporated into genomic DNA. They are removed by the RNase H2 enzyme in a process termed ribonucleotide excision repair (RER). When RER is defective, rNMPs accumulate in the genome and induce replication stress. Cullin 4 (CUL4)-based E3 ubiquitin ligases are required for DNA replication and repair in the presence of replicative DNA damage. In *Saccharomyces cerevisiae*, the CUL4 ortholog Rtt101 promotes DNA replication through damaged templates. However, the underlying mechanism and relevant ubiquitylation targets are poorly understood.

In this thesis we characterized the mechanism by which Rtt101 promotes DNA replication in the presence of the alkylating drug methyl methanesulfonate (MMS). We found that Rtt101, in complex with the putative substrate adaptor Mms22 ($Rtt101^{Mms22}$), counteracts a replicative function of the replisome component Mrc1. However, this does not alter Mrc1 protein levels. Instead, our genetic data suggests that interactions of Mrc1 with other replisome proteins are modulated. We propose that Rtt101 allows recombination-mediated fork restart at MMS-induced DNA lesions.

We further uncovered a novel role of $Rtt101^{Mms22}$ in the tolerance of misincorporated rNMPs that accumulate in the absence of RER. Cells lacking both Rtt101 and RER display reduced viability, which is not caused by increased levels of genomic rNMPs and can be partially offset by deletion of *MRC1*. Ubiquitin remnant profiling, a mass spectrometry-based approach, identified the leading strand polymerase ε subunit Dpb2 as a potential target of Rtt101. We suggest that Rtt101 ubiquitylates Dpb2 at replication forks that stall or break due to unrepaired rNMPs. This Rtt101-dependent ubiquitylation might facilitate replication fork restart or DNA synthesis repriming downstream of the site of damage.

We present evidence that underlines an important function of the Rtt101 E3 ubiquitin ligase to tolerate several aspects of faulty RER. Our data indicates a similar mechanism as under genotoxin-induced replication stress.

Zusammenfassung

Die Duplizierung des zellulären genetischen Materials muss genau reguliert werden, um die Integrität des Genoms aufrechtzuerhalten. Schäden, die durch eine Vielzahl von exogenen Faktoren verursacht und üblicherweise als Replikationsstress zusammengefasst werden, können die DNA-Replikation beeinträchtigen. Die Integrität des Genoms wird weiterhin durch endogen auftretende Strukturen wie Ribonukleotidmonophosphate (rNMP) bedroht, die häufig in genomische DNA eingebaut werden. Sie werden durch das Enzym RNase H2 in einem als Ribonukleotid-Exzisionsreparatur (RER) bezeichneten Prozess entfernt. Wenn RER defekt ist, akkumulieren rNMPs im Genom und induzieren Replikationsstress. Cullin 4 (CUL4) -basierte E3-Ubiquitin-Ligasen sind für die DNA-Replikation und -Reparatur in Gegenwart von replikativen DNA-Schäden erforderlich. In *Saccharomyces cerevisiae* fördert das CUL4-Ortholog Rtt101 die DNA-Replikation durch beschädigte DNA-Matrizen. Der zugrundeliegende Mechanismus und die relevanten Ziele der Ubiquitylierung sind jedoch kaum erforscht.

In dieser Dissertation haben wir den Mechanismus charakterisiert, durch den Rtt101 die DNA-Replikation in Gegenwart des alkylierenden Chemotherapeutikums Methylmethansulfonat (MMS) fördert. Wir haben herausgefunden, dass Rtt101 im Komplex mit dem mutmaßlichen Substratadapter Mms22 ($Rtt101^{Mms22}$) einer replikativen Funktion des Replisombestandteils Mrc1 entgegenwirkt. Dies ändert jedoch nicht die Mengen an Mrc1-Protein. Stattdessen legen unsere genetischen Daten nahe, dass Wechselwirkungen zwischen Mrc1 und anderen Replisomproteinen moduliert werden. Wir schlagen vor, dass Rtt101 einen Rekombinations-vermittelten Neustart der Replikationsgabel an MMS-induzierten DNA-Läsionen ermöglicht.

Wir haben außerdem eine neue Rolle von $Rtt101^{Mms22}$ in der Toleranz von fälschlicherweise eingebauten rNMPs aufgedeckt, die sich in Abwesenheit von RER anhäufen. Zellen, in welchen sowohl Rtt101 als auch RER fehlt, zeigen eine verminderte Lebensfähigkeit, die nicht durch erhöhte Mengen an genomischen rNMPs verursacht wird und durch die Deletion von *MRC1* teilweise ausgeglichen werden kann. Mithilfe der Profilerstellung von Ubiquitinresten, einem auf Massenspektrometrie basierenden Ansatz, haben wir Dpb2, eine Untereinheit von DNA-Polymerase ε am kontinuierlich replizierten Strang, als potentielles Ziel von Rtt101 identifiziert. Wir

schlagen vor, dass Rtt101 Dpb2 an Replikationsgabeln ubiquityliert, die aufgrund von nicht reparierten rNMPs ins Stocken geraten oder gebrochen sind. Diese Rtt101-abhängige Ubiquitylierung könnte den Neustart der Replikationsgabel oder die Wiederaufnahme der DNA-Synthese hinter der Schadensstelle erleichtern.

Wir präsentieren Beweise, die eine wichtige Funktion der Rtt101 E3-Ubiquitin-Ligase unterstreichen, die benötigt wird um verschiedene Aspekte fehlerhafter RER zu tolerieren. Unsere Daten weisen auf einen ähnlichen Mechanismus wie unter Genotoxin-induziertem Replikationsstress hin.

Introduction

Faithful DNA replication is essential for cells to duplicate their entire genome in an error-free manner during each cell cycle. Events that impede replication lead to replication stress and trigger the DNA damage response. Attempts to relieve replication stress or to repair DNA damage must be strictly regulated to avoid genome instability in the shape of chromosomal aberrations or mutations. An important layer of regulation is offered by posttranslational modifications of proteins, which allow for temporal or spatial fine-tuning of repair processes. The 76-amino-acid protein ubiquitin is highly conserved from yeast to human and a crucial signalling component during both unperturbed and challenged DNA replication (reviewed in (Villa-Hernández et al., 2017)).

1.1 Ubiquitylation – mechanism and functions

The attachment of ubiquitin moieties to a substrate requires a three-step enzymatic cascade. In an ATP-consuming initial step, a conserved cysteine in the active site of the E1 activating enzyme forms a covalent thioester with the C-terminal glycine of ubiquitin. Subsequently, the activated ubiquitin is passed on to an E2 conjugating enzyme via transesterification. The charged E2 can now associate with an E3 ubiquitin ligase that catalyses the transfer of ubiquitin to the ε-amino group of a substrate lysine. The *Saccharomyces cerevisiae* (*S. cerevisiae*) genome encodes for only one E1 enzyme (*UBA1*), while 11 genes encode for E2 ubiquitin conjugating enzymes. The ubiquitin system becomes strikingly more diverse considering the more than 60 different E3 ligases, which selectively bind the substrate, thereby achieving high specificity (reviewed in (Finley et al., 2012)).

E3 ubiquitin ligases are categorized into the HECT (homologous to E6-AP carboxy terminus) type and the RING (really interesting new gene)-based E3 ligases. The main difference between those classes is their mode of ubiquitin transfer to the substrate. HECT E3 ligases harbour a catalytical domain that forms an intermediate thioester with ubiquitin before transferring it to the target lysine residue. In contrast, RING E3 ligases do not undergo a covalent linkage with ubiquitin, but rather help to bring the substrate and the ubiquitin-charged E2 into close proximity, thereby facilitating the transfer of ubiquitin to the acceptor lysine. RING-domain proteins can either directly recruit

substrate proteins or they assemble with substrate-specific adaptors into multisubunit RING E3s as it is the case for the largest group of E3 ligases, the cullin-RING ligases (CRLs) (reviewed in (Zheng and Shabek, 2017)).

Ubiquitin is not only attached to lysine residues in substrate proteins, but can also be attached via its C-terminus to one of its seven internal lysines (K6, K11, K27, K29, K33, K48 and K63) or its N-terminal methionine (Peng et al., 2003; Kirisako et al., 2006). The resulting polyubiquitin chains adopt distinct topologies depending on the type of linkage with diverse consequences for the substrate protein. The most commonly found and thus best-studied linkage types are *via* K11, K48 and K63 (Xu et al., 2009). The classical signal for degradation through the ubiquitin-proteasome system (UPS) is mediated by K48-linked ubiquitin chains (Chau et al., 1989; Thrower et al., 2000). K11-linked polyubiquitin chains are implicated in the endoplasmic reticulum-associated degradation (ERAD) pathway. In contrast, ubiquitin chains linked through K63 have originally been proposed to serve a non-proteolytic function (Xu et al., 2009). However, the traditional view on the ubiquitin code has to be revised as emerging evidence suggests non-canonical functions for some linkage types (Saeki et al., 2009; Maric et al., 2014). Additionally, ubiquitin chains can contain mixed or branched chains, as well as a combination of ubiquitin and other small ubiquitin-like modifiers (reviewed in (Kravtsova-Ivantsiv and Ciechanover, 2012)).

A substrate protein can be either monoubiquitylated or subsequently modified with a polyubiquitin chain. Depending on which type of ubiquitylation is present, and in case of polyubiquitylation also depending on the type of chain linkage, the substrate will be directed to its distinct fate. This can range from a change in protein stability due to proteasomal degradation, to changed protein-protein interactions, protein localization, or activity (reviewed in (Komander and Rape, 2012)). Ubiquitin-specific proteases, termed deubiquitinases (DUBs), are required to recycle ubiquitin from targets that are on the way to be degraded, but also offer a possibility to make non-proteolytic ubiquitylation reversible (reviewed in (Mevissen and Komander, 2017)).

1.2 Ubiquitylation in DNA replication and repair

Ubiquitin is an essential signalling molecule for the regulation of cell cycle progression, DNA replication and the DNA damage response. These processes are mainly regulated by RING E3 ligases, more specifically by the CRLs and the anaphase promoting complex/cyclosome (APC/C).

The multisubunit APC/C promotes exit from mitosis and by this entry into G1 phase by inducing degradation of mitotic cyclins. Moreover, it is the main regulator of chromosome segregation through ubiquitylation of securin (Pds1), an inhibitor of the protease Esp1/separase that cleaves cohesin and thus allows separation of sister chromatids (Ciosk et al., 1998; Shirayama et al., 1999; Uhlmann et al., 1999).

In *S. cerevisiae,* the family of cullin-RING E3 ligases consists of three members. All CRLs interact with the E2 Cdc34 and the RING protein Hrt1/Roc1. The Cul1/Cdc53-based complexes, the SCF (Skp1-Cul1/Cdc53-F-box) ligases, recognize their substrates through the F-box protein that binds to Cdc53 *via* the bridging protein Skp1. The SCF complex employing Cdc4 as F-box protein (SCF^{Cdc4}) regulates entry into S phase by degrading the cyclin-dependent kinase (CDK) inhibitor Sic1 (Feldman et al., 1997; Skowyra et al., 1997). Moreover, SCF complexes also participate both in the initiation and in the termination of DNA replication, with SCF^{Cdc4} targeting the origin licencing factor Cdc6 to allow origin firing in S phase and SCF^{Dia2} inducing replisome disassembly at the end of replication by ubiquitylating the replicative helicase subunit Mcm7 (Drury et al., 1997; Maculins et al., 2015). Cul3 assembles a CRL with the linker protein Elc1 and induces degradation of the RNA polymerase II subunit Rpb1 upon DNA damage (Ribar et al., 2006, 2007). Finally, Rtt101 is found in a complex with the bridging protein Mms1 and the putative substrate adaptor Mms22 (Zaidi et al., 2008). The $Rtt101^{Mms22}$ E3 ligase promotes progression of replication forks through damaged DNA, thus becoming especially important during replication stress (Luke et al., 2006) (see section 1.3).

Ubiquitylation is further important for various DNA repair pathways (reviewed in (Villa-Hernández et al., 2017)). A prominent example among those is the DNA damage tolerance (DDT) pathway. It is regulated through ubiquitylation of proliferating cell nuclear antigen (PCNA). Depending on whether a monoubiquitin is attached by the E2 Rad6 and the E3 Rad18, or whether the monoubiquitylation is extended into a K63-

linked polyubiquitin chain by the E2 Mms2-Ubc13 and the E3 Rad5, cells will undergo error-prone translesion synthesis (TLS) or error-free template switch (TS), respectively (reviewed in (Finley et al., 2012) and see section 1.4.3).

1.3 The Cullin E3 ubiquitin ligase Rtt101 maintains genome stability

The *S. cerevisiae* cullin protein Rtt101 (Regulation of Ty1 Transposition) was initially identified in a screen for factors showing increased cDNA-mediated mobility of Ty1 (transposon of yeast 1) and regulating transposon mobility (Scholes et al., 2001).

The 842 amino acid-containing Rtt101 protein shares 21 % sequence homology with Cdc53/Cul1 in its carboxy terminus (Laplaza et al., 2004). This C-terminal cullin homology region of Rtt101 interacts with the RING domain protein Roc1/Hrt1 (Michel et al., 2003). Furthermore, the E2 conjugating enzyme Cdc34 binds to Rtt101 and delivers the enzymatic activity required for ubiquitylation of substrate proteins (Zaidi et al., 2008). As Cdc34 is able to both place the first ubiquitin moiety onto a substrate and to elongate polyubiquitin chains predominantly by K48 linkage (Sadowski et al., 2010), the Rtt101 complex is predicted to confer both monoubiquitylation and K48-linked polyubiquitin chains. However, Rtt101 has also been shown to be competent in attaching K63-linked polyubiquitin chains to a substrate, although it is unclear whether Cdc34 is the participating E2 enzyme in this case (Han et al., 2010).

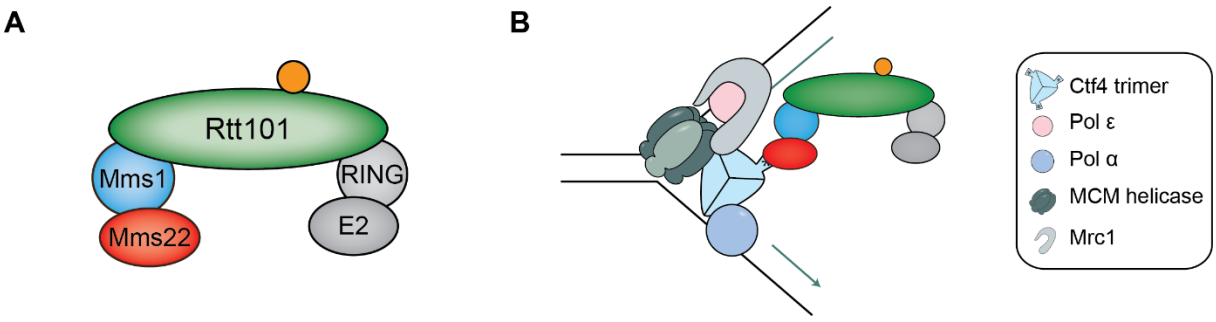

Figure 1. The Rtt101^{Mms22} E3 ubiquitin ligase. (**A**) The cullin Rtt101 scaffold brings together the RING protein Hrt1, the E2 conjugating enzyme Cdc34, the bridging protein Mms1 and the putative substrate adaptor Mms22. Rtt101 is neddylated as indicated by the orange sphere, which promotes cullin activity. (**B**) Rtt101^{Mms22} associates with active replisomes during S phase via an interaction between Mms22 and Ctf4. Panel (**B**) is modified from (Buser et al., 2016).

The bridging protein of the Rtt101 complex, Mms1, has been identified in a protein-protein interaction screen (Suter et al., 2007) and is recruited to the cullin complex by the Rtt101 N-terminus (Zaidi et al., 2008). Mms22 interacts with Rtt101 in an Mms1-dependent manner (Zaidi et al., 2008) and has first been identified in a screen for mutants that deliver sensitivity to the DNA damaging agent methyl methanesulfonate (MMS) (Chang et al., 2002). The interaction between Rtt101 and Mms22 is further detectable by yeast two-hybrid analysis (Ben-Aroya et al., 2010), suggesting that Rtt101 acts as a scaffold for a CRL employing Mms22 as a putative substrate-specific adaptor (Figure 1A). Finally, the replisome component Ctf4 physically interacts with Mms22 both by yeast two-hybrid assay (Gambus et al., 2009; Mimura et al., 2010) and immunoprecipitation experiments (Buser et al., 2016; Luciano et al., 2015). This is particularly interesting as Ctf4, the homolog of human AND1, plays a vital role as a central hub of the replisome. It bridges DNA polymerase α and the CMG (Cdc45-MCM-GINS) helicase complex (Gambus et al., 2009; Simon et al., 2014) while at the same time it coordinates the binding of multiple additional factors involved in DNA replication and repair (Villa et al., 2016). The above described discoveries and additional evidence (Buser et al., 2016) lead to a model in which the Rtt101-Mms1-Mms22 E3 ubiquitin ligase ($Rtt101^{Mms22}$) associates with active replication forks via the Mms22-Ctf4 interaction (Figure 1B).

Both in mammalian cells and in budding yeast, cullins are modified with the small ubiquitin-like protein Nedd8 (Neural precursor cell expressed developmentally down-regulated protein 8) (reviewed in (Brown and Jackson, 2015)) called Rub1 in yeast (Liakopoulos et al., 1998). This is also true for Rtt101: Rub1 is attached to K791 to achieve full E3 ligase activity (Laplaza et al., 2004; Michel et al., 2003). Interestingly, the same lysine residue can be modified with a single ubiquitin (Rabut et al., 2011). Ubiquitylation of Rtt101 relies on the E2 ubiquitin conjugating enzyme Ubc4, while Rub1-conjugation is mediated by the E2-like enzyme Ubc12 and the RING domain containing protein Tfb3, a subunit of transcription factor TFIIH (Rabut et al., 2011). Both modifications promote full activity of Rtt101. An indication for a difference between ubiquitylation and neddylation emerges from the difference in MMS sensitivity. While *rub1*Δ single mutants are not MMS sensitive, the expression of the *RTT101-K791R* mutant in *rub1*Δ cells increases sensitivity, suggesting that ubiquitin-conjugation is indeed important in the presence of DNA damage (Laplaza et al., 2004;

Rabut et al., 2011). However, how the choice for either of those modifications is made and how they differ in function remains to be investigated.

1.3.1 Cells lacking Rtt101^{Mms22} are sensitive to DNA damage in S phase

Cells lacking either *RTT101* or the E3 ligase complex members *MMS1* or *MMS22* display sensitivity to MMS (Chang et al., 2002; Hryciw et al., 2001). Moreover, the sensitivity towards the Top1 poison camptothecin (CPT) is increased in *rtt101Δ*, *mms1Δ* or *mms22Δ* cells, while sensitivity to hydroxyurea (HU) is only mildly elevated (Chang et al., 2002; Hryciw et al., 2001; Luke et al., 2006). Interestingly, the Rtt101^{Mms22} complex is not required when cells face DNA damage caused by ultraviolet (UV) irradiation or X-rays (Chang et al., 2002; Hryciw et al., 2001) or to repair and survive an induced DNA double-strand break (DSB) (Luke et al., 2006).

In *rtt101Δ* mutants, a defect in cell cycle progression causes a mitotic delay, which is dependent on the DNA damage checkpoint (Michel et al., 2003). This cell cycle defect is accompanied by the occurrence of spontaneous foci of the checkpoint sensor Ddc1 (Luke et al., 2006), phosphorylation of the checkpoint kinase Rad53 (Duro et al., 2008) and an accumulation of cells in G2/M phase (Luke et al., 2006). Taken together, these phenotypes suggest that Rtt101^{Mms22} is important to deal with damage arising in S phase, an idea further supported by the notion that cells lacking a functional Rtt101^{Mms22} complex are especially sensitive to agents that induce replication-born DSBs, but not to induced DSBs outside the context of replication. This is in line with its constitutive recruitment to active replisomes (Buser et al., 2016).

RTT101, *MMS1*, and *MMS22* have been assigned to an epistasis group further comprising the histone deacetylase *RTT109* and the histone chaperone *ASF1* based on SGA analysis of genetic interactions (Collins et al., 2007). Lysine 56 on histone H3 (H3K56) is acetylated by Rtt109 (Han et al., 2007a), and Asf1 promotes this reaction (Recht et al., 2006). H3K56Ac is important in both replication-coupled nucleosome assembly and chromatin assembly after repair of a DNA break. Importantly, like *rtt101*Δ, *rtt109Δ* and *asf1Δ* cells as well as non-acetylatable *H3K56R* mutants are sensitive to MMS and CPT (Masumoto et al., 2005; Schneider et al., 2006; Wurtele et al., 2012), suggesting that the Rtt101^{Mms22} E3 ligase and the regulation of H3K56Ac might act in concert in the presence of S phase damage.

An additional phenotype observed in all mutants of the H3K56Ac epistasis group is a checkpoint recovery defect. When cells lacking *RTT101*, *MMS1* or *MMS22* are treated with MMS, they initiate a checkpoint response but are unable to recover from this arrest once the drug is removed (Luke et al., 2006; Zaidi et al., 2008; Duro et al., 2008). This defect is shared by *rtt109Δ* and *asf1Δ* mutants (Collins et al., 2007). Conversely, HU treatment of cells lacking Rtt101 does not impair checkpoint recovery (Luke et al., 2006), suggesting that checkpoint recovery is only defective when the encountered DNA lesion requires a restart of replication forks, while extinguishing the checkpoint *per se* is not defective in *rtt101*△ mutants (Zaidi et al., 2008).

1.3.2 Rtt101^{Mms22} channels repair into an HR-dependent pathway

DNA damage in S phase leads to stalling of active replication forks. If at those forks DNA synthesis gets uncoupled from DNA unwinding, single-stranded DNA (ssDNA) accumulates and triggers the activation of the S phase checkpoint. Forks that cannot be protected will eventually break and need to be repaired to allow completion of DNA replication. HR proteins have been found to play important roles at different steps and in different pathways of replication fork restart (reviewed in (Costes and Lambert, 2013) and see section 1.4).

As described above, cells lacking a functional Rtt101^{Mms22} E3 ligase display an accumulation of spontaneous DNA damage during S phase. In line with that, *mms1Δ* cells exhibit a defect in HR, more specifically in unequal sister chromatid exchanges (uSCE) (Ui et al., 2007). This observation links Mms1 as part of the Rtt101^{Mms22} E3 ligase complex to a role in recombination-mediated processes. Consistently, the frequency of uSCEs in response to MMS- or CPT-induced DNA damage decreases in *mms1Δ* or *mms22Δ* cells, but is similar to wildtype cells when a DSB is induced by the expression of homothallic switching (HO) endonuclease. This phenotype is shared by *rtt101Δ* cells as well as mutants of the H3K56Ac pathway (*rtt109Δ* and *asf1Δ*) (Duro et al., 2008; Endo et al., 2010).

1.3.3 Rtt101 participates in replication-coupled nucleosome assembly and ubiquitylates histone H3 and FACT

Replication-coupled nucleosome assembly is the fast re-assembly of chromatin in the wake of a passing replication fork (reviewed in (Downs, 2008)). Parental histones ahead of the fork are recycled and randomly distributed to the daughter strands. However, in order to maintain nucleosome occupancy on both new strands, one half of all nucleosomes has to be produced in every S phase. Newly synthesized H3-H4 dimers are bound by Asf1 and presented to Rtt109, which acetylates histone H3 at lysine 56 (Han et al., 2007a; Recht et al., 2006). Subsequently, the modified H3-H4 dimer is passed on to the histone chaperone Rtt106 or to the CAF-1 complex. This step is facilitated by Rtt101-mediated ubiquitylation of H3 on lysine residues 121, 122 and 125, resulting in a reduced affinity of Asf1 to the modified H3-H4 dimer (Han et al., 2013). Consistently, H3K56Ac increases the binding affinity of Rtt106 and CAF-1 to H3 (Li et al., 2008). Finally, the H3-H4 dimer is assembled into the $(H3\text{-}H4)_2$ tetramer and deposited on DNA (Figure 2). This step is supposed to be the rate-limiting step of nucleosome assembly, followed by completion of the core histone octamer by two H2A-H2B dimers. The histone octamer is wrapped with ~147 bp of DNA wound 1.6 turns around the nucleosome (reviewed in (Li et al., 2012)).

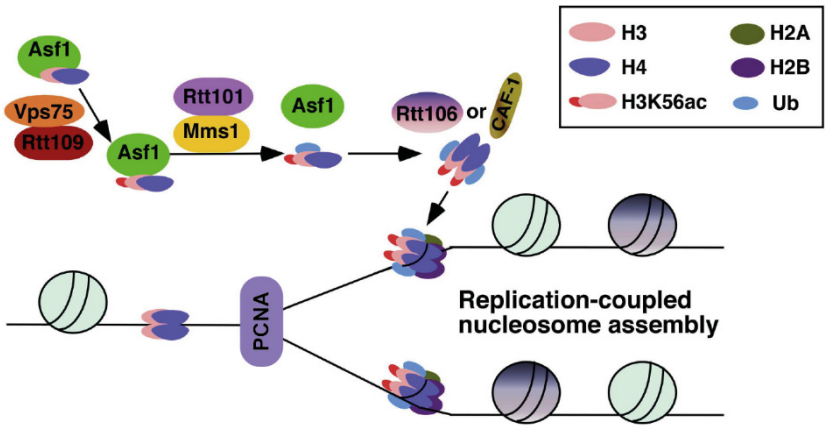

Figure 2. Rtt101 participates in replication-coupled nucleosome assembly. Newly synthesized H3-H4 dimers are bound by the histone chaperone Asf1 and presented to the histone acetyltransferase Rtt109 in complex with another histone chaperone, Vps75. Rtt109 acetylates H3 on lysine 56. This modification is recognized by $Rtt101^{Mms1}$ which ubiquitylates H3 on lysine 121, 122, and 125. As a consequence, the affinity between Asf1 and H3-H4 is reduced and H3-H4 is passed on to downstream histone chaperones Rtt106 or CAF-1 to be deposited on newly replicated DNA. Taken from (Han et al., 2013).

Ubiquitylation of H3 is dependent on the presence of Asf1 and H3K56Ac. While Mms1, which binds to H3, is also required, a strong dependency on Mms22 could not be observed. Therefore, the Rtt101-Mms1 E3 ligase promotes the deposition of H3K56Ac onto newly replicated DNA. Interestingly, mutation of the lysine residues targeted by Rtt101 to arginine renders cells sensitive to DNA damaging agents, such as MMS, CPT, and HU. Even though this sensitivity is additive with deletion of *RTT101*, it suggests that defective nucleosome assembly might contribute to the DNA damage that cells experience in the absence of Rtt101 (Han et al., 2013).

The histone chaperone complex FACT (facilitates chromatin transcription) comprised of Spt16 and Pob3 has recently been proposed to act in parallel to Rtt106 and CAF-1 in nucleosome assembly (Yang et al., 2016). The Spt16 subunit binds H3-H4 dimers and Rtt106 during S phase, and this interaction is enhanced by the prior acetylation of H3K56. Thus, also FACT promotes the deposition of H3K56Ac onto newly replicated DNA. This is of particular interest as the replicative function of FACT is regulated by Rtt101-dependent ubiquitylation of Spt16 (Han et al., 2010). This K63-linked polyubiquitylation does not cause degradation of Spt16 and is not dependent on Mms1 or Mms22. Consequently, the FACT complex is channelled into its function during DNA replication instead of its function during transcription. In the absence of Rtt101, the association of Spt16 with replication origins is reduced (Han et al., 2010). Taken together, Rtt101 might participate in replication-coupled nucleosome assembly at two different steps: by facilitating H3-H4 deposition onto replicated DNA through ubiquitylation of H3, and by directing the FACT complex to its role in DNA replication, presumably promoting its function in nucleosome assembly.

Acetylation of H3K56 is cell cycle-regulated: It rapidly emerges during S phase and disappears when cells reach G2 (Masumoto et al., 2005) due to the action of the histone deacetylases Hst3 and Hst4 expressed in late S/G2 phases (Celic et al., 2006). When cells activate the DNA damage checkpoint, Hst3 is degraded in a Mec1-dependent manner, leading to persistent H3K56Ac (Thaminy et al., 2007).

While the complete lack of H3K56 acetylation causes the aforementioned DNA damage-associated phenotypes, deregulation of its removal is equally deleterious. Cells lacking Hst3 and Hst4, or expressing the acetylation-mimetic *H3K56Q* mutant accumulate Rad52- and RPA-foci upon replication stress and are defective in checkpoint recovery (Simoneau et al., 2015). In a yeast strain harbouring a modified

version of chromosome III with extremely large inter-origin gaps, persistent H3K56Ac into the next S phase leads to increased loss of this chromosome (Irene et al., 2016). Further, the inability to remove H3K56Ac in *hst3Δ hst4Δ* mutant cells causes an SCE defect, and viability of those cells depends on a Rad51- or Pol32-dependent recombination pathway (Muñoz-Galván et al., 2013). While in this study H3K56Ac is proposed to help choosing the sister chromatid as the preferred substrate for repair, another study shows that the acetylation mark inhibits extensive break-induced replication (BIR) (Che et al., 2015).

Moreover, *rtt109*Δ, *asf1*Δ or *H3K56R* mutants are defective in recovery from the DNA damage checkpoint and show persistent Rad52 foci after experiencing DNA damage caused by CPT or MMS (Wurtele et al., 2012).

Finally, H3K56Ac is not only a mark of newly replicated chromatin, but is also necessary to signal the end of DNA repair (Chen et al., 2008). Cells that have repaired an induced DSB, require Rtt109 and Asf1 to re-assemble chromatin at the break site and subsequently switch off the DNA damage checkpoint. In line with this, loss of H3K56Ac causes a checkpoint recovery defect both in response to MMS or CPT treatment (Wurtele et al., 2012) and upon the induction of an ectopic DSB (Diao et al., 2017; Tsabar et al., 2016). Two current models try to explain the role of Rtt101 in checkpoint recovery. In the first model, Rtt101-mediated ubiquitylation and degradation of Mms22 (see section 1.3.4) is required to limit Rad51 loading on ssDNA (Diao et al., 2017), which if persisting leads to a checkpoint recovery defect (Yeung and Durocher, 2011). The second model attributes the checkpoint recovery defect of *rtt101Δ* cells to a direct role of Asf1 in turning off the DNA damage checkpoint (Tsabar et al., 2016). The interaction of Asf1 with the checkpoint kinase Rad53 is interrupted upon activation of the checkpoint, leading to increased association of Asf1 with H3 (Emili et al., 2001; Hu et al., 2001). This possibly supports nucleosome assembly on repaired DNA. Once the damage is repaired, Asf1 needs to re-associate with Rad53 to promote its full inactivation. This event could be facilitated by the Rtt101-mediated ubiquitylation of H3 that in turn reduces the interaction of H3 with Asf1 and would thus allow more Asf1 molecules to sequester Rad53 (Tsabar et al., 2016). As the two models for a role of Rtt101 in checkpoint recovery are not mutually exclusive, further investigations have to be performed to fully understand the origin of the checkpoint recovery defect of cells lacking Rtt101.

1.3.4 Rtt101 degrades Mms22 in response to DNA damage and controls Rad51 loading

All of the so far identified Rtt101 E3 ligase complexes seem to involve Mms1, whereas Mms22 is dispensable in certain situations. Moreover, while *mms22Δ* cells share most phenotypes, such as drug sensitivities and cell cycle progression defects with *rtt101Δ* mutants, a common observation is that loss of Mms22 has more severe effects than loss of Rtt101 or Mms1 (Mimura et al., 2010; Vaisica et al., 2011; Zaidi et al., 2008). This implies that Mms22 might have additional roles outside of the Rtt101 E3 ligase complex in response to DNA damage.

Two genome-wide screens for yeast mutants displaying chromosomal instability connected *MMS22* with proteasome subunits (Ben-Aroya et al., 2010; Yuen et al., 2007). Indeed, Rtt101-dependent ubiquitylation of Mms22 is induced by MMS treatment, resulting in increased recruitment of Mms22 to chromatin followed by its proteasomal degradation. Strikingly, the degradation of Mms22 is sufficient for cells to exit a G2/M arrest upon removal of the source of damage (Ben-Aroya et al., 2010). Thus, although being required for certain functions of the Rtt101 E3 ubiquitin ligase, Mms22 at the same time is one of its ubiquitylation targets. A functional consequence of this regulation has recently been proposed (Diao et al., 2017): Mms22 promotes loading of the Rad51 strand exchange protein onto ssDNA at a break site. Cells lacking Mms22 show decreased Rad51 loading, while cells lacking Rtt101 exhibit persistent loading of Rad51, clearly demonstrating an antagonistic regulation.

1.3.5 Further proposed roles for Rtt101

A recent study further implicates Rtt101 to be involved in the establishment of sister chromatid cohesion (SCC) (Zhang et al., 2017). SCC ensures the correct alignment and segregation of replicated sister chromatids during mitosis and meiosis, moreover it facilitates homologous recombination (HR) processes. The ring-shaped cohesin complex is loaded onto DNA in late G1, and during replication becomes stabilized due to acetylation of the Smc3 subunit by the acetyltransferase Eco1 (reviewed in (Bell and Labib, 2016)). Mms22 interacts with Eco1, and the deletion of *RTT101*, *MMS1* or *MMS22*, or the loss of interaction between Eco1 and Mms22 leads to reduced Eco1-dependent acetylation of Smc3 and consequently, to a defect in SCC (Zhang et al.,

2017). This defect seems to be in part coupled to the H3K56Ac pathway, which becomes essential in the absence of Eco1 function. Indeed, H3K56Ac needs to be tightly regulated as loss of Hst3 also leads to defective SCC (Thaminy et al., 2007). Moreover, the SCC defect in *mms22Δ* and *ctf4Δ* cells is epistatic (Zhang et al., 2017). Taken together, Rtt101^{Mms22} directly or indirectly regulates SCC establishment at active replisomes.

It should be noted that in addition to the above described Rtt101-Mms1-Mms22 complex, Rtt101 has the propensity to form another E3 ligase complex resulting in a non-DNA damage-related function. One such Rtt101 complex is involved in the process of non-functional rRNA decay (NRD) (Fujii et al., 2009). NRD is one of several RNA quality control pathways (reviewed in (Siwaszek et al., 2014)), and ensures the removal of aberrant 18S and 25S rRNA transcripts. Non-functional rRNA is produced by mutations, chemical agents or incorrect biogenesis and negatively affects ribosome function (LaRiviere et al., 2006). In a screen for factors regulating non-functional 25S rRNA decay, both *RTT101* and *MMS1* were detected (Fujii et al., 2009). In *rtt101Δ* and *mms1Δ* strains, the defective 25S rRNA accumulates in the cytoplasm. At the same time, proteins co-purifying with ribosomes containing the non-functional rRNA displayed reduced levels of ubiquitylation in the absence of Rtt101 or Mms1. Crt10, the transcriptional regulator of RNR levels in response to replication stress (Fu and Xiao, 2006) and interaction partner of Mms1 (Zaidi et al., 2008) is necessary to direct the Rtt101-Mms1 complex to its function in NRD (Sakata et al., 2015). This novel Rtt101^{Crt10} complex has a role separate from Rtt101^{Mms22} as *crt10Δ* cells do not show sensitivity to MMS and CPT (Sakata et al., 2015).

1.3.6 Conservation of Rtt101^{Mms22} in human cells

In human cells, the cullin 4 subfamily encompasses two members, CUL4A and CUL4B, which share 82 % identity of amino acid sequence and mainly differ in CUL4B bearing an additional N-terminal nuclear localization signal (NLS) of 149 amino acids (reviewed in (Hannah and Zhou, 2015)). Although CUL4A does not contain an intrinsic NLS and is mainly found in the cytoplasm, a subpopulation localizes to the nucleus. Due to their high similarity CUL4A and CUL4B often function in a redundant manner. However, increasing evidence suggests that in some cases there is a specific requirement for either of the two. The CUL4-based cullin-RING E3 ligase (CRL4) associates with the

RING protein RBX1 and the bridging protein DNA damage-binding protein 1 (DDB1). Substrate specificity is achieved through a selection of DDB1-CUL4-associated factors (DCAFs) (reviewed in (Hannah and Zhou, 2015)). Also in human cells, modification of the cullin subunit with NEDD8 on K619 enhances its function (Saha and Deshaies, 2008).

Although *S. cerevisiae* Rtt101 does not share sequence homology with human CUL4, it is forming CRL4-like complexes that fulfil similar functions. The Rtt101 adaptor protein Mms1 however does share limited sequence homology with human DDB1, and is conserved in domains that in DDB1 are important for its interaction with CUL4 and substrate adaptors (Zaidi et al., 2008). Thus, Rtt101 is considered to be a functional homolog of CUL4.

Within the same month, three independent research groups presented an uncharacterized ORF termed MMS22L (Mms22-like) as a putative homolog of *S. cerevisiae* Mms22. BLAST searches for Mms22 homologs revealed a conserved approximately 160 amino acid long region in the human protein (Duro et al., 2010). Additionally, MMS22L was identified in two independent RNAi screens as a mutant with increased 53BP1 foci formation (O'Donnell et al., 2010) and affecting the duration of the G2 cell cycle phase (Piwko et al., 2010). All three studies further identify TONSL/NFKBIL2 as a functionally relevant binding partner. MMS22L-TONSL interacts with histones, the histone chaperones FACT and ASF1, and DNA replication and repair factors such as the MCM and KU complexes (O'Donnell et al., 2010; Piwko et al., 2010). Although no direct interaction with CUL4A is detectable (O'Donnell et al., 2010), MMS22L is degraded in a CUL4A- and replication stress-dependent manner (Piwko et al., 2010). Consistent among the three reports, depletion of MMS22L or TONSL causes spontaneous DSBs and increased sensitivity to S phase damage such as caused by CPT. Moreover, MMS22L-TONSL accumulates at stressed or damaged forks, and regulates HR (O'Donnell et al., 2010) by stimulating RAD51-ssDNA nucleoprotein filament formation (Duro et al., 2010). This promotes replication fork reversal and HR-mediated restart (Piwko et al., 2016). Moreover, MMS22L-TONSL provides a potent link between the regulation of HR-dependent DNA repair and chromatin assembly based on two observations: First, the absence of H4K20 methylation on newly synthesized histones deposited behind the replication fork is recognized by TONSL and causes accumulation of MMS22L-TONSL on

post-replicative chromatin (Saredi et al., 2016). Second, MMS22L-TONSL is proposed to be recruited to ssDNA at a DSB in an ASF1-dependent manner to promote RAD51 loading onto damaged DNA (Huang et al., 2018). Consistently, localization of MMS22L to sites of DNA damage depends on the presence of RPA-bound ssDNA and resection of the break (O'Donnell et al., 2010; Piwko et al., 2016). The signal for MMS22L-TONSL recruitment has been proposed to stem from transient ASF1-mediated deposition of newly synthesized histones on RPA-covered ssDNA, which has been demonstrated in budding yeast and is speculated to happen in human cells (Huang et al., 2018).

1.3.7 CUL4 regulates nucleotide excision repair upon UV damage

CRL4 complexes target a wide range of proteins involved in cell cycle control, DNA replication and DNA repair. One important function in the maintenance of genome stability is the regulation of nucleotide excision repair (NER), which is required to repair DNA damage induced by UV-irradiation. The most common types of UV-induced DNA lesions, cyclobutane-pyrimidine dimers (CPDs) and 6-4 photoproducts (6-4PPs), are recognized by the heterodimeric UV-damaged DNA-binding protein (UV-DDB) complex comprised of DDB1 and DDB2, which recruits CUL4A to assemble a CRL4 complex. CUL4A efficiently activates global genome NER (GG-NER) through polyubiquitylation of xeroderma pigmentosum group C (XPC) protein and at the same time restricts NER activity by inducing proteasomal degradation of DDB2 (Sugasawa et al., 2005; Chen et al., 2001; Liu et al., 2009). In contrast to GG-NER, transcription-coupled NER (TC-NER) is activated when CPDs or 6-4PPs occur in the context of transcribed chromatin, where they are recognized by stalled RNA polymerase II. Subsequently, CUL4A-DDB1 is recruited through Cockayne Syndrome Protein A (CSA) to form a CRL4 complex in analogy to the CUL4A-DDB1-DDB2 complex involved in GG-NER (Groisman et al., 2003). While GG-NER and TC-NER differ in the sensor that initially recognizes the UV lesion, the downstream processing and repair of the DNA is identical in both NER subpathways. Briefly, NER involves the opening of the DNA duplex, the excision of a stretch of ssDNA harbouring the lesion, the subsequent gap filling using DNA polymerases and ligation of the remaining nick (reviewed in (Nouspikel, 2009)). An important regulator of CRL4 function in NER is the COP9 signalosome (CSN) (Groisman et al., 2003). The CSN binds to CUL4 complexes

and keeps them inactive through deneddylation of the cullin. Upon UV irradiation, the CUL4-DDB1-DDB2 complex dissociates from CSN, thus being activated for GG-NER. At the same time, CUL4A-DDB1-CSA is inactivated through association with CSN. Interfering with CSN function *via* knockdown of the isopeptidase subunit CSN5 results in defects in both GG-NER and TC-NER (Groisman et al., 2003).

1.3.8 CUL4 regulates cell cycle progression and replication in S phase and in the presence of DNA damage

The CRL4 complex employing the DCAF subunit CDT2 regulates key components involved in cell cycle regulation and DNA replication. The replication licensing factor p21 regulates cell cycle progression at different stages through its role in CDK inhibition (reviewed in (Abbas and Dutta, 2009)). The stabilization of p53 upon UV-irradiation induces a transcriptional upregulation of p21, thus reinforcing the G1/S checkpoint to prevent replication in the presence of DNA damage (reviewed in (Fotedar et al., 2004)). p21 is ubiquitylated and degraded throughout unperturbed S phase and upon UV damage in a CUL4A-DDB1-CDT2-dependent manner, thereby preventing re-replication of DNA (Abbas et al., 2008; Kim et al., 2008; Nishitani et al., 2008). The prevention of re-replication is further achieved by CRL4-CDT2-mediated degradation of the replication licensing factor CDT1 which is rapidly degraded in response to UV- or γ-irradiation (Higa et al., 2003; Hu et al., 2004).

Additionally, in response to UV damage CRL4 directly regulates replication progression. The CRL4 complex with VprBP acting as DCAF targets MCM10, a factor involved in the initiation of DNA synthesis at origins of replication, for proteasomal degradation. This halts ongoing replication in the face of UV-induced DNA damage (Kaur et al., 2012). In parallel, CRL4-CDT2 induces degradation of the DNA polymerase δ subunit p12 (Zhang et al., 2013). This leads to a switch from the four-subunit Pol δ to its three-subunit version and provides an important mechanism to inhibit replication fork progression in response to UV irradiation (Terai et al., 2013).

Besides regulating cell cycle progression and DNA replication upon DNA damage, CUL4 moreover directly controls the replication checkpoint response through checkpoint kinase 1 (CHK1). CUL4A-DDB1 interacts with and destabilizes CHK1 protein, a regulation that is enhanced upon ATR-mediated phosphorylation of CHK1

and in response to several types of replication stress (Van Leung-Pineda et al., 2009; Zhang et al., 2005). This regulation of CHK1 prevents a delay in DNA replication that would be caused by an accumulation of active CHK1 and might promote the termination of the replication checkpoint during unperturbed S phase (Zhang et al., 2005).

1.3.9 CUL4 targets histones and affects chromatin state

Histone ubiquitylation at sites of UV-induced DNA damage depends on the CUL4-DDB1-DDB2 complex and targets H3 and H4 both *in vitro* and *in vivo*. Consequently, the NER factor XPC is recruited more efficiently to sites of damage. Moreover, histone eviction from damaged DNA could contribute to making the damaged site more accessible for repair enzymes (Wang et al., 2006). In the absence of damage, budding yeast Rtt101 ubiquitylates H3 during *de novo* nucleosome assembly (see section 1.3.3), thereby facilitating the transfer of newly synthesized H3-H4 dimers from the histone chaperone Asf1 to downstream chaperones like CAF-1 (Han et al., 2013). The same study shows that in human cells the deposition of newly synthesized H3 on replicated DNA is CUL4-DDB1-dependent. Moreover, in the absence of CUL4-DDB1 the association of H3 with ASF1 is increased, indicating a conserved function of Rtt101/CUL4-mediated histone ubiquitylation (Han et al., 2013). After DNA repair, CUL4-DDB1-DDB2 drives chromatin re-assembly and deposition of H3K56Ac in a CAF-1-dependent fashion (Zhu et al., 2017). Intriguingly, CAF-1-mediated chromatin assembly after repair is acting in concert with Rtt101-driven checkpoint recovery in *S. cerevisiae* (Diao et al., 2017), thereby supporting a potential link between CUL4/Rtt101 and chromatin-related processes.

This role is further supported by the notion that CUL4-CDT2 prevents H4K20 monomethylation by ubiquitylating and degrading the histone methyltransferase SET8 during unperturbed S phase and upon DNA damage (Abbas et al., 2010; Centore et al., 2010; Oda et al., 2010). Unscheduled SET8-mediated H4K20me1 during S phase leads to checkpoint-dependent G2 arrest and aberrant chromatin compaction. Of note, CUL4 thus directly prevents the deposition of the histone mark that has to be absent (H4K20me0) for the recruitment of MMS22L-TONSL (Saredi et al., 2016).

1.3.10 CUL4 in human disease and cancer

With CRL4 complexes playing important roles in ensuring cell cycle progression and faithful DNA replication, it is conceivable how their deregulation can drive cancer progression. Increased CUL4 expression levels have originally been reported in breast cancer cells (Chen et al., 1998). However, CUL4 overexpression mainly stemming from gene amplification is now connected with a wide range of tumours, such as in colorectal, lung, prostate or liver cancer, and often correlates with poor prognosis, tumour progression and metastasis (reviewed in (Hannah and Zhou, 2015)). Interestingly, the abrogation of CUL4 function in mice can protect skin cells from UV-induced skin carcinogenesis (Liu et al., 2009). This is achieved by upregulation of GG-NER due to stabilization of DDB2 and XPC, and an enhanced G1 DNA damage checkpoint due to stabilization of p21.

CUL4B deficiency has been identified to be causative for an X-linked mental retardation syndrome (Tarpey et al., 2007; Zou et al., 2007). Despite displaying normal levels of CUL4A, patient cells lacking functional CUL4B are highly sensitive to the Topoisomerase 1 (Top1) poison camptothecin (CPT) and exhibit increased DNA breaks and cell death (Kerzendorfer et al., 2010). To remove covalently bound Top1 from DNA and allow repair, Top1 has to be partially degraded followed by the removal of the remnant peptide by the tyrosyl-phosphodiesterase TDP1 (Lin et al., 2008, 2009). This proteolytic removal of Top1 is dependent on a CUL4B-based CRL complex, which explains the CPT hypersensitivity observed in patient-derived cells (Kerzendorfer et al., 2010).

Targeting CUL4 activity in tumours offers an attractive therapy option. Up to now, this can only be achieved by general inhibition of the proteasome or more specifically by inhibiting cullin activity through the inhibition of neddylation. Bortezomib is an FDA-approved proteasome inhibitor (Fisher et al., 2006; Richardson et al., 2003) while MLN4924 is an inhibitor of neddylation still undergoing phase I and II clinical trials that specifically blocks the NEDD8-E1 enzyme (Soucy et al., 2009). The direct targeting of CRL activity through the prevention of NEDD8-attachment is usually combined with anti-tumour drugs or irradiation to achieve selective killing of tumour cells (reviewed in (Jang et al., 2018)). However, the development of inhibitors specifically targeting CUL4-containing E3 ligases will be of great importance. Particularly, the specific inhibition of CUL4B could sensitize tumour cells in patients that exhibit resistance to

chemotherapeutic agents targeting Top1. Those patients would greatly benefit from a combinational treatment with CPT or its derivatives and CUL4B inhibitors due to the stabilization of Top1 cleavage complexes (reviewed in (Sang et al., 2015)).

The possibility of CUL4B inhibition is also intriguing considering neurological disorders, such as spinocerebellar ataxia with axonal neuropathy (SCAN1). SCAN1 is caused by a mutation in TDP1 (Takashima et al., 2002), and is attributed to impaired processing of Top1 cleavage complexes and transcription-induced DNA breaks (Katyal et al., 2007, 2014; Miao et al., 2006; Sordet et al., 2009). Avoiding the initial degradation of Top1 would make TDP1 dispensable as Top1 complexes on DNA can also be repaired by a TDP1-independent pathway (Zhang et al., 2011).

1.4 Replication fork stalling and restart

The maintenance of genome integrity is inherent to the correct and complete duplication of eukaryotic chromosomes. DNA replication initiates in S phase with the process of origin firing when the parental duplex DNA is unwound by the CMG helicase consisting of Cdc45, the minichromosome maintenance (MCM) helicase and the tetrameric GINS complex (Sld5-Psf1-Psf2-Psf3). DNA synthesis is carried out by the DNA polymerases with Pol ε acting on the leading strand and Pol δ elongating the RNA primers deposited by Pol α/primase on the lagging strand into discontinuous Okazaki fragments (reviewed in (Bell and Labib, 2016)). Pol ε is a tetrameric complex consisting of the essential subunits Pol2 and Dpb2 accompanied by the non-essential subunits Dpb3 and Dpb4 (reviewed in (Hogg and Johansson, 2012)). Pol δ is built up of the essential subunits Pol3 and Pol31, as well as the accessory subunit Pol32 (reviewed in (Prindle and Loeb, 2012)). Replication processivity on both strands is enhanced by the sliding clamp PCNA (reviewed in (Bell and Labib, 2016)). Additional regulatory proteins assemble with the CMG to form the ‘Replisome Progression Complex’ (RPC) (Gambus et al., 2006). Among those are the replication fork pausing complex (FPC) members Csm3 and Tof1 (Calzada et al., 2005; Hodgson et al., 2007), and Mrc1 which interacts with both Pol ε (Lou et al., 2008) and the MCM subunit Mcm6 (Komata et al., 2009). Mrc1 is additionally required to activate the S phase checkpoint in response to replication stress (Alcasabas et al., 2001). Moreover, the histone chaperone complex FACT with roles in both transcription and replication through chromatin (Orphanides et

al., 1998; Schlesinger and Formosa, 2000) is part of the RPC. Finally, Ctf4 couples DNA Pol α with the CMG (Gambus et al., 2009; Tanaka et al., 2009) while at the same time acting as a platform for the recruitment of further proteins (Villa et al., 2016). The active replisome is accompanied by many additional proteins throughout S phase and upon replication fork stalling.

1.4.1 Causes of replication fork stalling

A large variety of exogenous and endogenous factors can interfere with DNA replication processes. In the following, some of those factors will be introduced with a focus on the causes of replication fork stalling and DNA damage relevant for this thesis.

The most commonly used agent to induce DNA replication stress is hydroxyurea (HU). HU is a potent inhibitor of ribonucleotide reductase (RNR), the enzyme complex responsible for the rate-limiting step in the biosynthesis of deoxynucleotide triphosphate (dNTP) (Krakoff et al., 1968). Consequently, HU induces nucleotide depletion and influences the cellular balance between rNTPs and dNTPs, leading to fork stalling and a reversible S phase arrest (reviewed in (Singh and Xu, 2016)). Intriguingly, a prolonged HU-induced arrest leads to the accumulation of DSBs as a result of fork collapse, which in human cells rely on RAD51-mediated processes to restart replication (Petermann et al., 2010; Saintigny et al., 2001).

Another frequently used DNA damaging drug that causes replication stress is methyl methanesulfonate (MMS). Methylation of DNA bases at different positions leads to the formation of a mix of modifications with 7-methylguanine being by far the most abundant (82 %) followed by 3-methylguanine (11 %) and a small fraction of 3-methyladenine (Beranek, 1990). These base modifications are not necessarily cytotoxic or mutagenic *per se*, but upon spontaneous hydrolysis or depurination, toxic apurinic (AP) sites can arise (reviewed in (Shrivastav et al., 2009)). Moreover, throughout the repair of the alkylation adducts *via* the base excision repair (BER) pathway, additional toxic intermediates including AP sites can accumulate (Xiao and Samson, 1993; Glassner et al., 1998). Treatment of cells with MMS leads to a dose-dependent physical block of replication forks that is independent of DNA damage signalling and can cause the formation of DSBs (Groth et al., 2010). Those replication-

dependent DSBs induced by the N-alkylpurines rely on homologous recombination (HR) for their repair (Nikolova et al., 2010).

To study replication-dependent DSBs, drugs targeting topoisomerases are widely used. Top1 is important during DNA replication and transcription as it can relieve both positive and negative supercoiling of DNA and thus reduces torsional stress during those processes (reviewed in (Pommier et al., 2016)). Mechanistically, a tyrosine residue in the catalytic core of Top1 can covalently bind to the 3'-phosphate in dsDNA by nucleophilic attack and the formation of a phosphodiester bond. The resulting single-stranded DNA nick allows rotation of the DNA, thereby reducing supercoiling within the DNA molecule. Once the 5'-hydroxylgroup of the incised DNA is aligned back with the tyrosine-DNA phosphodiester bond, Top1 can religate the DNA backbone. This reaction, as well as the formation of the covalent Top1 cleavage complex (Top1cc) is usually very transient (reviewed in (Pommier et al., 2006)). Camptothecin (CPT) exerts its poisoning effect by trapping the Top1cc intermediate on DNA, thereby reversibly stabilizing it (Staker et al., 2002). Consequently, damage caused by CPT is not due to the drug itself, but requires cells to proceed through S phase (Degrassi et al., 1989). DSBs are generated during transcription or because a replication fork 'runs off' the leading strand once it reaches the nicked DNA accompanying the stabilized Top1cc (Sordet et al., 2009; Strumberg et al., 2000). Interestingly, Top1ccs can also be stabilized in the absence of CPT when aberrant DNA structures are present at or close to the site of incision. Among those structures are oxidative base damage (Pourquier et al., 1999; Lesher et al., 2002), abasic sites (Pourquier et al., 1997a), and DNA nicks or gaps (Pourquier et al., 1997b). More recently, Top1-mediated processing of misincorporated genomic ribonucleotides has been shown to cause genome instability although through mechanisms that do not directly involve stabilization of Top1ccs (Sekiguchi and Shuman, 1997; Kim et al., 2011; Huang et al., 2015, 2017) (see section 1.5).

Even in unchallenged cells, endogenously occurring structures can impair DNA replication progression. Natural pause sites such as the replication fork barrier (RFB) within the ribosomal DNA locus induce fork stalling via the Fob1 protein that binds to a specific sequence in the DNA (Kobayashi and Horiuchi, 1996; Kobayashi, 2003). Moreover, co-transcriptionally arising R-loops, three-stranded structures in which an RNA molecule anneals to its complement DNA strand while displacing the second DNA

strand, can interfere with DNA replication and transcription, and cause a major threat for genome stability (reviewed in (Aguilera and García-Muse, 2012)). Another potential threat on DNA replication is imposed by G-quadruplexes that can form in G-rich DNA sequences through stacking of guanines and interfere with replication fork progression (reviewed in (Gadaleta and Noguchi, 2017)). Finally, changes in the DNA structure can directly affect DNA replication. One such structural change is caused by the accumulation of ribonucleotides in the duplex DNA, shifting the overall conformation from the B-form to the A-form associated with RNA molecules (Ban et al., 1994; Clausen et al., 2013a; Egli et al., 1993) (see section 1.5.1).

DNA replication can be perturbed by a wide range of exogenous and endogenous cues that cause frequent DNA replication fork stalling and replication-associated DSBs. Thus, it is important to understand the mechanisms that sense and repair those structures to maintain genome integrity.

1.4.2 Checkpoint activation

The active slow-down of replication in the presence of DNA lesions has been described as the result of an ‘intra-S phase’ checkpoint. This checkpoint is different from the DNA damage checkpoint that prevents entry into mitosis in the presence of DNA damage (Liang and Wang, 2007; Paulovich and Hartwell, 1995). The important functions of this replication checkpoint can be divided into three main aspects. First, inhibition of origin firing to prevent stalling of additional forks. Second, an increase of nucleotide levels as a substrate for subsequent repair processes. And third, stabilization of the stalled replication forks. The main players involved in this checkpoint are the apical kinase Mec1 (ATR in human cells) and the downstream checkpoint kinase Rad53 (human CHK1). The inhibition of late origin firing is achieved through direct Rad53-mediated phosphorylation of proteins required for the initiation of replication, Sld3 and Dbf4 (Santocanale and Diffley, 1998; Lopez-Mosqueda et al., 2010; Zegerman and Diffley, 2010). The balance of dNTP levels upon replication stress is regulated by Dun1, a downstream effector kinase of Rad53. Dun1 controls dNTP levels in the presence of replication stress by inducing the degradation of Sml1, an inhibitor of ribonucleotide reductase, thus allowing for increased dNTP synthesis (Zhao et al., 1998; Zhao and Rothstein, 2002). Moreover, Dun1 controls RNR gene expression on the transcriptional level through Crt10 (Fu and Xiao, 2006). The third important function of the S phase

checkpoint is the prevention of replication fork collapse upon fork stalling (Lopes et al., 2001; Tercero and Diffley, 2001). Although previous work suggested that the checkpoint stabilizes replisome components at a stalled fork (Cobb et al., 2003), more recent evidence from work in both yeast and human cells indicates that the checkpoint is dispensable for the stable association of the replisome with DNA replication forks upon replication stress (Dungrawala et al., 2015; De Piccoli et al., 2012). This suggests that the S phase checkpoint modulates replisome function rather than its stability. Checkpoint-defective yeast and human cells accumulate long stretches of ssDNA when replication is stalled (Buisson et al., 2015; Sogo et al., 2002). Thus, checkpoint proteins have been suggested to be involved in the restriction of uncoupling at stalled forks (Nedelcheva et al., 2005). Indeed, extensive accumulation of ssDNA is implicated in being the cause of increased fork breakage in checkpoint mutants, presumably through exhausting the nuclear pool of replication protein A (RPA) that helps to protect ssDNA (Toledo et al., 2014). Strand-specific DNA sequencing methods reveal that Rad53 prevents the accumulation of ssDNA by coupling leading and lagging strand DNA synthesis upon replication stress (Gan et al., 2017). In the absence of a functional S phase checkpoint, lagging strand synthesis proceeds after fork stalling while the leading strand accumulates as a long RPA-coated, single-stranded template.

At a stalled replication fork, ssDNA accumulates and is rapidly coated by RPA. This structure is recognized by the sensor complexes Mec1-Ddc2 (ATR-ATRIP in human cells) through interaction with RPA-ssDNA (Zou and Elledge, 2003) or the PCNA-like checkpoint clamp Rad17-Mec3-Ddc1 (human RAD9-RAD1-HUS1, or 9-1-1) together with Dpb11 (human TopBP1) and the replication initiation protein Sld2 (Kondo et al., 1999; Wang and Elledge, 1999; Zou et al., 2003). Checkpoint activation is enhanced through the continuation of lagging strand replication at stalled forks, as recruitment of the 9-1-1 clamp is facilitated by the presence of ssDNA-dsDNA junctions such as created by primers on the lagging strand (Majka et al., 2006; Van et al., 2010). Interestingly, DNA Pol ε itself has been implicated in the direct activation of Mec1 both through the C-terminal domain of the catalytic subunit Pol2 and through the accessory subunit Dpb4 in a pathway independent of the 9-1-1 clamp (Navas et al., 1995; Puddu et al., 2011). Moreover, the replisome component Mrc1 is a mediator of the replication checkpoint and transduces signalling from Mec1 to Rad53 through its interaction with Mec1 (Alcasabas et al., 2001; Berens and Toczyski, 2012; Osborn and Elledge, 2003).

This checkpoint mediator function of Mrc1 can be uncoupled from its other functions within the replisome (Osborn and Elledge, 2003). Interestingly, Mrc1 interacts with both the N-terminus and C-terminus of Pol2. The interaction with the N-terminal domain of Pol2 implicated in its catalytic activity is lost upon activation of the S phase checkpoint while the C-terminal domain of Pol2 that plays a structural role maintains its interaction with Mrc1. Additionally, the absence of Mrc1 leads to a destabilization of Pol2 at stalled forks (Lou et al., 2008). Thus, Mrc1 might play a dual role in the response to stalled replication forks by directly activating Rad53 and by its interaction with Pol ε. This is further emphasized by a very recent study showing that Mrc1 enhances Pol ε DNA synthesis activity *in vitro*, a function that is abrogated when Mrc1 gets phosphorylated by Mec1 (Zhang et al., 2018).

1.4.3 DNA damage tolerance and post-replicative repair

When replication forks stall due to a lesion in the DNA template, the favoured consequence for the cell is to avoid prolonged replication fork arrest that could potentially lead to fork breakage and thus deleterious DSBs. The DNA damage tolerance (DDT) pathways offer an elegant way to allow replication to continue across a lesion (Figure 3). DDT can be separated into the error-prone translesion synthesis (TLS) and the error-free template switch (TS) pathway. Both pathways allow replication to skip the lesion and continue with bulk replication, as DDT can be genetically separated from DNA synthesis and postponed until G2 phase (Daigaku et al., 2010; Karras and Jentsch, 2010). Damage tolerance is regulated by the posttranslational modification status of the homotrimeric DNA replication clamp PCNA, Pol30 in yeast. During unperturbed replication, PCNA is found to be SUMOylated on K164 by Siz1 (Hoege et al., 2002). This modification signals for the recruitment of the antirecombinase Srs2 to prevent unscheduled HR at the replication fork (Papouli et al., 2005; Pfander et al., 2005). Upon replication fork stalling at the site of a lesion, the accumulation of RPA-covered ssDNA recruits the E3 ubiquitin ligase Rad18 (Davies et al., 2008), which together with the E2 ubiquitin conjugating enzyme Rad6 monoubiquitylates PCNA on K164 (Hoege et al., 2002). This modification allows direct recruitment of TLS polymerases *via* their ubiquitin-interacting domains (Bienko et al., 2005; Watanabe et al., 2004). Those specified DNA polymerases, in budding yeast mainly Rad30 (Pol η/eta) and Rev1 in complex with Rev3-Rev7 (Pol ζ/zeta) can extend

the newly synthesized DNA strand across the lesion (Stelter and Ulrich, 2003). However, due to the low fidelity of these polymerases, the TLS mechanism is a potent source of damage-induced mutations (Garg and Burgers, 2005; Guo et al., 2006; Parker et al., 2007). The single ubiquitin molecule on PCNA can be further extended into K63-linked polyubiquitin chains by the concerted action of the E2 enzyme complex Mms2-Ubc13 and the E3 ligase Rad5 (Ulrich and Jentsch, 2000). If this happens, the postreplicative DNA gap on the daughter strand will be repaired by the TS mechanism. This offers an error-free mode of damage tolerance, as the gap will be filled using the undamaged sister strand as a template (Zhang and Lawrence, 2005). A plasmid-based *in vivo* assay that induces site-specific replication fork stalling revealed that the completion of DNA replication in more than 90 % of events relies on recombination (Zhang and Lawrence, 2005). Roughly two thirds of these recombination events require the *RAD6/RAD18* pathway, while the remaining ones are *RAD52*-dependent. The authors speculate that the portion of *RAD52*-dependent events might involve strand breakage and thus need Rad52 to facilitate single-strand invasion and HR-dependent repair (see section 1.4.5). Indeed, two proposed models for error-free DDT that are not mutually exclusive are under debate (reviewed in (Xu et al., 2015)): One of those models suggests the involvement of strand invasion, which in turn would at least partially require the conventional HR machinery. After completion of DNA synthesis across the lesion using the newly synthesized sister strand as a template, the resulting double Holliday junction (dHJ) structure can be resolved by Sgs1 and Top3. In the alternative model, Rad5 *via* its helicase activity can unwind the nascent strands, followed by their subsequent annealing (Blastyák et al., 2007). This creates a so-called chicken foot structure or regressed replication fork. In a subsequent step, the original fork is restored (see section 1.4.4). In support of the fork regression model of DDT, the formation of K63-linked ubiquitin chains on PCNA is a prerequisite for replication fork regression in mammalian cells (Vujanovic et al., 2017).

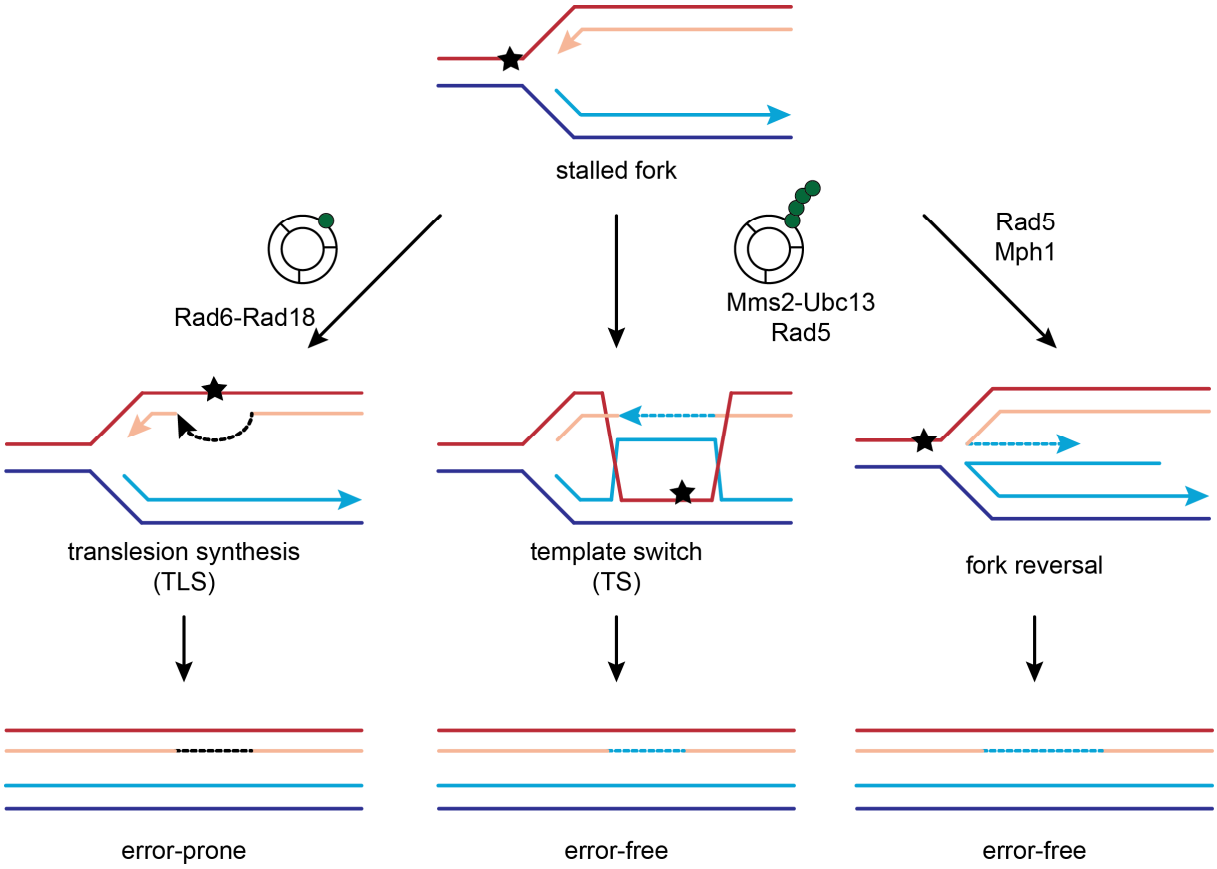

Figure 3. Stalled replication forks and possible repair outcomes. Replication fork stalling is induced by a variety of DNA lesions (symbolized by the star). Postreplicative repair (PRR) or the DNA damage tolerance (DDT) pathway is initiated by the ubiquitylation of PCNA (depicted by the ring, green spheres stand for ubiquitin) on K164. Monoubiquitylation by the E2 enzyme Rad6 and the E3 ligase Rad18 leads to the recruitment of translesion synthesis (TLS) DNA polymerases that can replicate across the lesion. Due to the low fidelity of TLS polymerases, this pathway is mutagenic and error-prone. When the monoubiquitin on PCNA gets elongated into a K63-linked polyubiquitin chain by the E2 Mms2-Ubc13 and the E3 Rad5, template switch (TS) is activated. This pathway involves the use of the nascent sister strand as a template. Alternatively, the nascent strands can anneal to form a 'chicken foot structure' referred to as reversed fork. This process requires Rad5 and the helicase Mph1 and might depend on PCNA polyubiquitylation. Both TS and fork reversal lead to an error-free outcome.

Although increasing insight into the mechanisms of error-prone and error-free DDT is available, the exact regulation of the different pathways and what determines the pathway choice is still under investigation. Moreover, the possibility that each of the three Pol30 subunits within PCNA could be modified differentially offers multiple layers of regulation that remain to be clarified.

1.4.4 Replication fork reversal

An important consequence of the above described damage tolerance pathways is that cells avoid the creation of a DSB upon fork stalling. One option to avoid the breakdown of a stalled fork offers repriming of DNA synthesis downstream of the lesion, which leaves a ssDNA gap on the DNA strand opposite of the lesion (Lopes et al., 2006). This gap can then be repaired by HR-mediated template switch (Zhang and Lawrence, 2005). Another frequently observed scenario is the uncoupling of leading and lagging strand synthesis at the site of replication fork stalling. The continuous unwinding of template DNA with the simultaneous block of leading strand polymerase progression leads to the accumulation of large regions of ssDNA on one arm of the replication fork (Lopes et al., 2006; Yeeles and Marians, 2013). Replisome uncoupling is likely a prerequisite for replication fork reversal, a DNA structure observed in response to a large variety of replication stressors (Zellweger et al., 2015) (Figure 3). More than 40 years ago, the existence of four-way junctions at replication forks presumably caused by annealing of the newly synthesized strands was shown by electron microscopy (Fujiwara and Tatsumi, 1976; Higgins et al., 1976). In budding yeast, fork regression or reversal could initially only be detected in checkpoint-deficient mutants (Sogo et al., 2002). The first evidence of fork reversal in wildtype yeast cells stems from treatment of cells with CPT (Ray Chaudhuri et al., 2012). At the concentrations used in that study, CPT-induced damage is checkpoint-blind and does not lead to activation of the intra S checkpoint (Redon et al., 2003). Thus, fork regression might be a consequence of increased topological stress due to poisoning of topoisomerases. Similarly, the failure of highly transcribed loci to detach from nuclear pore complexes upon checkpoint activation results in increased fork reversal due to structural tension (Bermejo et al., 2011). In budding yeast, Rad5 and Mph1 as well as Rad51 are implicated in the remodelling of stalled forks into regressed ‘chicken foot structures’ (Blastyák et al., 2007; Zellweger et al., 2015; Zheng et al., 2011), with Mph1 being negatively regulated by the Smc5/Smc6 complex (Xue et al., 2014).

However, although yeast cells might employ fork reversal only in response to certain types of replication stress or when the checkpoint is non-functional, recent discoveries in human cells characterize fork regression as a process that is both reversible and highly regulated (reviewed in (Neelsen and Lopes, 2015)). Reversed forks are observed in response to CPT as well as several other types of DNA damage including

DNA crosslinks, nucleotide depletion and DNA base damage. Their formation depends on RAD51 as well as poly(ADP-ribose) polymerase 1 (PARP1) activity (Ray Chaudhuri et al., 2012; Zellweger et al., 2015). Moreover, the SWI/SNF protein family translocases ZRANB3 and SMARCAL1 as well as the Rad5 homolog HLTF induce fork regression *in vivo* (Kolinjivadi et al., 2017; Taglialatela et al., 2017; Vujanovic et al., 2017). Other DNA translocases such as the Mph1 homolog FANCM and RAD54 display fork regression activity *in vitro* (Bugreev et al., 2011; Gari et al., 2008). The breast cancer susceptibility gene products BRCA1 and BRCA2, together with RAD51 protect reversed forks from degradation mediated by the combined action of the nucleases CtIP, MRE11 and EXO1 (Kolinjivadi et al., 2017; Lemaçon et al., 2017). Finally, proteins with the capability to restart regressed forks have been identified: the RECQ1 helicase as well as DNA2 nuclease in concert with WRN helicase promote restart of a regressed fork (Berti et al., 2013; Thangavel et al., 2015). Depending on the situation and the type of damage that causes fork stalling, a regulated subset of the above-mentioned factors might be employed to either restart a stalled fork or stabilize it until an incoming fork arrives to ensure complete replication of chromosomes. Since many of those enzymes are conserved, their homologs might be similarly involved in the probably less frequent replication fork regression in budding yeast.

1.4.5 HR-dependent repair of broken replication forks

As described above, uncoupling of leading and lagging strand DNA synthesis is a common response to lesions that block replication fork progression. If a fork is stalled for a prolonged time, it becomes more susceptible to the action of nucleases and might ultimately break down (Hanada et al., 2007). Moreover, unrepaired ssDNA gaps or nicks in the template duplex DNA can cause replication fork run-off in the subsequent S phase (Strumberg et al., 2000). Both fork breakdown and fork run-off result in the creation of a one-ended DSB (Figure 4A). As DSBs are considered the most toxic type of DNA damage, their repair is tightly regulated. During S and G2 phase, homologous recombination (HR) is the prevalent choice of repair for DSBs. While in G1 phase HR is actively inhibited (Orthwein et al., 2015), the presence of a nascent sister chromatid in S and G2 phase offers a chance to minimize loss of DNA sequences surrounding the break. HR-based repair of DNA replication-associated DSBs leads to the exchange

of varying amounts of genetic material between the sister chromatids, an event termed sister chromatid exchange (SCE) (Sonoda et al., 1999).

The initial step for all HR-mediated pathways is the resection of the broken DNA end to create ssDNA that can subsequently search for homology on the sister chromatid or within other genomic loci (Figure 4B). Resection is carried out by a two-step mechanism: the Mre11-Rad50-Xrs2 (MRX) complex (MRE11-RAD50-NBS1, MRN in mammals) together with Sae2 (human CtIP) initiates short-range resection followed by extensive long-range resection mediated by Exo1 or Sgs1 and Dna2 (Gravel et al., 2008; Mimitou and Symington, 2008; Zhu et al., 2008). The resulting 3' ssDNA overhang is rapidly covered by the single-strand binding protein RPA (Replication Protein A). While initially RPA-coated single-stranded DNA serves as a signal to activate the Mec1-Ddc2 (human ATR/ATRIP) DNA damage checkpoint (Zou and Elledge, 2003), it is subsequently replaced by Rad51 to form the Rad51 nucleoprotein or presynaptic filament.

The Rad51 presynaptic filament is central to virtually all recombination-dependent repair pathways of one-ended DSBs (Figure 4). Coherently, its formation, stability and dissolution are tightly regulated by a wide range of factors. While during unperturbed S phase the formation of Rad51 filaments is prevented by the strippase activity of Srs2 (Krejci et al., 2003; Papouli et al., 2005; Pfander et al., 2005), the initial steps of recombination, namely search for homology and strand invasion into the homologous duplex DNA, are catalysed by the Rad51 presynaptic filament (Baumann et al., 1996; Sung, 1994). Recombination mediator proteins stimulate the replacement of RPA on the resected ssDNA with Rad51. Yeast Rad52 has an important stimulatory role in this process (Benson et al., 1998; Song and Sung, 2000). Further, the Rad51 paralogs Rad55-Rad57 and the Shu complex, as well as the Rad54 translocase have been implicated in the formation of Rad51 nucleoprotein filaments (Sung, 1997; Liu et al., 2011; Gaines et al., 2015; Sugawara et al., 2003; Wolner et al., 2003).

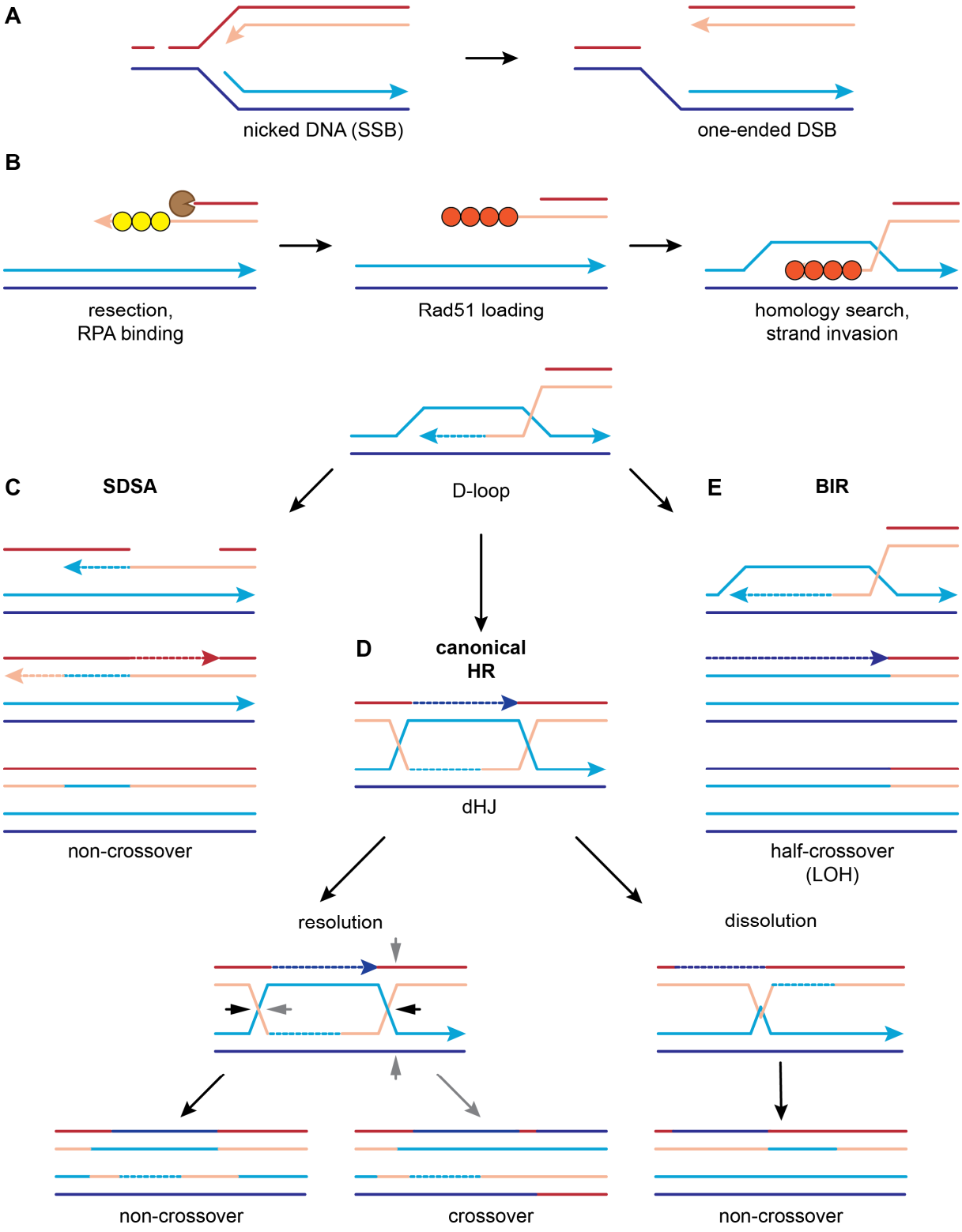

Figure 4. Homologous recombination-dependent repair of broken replication forks. *Figure legend: see next page.*

Figure 4. Homologous recombination-dependent repair of broken replication forks. (**A**) When replication encounters a single-stranded break (SSB) or nick in the template, a one-ended double-strand break (DSB) will occur. Alternatively, prolonged fork stalling can lead to fork breakdown, which also results in a one-ended DSB. (**B**) The broken end gets resected by nucleases, the resulting 3' ssDNA overhang is covered by replication protein A (RPA). RPA then is replaced by Rad51. The resulting Rad51-presynaptic filament finds a homologous DNA region and invades the duplex DNA. Upon stripping of Rad51 from the DNA, the invaded end is elongated by DNA polymerases to form the D-loop, which can be processed by different pathways. (**C**) Synthesis-dependent strand annealing (SDSA) depends on disruption of the D-loop and the capture of a second end. Repair will result in a non-crossover product. (**D**) The D-loop can be stabilized upon second end capture to form a double Holliday junction (dHJ). This is the central intermediate of canonical HR and can be processed by resolution or dissolution. Dissolution is mediated by Sgs1-Top3-Rmi1: the two branch points converge towards one another and are finally dissolved by Top3 activity. For resolution, structure-specific endonucleases Mus81-Mms4, Slx1-Slx4 or Yen1 can target the dHJ in different ways (depicted by the black or grey arrowheads). While dissolution always results in non-crossover products, resolution can lead to the formation of both non-crossover and crossover products. (**E**) If a second end of the break is not found, break-induced replication (BIR) allows the completion of chromosome duplication. Initiating within the D-loop, a migrating bubble copies DNA from the sister strand in a conservative fashion to the end of the chromosome. This results in a half-crossover that can lead to loss of heterozygosity (LOH). BIR depends on Pol32 and Pif1 and is regulated by Sgs1 and Mph1.

In human cells, BRCA2 and its homologs as well as a group of RAD51 paralogs participate in the regulation of RAD51 presynaptic filament formation (reviewed in (Ranjha et al., 2018)). Recently, the budding yeast Mms22 homolog MMS22L in complex with TONSL has been shown to be required for efficient loading of RAD51 onto RPA-coated ssDNA (Piwko et al., 2016). Although in yeast cells a direct involvement of Mms22 in Rad51 filament formation has not been shown, reduced levels of Rad51 at a DSB in *mms22Δ* cells lead to the speculation about a similar role for Mms22 (Diao et al., 2017).

When the Rad51-coated presynaptic filament finds a homologous sequence, it has to invade the duplex DNA to form a stable displacement loop (D-loop). The displaced DNA strand is bound and protected by RPA (Eggler et al., 2002). Once the invading Rad51 nucleoprotein filament base-pairs with homologous sequences within the D-loop, Rad54 promotes displacement of Rad51 molecules from the resulting dsDNA (Solinger et al., 2002). This allows for the initiation of DNA synthesis on the free 3' end mainly by Pol δ, although Pol ε has also been implicated to drive DNA synthesis in the context of HR (Hicks et al., 2010; Li et al., 2009; Wilson et al., 2013).

After DNA synthesis the extended D-loop can be disrupted, thus the DNA end which has now been elongated past the damaged site is released and can anneal back to its

original template strand (Figure 4C). This synthesis-dependent strand-annealing (SDSA) pathway is estimated to account for approximately 80 % of recombination events (Malkova et al., 1996) and is the preferred repair outcome as it prevents crossover formation, meaning the exchange of genetic material between regions flanking the break (Ira et al., 2006). SDSA is promoted by the D-loop disruption/branch migration activity of Mph1 (Zheng et al., 2011). Moreover, Top3 can catalytically dissolve D-loops, thus is also able to promote SDSA (Fasching et al., 2015).

If the second end of the break is in close proximity, Rad52-dependent annealing of that end to the displaced strand of the D-loop and subsequent ligation leads to the formation of a double Holliday junction (dHJ) (Nimonkar et al., 2009) (Figure 4D). This key structure of canonical HR leads to genome instability if not properly repaired (Wechsler et al., 2011) and can either be subjected to dissolution or resolution. When Sgs1 and Top3 catalyse a converging of the two branch points towards one another, the strand passage activity of Top3, stimulated by Rmi1, leads to dissolution of the dHJ thereby forming a non-crossover repair product (Cejka et al., 2010). Alternatively, the resolution of the dHJ by nucleases can result either in a non-crossover or a crossover product. Mus81-Mms4 (human MUS81-EME1), Slx1-Slx4 (human SLX1-SLX4) and Yen1 (human GEN1) have all been shown to target dHJs leading to their resolution (reviewed in (Wyatt and West, 2014)).

When the second homologous end of a break is not available or is too far away to be captured, break-induced replication (BIR) offers an emergency route that ensures the complete duplication of a chromosome, albeit at a substantial risk for genome integrity (Figure 4E). Initiating within the D-loop, break-induced replication can proceed over long distances to the end of the chromosome. This unusual DNA synthesis mode uses most of the conventional DNA replication factors such as the CMG helicase and the three replicative DNA polymerases (Lydeard et al., 2007, 2010). Despite sharing a similar set of replication proteins used in semi-conservative S phase replication, BIR employs a conservative mode of DNA synthesis, in which a migrating bubble travels long distances along the chromosome (Donnianni and Symington, 2013; Lydeard et al., 2007; Saini et al., 2013). Migration of this bubble is dependent on the Pif1 helicase and the Pol δ subunit Pol32, which during normal S phase replication is dispensable (Lydeard et al., 2007; Saini et al., 2013; Wilson et al., 2013). Additionally, lagging strand synthesis is largely uncoupled from the synthesis of the invaded leading strand,

resulting in the accumulation of a long ssDNA tail behind the migrating bubble (Saini et al., 2013) which is covered by RPA (Ruff et al., 2016). The decision to commit to the BIR pathway is controlled by the replication execution checkpoint that delays the initiation of BIR for several hours (Donnianni and Symington, 2013; Malkova et al., 2005). This pathway choice is regulated by the Mph1 and Sgs1 helicases. The concomitant loss of both Mph1 and Sgs1 abolishes the delay in initiation of BIR (Jain et al., 2009; Mehta et al., 2017; Štafa et al., 2014). One reason why BIR has such detrimental consequences on genome stability is that it results in a half-crossover outcome that causes loss of heterozygosity (LOH). Additionally, BIR is highly inaccurate and increases the frequency of frameshift mutations as well as base substitutions (Deem et al., 2011; Saini et al., 2013). While frameshifts are attributed to the more inaccurate mode of replication of Pol δ, base substitution mutations might accumulate on the long ssDNA tail that persists behind the migrating bubble until the lagging strand is fully replicated.

In conclusion, the fate of a one-ended DSB is closely related to the fate of the Rad51 nucleofilament that is formed in an early step and multiple proteins have evolved to control repair outcomes in a way that maintains genome integrity.

1.5 Genomic ribonucleotides and their repair

While DNA replication requires dNTPs to faithfully duplicate the genome, transcription processes need considerable amounts of rNTPs. As a consequence, the intracellular concentrations of rNTPs highly exceed those of dNTPs with 500-3000 µM compared to 12-30 µM (Nick McElhinny et al., 2010a). DNA polymerases harbour a tyrosine residue within their ‘steric gate’ that collides with the OH-group of an rNTP, thus allowing for discrimination between the different sugars to a certain extent (reviewed in (Brown and Suo, 2011)). However, this discrimination is imperfect and *in vitro* studies using endogenous concentrations of rNTPs and dNTPs suggest that in the *S. cerevisiae* genome approximately 13000 ribonucleotides get incorporated within a single round of replication. This incorporation frequency is recapitulated *in vivo* (Nick McElhinny et al., 2010a), resulting in an incorporation rate of approximately 1 rNMP incorporation per 6500 bases (Lujan et al., 2012). Counted among them are also the RNA primers synthesized by Pol α/Primase at each Okazaki fragment during lagging

strand synthesis, although those rNMPs get very efficiently removed and are thus only transient (reviewed in (Zheng and Shen, 2011)). Accordingly, in human cells the number of incorporated ribonucleotides per cell cycle is estimated to reach 1 million (Clausen et al., 2013b).

1.5.1 Direct consequences of misincorporated genomic ribonucleotides

All three replicative polymerases in budding yeast can bypass single ribonucleotides within duplex DNA, although with reduced efficiency. The bypass efficiency for Pol ε lies at 66 % for a single rNMP, but rapidly drops to 3 % when three consecutive rNMPs are incorporated. Stretches of four or more rNMPs cannot be bypassed by Pol ε anymore (Watt et al., 2011). Similar observations are made for the human replicative polymerases Pol ε and Pol δ (Clausen et al., 2013b; Göksenin et al., 2012). Together with the high numbers of misincorporated rNMPs in every cell cycle this strongly puts forward the existence of dedicated mechanisms to remove most of the rNMPs incorporated by DNA polymerases.

Consistent with the reduced efficiency of DNA polymerases to replicate across an incorporated rNMP, several studies show that even a single rNMP within duplex DNA has an impact on the structure of the DNA molecule. It locally changes the helix structure from the B-form commonly adopted by DNA to the A-form characteristic for RNA molecules (Derose et al., 2012; Jaishree et al., 1993; Rychlik et al., 2010) and affects the elastic properties of DNA (Chiu et al., 2014). As a consequence, interactions between DNA and certain proteins could be impaired (Tumbale et al., 2014). This might be especially problematic for nucleosome formation as proposed by *in vitro* studies (Dunn and Griffith, 1980; Hovatter and Martinson, 1987). Moreover, due to the 2'OH group rNMPs are more susceptible to spontaneous hydrolysation, thus creating single-stranded breaks (SSBs) in the DNA backbone (Li and Breaker, 1999). Another structure with potentially harmful consequences arises from abortive ligation of a single-stranded nick, as it could be induced by RNase H2 (reviewed in (Schellenberg et al., 2015)). The resulting bulky adenylated 5' DNA end requires resolution by the deadenylase aprataxin (Hnt3 in yeast) to avoid induction of replication stress (Tumbale et al., 2014).

Both yeast and mammalian cells lacking RNase H2, the enzyme responsible for the majority of ribonucleotide repair (see section 1.5.2), display signs of replication stress. In yeast, the S phase checkpoint as well as the PRR pathway is constitutively activated and cells exhibit a cell cycle progression defect (Nick McElhinny et al., 2010b; Lazzaro et al., 2012; Williams et al., 2013). The same defects are observed in RNase H2-depleted human cells as well as cells from patients suffering from Aicardi-Goutières syndrome (AGS) associated with mutations in RNase H2 (see section 1.5.3) (Pizzi et al., 2015). Similarly, the loss of RNase H2 in mouse cells results in a slower cell cycle, accumulation of cells in G2/M phase, a chronic activation of the DNA damage response, an increase in SSBs, and the formation of γH2AX foci (Hiller et al., 2012).

1.5.2 Repair of misincorporated genomic ribonucleotides

The efficiency of polymerases to recognize and excise rNMPs is weak compared to their proofreading of incorrect base-base pairing (approximately 30 % compared to 92 % for Pol ε) (Shcherbakova et al., 2003; Williams et al., 2012). Thus, additional repair pathways must have evolved. The eukaryotic RNase H family consists of the trimeric RNase H2 and the monomeric RNase H1 and removes RNA-DNA hybrid structures occurring in the genome (reviewed in (Cerritelli and Crouch, 2009)). Besides accidently incorporated rNMPs found both as single bases and in longer stretches, RNA-DNA hybrids can form when RNA molecules anneal to a complementary DNA strand, thereby displacing the second strand. This three-stranded structure termed R-loop can have detrimental consequences on genome stability (reviewed in (Santos-Pereira and Aguilera, 2015)). While RNase H1 requires at least four consecutive rNMPs to recognize RNA-DNA hybrid structures, RNase H2 can act both on stretches of rNMPs such as found in R-loops and on single rNMPs in the context of dsDNA (Figure 5A). RNase H2 consists of the catalytic subunit Rnh201 and the accessory subunits Rnh202 and Rnh203. Loss of any of its subunits renders the enzyme inactive (Jeong et al., 2004). A separation-of-function allele of the catalytic Rnh201 subunit, *RNH201-P45D-Y219A* (or *RNH201-RED* for ribonucleotide excision defective) is almost completely deficient in the removal of single rNMPs in duplex DNA, but still proficient in the removal of longer rNMP stretches and R-loops, albeit with slightly reduced enzymatic activity compared to wildtype enzyme (Chon et al., 2013). The use of this allele in various succeeding studies helped to clarify that in eukaryotic cells

RNase H2 is the main enzyme to repair misincorporated genomic rNMPs in a process termed ribonucleotide excision repair (RER) (Figure 5B).

Upon recognition of an rNMP, RNase H2 incises the DNA backbone 5' of the ribonucleotide to allow its subsequent repair and removal (Eder et al., 1993; Rydberg and Game, 2002). The detailed mechanism of RER has been reconstituted *in vitro*: after the initial incision mediated by RNase H2, Pol ε or, less efficiently, Pol δ perform strand displacement synthesis and create a flap structure harbouring the rNMP. This flap subsequently gets removed by the flap endonuclease Rad27 (human FEN1) or by the exonuclease Exo1. Finally, the remaining single-stranded nick is sealed by DNA ligase (Sparks et al., 2012).

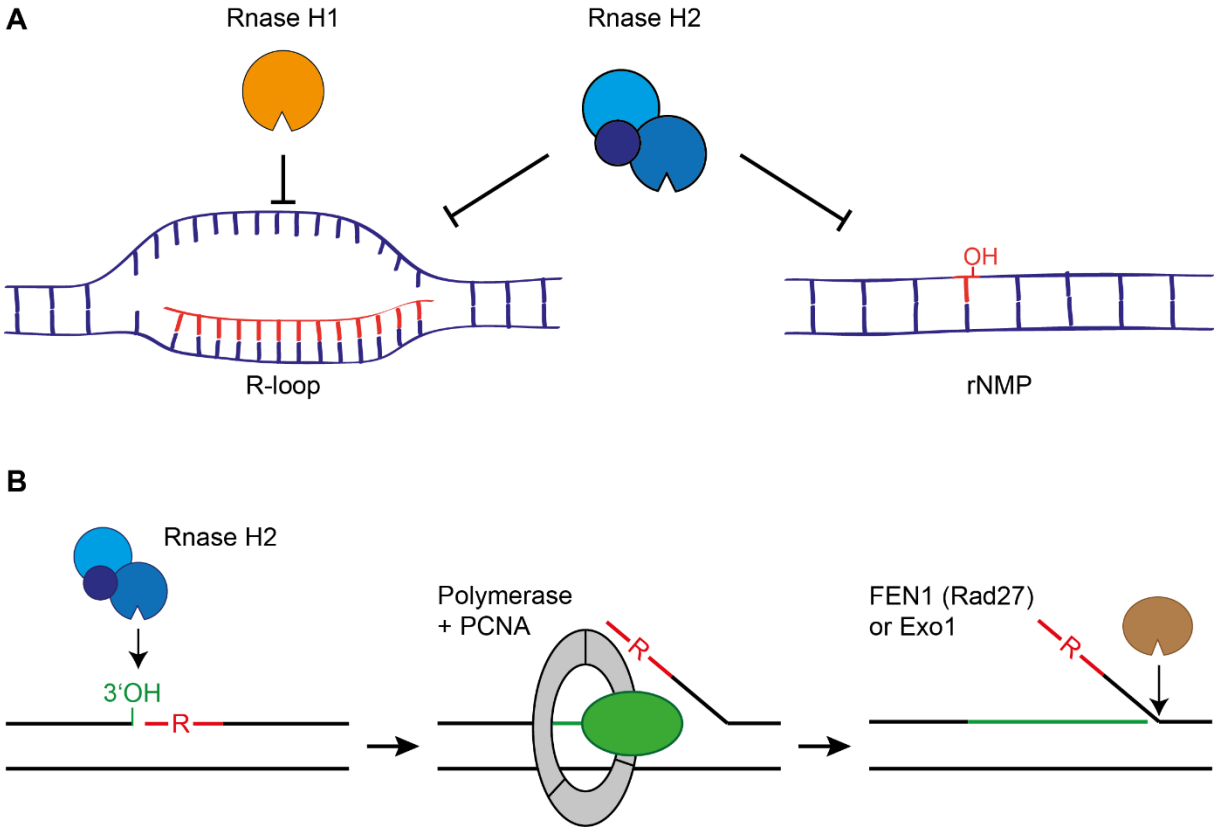

Figure 5. RNase H enzymes and ribonucleotide excision repair (RER). (**A**) Monomeric RNase H1 recognizes R-loops and stretches of at least four consecutive rNMPs. The heterotrimeric RNase H2 enzyme can degrade the RNA moiety of an R-loop and can excise single misincorporated rNMPs from genomic DNA. (**B**) To remove rNMPs from DNA, RNase H2 incises 5' of the rNMP. The resulting free 3'OH end can be extended by DNA polymerase δ or ε via strand displacement synthesis. The displaced strand containing the rNMP is then removed by the flap endonuclease Rad27 or by Exo1 and the remaining nick sealed by DNA ligase.

Human RNase H2 contains a PCNA-interacting protein (PIP) box which might direct the enzyme to sites of DNA replication (Bubeck et al., 2011). In the yeast Rnh202 subunit, the same motif is found but its importance remains to be clarified (Chon et al., 2013). To note, RNase H2 is involved in a backup pathway to remove Okazaki primers on the lagging strand (Qiu et al., 1999), although Rad27 and Dna2 are performing the majority of RNA primer removal (reviewed in (Zheng and Shen, 2011)).

In prokaryotes, it has recently been suggested that nucleotide excision repair (NER) can provide a backup pathway when RER is defective (Cai et al., 2014; Vaisman et al., 2013). However, in human cells NER proved to be inefficient to substitute for a loss of RNase H2 (Lindsey-Boltz et al., 2015). Genetic studies in yeast also exclude NER as a potent backup mechanism in the absence of RER (Lazzaro et al., 2012), thus suggesting that in eukaryotes other backup mechanisms might have evolved.

Even before the RER mechanism was unravelled, an *in vitro* study showed that Top1 can process an rNMP-containing DNA substrate (Sekiguchi and Shuman, 1997). The tyrosine residue of Top1 can form a covalent intermediate via a transesterification reaction with the 3' end of the rNMP. This bond is subsequently attacked by the adjacent 2'OH of the ribose moiety which results in a DNA nick that is flanked by an unligatable 2',3'-cyclic phosphate and a free 5'OH end (Sekiguchi and Shuman, 1997). More than 15 years later this Top1-dependent mechanism was described to remove rNMPs from DNA *in vivo* and thus to represent an important backup mechanism in RER-defective cells (Williams et al., 2013) (Figure 6). Being specific for rNMPs incorporated by the leading strand DNA polymerase, Top1 creates a nick that can subsequently be repaired by different means (Cho et al., 2015; Williams et al., 2013, 2015). Top1 can initiate a second cut on a dNMP 2 bp upstream of the initial cut leading to the release of the rNMP-dNMP dinucleotide (Sparks and Burgers, 2015). In this case, Top1 remains covalently bound to the DNA. The resulting Top1cc is proteolytically processed by Tdp1, leaving a 2 nt gap that can be repaired in an error-free manner. As an alternative to this Tdp1-dependent pathway, Top1 can also realign the DNA backbone and ligate the nick (Huang et al., 2015; Sparks and Burgers, 2015). If this happens within repetitive DNA sequences, ligation by Top1 leads to characteristic slippage mutations consisting of 2-5 bp deletions (Δ2-5 bp) (Kim et al., 2011; Nick McElhinny et al., 2010b). Srs2 together with Exo1 reduces the risk of acquiring those slippage mutations by processing the 5'OH end created by the initial

Top1 cleavage (Potenski et al., 2014). The 3'-5' helicase activity of Srs2 unwinds the DNA from this free end, followed by flap processing by Exo1. This results in a single-stranded DNA gap that can be repaired via an error-free gap repair pathway. Alternatively, a second Top1-mediated cut on the DNA strand opposing the rNMP leads to the creation of DSBs and employs Rad51/Rad52-dependent HR (Huang et al., 2016).

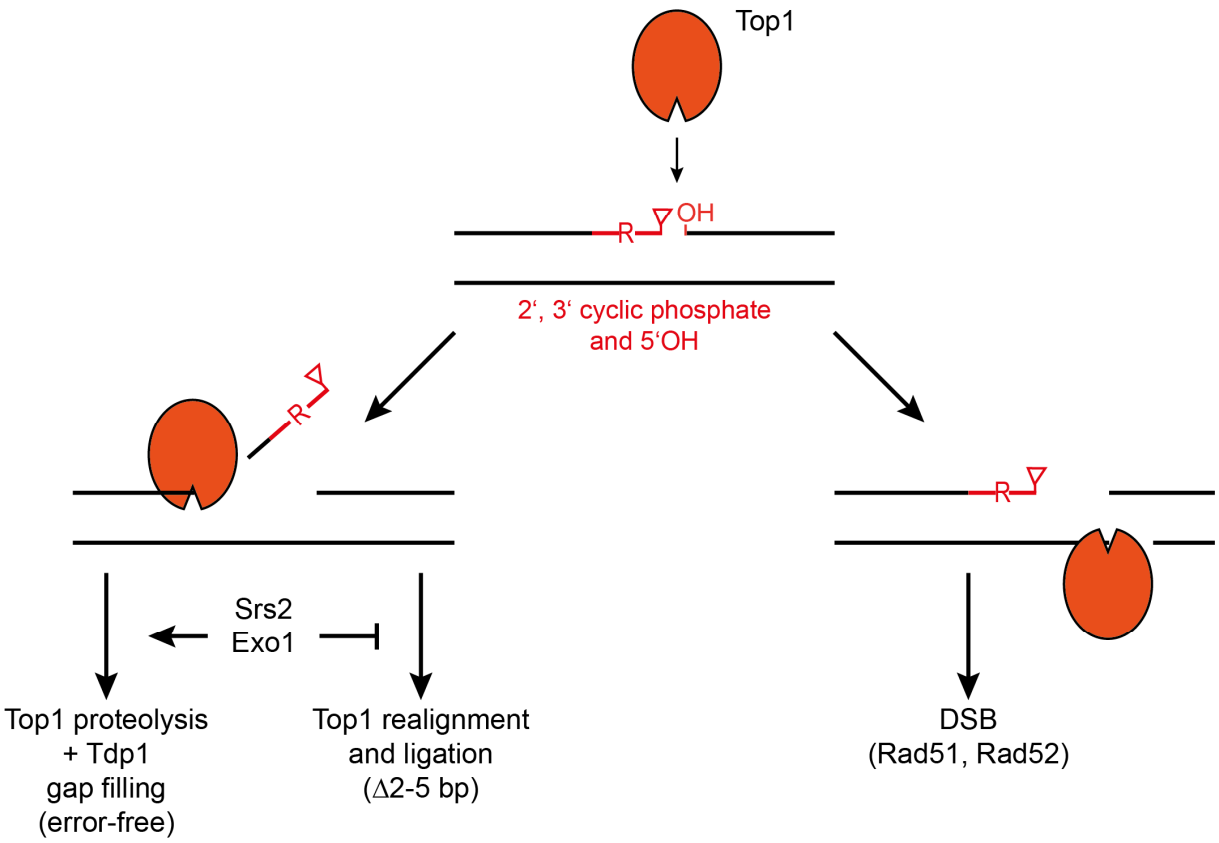

Figure 6. Top1-dependent rNMP removal. Top1 can incise 3' of an rNMP. The resulting 2', 3' cyclic phosphate and 5'OH cannot be re-ligated and cannot be used for strand displacement synthesis. Top1 can make a second cut 2 nucleotides upstream of the initial cut to release a dinucleotide containing the rNMP. At this point, the covalently bound Top1 (Top1 cleavage complex, Top1cc) can either be processed by proteolysis followed by removal of the remaining peptide by Tdp1. In this case, a gap will remain that can be filled in an error-free manner. Top1 can also realign the two ends of the 2 nt gap and ligate them. This results in 2-5 bp slippage mutations. Srs2 and Exo1 can prevent relegation by displacement and flap removal of the 5'OH end, thereby promoting gap repair. Alternatively, Top1 can make a second cut on the strand opposite of the nicked rNMP. This results in DSBs that have to be repaired by HR and require Rad51 and Rad52.

It remains unclear whether a similar, Top1-mediated, ribonucleotide excision repair also exists in mammalian cells. Intriguingly, the lethality of *rnh1Δ rnh201Δ top1Δ* cells can be rescued with the *RNH201-RED* allele (Chon et al., 2013), suggesting that rNMPs are still tolerated in the genome when both RER and Top1-dependent repair are lacking. Thus, a yet unknown backup pathway might exist.

1.5.3 Impact of misincorporated ribonucleotides on genome stability

As described above (section 1.5.1), loss of RNase H2 induces replication stress in both mammalian and yeast cells. Especially in yeast, genome stability is highly compromised when RER is defective. In the absence of RNase H2, spontaneous mutation rates and gene conversion events are increased (Ii et al., 2011; Potenski et al., 2014). Moreover, rNMP-dependent gross chromosomal rearrangements (GCRs) are observed when HR-mediated repair is compromised (Allen-Soltero et al., 2014). The most prominent type of genome instability in cells that lack RNase H2 is given by short deletions in dinucleotide repeat sequences, mostly between 2 and 5 bp in length (Chen et al., 2000; Nick McElhinny et al., 2010b). These ∆2-5 bp slippage mutations are a consequence of accumulating rNMPs but not of increased R-loop formation (Chon et al., 2013; Williams et al., 2017). Intriguingly, *TOP1* deletion completely suppresses the ∆2-5 bp slippage mutations, which are attributed to faulty Top1-dependent alignment and ligation (Kim et al., 2011; Williams et al., 2017). Mutation rates are similarly Top1-dependent (Potenski et al., 2014). In RER-defective diploid cells, both nonallelic HR and loss of heterozygosity (LOH) events increase in a Top1-dependent manner (Conover et al., 2015).

Conclusively, in *S. cerevisiae* the processing of rNMPs by Top1 in the absence of RER leads to genome instability most likely through aberrant processing of repair intermediates rather than through the misincorporated rNMP *per se*. As mentioned above, there is no evidence for a Top1-dependent repair of rNMPs in human cells yet. However, genome instability due to unrepaired rNMPs is observed in mammalian cells as large scale chromosomal rearrangements and the formation of micronuclei (Reijns et al., 2012).

1.5.4 Implications on human health and disease

Single missense mutations in either of the three human RNase H2 genes, RNASEH2A, RNASEH2B and RNASEH2C, are found in a majority of patients suffering from the early childhood autoinflammatory disorder Aicardi-Goutières syndrome (AGS) (Crow et al., 2006; Rice et al., 2007). AGS is an autosomal recessive genetic disease that manifests with severe neurological dysfunction (reviewed in (Crow and Manel, 2015)). Modelling of AGS-associated mutations in budding yeast shows that mutations in any of the subunits do not affect formation of the trimeric complex, and only a mutation in the catalytic subunit (RNASEH2A-G37S and *RNH201-G42S* in human and yeast, respectively) reduces enzymatic activity compared to wildtype (Crow et al., 2006; Perrino et al., 2009; Rohman et al., 2008). Intriguingly, AGS mutations have an impact on localization of the RNase H2 complex: in human control cells, RNase H2 is recruited to sites of DNA replication and PCNA-dependent repair, while in cells expressing one of the AGS-associated mutant subunits this recruitment is impaired (Kind et al., 2014). An altered repair efficiency might therefore be the underlying cause of replication stress and increased genome instability in AGS patient cells (Pizzi et al., 2015). Interestingly, AGS shares common features with the autoimmune disease systemic lupus erythematosus (SLE). Indeed, several mutations throughout all RNase H2 subunits lead to accumulation of rNMPs in genomic DNA of SLE patient cells and correlate with a constitutive upregulation of interferon-stimulated genes (Günther et al., 2015). Thus, RNase H2 and DNA damage-associated pathways are implicated in the initiation of autoimmunity. Work in AGS mouse models identified the responsible pathway for the inflammatory response: the immune sensor cyclic GMP-AMP synthase (cGAS) with the adaptor protein stimulator of interferon genes (STING) (Mackenzie et al., 2016; Pokatayev et al., 2016). This immune sensor recognizes free DNA in the cytoplasm derived from pathogens, endogenous retroviral elements, mitochondrial DNA or chromatinized nuclear DNA and elicits an innate immune response upon binding to cytoplasmic DNA (reviewed in (Dhanwani et al., 2018)). Indeed, both RNase H2 knockout cells and AGS mouse model cells accumulate micronuclei which colocalize with cGAS. Upon breakdown of the nuclear envelope encompassing the micronucleus, cGAS-STING-mediated signalling induces the expression of interferon-stimulated genes (Bartsch et al., 2017; MacKenzie et al., 2017).

Besides underlying the pathogeny of AGS, an increased accumulation of rNMPs can further contribute to the neurological disease ataxia with oculomotor apraxia 1 (AOA1) (Tumbale et al., 2014). Mutations in the aprataxin-coding gene APTX lead to reduced 'proofreading' for abortive ligation products that can impact DNA replication processes. Since these bulky adducts also form at misincorporated rNMPs, they connect the formation of toxic intermediates formed by RER with a neurological disorder, AOA1 (reviewed in (Williams and Kunkel, 2014)).

1.6 Scope of this thesis

DNA replication and especially the response to DNA replication stress is regulated by posttranslational modifications such as ubiquitylation. The cullin family of E3 ubiquitin ligases is conserved from yeast to man and regulates many important steps of cell cycle progression, DNA replication and DNA repair. The yeast cullin Rtt101 is required for faithful DNA replication through damaged templates (Luke et al., 2006). In the absence of Rtt101 cells are highly sensitive to drugs that cause replicative DNA damage, such as MMS or CPT (Chang et al., 2002; Hryciw et al., 2001; Luke et al., 2006). Although some insight into a potential mechanism of how Rtt101 ensures genome integrity has been gained by the identification of some of its targets (Ben-Aroya et al., 2010; Han et al., 2010, 2013), a comprehensive model implementing all of those discoveries is still lacking.

We have previously performed an SGA approach to identify suppressors of the MMS and CPT sensitivities of *rtt101Δ* cells (Buser et al., 2016). Among the identified candidates, *MRC1* was the only gene that when deleted in *rtt101Δ* cells conferred resistance to both drugs tested. Moreover, *MRC1* was the strongest candidate in the rescue of MMS sensitivity. In this thesis we aim to dissect how *MRC1* deletion alleviates MMS sensitivity.

One of the most frequent endogenous obstacles for DNA replication are RNA-DNA hybrids, especially misincorporated ribonucleotides (rNMPs) (Clausen et al., 2013b; Lujan et al., 2013; Nick McElhinny et al., 2010a). In healthy cells, ribonucleotide excision repair (RER) mediated by RNase H2 prevents those rNMPs from becoming harmful by removing them from genomic DNA. At the same time, RNase H2 together with RNase H1 also resolves R-loops (reviewed in (Cerritelli and Crouch, 2009)),

another harmful endogenous structure threatening genome integrity. Since misregulation of RNase H2 is associated with Aicardi-Goutières syndrome (AGS), a severe genetic neurological disorder (Crow et al., 2006; Rice et al., 2007), in this thesis we further investigate a potential role of Rtt101 when RNase H2 is non-functional.

Finally, we aim to identify ubiquitylation targets of Rtt101 when cells face DNA replication stress. To this end, we use ubiquitin remnant profiling, an unbiased approach employing SILAC-based mass spectrometry (Xu et al., 2010). This method allows to identify ubiquitylated peptides and, by comparing wildtype and *rtt101Δ* cells, reveals candidate targets of Rtt101.

Results

2.1 Rtt101 is required to survive MMS-induced DNA damage

In *Saccharomyces cerevisiae*, the cullin-type E3 ubiquitin ligase Rtt101 has been shown to promote replication of damaged DNA templates (Luke et al., 2006; Zaidi et al., 2008) and loss of its subunits Rtt101, Mms1 or Mms22 renders cells highly sensitive to the Top1 poison CPT and the alkylating agent MMS (Chang et al., 2002; Luke et al., 2006). A synthetic genetic growth array (SGA) performed in our laboratory as part of my master thesis identified the replication checkpoint gene *MRC1* as a suppressor of both the CPT and MMS sensitivity of *rtt101Δ* cells (master thesis (Kellner, 2014) and published in (Buser et al., 2016)).

2.1.1 Loss of Mrc1 suppresses MMS sensitivity of cells lacking a functional Rtt101 E3 ubiquitin ligase

We corroborated the result of the SGA screen by manually crossing an independent *rtt101Δ* strain to a strain deleted for *MRC1.* Upon sporulation of this diploid, manual tetrad dissection and spotting of the resulting haploid mutant strains on MMS-containing agar plates, confirmed the suppressive effect of *MRC1* deletion in the absence Rtt101 (Figure 7A). Rtt101 has been suggested to assemble a functional E3 ubiquitin ligase complex with the bridging protein Mms1 and the putative substrate adapter Mms22 (Zaidi et al., 2008) (Figure 1A). Therefore, we tested whether in cells lacking these complex members *MRC1* deletion could also restore viability in the presence of MMS. Indeed, in both *mms1Δ* and *mms22Δ* cells the loss of Mrc1 abolished or reduced sensitivity towards MMS, respectively (Figure 7B), indicating that the suppressive effect of *MRC1* deletion affects the Rtt101-Mms1-Mms22 E3 ligase ($Rtt101^{Mms22}$) rather than the Rtt101 subunit alone. Of note, while the MMS sensitivity of *mms1Δ* cells was comparable to that of *rtt101Δ* cells, deletion of *MMS22* rendered cells more sensitive to MMS. Moreover, the additional deletion of *MRC1* did only partially rescue the drug sensitivity of *mms22Δ* cells.

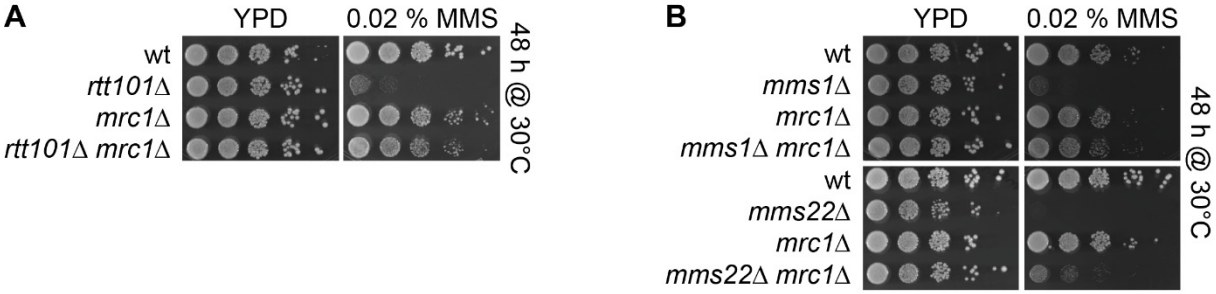

Figure 7. Deletion of *MRC1* rescues the MMS sensitivity of cells lacking the Rtt101^{Mms22} E3 ubiquitin ligase. (**A**) and (**B**) Haploid yeast strains of the indicated genotypes were grown overnight in liquid culture and the same number of cells was spotted in 10-fold serial dilutions onto YPD agar plates and YPD agar plates containing 0.02 % MMS. Images were taken after 48 hours of incubation at 30°C.

2.1.2 Mrc1 protein levels are not regulated by Rtt101 upon MMS-induced damage

Since ubiquitylation of target proteins frequently leads to their proteasomal degradation, Rtt101-mediated regulation of Mrc1 protein levels in the presence of DNA damage could be an explanation for how the loss of Mrc1 is improving viability of cells lacking Rtt101^{Mms22}. We therefore tested whether Mrc1 protein stability depends on Rtt101^{Mms22}. Mrc1 has been previously shown to be ubiquitylated both *in vitro* and *in vivo* by the SCF E3 ubiquitin ligase in complex with the F-box protein Dia2 (Mimura et al., 2009). Moreover, the strong MMS-sensitivity of *dia2Δ* cells could be reverted by deleting *MRC1,* and induced degradation of Mrc1 could rescue the defect of *dia2Δ* cells to recover from an MMS-induced S phase checkpoint arrest (Fong et al., 2013). Thus, we set out to analyse Mrc1 stability both in *rtt101Δ* cells and as a control also in *dia2Δ* cells. To this end, we integrated a galactose-inducible and hence glucose-repressible promoter into the endogenous *MRC1* locus to selectively induce or inhibit expression of Mrc1 tagged with an HA-epitope (pGal-3HA-Mrc1). Wildtype cells and *rtt101Δ* or *dia2Δ* mutants expressing 3HA-Mrc1 were synchronized in G1 by the addition of alpha factor mating pheromone (α-factor) in the presence of galactose (Figure 8A). The synchronized cultures were then released into S phase for 15 minutes to allow replication to initiate while still expressing 3HA-Mrc1, then damage was induced by the addition of 0.03 % MMS. Simultaneously, 3HA-Mrc1 expression was shut off by adding glucose. 3HA-Mrc1 protein levels were monitored over time by immunoblotting (Figure 8B) and band intensities were quantified and normalized to the

loading control, Pgk1 (Figure 8C). Consistent with published results, Mrc1 was partially stabilized in *dia2Δ* cells. The absence of Rtt101 however did not reveal any difference in Mrc1 stability as compared to wildtype cells, indicating that Rtt101 is not directly regulating Mrc1 protein levels in response to MMS-induced DNA damage. This result was further confirmed by cycloheximide chase experiments (our unpublished results and (Buser et al., 2016)) as well as by using a quantitative mass spectrometry approach (Buser et al., 2016).

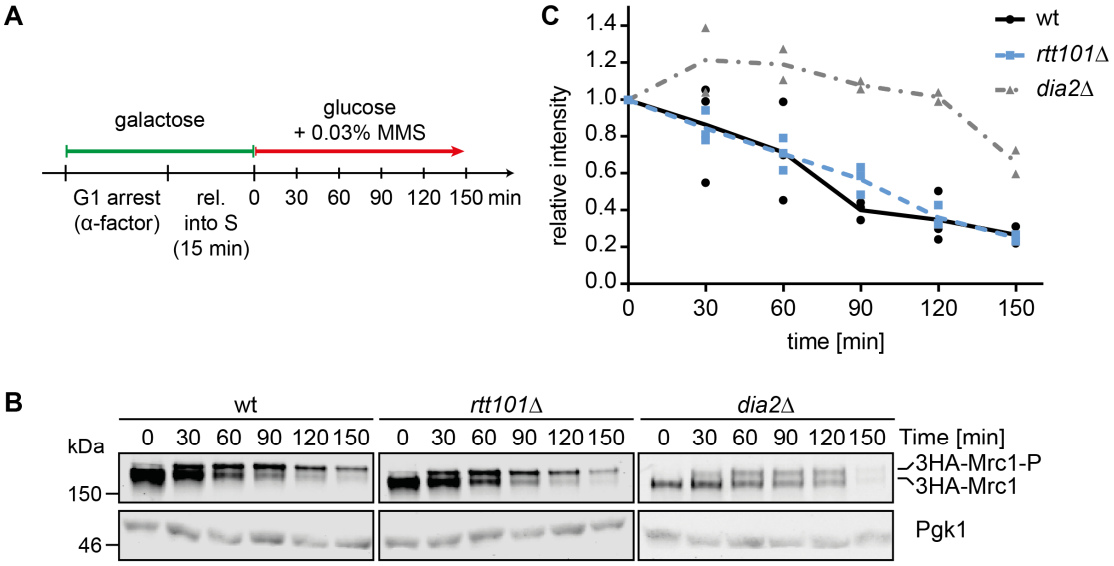

Figure 8. Rtt101 does not regulate Mrc1 protein levels upon MMS-induced DNA damage. (**A**) Scheme of the experimental setup. Wildtype, *rtt101*Δ and *dia2*Δ cells expressing 3HA-Mrc1 from the galactose-inducible promoter were grown to mid-log phase in YP medium containing 1 % raffinose (YPRaf) at 30°C, and subsequently arrested in G1 phase by the addition of 2 µM α-factor for 2 hours 30 minutes. During this time, expression of 3HA-Mrc1 was induced with 2 % galactose. After α-factor washout, cells were released into fresh YPRaf supplemented with 2 % galactose. After 15 minutes, transcription was inhibited, and damage was induced by the addition of 2 % glucose and 0.03 % MMS, respectively. Samples for protein extraction were taken at the indicated time points. (**B**) Protein lysates were prepared from the samples indicated in (**A**) and separated on a 7.5 % polyacrylamide gel followed by immunoblotting for 3HA-Mrc1 and Pgk1. Signals were detected by fluorescence. Representative blots are shown. (**C**) Quantification of band intensities in (**B**) from at least 2 independent experiments. The relative intensity of 3HA-Mrc1 bands was normalized to the band intensity of the corresponding Pgk1 band. The value at time point 0 minutes (t_0) is set to 1, every following time point is expressed relative to t_0.

2.1.3 Rtt101 counteracts a replicative function of Mrc1 to promote survival in the presence of MMS

As we were unable to detect Rtt101-mediated destabilization of Mrc1, we assumed that Rtt101 might rather modulate a specific function of Mrc1. The Rtt101^{Mms22} E3 ubiquitin ligase associates with active replisomes independent of DNA damage via an interaction between Mms22 and the replisome component Ctf4 (Buser et al., 2016). This observation strongly suggests that a regulation of Mrc1 might occur at the level of stalled or arrested replication forks caused by MMS.

We first addressed the possibility that deletion of *MRC1* confers a genetic rescue because it disrupts the fork pausing complex (FPC). This heterotrimeric complex consisting of Mrc1, Tof1, and Csm3, interacts with the replication machinery (Katou et al., 2003) and upon fork stalling prevents replisome uncoupling (Nedelcheva et al., 2005). Surprisingly, neither the deletion of *TOF1* or *CSM3* alone, nor the combinatorial deletion of both genes was able to suppress sensitivity of *rtt101Δ* cells to MMS (Figure 9A), suggesting that the function of Mrc1 in the context of the FPC is likely not to be regulated by Rtt101^{Mms22}. We confirmed these observations by repeating the experiment in an *mms22Δ* background (data not shown).

Mrc1 is further a central component of the S phase checkpoint: In response to replication stress caused by HU or MMS, Mec1-dependent phosphorylation of Mrc1 is required to activate Rad53 and consequently halt the cell cycle and inhibit late origin firing (Alcasabas et al., 2001). The simultaneous mutation of all 17 Mec1-dependent SQ and TQ consensus phosphorylation sites within Mrc1 results in a separation-of-function mutant, *mrc1$_{AQ}$*, that is unable to activate Rad53 in response to replication stress while maintaining normal S phase progression kinetics (Osborn and Elledge, 2003). We introduced this checkpoint-defective but replication-proficient *mrc1$_{AQ}$* allele into *rtt101Δ mrc1Δ* double mutant cells and analysed their resistance to MMS in a spotting assay (Figure 9B). Compared to *rtt101Δ mrc1Δ* cells transformed with the vector control (vc), expression of the *mrc1$_{AQ}$* allele resulted in highly increased sensitivity to MMS as seen for *rtt101Δ* cells (*rtt101Δ* + vc), indicating that the checkpoint function of Mrc1 is not causing toxicity in cells lacking Rtt101. Again, using *mms22Δ* cells instead of *rtt101Δ* cells resulted in the same observation (data not shown), emphasizing that the suppressive mechanism is common for the whole Rtt101^{Mms22} E3 ligase complex.

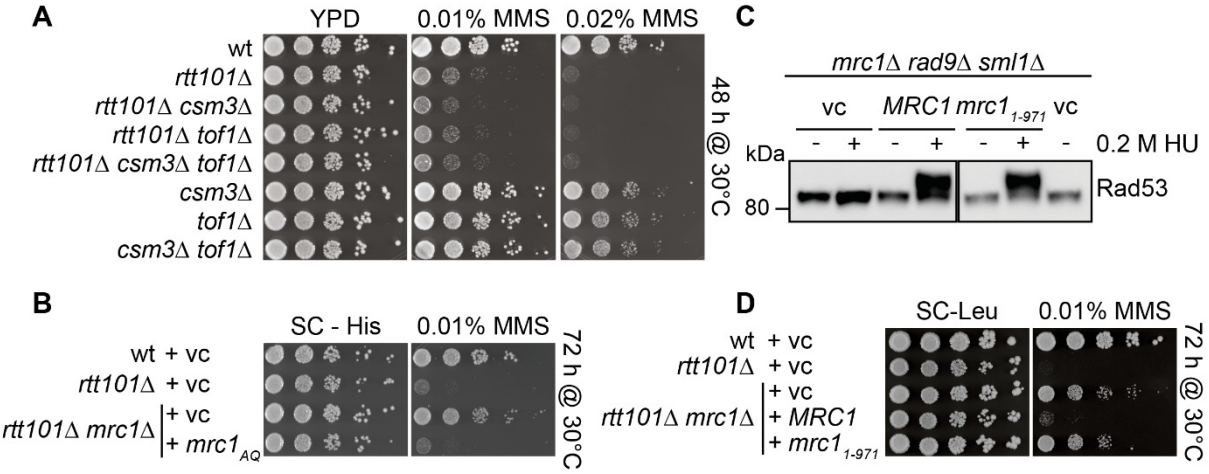

Figure 9. Loss of a replicative function of Mrc1 rescues the MMS sensitivity of *rtt101*Δ cells. (**A**) Haploid yeast strains of the indicated genotypes were grown overnight in liquid culture and the same number of cells was spotted in 10-fold serial dilutions onto YPD agar plates and YPD agar plates containing 0.01 % or 0.02 % MMS. Images were taken after 48 hours of incubation at 30°C. (**B**) Wildtype yeast, *rtt101*Δ and *rtt101*Δ *mrc1*Δ cells were transformed with the control plasmid (vc) or a plasmid expressing the checkpoint-defective $mrc1_{AQ}$ allele. The resulting strains were grown overnight in SC-His liquid medium and the same number of cells was spotted in 10-fold serial dilutions onto SC-His agar plates and SC-His agar plates containing 0.01 % MMS. Images were taken after 72 hours of incubation at 30°C. (**C**) *mrc1*Δ *rad9*Δ *sml1*Δ cells were transformed with the control plasmid (vc), a plasmid expressing wildtype *MRC1* or a plasmid expressing the C-terminal truncation mutant $mrc1_{1\text{-}971}$. The resulting strains were grown to mid-log phase in SC-Leu liquid medium at 30°C. The cultures were split in two and were either left untreated (-) or treated with 0.2 M HU (+) for 1 hour. Protein were extracted, and lysates were separated on a 7.5 % polyacrylamide gel and subjected to immunoblotting for Rad53 protein. Signal was detected using chemiluminescence. (**D**) Wildtype yeast, *rtt101*Δ and *rtt101*Δ *mrc1*Δ cells were transformed with the control plasmid (vc) or a plasmid expressing the C-terminally truncated $mrc1_{1\text{-}971}$ allele as indicated. The resulting strains were grown in SC-Leu liquid medium and spotted as described in (**B**) onto SD-Leu agar plates and SC-Leu agar plates containing 0.01 % MMS. Images were taken after 72 hours of incubation at 30°C.

To corroborate the result that suppression of the MMS sensitivity in *rtt101Δ* cells by deleting *MRC1* is independent of the S phase checkpoint, we employed a C-terminal truncation mutant of Mrc1, the $mrc1_{1\text{-}971}$ allele. This truncation mutant has been reported to be DNA replication-proficient, but upon MMS treatment was unable to activate Rad53 in a *rad9Δ* background (Fong et al., 2013). We first wanted to confirm the defect in replication checkpoint activation by monitoring HU-induced phosphorylation of Rad53 by immunoblotting (Figure 9C). Surprisingly, expressing the $mrc1_{1\text{-}971}$ allele in an *mrc1Δ rad9Δ sml1Δ* background resulted in Rad53 phosphorylation to a similar extent as in *mrc1Δ rad9Δ sml1Δ* cells expressing wildtype Mrc1 from a plasmid. This raises the possibility that the $mrc1_{1\text{-}971}$ allele is competent in

activating the S phase checkpoint and contradicts the observation reported by Fong and colleagues (Fong et al., 2013). Further support comes from the notion that a C-terminal truncation of Mrc1 retaining residues 1-820 or more can still activate Rad53 (Naylor et al., 2009).

Interestingly, when we introduced the *mrc1*$_{1-971}$ allele into *rtt101Δ mrc1Δ* cells, we found that expression of this truncation mutant could suppress the MMS sensitivity of *rtt101Δ* cells almost as well as the complete deletion of *MRC1* (Figure 9D), indicating that a function of Mrc1 residing in its C-terminal domain might be involved in the suppression of *rtt101Δ* MMS-sensitivity. Consistently, the MMS-sensitivity of *mms22Δ* cells could be rescued by expression of the *mrc1*$_{1-971}$ allele as the sole source of Mrc1 (data not shown). In line with this, the use of the *sld3-37A dbf4-4A* mutant that is genetically de-repressing late origin firing (Zegerman and Diffley, 2010) could not mimic the suppressive effect of *MRC1* deletion on MMS-sensitivity of *rtt101Δ* cells (Buser et al., 2016). This speaks against the hypothesis that late origin firing due to loss of a functional S phase checkpoint suppresses toxicity in *rtt101Δ* cells and furthermore argues against the S phase checkpoint as the cause of toxicity upon MMS treatment. In summary, we conclude that Rtt101^{Mms22} is required in the presence of MMS-induced DNA damage to counteract a replicative function of Mrc1 that most likely resides within its C-terminus.

2.1.4 The checkpoint recovery defect of *rtt101*△ cells is alleviated by *MRC1* deletion

Cells lacking Rtt101 are unable to recover from an MMS-induced DNA damage checkpoint arrest, but are proficient in recovering from replication stress due to HU treatment (Luke et al., 2006). To better understand the mechanism by which *MRC1* deletion restores viability of *rtt101Δ* and *mms22Δ* cells in the presence of MMS, we synchronized wildtype cells, *rtt101Δ* and *mms22Δ* single mutants or the *rtt101Δ mrc1Δ* and *mms22Δ mrc1Δ* double mutants in G1 using α-factor, and subsequently released them into medium containing 0.01 % MMS. After 60 minutes, the drug was quenched and washed out and cells were released into rich YPD medium. The recovery from the MMS-induced checkpoint arrest was monitored by immunoblotting of Rad53 (Figure 10A) and by flow cytometry to determine the cell cycle phase (Figure 10B). While *rtt101Δ* and *mms22Δ* single mutants were unable to dephosphorylate Rad53

after removal of the damage as previously reported (Duro et al., 2008; Luke et al., 2006; Zaidi et al., 2008), the concomitant deletion of *MRC1* allowed cells to deactivate the checkpoint within 4 hours of recovery (Figure 10A). Consistently, while *rtt101Δ* cells remained arrested with a G2/M DNA content, deletion of *MRC1* enabled *rtt101Δ* cells to re-enter the cell cycle as cultures started to accumulate a G1 peak within 4 hours of recovery (Figure 10B). The checkpoint recovery defect of cells lacking Rtt101^{Mms22} has been attributed to their inability to complete DNA replication upon DNA damage-induced replication fork arrest (Zaidi et al., 2008). Moreover, our results implicate that the presence of Mrc1 in those cells might be what prevents replication fork restart and completion of DNA replication.

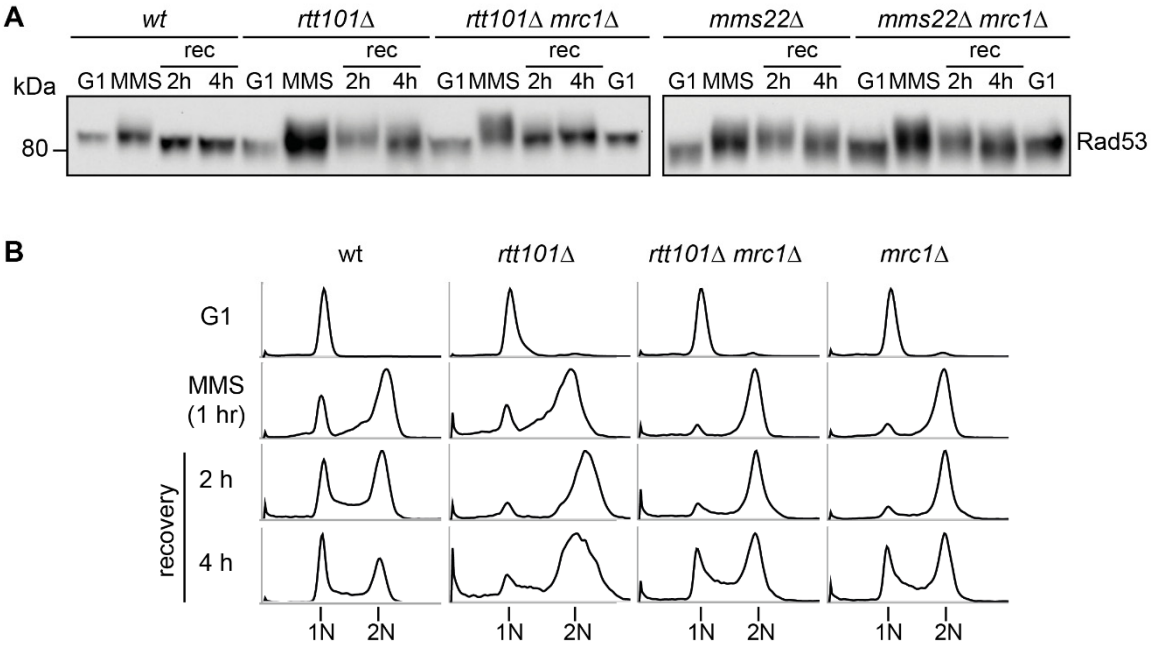

Figure 10. *MRC1* deletion allows *rtt101*Δ and *mms22*Δ cells to turn off the checkpoint during recovery from MMS-induced DNA damage. (**A**) Cells of the indicated genotypes were grown in YPD liquid medium to mid-log phase at 30°C and arrested in G1 phase with 2 µM α-factor for 2 hours 15 minutes. Arrested cells were then synchronously released into YPD containing 0.03 % MMS for 1 hour. MMS was quenched by the addition of 2.5 % sodium thiosulfate, cells were washed and released into fresh YPD medium. Samples for protein extraction (**A**) and flow cytometry (**B**) were taken prior to release into MMS (G1), after MMS treatment (MMS) and after 2 and 4 hours of recovery in fresh YPD medium (2h and 4h rec). (**A**) Protein lysates were separated on 7.5 % polyacrylamide gels, subjected to immunoblotting and probed for Rad53 protein. Signals were detected using chemiluminescence. (**B**) DNA content of the cultures at the indicated time points was assessed by flow cytometry analysis after staining with Sytox® Green.

2.1.5 Rtt101 promotes recombination-mediated fork restart by counteracting Mrc1

It has become widely accepted that HR is playing a central role in the protection and restart of stalled replication forks (reviewed in (Costes and Lambert, 2013)). Moreover, Mms1 and Mms22 have been shown to be required for efficient HR in response to MMS-induced DNA damage, but not for HR to repair an induced DSB (Duro et al., 2008). In contrast, loss of Mrc1 increases HR as evident from both increased levels of Rad52 foci (Alabert et al., 2009) and from using an intrachromosomal recombination assay (Xu et al., 2004).

Taken together, this suggests that loss of Mrc1 in cells lacking a functional $Rtt101^{Mms22}$ E3 ubiquitin ligase might enable cells to restart stalled replication forks by a mechanism involving HR. To test this hypothesis, we deleted *RAD52*, the key player of all HR-dependent repair mechanisms (Bärtsch et al., 2000). Indeed, preventing global HR in the *rad52Δ* background resulted in abolishment of the suppressive effect that *MRC1* deletion showed in *rtt101Δ* cells (Figure 11A). We therefore set out to investigate the role of HR in this scenario in more detail. To this end, we expressed Rad52 fused to the mCherry fluorophore (Rad52-mCherry) in order to follow HR by imaging the occurrence of Rad52-mCherry foci (Lisby et al., 2001). Wildtype or mutant cells expressing Rad52-mCherry from the endogenous promoter were synchronized in G1 using α-factor and subsequently released into 0.03 % MMS for 60 minutes. The formation of Rad52-mCherry foci was scored immediately by taking images of living cells with a fluorescence microscope and quantified by counting the number of cells that harboured at least one focus. In wildtype cells, MMS treatment resulted in a frequency of Rad52-mCherry foci formation of 27.0 ± 4.0 % (Figure 11B, 11C). Deletion of *RTT101* significantly decreased the formation of Rad52-mCherry foci to 13.5 ± 1.1 %. In the *rtt101Δ mrc1Δ* double mutant, the percentage of cells displaying Rad52-mCherry foci was comparable to wildtype levels, with 28.9 ± 2.3 % of cells showing Rad52-mCherry foci, suggesting that the absence of Mrc1 restored the HR capability of *rtt101Δ* cells. This was further confirmed in *mms22Δ* cells, where deletion of *MRC1* increased the formation of Rad52-mCherry foci from 20.0 ± 0.8 % to 26.9 ± 3.3 %. In summary, both the genetic data and the analysis of Rad52-mCherry foci formation strongly suggest that in cells lacking a functional $Rtt101^{Mms22}$ E3 ligase, loss of a replicative Mrc1 function upregulates HR and might thereby allow for efficient replication fork restart/repair.

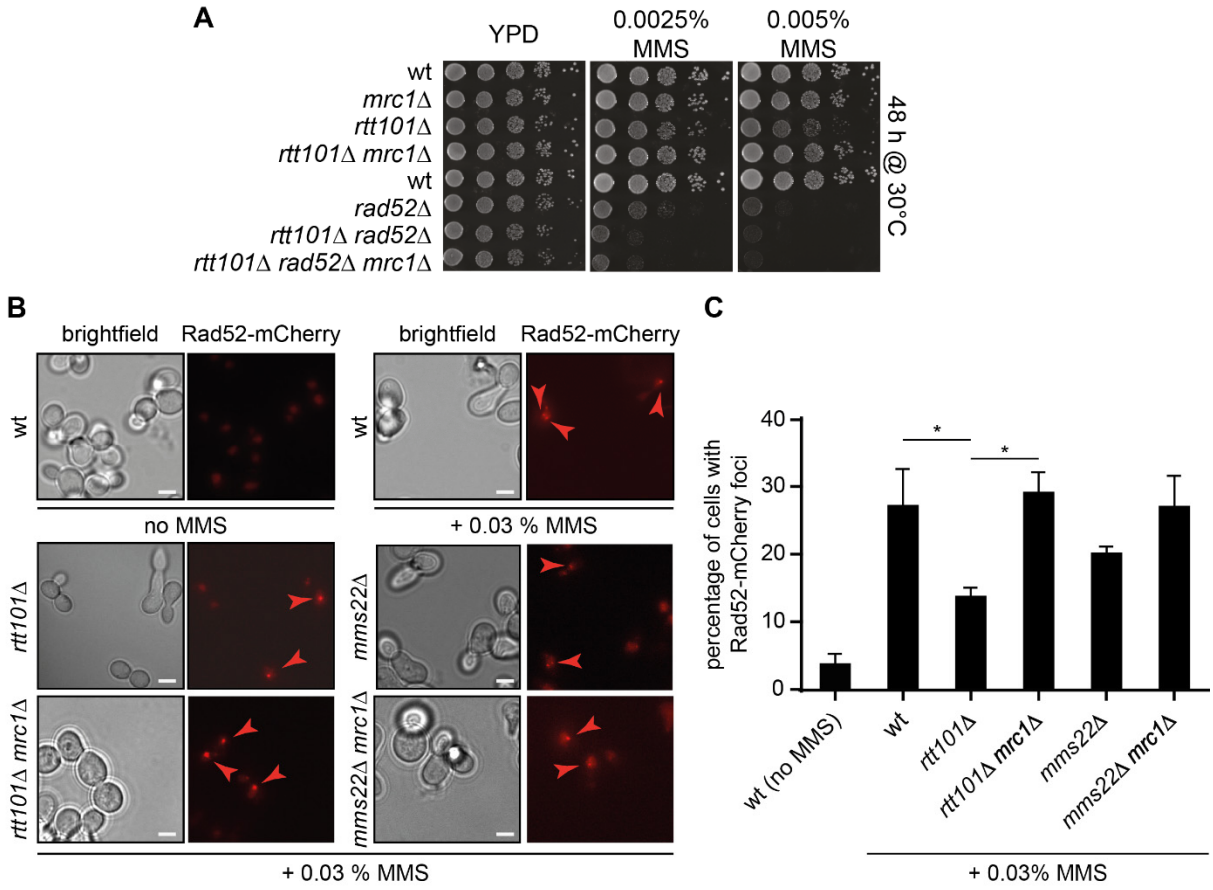

Figure 11. Rad52-mediated HR in *rtt101*Δ and *mms22*Δ cells is suppressed in the presence of Mrc1. (**A**) Haploid yeast strains of the indicated genotypes were grown overnight in YPD medium and the same number of cells was spotted in 10-fold serial dilutions onto YPD agar plates and YPD agar plates containing 0.0025 % or 0.005 % MMS. Images were taken after 48 hours of incubation at 30°C. (**B+C**) Strains of the indicated genotypes expressing Rad52-mCherry were grown to mid-log phase and arrested in G1 phase using 1 µM α-factor. Following a synchronous release into YPD medium containing 0.03 % MMS for one hour, cell aliquots were resuspended in SC-Trp liquid medium and imaged using a widefield microscope. (**B**) Exemplary images of MMS-treated cells from each genotype are shown. Red arrows indicate Rad52-mCherry foci. The scale bar is 5 µM. (**C**) Quantification of Rad52-mCherry foci. Two biological replicates per genotype were measured in independent experiments, and approximately 400 cells per replicate were counted. The mean percentage of cells with at least one Rad52-mCherry focus is displayed with error bars indicating standard deviation. *: $p < 0.05$ (one-way ANOVA analysis).

2.1.6 Genetic uncoupling of the CMG from DNA synthesis relieves MMS sensitivity of *rtt101Δ* cells

Within the replisome, Mrc1 interacts with both the N- and C-terminus of the DNA Polymerase ε subunit Pol2 (Lou et al., 2008). Moreover, the Mcm6 subunit of the CMG helicase physically interacts with Mrc1 via two critical residues of Mcm6, I973 and L974 (Komata et al., 2009). It is thus conceivable that Mrc1 might function in coupling DNA synthesis with DNA unwinding by the CMG helicase (Lou et al., 2008). Therefore, we wanted to address whether the disruption of the Mrc1-Mcm6 interaction might be sufficient to relieve the MMS toxicity in *rtt101Δ* cells. To this end, we made use of the *mcm6IL* allele, in which I973 and L974 are both mutated to alanine, thereby completely abolishing the interaction with Mrc1 (Komata et al., 2009). Expression of the *mcm6IL* point mutant in *rtt101Δ* cells allowed a partial suppression of the MMS sensitivity (Figure 12A). More importantly, the *mcm6IL* allele was epistatic with the deletion of *MRC1*, suggesting that the rescue mediated by *mcm6IL* and *mrc1Δ* is based on the same genetic pathway.

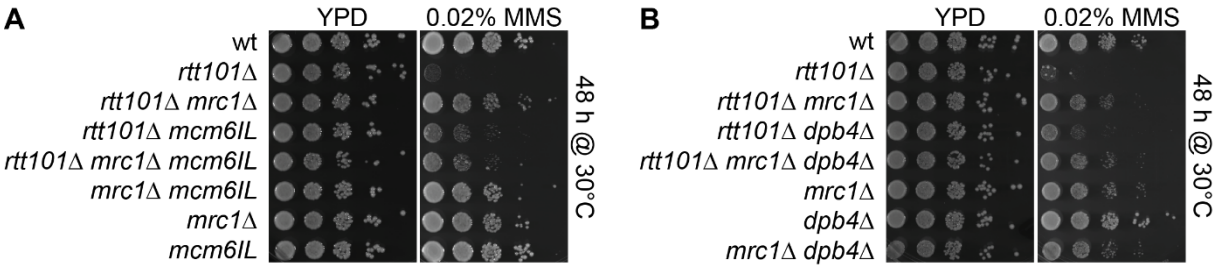

Figure 12. Deletion of *MRC1* is epistatic with altered interactions of replisome components when Rtt101 is absent. (**A**) and (**B**) Haploid yeast strains of the indicated genotypes were grown overnight in liquid culture and the same number of cells was spotted in 10-fold serial dilutions onto YPD agar plates and YPD agar plates containing 0.02 % MMS. Images were taken after 48 hours of incubation at 30°C.

Finally, we set out to test whether deletion of the only other identified suppressor of *rtt101Δ* MMS sensitivity in our SGA screen, *DPB4* (Buser et al., 2016), might also be epistatic with *mrc1Δ* in the rescue of *rtt101Δ* cells. Dpb4 is a component of DNA polymerase ε (Hamatake et al., 1990), which, although non-essential, is thought to stabilize the interaction of Pol ε with dsDNA to enhance its processivity and exonuclease activity (Aksenova et al., 2010). The initial SGA screen identified *DPB4* as a weak suppressor of *rtt101Δ* cells on MMS, a phenotype we could reproduce in a

spotting assay using haploid mutants coming from an independent diploid strain (Figure 12B). More importantly, the additional deletion of *DPB4* in the *rtt101Δ mrc1Δ* double mutant did not further increase the suppressive effect, suggesting that deletion of *DPB4* and *MRC1* is acting through the same pathway.

In summary, we could show that the genetic interference with replisome integrity by altering physical properties of replisome components is beneficial for *rtt101Δ* cells to survive MMS-induced DNA damage.

2.2 Rtt101 is required to survive accumulating genomic ribonucleotides

Cells lacking Rtt101 exhibit a slow growth phenotype even in the absence of exogenous damage (Michel et al., 2003). This implies that a naturally occurring structure in cells may compromise cell cycle progression in *rtt101Δ* cells. Ribonucleotide monophosphates (rNMPs) get incorporated into the genome at surprisingly high rates throughout each round of DNA replication (Nick McElhinny et al., 2010a) and are possibly the most abundant type of noncanonical nucleotides. Moreover, RNA-DNA hybrids caused by the re-annealing of a transcribed RNA with its respective complementary template DNA strand, a structure referred to as an R-loop, has been shown to impose a threat on genome stability and to create replication stress (reviewed in (Aguilera and García-Muse, 2012)). As both of these structures occur *in vivo* in the absence of exogenous DNA damage, we hypothesized that Rtt101 might be required for cell viability when these natural sources of replication stress accumulate.

2.2.1 Loss of Rtt101 is toxic for cells that accumulate genomic ribonucleotides

To investigate the importance of Rtt101 when RNA-DNA hybrids accumulate, we created a scenario in which the removal of both rNMPs and R-loops is impaired. To this end, we crossed a strain in which both RNase H enzymes were non-functional (*rnh1Δ rnh201Δ*) to a strain deleted for *RTT101* and assessed viability of the resulting *rtt101Δ rnh1Δ* and *rtt101Δ rnh201Δ* double mutants in comparison to the respective single mutants by performing a liquid culture growth assay in unchallenged conditions. Briefly, saturated cultures were diluted to a low density (OD_{600} of 0.01) and growth was monitored by measuring the OD_{600} of those cultures every hour. To our surprise, the slow growth phenotype of *rtt101Δ* cells was further slowed down when *RNH201* was deleted, but not in the absence of Rnh1, while the single RNase H mutants showed wildtype-like growth kinetics (Figure 13A). We further confirmed the genetic interaction between *RTT101* and genes encoding for the trimeric RNase H2 complex by investigating viability of *rtt101Δ rnh202Δ* cells on HU-containing plates (Figure 13B). While RNase H1 is mainly responsible for the removal of R-loops, RNase H2 is competent in removing both R-loops and genomic rNMPs (reviewed in (Cerritelli and Crouch, 2009)). To discriminate between the two functions of RNase H2 and address which of them affects viability in *rtt101Δ* cells, we first overexpressed *RNH1* in an

rtt101Δ rnh201Δ mutant in order to compensate for the loss of the R-loop removal function of RNase H2 (Huertas and Aguilera, 2003). However, this proved to be insufficient to rescue the HU sensitivity of those cells (Figure 13B), suggesting that an accumulation of R-loops is unlikely to be the cause of decreased viability and increased HU sensitivity of *rtt101Δ rnh201Δ* cells. We next employed the separation-of-function mutant *RNH201-P45D-Y219A* (or *RNH201-RED* for Ribonucleotide-Excision-Defective) that is specifically impaired in the rNMP removal function of RNase H2 (Chon et al., 2013). In contrast to the expression of wildtype *RNH201*, expression of the *RNH201-RED* allele did not restore HU resistance of *rtt101Δ rnh201Δ* cells (Figure 13C), strongly pointing towards unrepaired rNMPs as the main cause for the viability loss of cells lacking both Rtt101 and RNase H2.

s

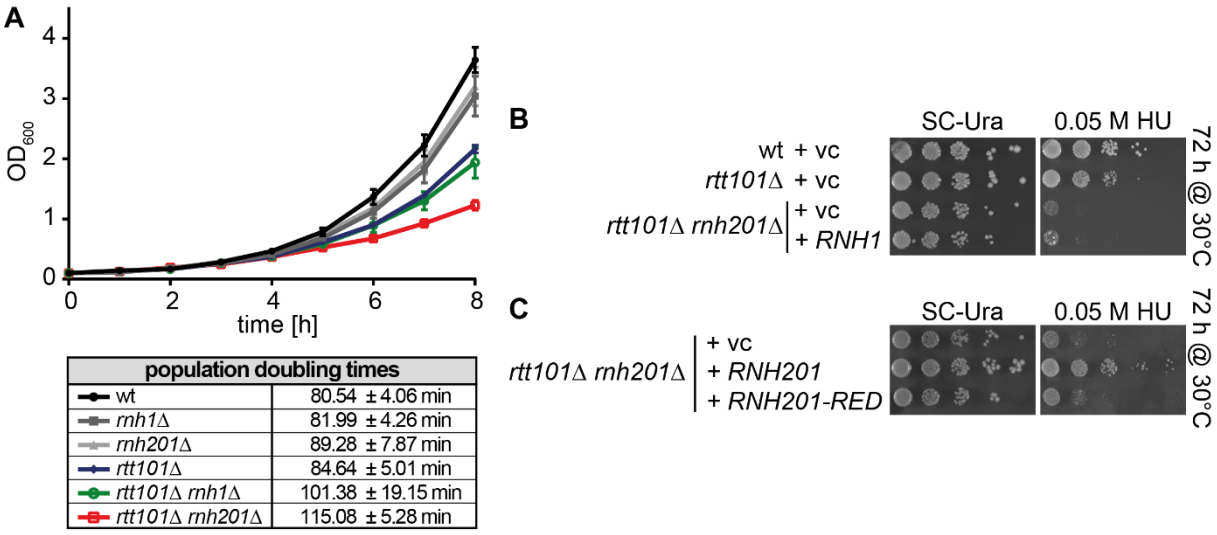

population doubling times	
wt	80.54 ± 4.06 min
rnh1Δ	81.99 ± 4.26 min
rnh201Δ	89.28 ± 7.87 min
rtt101Δ	84.64 ± 5.01 min
rtt101Δ rnh1Δ	101.38 ± 19.15 min
rtt101Δ rnh201Δ	115.08 ± 5.28 min

Figure 13. Rtt101 is important for cell viability when genomic ribonucleotides accumulate in the absence of RER. (**A**) Isogenic strains of the indicated genotypes were grown overnight in YPD medium and diluted to an OD_{600} of 0.1. Cell density was measured every hour and the mean of three biological replicates (n=3) was plotted with error bars indicating SEM. Doubling times shown in the table below were generated from the growth curve and are depicted as the mean of 3 replicates ± standard deviation. (**B**) Wildtype yeast, *rtt101Δ, rnh201Δ* and *rtt101Δ rnh201Δ* cells were transformed with the control plasmid (vc) or a plasmid constitutively overexpressing *RNH1* (**C**). Moreover, *rtt101Δ rnh201Δ* cells were transformed with the control plasmid (vc) or a plasmid expressing wildtype *RNH201* or the *RNH201-RED* allele. (**B+C**) The same number of cells was spotted in 10-fold serial dilutions onto SC-Ura agar plates and SC-Ura agar plates containing 0.05 M HU. Images were taken after 72 hours of incubation at 30°C. Strains used in (**B**) were generated and spotting was performed by Stefanie Grimm.

As *rtt101Δ rnh201Δ* cells displayed a reduced fitness already in the absence of any exogenous damage, we sought for an inducible system to deplete RNase H2 activity in a timely controlled manner. We chose the auxin-inducible system (Morawska and Ulrich, 2013) in which a C-terminally fused auxin-inducible degron (AID) allows rapid degradation of Rnh201 by adding the plant hormone auxin (indole-3-acetic acid, IAA) to the medium. Unlike deletion of *RNH201*, expression of AID*-tagged *RNH201* in the absence of IAA (Figure 14A) prevents MMS sensitivity in *rnh1Δ* cells (Arudchandran et al., 2000) confirming that the allele is functional. Upon addition of auxin, *rnh1Δ RNH201-AID** double mutants show decreased resistance to MMS (Figure 14B). Protein expression and auxin-induced degradation were confirmed in both wildtype and *rtt101Δ* cells (Figure 14C).

Through the inhibition of ribonucleotide reductase (RNR), HU directly affects the ratio between dNTPs and rNTPs in the cell; this in turn has implications on the fidelity of DNA polymerases (Watt et al., 2011) and might further increase the load of rNMPs incorporated into the genome (Reijns et al., 2012). To prove that an increased frequency of rNMP incorporation affects viability of *rtt101Δ* cells, we introduced the DNA polymerase ε mutant *pol2-M644G*. In this point mutant, a methionine adjacent to the steric gate tyrosine 645 decreases the ability of Pol ε to discriminate between dNTPs and rNTPs and thus, rNMPs are incorporated more frequently during replication than in wildtype cells (Nick McElhinny et al., 2010b). Notably, although this mutant alone did not have an effect on viability of *rtt101Δ* cells, the depletion of Rnh201-AID* strongly affected survival in *rtt101Δ pol2-M644G* cells even in the absence of HU (Figure 14D). This substantial negative genetic interaction could be completely reverted by the expression of wildtype *RNH201*, but not *RNH201-RED*.

In conclusion, we revealed an important role for Rtt101 when cells accumulate genomic ribonucleotides in the absence of RNase H2 activity.

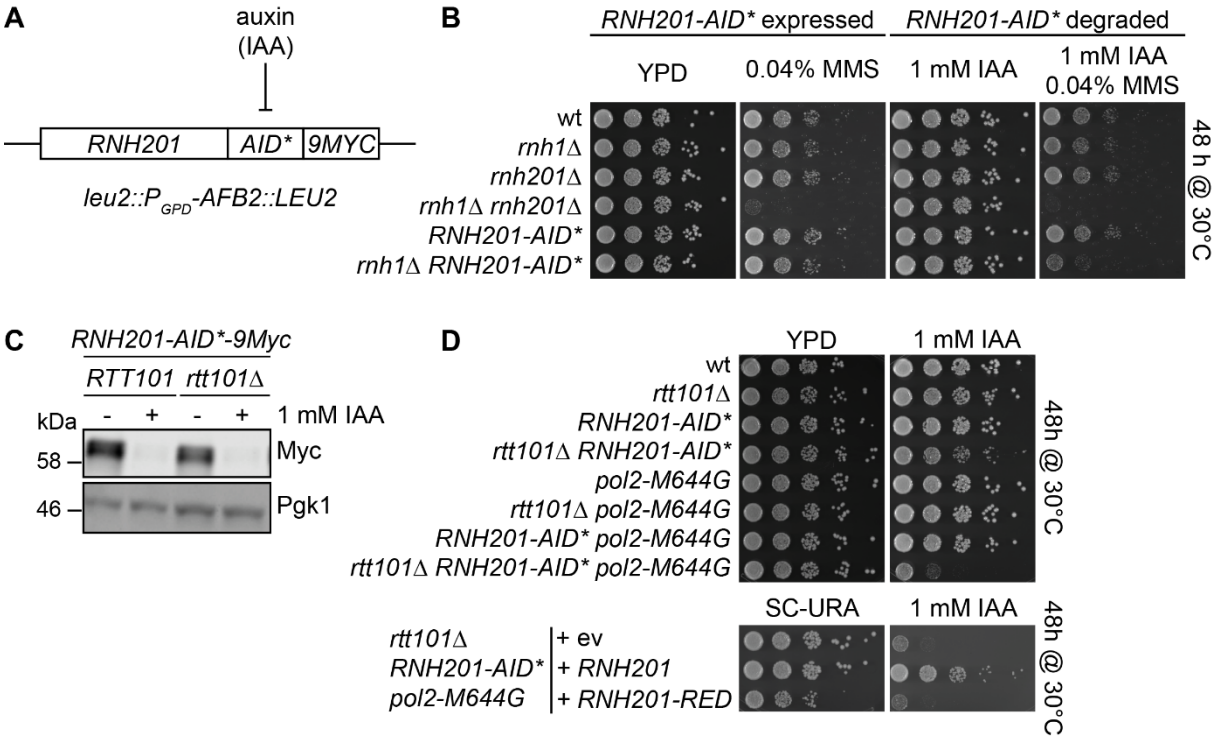

Figure 14. The auxin-inducible *RNH201-AID*-9MYC* degron is functional and renders *rtt101*Δ cells sensitive to an increased accumulation of genomic rNMPs. (**A**) Schematic view of the auxin-inducible degron (AID*)-tag. The *AID** sequence and a *9MYC* epitope tag were fused in frame to the 3' end of the *RNH201* gene. This allows for expression of the Rnh201-AID*-9Myc fusion protein in a strain expressing the *Arabidopsis thaliana* F-box protein AFB2 from the GPD promoter. After the addition of auxin (IAA), the protein is recognized by the F-box protein AFB2 and degraded by the 26S proteasome. (**B**) The function of the Rnh201-AID*-9Myc fusion protein was confirmed by spotting haploid yeast cells of the indicated genotypes on YPD plates and YPD plates containing 0.04 % MMS (*RNH201-AID*-9MYC* is expressed and should behave as wildtype *RNH201*) and on YPD agar plates containing 1 mM IAA or 1 mM IAA and 0.04 % MMS (*RNH201-AID*-9MYC* is degraded and should behave like *rnh201*Δ). Images were taken after 48 hours of incubation at 30°C. (**C**) *RNH201-AID*-9MYC* was expressed both in wildtype cells (*RTT101*) and in *rtt101*Δ cells. Cultures in mid-log phase were treated for one hour with 1 mM IAA, then cells were harvested for protein extraction. Subsequently, the protein lysates were separated on a 4-15 % polyacrylamide gradient gel and immunoblotted using antibodies detecting Myc-tagged species and Pgk1. (**D**) Haploid yeast strains of the indicated genotypes, or the *rtt101*Δ *RNH201-AID* pol2-M644G* mutant transformed with either control plasmid (vc) or expressing wildtype *RNH201* or the *RNH201-RED* allele were grown overnight in the appropriate liquid medium and the same number of cells was spotted in 10-fold serial dilutions onto the appropriate agar plates in the absence and presence of 1 mM IAA. Images were taken after 48 hours of incubation at 30°C.

Next, we investigated whether the functional Rtt101^{Mms22} E3 ubiquitin ligase is required when rNMPs accumulate genome wide in the absence of ribonucleotide excision repair (RER). To address this question, we crossed the *RNH201-AID* pol2-M644G* strain to *mms1Δ* and *mms22Δ* cells and assessed viability of the resulting haploid mutants in the presence of IAA (Figures 15A and 15B). In agreement with our results obtained in

the *rtt101Δ* mutant (Figure 14D), increasing the frequency of rNMP incorporation in *pol2-M644G* cells exacerbated the negative effect on viability observed upon concomitant loss of Rnh201 function and Mms1 or Mms22. In line with this observation, preventing the full activation of Rtt101 E3 ligase function using the Rtt101-K791R mutant that can neither be neddylated nor ubiquitylated (Rabut et al., 2011) significantly reduced HU resistance of *rtt101Δ rnh201Δ* cells when compared to the expression of wildtype *RTT101* in the same cells (Figure 15C). Taken together, the functional Rtt101-Mms1-Mms22 E3 ubiquitin ligase is required for viability when cells accumulate genomic ribonucleotides in the absence of RER.

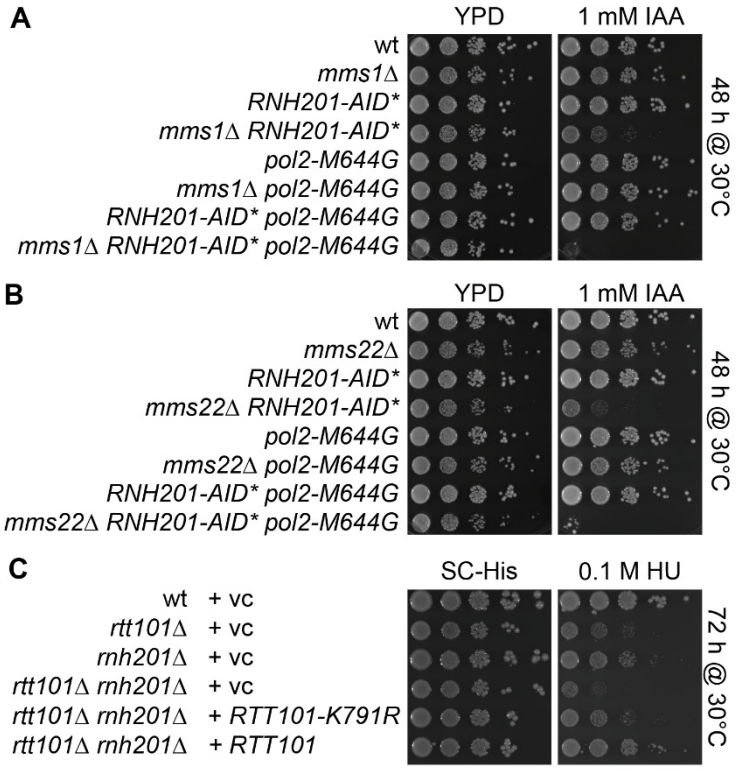

Figure 15. The functional Rtt101-Mms1-Mms22 E3 ligase is required for viability when genomic rNMPs accumulate. (**A+B**) Haploid yeast strains of the indicated genotypes were grown overnight in liquid culture and the same number of cells was spotted in 10-fold serial dilutions onto YPD agar plates and YPD agar plates containing 1 mM IAA. Images were taken after 48 hours of incubation at 30°C. (**C**) Wildtype yeast, *rtt101Δ, rnh201Δ* and *rtt101Δ rnh201Δ* cells were transformed with the control plasmid (vc) or a plasmid expressing wildtype *RTT101* or the neddylation-defective *RTT101-K791R* mutant. The same number of cells was spotted in 10-fold serial dilutions onto SC-His agar plates and SC-His agar plates containing 0.1 M HU. Images were taken after 72 hours of incubation at 30°C. Strains used in (**C**) were generated and spotting was performed by Stefanie Grimm.

2.2.2 Rtt101 is dispensable for efficient removal of genomic ribonucleotides

A first intriguing hypothesis would be that Rtt101^{Mms22} is directly involved in the removal of genomic rNMPs and that cells with a non-functional Rtt101 complex consequently accumulate more rNMPs than wildtype cells. The amount of incorporated ribonucleotides in the genome can be measured by alkaline hydrolysis. The Kunkel lab is frequently performing this type of analysis (Nick McElhinny et al., 2010a; Williams et al., 2015) and they kindly agreed to test our strains using this assay. Briefly, isolated genomic DNA was treated with the alkaline agent potassium hydroxide (0.3 M KOH). This leads to the creation of nicks at incorporated ribonucleotides since the 2'-OH of the ribose moiety is susceptive to hydrolysis while the sugar-phosphate backbone at dNMPs is not affected. Subsequent separation of the treated DNA on a denaturing alkaline gel allows comparison of the frequency of nicks and thus of the overall load of genomic rNMPs. In wildtype cells, the loss of RNase H2 generated more fragments with high mobility, indicative of more incorporated rNMPs (compare lanes 1 and 3, Figure 16A). The expression of *pol2-M644G* further increased the mobility of DNA fragments (lane 4), consistent with an increase in the frequency of rNMP incorporation in this mutant. Loss of *MMS22* (lanes 5-8) or *RTT101* (lanes 9-12), respectively, did not result in a further increase of alkali-sensitive sites in these genetic backgrounds.

Consistent with DNA Pol ε being the major DNA polymerase to replicate the leading strand (Pursell et al., 2007), the *pol2-M644G* mutant accumulates rNMPs especially in the leading strand (Williams et al., 2015). However, RNase H2-mediated RER has been shown to act on both the leading and the lagging strand (Williams et al., 2015). In order to discriminate between rNMPs incorporated into the leading versus the lagging strand, the DNA separated on the alkaline gel was transferred to a nylon membrane. Subsequently, strand-specific radiolabelled probes detecting the *AGP1* gene locus on chromosome III allowed specific analysis of either leading strand or lagging strand DNA (Figure 16B). Comparisons of lanes 1, 5 and 9 shows that in RER-proficient cells, the loss of Rtt101 or Mms22 does not increase the amount of alkali-sensitive sites as observed upon loss of Rnh201 (compare lanes 1 and 3). In line with that, deletion of *RNH201* and/or introducing the *pol2-M644G* mutant in *mms22Δ* (lanes 7 and 8) or *rtt101Δ* cells (lanes 11 and 12) resulted in a fragment distribution similar to *MMS22* and *RTT101* cells (lanes 3 and 4). In summary, the loss of Rtt101^{Mms22} is not causing toxicity in RER-defective cells by further increasing the load of genomic rNMPs.

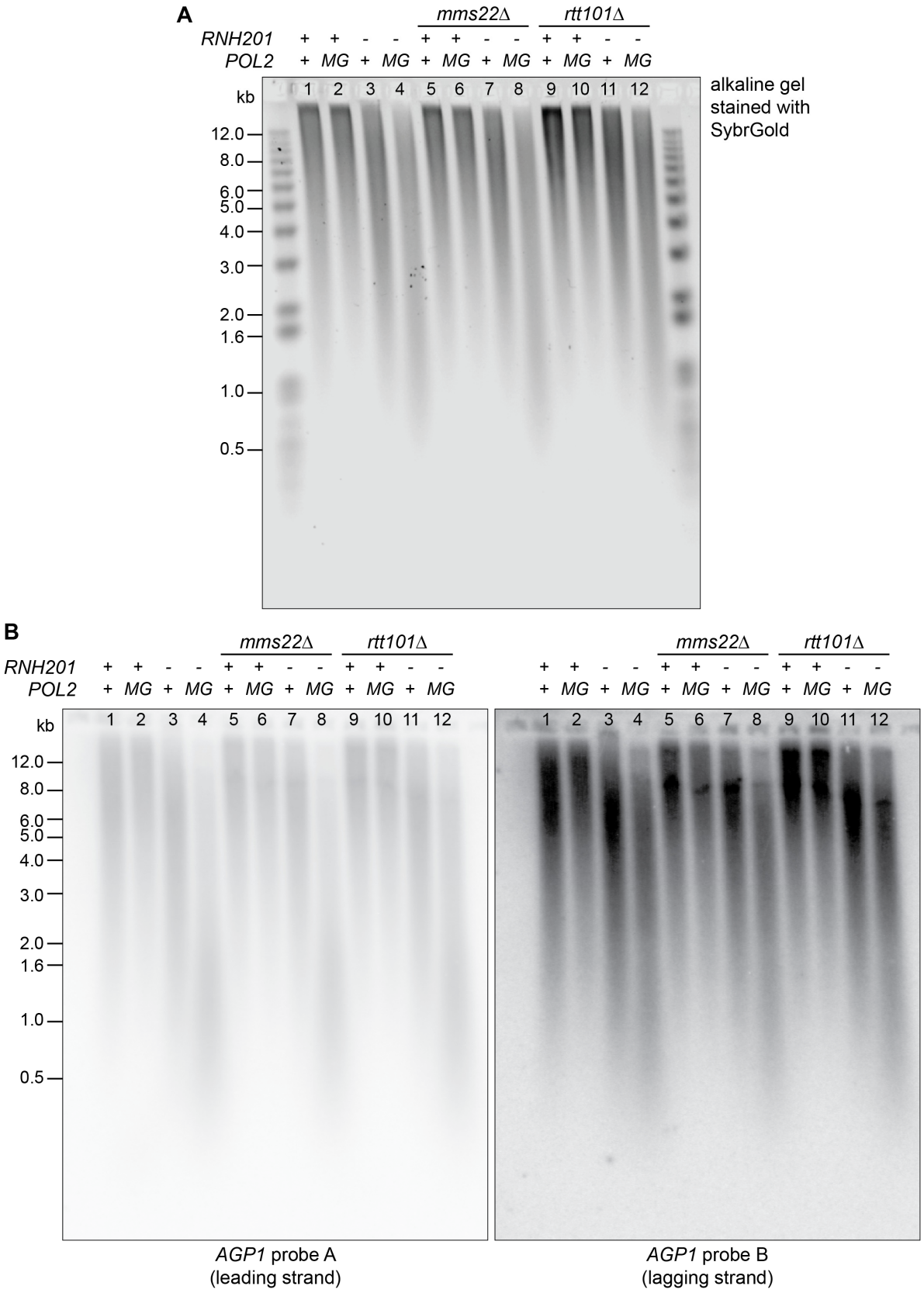

Figure 16. Loss of Rtt101^{Mms22} does not further increase the load of genomic rNMPs in RER-defective cells. *Figure legend: see next page.*

Figure 16. Loss of Rtt101^{Mms22} does not further increase the load of genomic rNMPs in RER-defective cells. (**A**) Genomic DNA was extracted from wildtype, *rtt101*Δ or *mms22*Δ cells either expressing *RNH201* (*RNH201* +) or with an *RNH201* deletion (*RNH201* -) and expressing either wildtype *POL2* (*POL2* +) or the *pol2-M644G* mutant (*POL2 MG*). 5 µg DNA was treated with 0.3 M KOH and alkaline-agarose gel electrophoresis was performed. After neutralization of the gel, the DNA was stained with SyBr Gold and imaged. (**B**) The gel shown in (**A**) was subjected to Southern blotting and the DNA was detected with radioactively labelled probes recognizing the *AGP1* locus in a strand-specific manner (probe A – leading strand, probe B – lagging strand). Experiments shown in (**A**) and (**B**) were performed and data was provided by Jessica Williams (Thomas Kunkel lab). Strains were generated by Vanessa Kellner.

2.2.3 Rtt101 is not required to deal with Top1-mediated damage

In the absence of RNase H2-mediated RER, genomic rNMPs can also be excised by Top1 (Sekiguchi and Shuman, 1997; Williams et al., 2013). However, this Top1-mediated removal of leading strand rNMPs (Williams et al., 2015) is error-prone and associated with deletions of 2-5 bp, DSBs and generally high mutation rates (Huang et al., 2017, 2016; Potenski et al., 2014; Williams et al., 2013). In most of the studies, the aforementioned defects could be completely reverted by the deletion of *TOP1*. We speculated that Rtt101^{Mms22} might regulate this Top1-dependent branch of RER and that loss of the E3 ligase might increase the load of Top1-mediated damage. If this was true, deletion of *TOP1* should greatly improve the viability of rNMP-accumulating strains that lack Rtt101. To our surprise, loss of Top1 did not have any effect on the viability of rNMP-accumulating strains when Rtt101^{Mms22} function was compromised in the absence of *RTT101* (Figure 17A), *MMS1* (Figure 17B) or *MMS22* (Figure 17C). This suggests that Rtt101^{Mms22} is not directly involved in the removal of genomic rNMPs but might instead be required to tolerate rNMPs that remain.

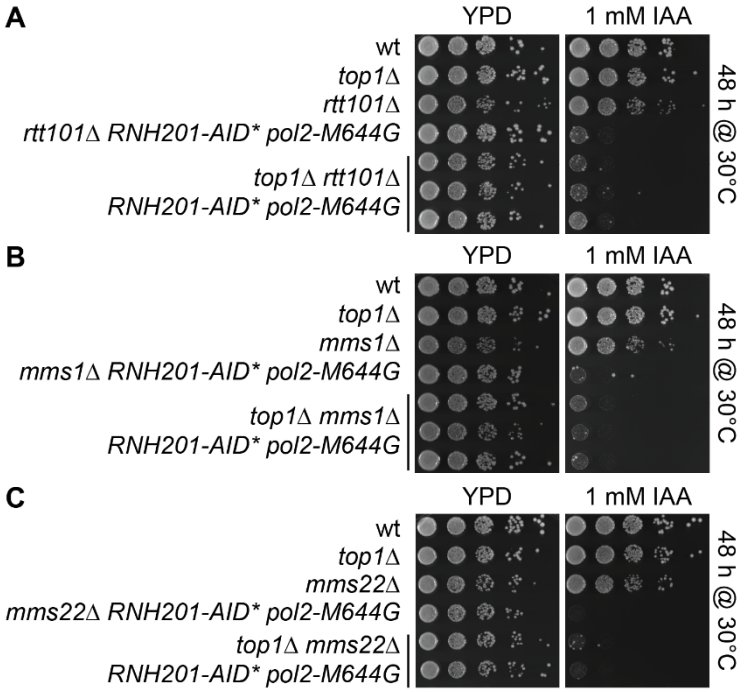

Figure 17. Toxicity in RER-defective cells lacking Rtt101^{Mms22} is not caused by Top1-dependent processing of rNMPs. (**A-C**) Haploid yeast strains of the indicated genotypes were grown overnight in liquid culture and the same number of cells was spotted in 10-fold serial dilutions onto YPD agar plates and YPD agar plates containing 1 mM IAA. Images were taken after 48 hours of incubation at 30°C.

2.2.4 *RAD51*-dependent HR is not epistatic with *RTT101* and *MRC1* deletion suppresses toxicity caused by accumulated genomic rNMPs

We previously proposed a model in which Rtt101^{Mms22} counteracts Mrc1 function in response to MMS-induced replication fork stalling to allow HR-mediated replication fork restart. HR has further been shown to be vital for cells in the absence of RNase H2: *rad52Δ rnh201Δ pol2-M644G* cells are inviable, while *rad51Δ rnh201Δ pol2-M644G* cells exhibit a highly reduced fitness (Huang et al., 2017). This strong need for HR can be offset by deleting *TOP1*. In our hands, the requirement for the Rtt101^{Mms22} E3 ligase did not depend on the presence of Top1. We thus analysed the importance of HR in *rtt101Δ* cells that are RER-defective by deleting *RAD51*. Consistent with the observations of Huang and colleagues, *rad51Δ RNH201-AID** cells showed a moderately decreased viability compared to either of the single mutants, most likely through the incapability to deal with Top1-mediated DSBs (Huang et al., 2017). The combined loss of Rad51 and Rtt101 in *RNH201-AID** cells was additive (Figure 18A), suggesting that Rtt101 functions in a pathway different from the Rad51-dependent

pathway to repair Top1-mediated DSBs. This is plausible as we showed before that Top1 is not the source of toxicity in *rtt101Δ* cells that accumulate genomic rNMPs (Figure 17A). Yet, based on this result we cannot omit that the concomitant loss of Rtt101 and Rad51 in *RNH201-AID** cells is synergistic instead of being merely the additive effect of the growth impairment of *rad51Δ RNH201-AID** and *rtt101Δ RNH201-AID**. This means that at this point we cannot exclude a requirement for Rad51 in *rtt101Δ RNH201-AID** cells besides the repair of Top1-mediated DSBs, for instance to process structures arising due to the absence of Rtt101.

We next asked whether deletion of *MRC1* might be beneficial in *rtt101Δ* cells that accumulate genomic rNMPs. Indeed, the viability of *rtt101Δ RNH201-AID* pol2-M644G* cells in the presence of IAA was improved in the absence of Mrc1 (Figure 18B), raising the possibility that similar to MMS-induced damage, Rtt101^{Mms22} allows tolerance of genomic ribonucleotides through a modulation of Mrc1. Intriguingly, when we analysed the checkpoint status in those cells both by immunoblotting for Rad53 phosphorylation and *RNR3* expression (Figure 18C) and by monitoring the cell cycle distribution via flow cytometry (Figure 18D), we found that *rtt101Δ RNH201-AID* pol2-M644G* cells accumulated in G2/M and exhibited increased checkpoint activation after Rnh201-AID* depletion.

In addition, *mrc1Δ RNH201-AID* pol2-M644G* mutants also accumulated at the G2/M border with an active checkpoint which might be at least partially attributable to the already active checkpoint in *pol2-M644G* cells lacking Rnh201 (Williams et al., 2013). Instead of alleviating the checkpoint arrest of *rtt101Δ RNH201-AID* pol2-M644G* cells, deletion of *MRC1* rather seemed to increase the checkpoint activation albeit allowing cells to grow better. To clarify this observation in more detail, we employed the checkpoint-defective *mrc1$_{AQ}$* allele (Osborn and Elledge, 2003). As in the presence of MMS-induced DNA damage, the checkpoint function of Mrc1 was not responsible for a decreased cell viability (Figure 18E). In summary, the data shown here suggest that when genomic rNMPs accumulate, a function of Mrc1 unrelated to its role in activating the S phase checkpoint has to be counteracted by Rtt101.

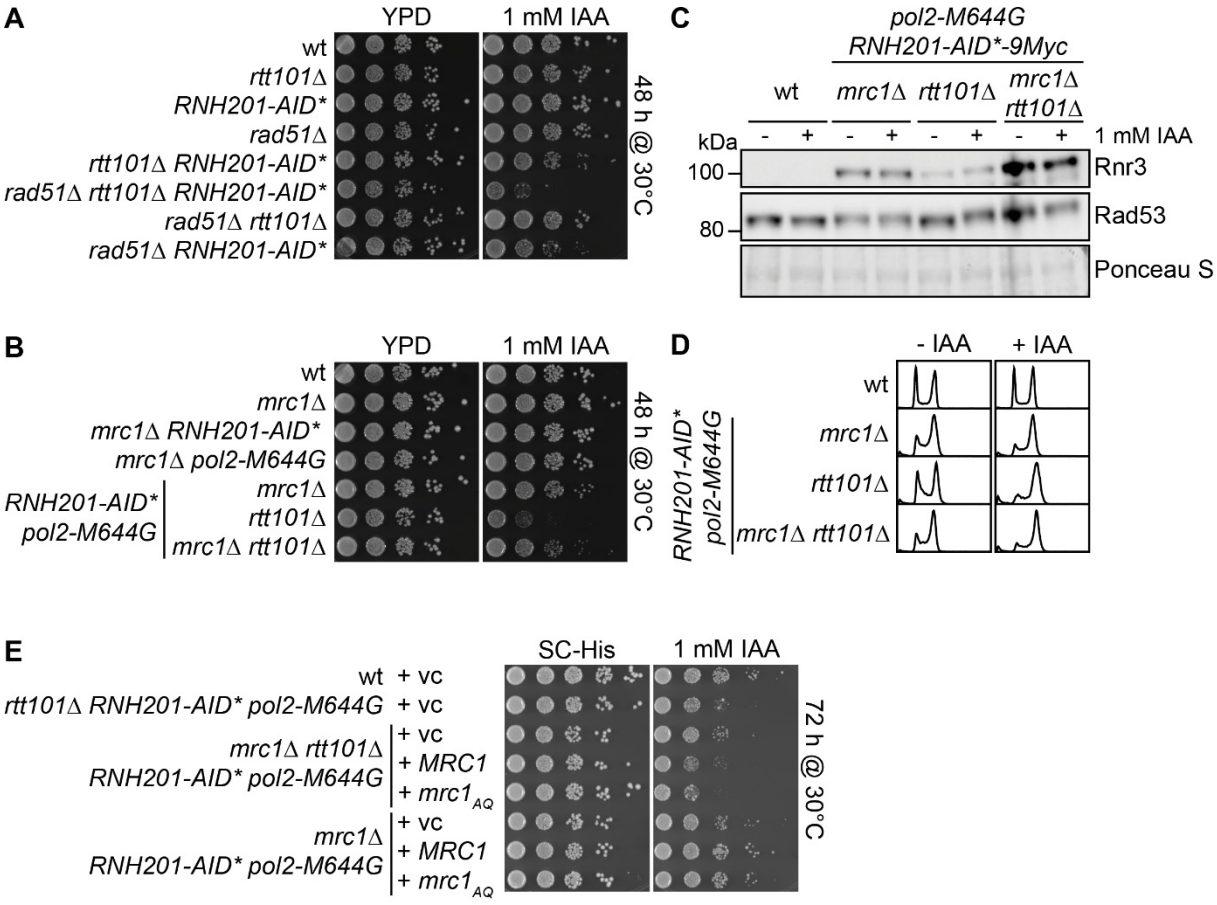

Figure 18. Rad51-mediated recombination is required and Rtt101 counteracts a replicative function of Mrc1 when rNMPs accumulate. (**A+B**) Haploid yeast strains of the indicated genotypes were grown overnight in liquid culture and the same number of cells was spotted in 10-fold serial dilutions onto YPD agar plates and YPD agar plates containing 1 mM IAA. Images were taken after 48 hours of incubation at 30°C. (**C**) Wildtype cells and *RNH201-AID*-9MYC pol2-M644G* mutants with the additional deletion of *RTT101, MRC1* or both were grown to mid-log phase in the absence (-) or presence (+) of 1 mM IAA. Cells were harvested for protein extraction and protein lysates were separated on a 7.5 % polyacrylamide gel followed by immunoblotting for Rad53 and Rnr3 protein. Signal was obtained by chemiluminescence. The Ponceau S-stained membrane serves as a proxy for equal loading. (**D**) DNA content of an aliquot of the same cell cultures as in (**C**) was determined by flow cytometry after staining with Sytox® Green. (**E**) Strains of the indicated genotypes were transformed with the control plasmid (vc) or a plasmid expressing either wildtype *MRC1* or the $mrc1_{AQ}$ mutant. In analogy to (**A+B**), cells were grown in SC-His liquid medium overnight and spotted onto SC-His agar plates and SC-His agar plates with 1 mM IAA. Images were taken after 72 hours at 30°C.

2.2.5 RNase H2 is required post-replicatively in the absence of Rtt101

We hypothesized that the damage caused by an accumulation of genomic rNMPs in the absence of Rtt101 is interfering with DNA replication and thus causing replication stress. To test this hypothesis, we made use of a system that allows the restriction of protein expression to a specific phase of the cell cycle (Hombauer et al., 2011; Karras and Jentsch, 2010). In this elegant system, the endogenous promoter of a gene is replaced by the promoter of a cyclin, in this case of the S phase cyclin *CLB6* or the G2/M cyclin *CLB2* (Figure 19A). Moreover, the N-terminal portion of the respective cyclin gene is fused in frame to the 5' end of the gene of interest. Consequently, transcription and degradation of the resulting fusion proteins mimic the cell cycle regulated timing of the cyclins. The described constructs were introduced into the *RNH202* locus which additionally contained a C-terminal TAP epitope tag to easily monitor protein levels by immunoblotting. The G2/M-restricted *CLB2-RNH202-TAP* (*G2-RNH202-TAP*) allele was created as part of this study, while the S phase-restricted *CLB6-RNH202-TAP* (*S-RNH202-TAP*) allele was kindly provided by Arianna Lockhart.

To confirm that the created Rnh202 constructs were indeed restricted to the desired cell cycle stages, we synchronously released *RNH202-TAP*, *S-RNH202-TAP* and *G2-RNH202-TAP* cells from a G1 arrest induced by α-factor and followed protein levels of the Rnh202 constructs over time by immunoblotting. Cell cycle arrest and release were controlled by flow cytometry and showed that all strains progressed through the cell cycle with similar kinetics (Figure 19B). While Rnh202-TAP levels did not fluctuate throughout the time course (Figure 19C), S-Rnh202-TAP levels started to rise when the G1-specific CDK inhibitor Sic1 disappeared, reaching a maximum level between 30 and 45 minutes when the majority of cells had entered S phase according to the flow cytometry results. S-Rnh202-TAP levels dropped after 60 to 75 minutes when the G2/M cyclin Clb2 was expressed and most of the cells reached a 2C DNA content, indicative of a restriction of S-Rnh202-TAP expression exclusively to S phase. Similarly, expression of G2-Rnh202-TAP initiated between 45 and 60 minutes and perfectly mirrored the appearance of Clb2 itself. At the 90 minutes time point, G2-Rnh202-TAP levels dropped, consistent with the re-appearance of Sic1. The temporal expression and degradation of G2-Rnh202-TAP was also in accordance with cell cycle progression of the culture as seen in the DNA content profiles assessed by flow cytometry.

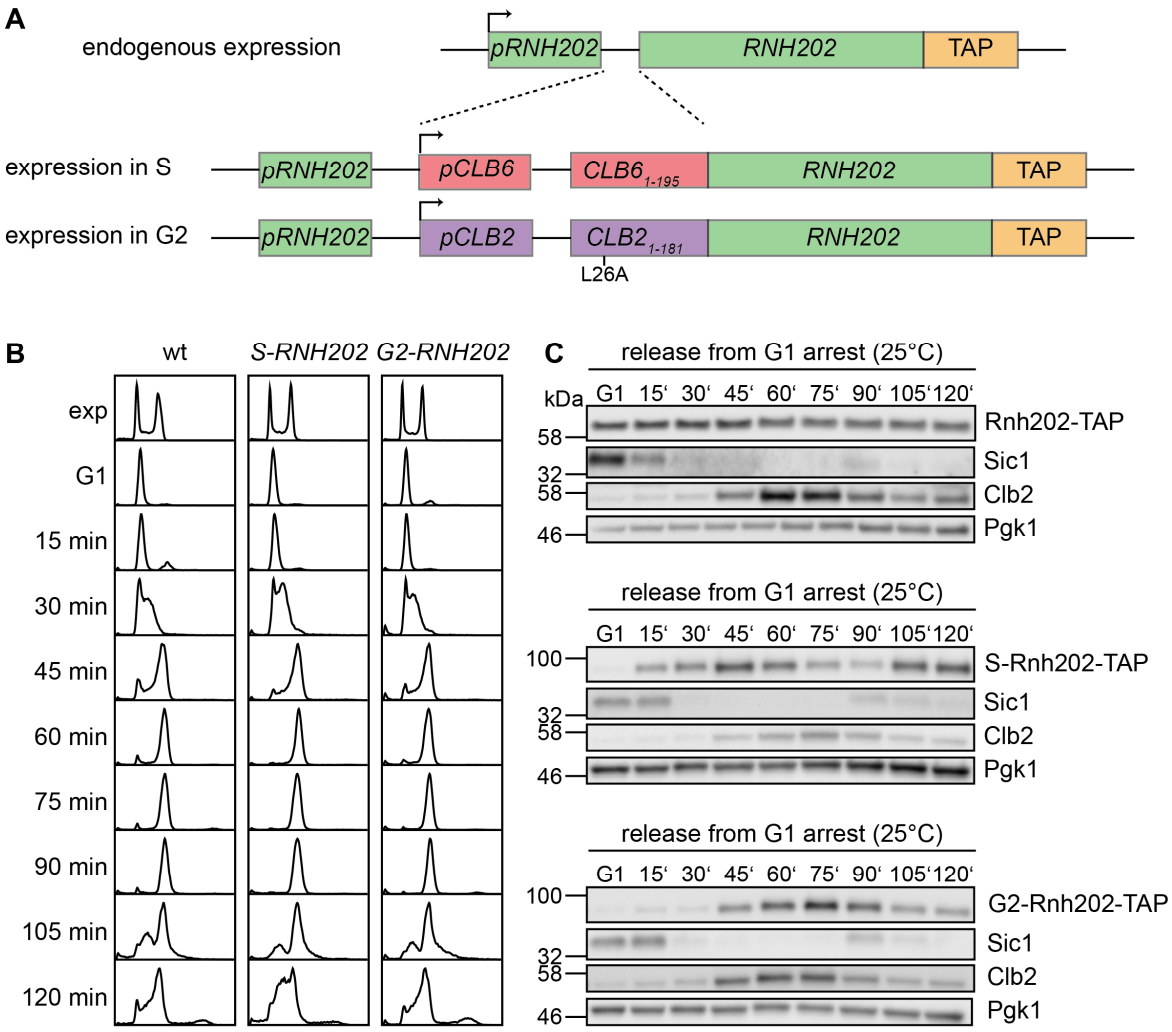

Figure 19. Cell cycle-restricted expression of *RNH202*. (**A**) Schematic view of the cell cycle-restricted *RNH202* alleles. Either the *CLB6* promoter and the N-terminal portion of the Clb6 protein (restriction to S phase, resulting in *S-RNH202-TAP*) or the *CLB2* promoter and the N-terminal portion of the Clb2 protein (restriction to G2/M, resulting in G2-*RNH202-TAP*) were integrated upstream of the *RNH202-TAP* ORF, thereby allowing transcription from the *CLB6*/*CLB2* promoters while inactivating the *RNH202* endogenous promoter. The *S-RNH202-TAP* strain was generated by Arianna Lockhart. (**B+C**) Cells expressing *RNH202-TAP*, *S-RNH202-TAP* or *G2-RNH202-TAP* were synchronized in G1 phase using 2.4 µM α-factor at 30°C and synchronously released into S phase at 25°C. Every 15 minutes, an aliquot of cells was taken for DNA content analysis by flow cytometry (**B**) and for protein extraction (**C**). Cell lysates were separated on a 4-15 % polyacrylamide gradient gel and immunoblotted using the PAP antibody to detect wildtype or cell cycle-restricted Rnh202-TAP levels, antibodies against Sic1 and Clb2 to determine the cell cycle phase for every time point and against Pgk1 as loading control. Signals were detected using chemiluminescence.

With this tool in hand, we next wanted to see whether expression of *RNH202* restricted to either S or G2/M phase was sufficient to restore full viability of *rtt101Δ* cells lacking RNase H2 activity. We therefore crossed cells deleted for *RTT101* to cells harbouring either the *S-RNH202-TAP* or the *G2-RNH202-TAP* allele and analysed the spore

viability of the resulting double mutants (Figure 20A). While the full deletion of the *RNH202* gene did not show significant differences in colony size between the single and double mutants, restricting Rnh202 expression in *rtt101Δ* cells to S phase caused a severe growth defect. In contrast, the restriction of Rnh202 expression to G2/M phase did not reveal any obvious growth defect of the spores in the absence of Rtt101. This result implies that RNase H2 might act outside of S phase and thus might have a role in a post-replicative repair pathway.

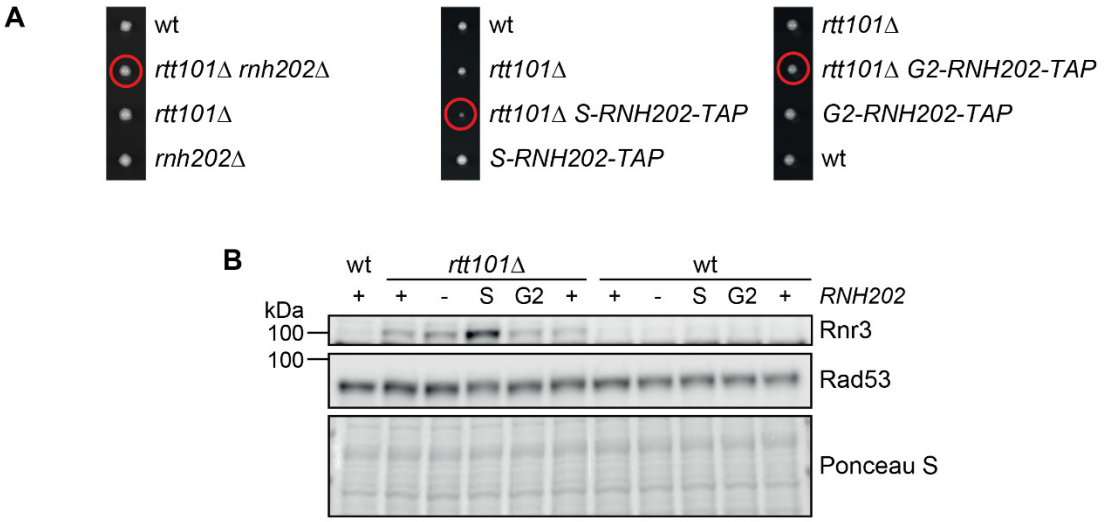

Figure 20. Restricting *RNH202* expression to S phase is not sufficient to maintain viability of *rtt101*Δ cells. (**A**) Heterozygous diploid *rtt101*Δ cells harbouring one wildtype copy of *RNH202* and either *rnh202*Δ, *S-RNH202-TAP* or *G2-RNH202-TAP* were sporulated, tetrads were manually dissected and after 3 days at 30°C the viability of the spore colonies was visually assessed. Red circles indicate the resulting haploid double mutants. (**B**) Wildtype or *rtt101*Δ cells expressing either wildtype *RNH202* (+), *S-RNH202-TAP* (S), *G2-RNH202-TAP* (G2) or being *rnh202*Δ (-) were grown to mid-log phase in YPD medium at 30°C. Proteins were extracted and cell lysates were separated on a 7.5 % polyacrylamide gel followed by immunoblotting for Rnr3 and Rad53 protein. Signal was obtained by chemiluminescence. The Ponceau S-stained membrane serves as a control for equal loading.

We could previously show that *rtt101Δ* cells accumulating genomic ribonucleotides elicit a checkpoint response (Figure 18C). Therefore, we compared the status of the DNA damage checkpoint in Rtt101-proficient and -deficient cells expressing either wildtype Rnh202, S-Rnh202-TAP, G2-Rnh202-TAP or lacking *RNH202* by immunoblotting Rad53 phosphorylation and Rnr3 expression (Figure 20B). In unchallenged cells, the loss of Rtt101 caused a moderate activation of the checkpoint, which was not obviously influenced by either loss of Rnh202 or by restriction of its

expression to G2/M. In contrast, the expression of Rnh202 exclusively in S phase further increased the activation of the checkpoint consistent with the reduced viability of *rtt101Δ S-RNH202-TAP* spores (Figure 20A). Besides clearly demonstrating a requirement for RNase H2 outside of S phase, the more pronounced effect of S phase-restricted expression compared to a complete loss of RNase H2 function also puts forward the possibility that RNase H2 activity has to be tightly controlled during DNA replication and that loss of Rtt101 might interfere with this regulation.

2.2.6 H3K56Ac is required when genomic ribonucleotides accumulate

Histone H3 constitutes one of the few characterized targets of the Rtt101 E3 ubiquitin ligase, and its ubiquitylation on three lysine residues (K121, K122, K125) has been proposed to promote replication-coupled nucleosome assembly (Han et al., 2013). A crucial upstream step of H3 ubiquitylation is the Rtt109-dependent modification of lysine 56 on H3 with an acetyl group (H3K56Ac) (Han et al., 2007a; Li et al., 2008), which is absent not only in *rtt109Δ* cells but also in cells lacking the histone chaperone Asf1 (Schneider et al., 2006). To address the question whether Rtt101 is required due to its function in replication-coupled nucleosome assembly, we tested the importance of the upstream factors Rtt109 and Asf1 when rNMPs accumulate. We analysed viability of rNMP-accumulating cells in the absence of Rtt109 or Asf1 using a spotting assay.

We found that loss of Rtt109 (Figure 21A) or Asf1 (Figure 21B) reduced the growth of rNMP accumulating *RNH201-AID** cells in the presence of auxin, and cells additionally expressing *pol2-M644G* to further increase aberrant rNMP incorporation were barely viable on auxin-containing plates. This strongly implies that the deposition of H3K56Ac is crucial for cells accumulating genomic rNMPs. This result is an indication that Rtt101 might be crucial when rNMPs accumulate due to its role in modification of H3 as H3 ubiquitylation functions within the same pathway as Rtt109-mediated and Asf1-dependent H3K56Ac. However, Rtt101-mediated H3 ubiquitylation depends on the preceding acetylation of K56 and thus happens downstream of H3K56Ac.

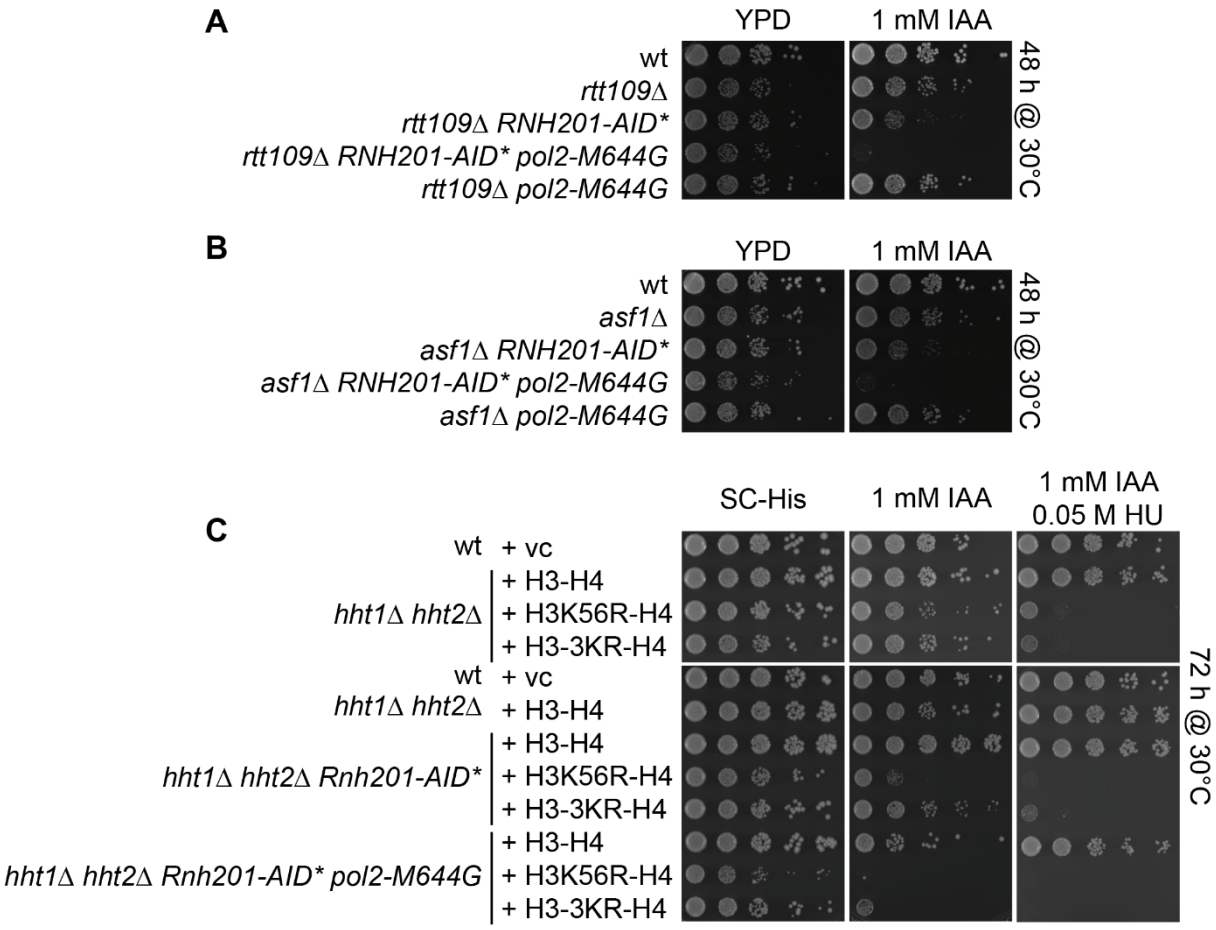

Figure 21. The H3K56Ac pathway is crucial when cells accumulate genomic rNMPs. (**A+B**) Haploid yeast strains of the indicated genotypes were grown overnight in liquid culture and the same number of cells was spotted in 10-fold serial dilutions onto YPD agar plates and YPD agar plates containing 1 mM IAA. Images were taken after 48 hours of incubation at 30°C. (**C**) Heterozygous diploid *hht1Δ hht2Δ RNH201-AID*-9MYC pol2-M644G* mutants were transformed with a centromeric plasmid encoding either wildtype histone H3 and H4 (*H3-H4*), the non-acetylatable H3K56R mutant and wildtype H4 (*H3K56R-H4*) or the non-ubiquitylatable H3-K121,122,125R mutant and wildtype H4 (*H3-3KR-H4*). The plasmid-containing diploids were sporulated and the indicated haploid mutants carrying either of the plasmids were grown in SC-His liquid medium overnight at 30°C and spotted on SC-His agar plates, SC-His agar plates containing 1 mM IAA and SC-His agar plates containing 1 mM IAA and 0.05 M HU. Images were taken after 72 hours at 30°C.

One could envision that loss of Rtt101 causes toxicity in cells accumulating rNMPs because H3 is no longer ubiquitylated and thus replication-coupled nucleosome assembly might be perturbed. To test this idea, we employed H3 point mutants in which the lysines shown to be ubiquitylated by Rtt101 or acetylated by Rtt109 were substituted by arginine (*H3-3KR* or *H3K56R*, respectively). The resulting H3 point mutants or wildtype H3 as a control were expressed from a centromeric plasmid together with wildtype H4. The plasmids were transformed into diploid yeast cells

lacking both copies of H3 (*HHT1* and *HHT2*) but being homozygous for the *RNH201-AID** and *pol2-M644G* alleles. After diploid sporulation and manual tetrad dissection, viability of *hht1Δ hht2Δ RNH201-AID* pol2-M644G* cells expressing either mutant or wildtype H3 was analysed in a spotting assay (Figure 21C). The presence of an additional copy of H4 in general did not affect viability of cells, as *hht1Δ hht2Δ* cells expressing *H3-H4* showed neither compromised growth when compared to wildtype cells transformed with the vector control (wt + vc) nor increased HU sensitivity (upper panel, Figure 21C). In contrast, the expression of non-acetylatable *H3K56R-H4* or non-ubiquitylatable *H3-3KR-H4* highly increased the sensitivity of *hht1Δ hht2Δ* cells to HU, consistent with a previous report (Han et al., 2013). Moreover, the use of the *H3K56R* mutant showed that deletion of *RTT109* is indeed causing toxicity in *RNH201-AID** and *RNH201-AID* pol2-M644G* cells due to loss of H3K56Ac, further emphasizing the importance of this acetylation mark when genomic rNMPs accumulate (lower panel, Figure 21C). Strikingly, a slightly reduced growth rate of cells expressing *H3-3KR-H4* and lacking RNase H2 activity was highly exacerbated in cells additionally expressing *pol2-M644G* (lower panel, Figure 21C and Natalie Schindler, personal communication). This increased toxicity is reminiscent of a loss of Rtt101 in cells accumulating genomic rNMPs (Figure 14D) and strongly suggests that in the presence of unrepaired genomic rNMPs, one crucial function of Rtt101 is the ubiquitylation of H3 on K121, K122 and K125.

2.2.7 Nucleosome deposition in RER-defective cells is not altered

In budding yeast, acetylation of H3K56 has been shown to be a modification deposited onto replicated or repaired DNA (Li et al., 2008; Masumoto et al., 2005) and is attached to newly synthesized H3 molecules that are not yet assembled into nucleosomes (Han et al., 2007b). In cells lacking Rtt101, H3K56Ac levels on replicated DNA have been shown to be reduced due to the inability to ubiquitylate H3 which would in turn facilitate nucleosome assembly (Han et al., 2013). Ribonucleotides incorporated into stretches of DNA have the potential to alter DNA structure (Derose et al., 2012; Egli et al., 1993; Jaishree et al., 1993) and might interfere with DNA-nucleosome interactions. Therefore, we aimed to address whether the reported reduced nucleosome assembly in *rtt101Δ* cells might result in additive disturbance of DNA-histone interactions when genomic rNMPs accumulate. To test this, we performed chromatin immunoprecipitation (ChIP) experiments using antibodies specific for H3 to monitor

total nucleosome occupancy and H3K56Ac to monitor replication-coupled nucleosome assembly.

Occupation of total H3 and H3K56Ac was quantified by qPCR at three different gene loci, *ACT1, GCN4,* and *PDC1*. The H3K56Ac signal was normalized to the respective signal for total H3 to account for potential differences in H3 occupancy in the mutants. We first performed the described ChIP experiment comparing exponentially growing wildtype cells with *rtt101Δ*, *asf1Δ*, *rtt109Δ* and auxin-treated *RNH201-AID* pol2-M644G* cells (Figure 22). As measured by immunoblotting, H3K56Ac is absent in *asf1Δ* and *rtt109Δ* cells, but detectable in both *rtt101Δ* and *RNH201-AID pol2-M644G* cells (Figure 22A). At the timepoint of crosslinking the cultures, DNA content was monitored by flow cytometry (Figure 22B). While the pulldown of H3 did not reveal any differences between all strains tested (Figure 22C), the H3K56Ac signal was significantly reduced in *asf1Δ* and *rtt109Δ* cells as expected (Figure 22D). Unexpectedly, exponentially growing *rtt101Δ* cells showed wildtype-like levels of H3K56Ac at the tested loci. This seems contradictory to a previous study reporting that the ubiquitylation of H3 by Rtt101 is required to ensure deposition of H3K56Ac on chromatin (Han et al., 2013). In *RNH201-AID* pol2-M644G* cells, depletion of Rnh201-AID* in cycling cells for at least 6 hours, and therefore multiple S phases, did not change H3 and H3K56Ac occupation as compared to wildtype.

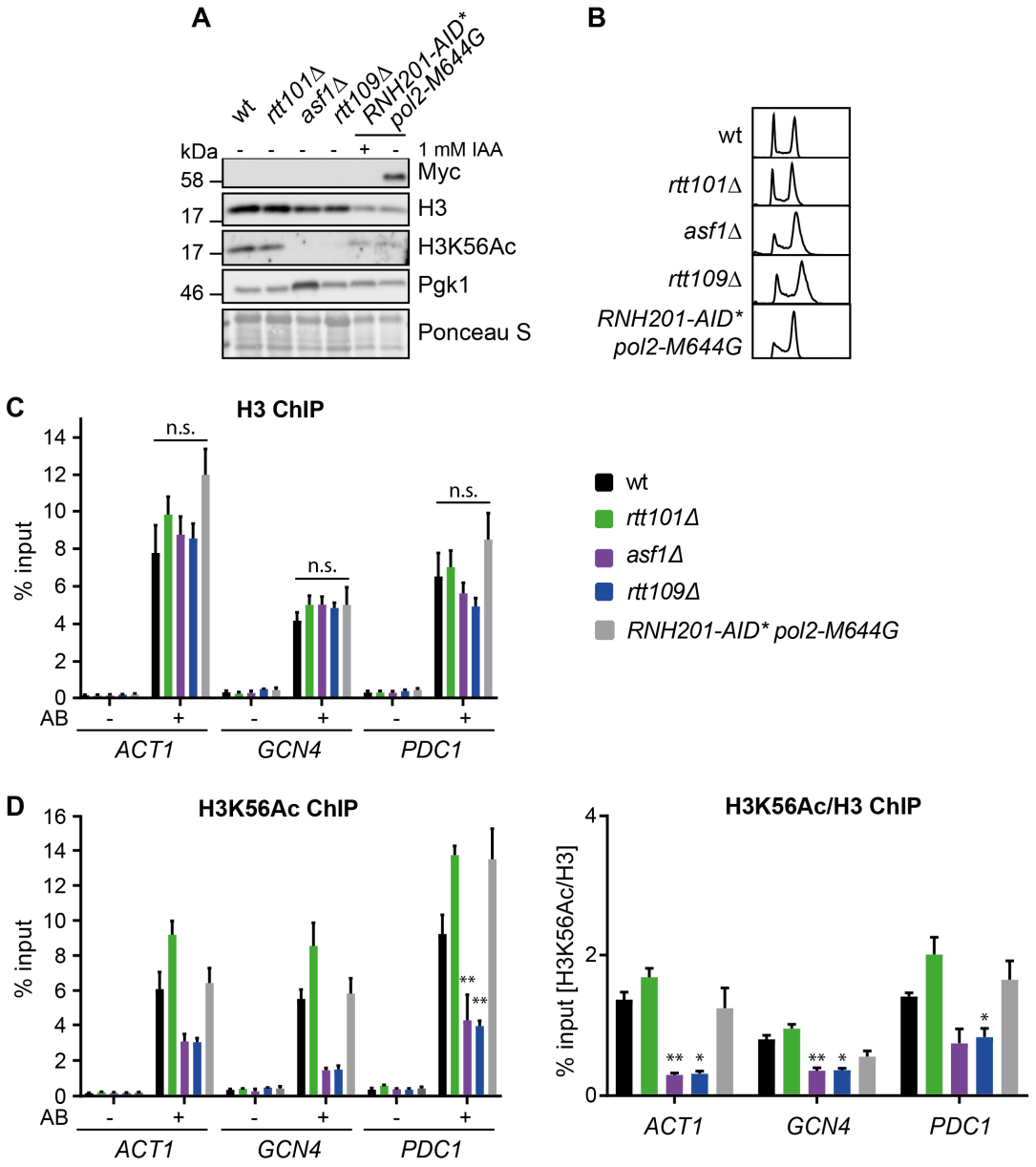

Figure 22. Histone H3 occupancy and H3K56Ac deposition onto DNA is not affected when cells accumulate rNMPs. (**A-D**) Strains of the indicated genotypes were grown to mid-log phase in YPD medium. *RNH201-AID*-9MYC pol2-M644G* mutants were treated with 1 mM IAA during exponential growth. An aliquot of each culture was taken for protein extraction (**A**) and flow cytometry (**B**), the remaining culture was crosslinked and assessed by ChIP. (**A**) Protein lysates were separated on a 4-15 % polyacrylamide gradient gel and immunoblotted using antibodies targeting Rnh201-AID*-9Myc, H3, H3K56Ac and Pgk1. Signal was obtained by chemiluminescence. The Ponceau S-stained membrane serves as a control for equal loading. (**B**) DNA content analysis by flow cytometry after staining with Sytox® Green. (**C+D**) Chromatin associated with H3 (**C**) and H3K56Ac (**D**) was quantified at three transcribed loci (*ACT1, GCN4,* and *PDC1*) by qRT-PCR. Mean % input values + SEM are shown from 3 biological replicates. Additionally, the mean % input of the H3K56Ac IP was normalized to the mean % input of the H3 IP (**D**). Statistically significant differences from wildtype are indicated. *: $p < 0.05$; **: $p < 0.01$ (Student's t-test).

A reduced deposition of H3K56Ac in *rtt101Δ* cells was reported during replication-coupled nucleosome assembly (Han et al., 2013). In order to reproduce the published results, we synchronously released G1-arrested cultures into 0.2 M HU at 25°C to slow down S phase, crosslinked after 45 minutes and performed the ChIP approach as described above. In addition to the loci previously tested by qPCR (Figure 22), we also assessed the H3 and H3K56Ac signals at an early replicating origin (*ARS607*) and in a distance from this origin (*ARS607* + 14 kb) (Han et al., 2013; Li et al., 2008). Total H3 and H3K56Ac levels at the time of crosslinking were monitored by immunoblotting (Figure 23A) and the G1 arrest and release into HU were controlled by flow cytometry for DNA content (Figure 23B). In the case of *rtt101Δ RNH201-AID* pol2-M644G* and *rtt109Δ RNH201-AID* pol2-M644G*, a substantial fraction of cells seemed to be arrested in G2/M since treatment with α-factor did not result in a single G1 peak. However, the portion of cells that did arrest in those strains clearly exited the G1 arrest when cells were released into HU as seen for the remaining strains. In wildtype cells, H3K56Ac incorporation was observable for the *GCN4* and *PDC1* loci (Figure 23C) as well as for *ARS607* (Figure 23D), while at the *ACT1* locus and in 14 kb distance to *ARS607* no H3K56Ac signal was detected. This is consistent with *GCN4* and *PDC1* being close to early firing origins (6 kb and 1 kb), while the distance of *ACT1* to the next origin (14 kb) is comparable to the *ARS607* + 14 kb locus tested. In agreement with previous reports (Li et al., 2008), cells lacking Rtt109 consistently showed low levels of H3K56Ac at all loci tested. However, in our hands *rtt101Δ* cells did not show a defective incorporation of H3 acetylated at K56. Moreover, the release into S phase while depleting Rnh201-AID* did not significantly change H3K56Ac levels on replicated DNA compared to wildtype cells. Thus, combining *RTT101* deletion with *RNH201-AID* pol2-M644G* also resembled the wildtype situation in terms of nucleosome assembly on replicated DNA. Importantly, different groups discovered that most of the commercially available antibodies raised against H3K56Ac might also cross-react with other acetylation sites on H3, such as H3K9Ac or H3K27Ac (Drogaris et al., 2012; Pal et al., 2016). Thus, we cannot exclude that the signal obtained in the H3K56Ac ChIP experiments might be partially due to other acetylated residues in H3. However, based on the results obtained by ChIP, we suggest that nucleosome occupancy and deposition of H3K56Ac onto newly replicated DNA is not defective in the absence or Rtt101 or when cells accumulate rNMPs during a single S phase due to the lack of RNase H2. Moreover, the genetic interaction observed for *rtt101Δ RNH201-AID* pol2-*

M644G mutants is likely not due to an exacerbated disturbance of nucleosome-DNA interactions in these cells.

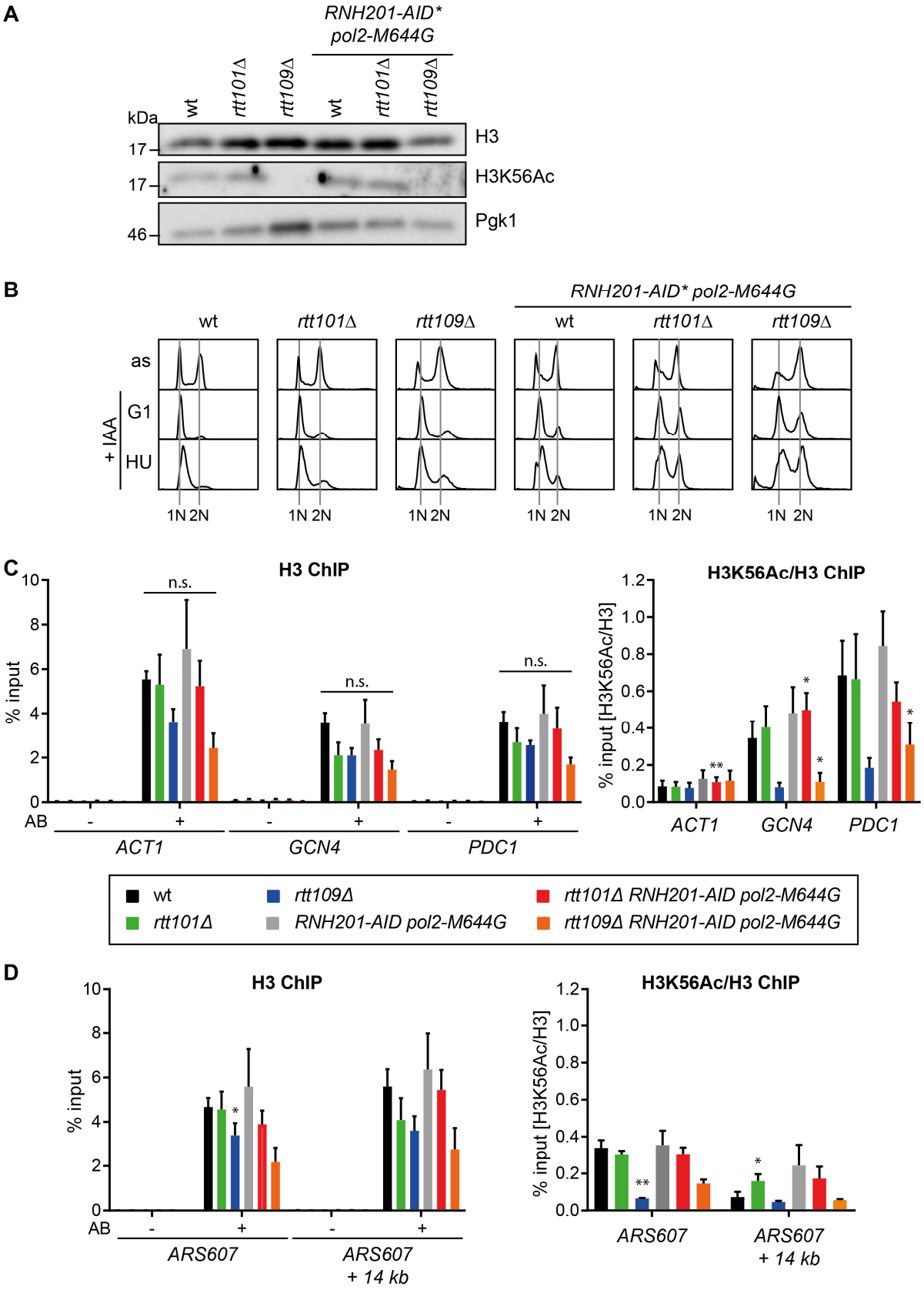

Figure 23. Histone H3 occupancy and H3K56Ac deposition onto DNA is not affected when cells cannot repair rNMPs during replication. *Figure legend: see next page.*

Figure 23. Histone H3 occupancy and H3K56Ac deposition onto DNA is not affected when cells cannot repair rNMPs during replication. (**A-D**) Strains of the indicated genotype were arrested in G1 phase and synchronously released into YPD medium containing 0.2 M HU and 1 mM IAA at 25°C. Degradation of the AID*-tagged Rnh201 protein was induced during the G1 arrest and maintained during the release into HU. Samples for protein extraction were taken immediately prior to crosslinking, samples for flow cytometry were obtained from asynchronous cells before the α-factor arrest (as), at the time point of release into HU (G1) and at the time point of crosslinking after 45 min in HU (HU). (**A**) Cell extracts were separated on a 4-15 % polyacrylamide gradient gel and immunoblotted using antibodies targeting Rnh201-AID*-9Myc, H3, H3K56Ac and Pgk1. Signal was obtained by chemiluminescence. The Ponceau S-stained membrane serves as a control for equal loading. (**B**) DNA content analysis by flow cytometry after staining with Sytox® Green. (**C+D**) Chromatin associated with H3 and H3K56Ac was quantified at three transcribed loci (*ACT1, GCN4,* and *PDC1*) (**C**) and at the early firing origin *ARS607* as well as 14 kB away from this origin (*ARS607* + 14 kB) (**D**). Data was obtained by qRT-PCR and is presented as mean % input values + SEM from three biological replicates tested in independent experiments. The H3K56Ac signal is normalized to the signal for total H3 at the respective loci. Statistically significant differences from wildtype are indicated. *: $p < 0.05$; **: $p < 0.01$ (Student's t-test).

2.2.8 SILAC-based approach to identify relevant targets of Rtt101 in RER-defective cells

To fully understand the requirement for Rtt101 when rNMPs accumulate it is important to identify the relevant targets whose ubiquitylation depends on Rtt101. The lab of Petra Beli has optimized a mass spectrometric approach termed di-glycine remnant profiling to identify DNA damage-induced ubiquitylation sites (Heidelberger et al., 2016). The basic principle of this method is that upon digestion of proteins with trypsin, a protease that cleaves peptide bonds exclusively C-terminally after arginine and lysine residues (Olsen et al., 2004), ubiquitin that is covalently bound to a target lysine *via* its C-terminal RGG sequence will leave a di-glycine remnant still attached to this lysine (Peng et al., 2003). Di-glycine-modified peptides can be enriched using a monoclonal antibody that recognizes this adduct (Xu et al., 2010) and identified by mass spectrometry. In combination with SILAC (stable isotope labelling with amino acids in cell culture), this method allows a site-specific quantitative comparison of ubiquitylated peptides in cells grown either in different conditions or, as in our case, in the presence and absence of the E3 ubiquitin ligase to be investigated.

To this end, *RNH201-AID*-9MYC pol2-M644G* ('wildtype') cells and *rtt101Δ RNH201-AID*-9MYC pol2-M644G* ('*rtt101Δ*') were grown in heavy and light SILAC medium, respectively (Figure 24A). Auxin was omitted from the medium to allow expression of RNase H2 and thus constant removal of rNMPs. Exponentially growing cells were arrested in G1 phase using α-factor. Subsequently, auxin was added to degrade

Rnh201-AID* before the synchronized cultures were released for one hour into the respective SILAC medium containing auxin and proteasome inhibitor (MG-132). Consequently, cells progressed into S phase in the absence of RER. The same number of cells from wildtype and *rtt101*Δ cultures with opposite SILAC label were combined in a 1:1 ratio, and proteins were extracted from this mixed culture. Moreover, this experiment was simultaneously performed as a reverse experiment defined by a label switch: *rtt101*Δ cells were grown in heavy and wildtype cells in light medium. The extracted protein lysates of both experiments were handed over to Thomas Juretschke in the Beli lab who performed the di-glycine remnant profiling and mass spectrometric measurement as described above (Figure 24B). By this approach we obtained 17 different di-glycine peptides mapped to 14 different proteins that were significantly enriched in wildtype cells compared to *rtt101*Δ cells in both the forward and reverse experiment. These identified candidate targets of Rtt101 are summarized in Figure 24C and 24D.

One peptide especially caught our attention as it is directly involved in DNA metabolism: Dpb2, the second largest subunit of DNA polymerase ε, exhibited a di-glycine remnant on K419 with a strong enrichment in wildtype over *rtt101*Δ cells in both the forward and reverse experiment (Figure 24C, 24D). Careful analysis of the MS parent ion scan (Figure 25A) and the MS-MS fragment spectrum (Figure 25B) confirmed the identity of an Rtt101-dependent ubiquitylation site on K419 of Dpb2 when rNMPs accumulate during S phase in the absence of RNase H2.

Figure 24 Di-glycine remnant profiling identifies putative targets of Rtt101 when rNMPs accumulate. (**A**) Scheme of the experimental strategy. *RNH201-AID*-9MYC pol2-M644G* cells either expressing *RTT101* ('wt') or with a deletion of *RTT101* ('*rtt101Δ*') were grown in heavy and light SILAC medium (SC-Lys supplemented with Lys^8 or Lys^0), respectively. Cells were arrested in G1 using α-factor, and approximately one hour prior to release 1 mM IAA (auxin) was added to deplete Rnh201-AID*-9Myc protein. Subsequently, cells were released into S phase into heavy/light SILAC medium supplemented with 1 mM IAA and 75 µM MG132 (proteasome inhibition) for 1 hour at 25°C. Then heavy and light cultures were combined in a 1:1 ratio and both soluble and chromatin-associated proteins were extracted. The protein extract was handed over to Thomas Juretschke (Beli lab). (**B**) Scheme depicting the di-glycine remnant profiling approach. Modified from (Xu and Jaffrey, 2011). Proteins were digested with trypsin, then di-glycine-modified peptides were enriched by IP. The eluted peptides were subjected to LC-MS/MS. (**C**) Scatter plot depicting the logarithmic SILAC ratios of sites quantified in both experiments. The dotted lines represent the threshold of a heavy/light (H/L) ratio of 1.5 that has to be reached for significance. (**D**) Bar plot showing logarithmic H/L SILAC ratios for both experiments. The dotted lines represent an H/L ratio of 2. Sample preparation for mass spectrometry (trypsin

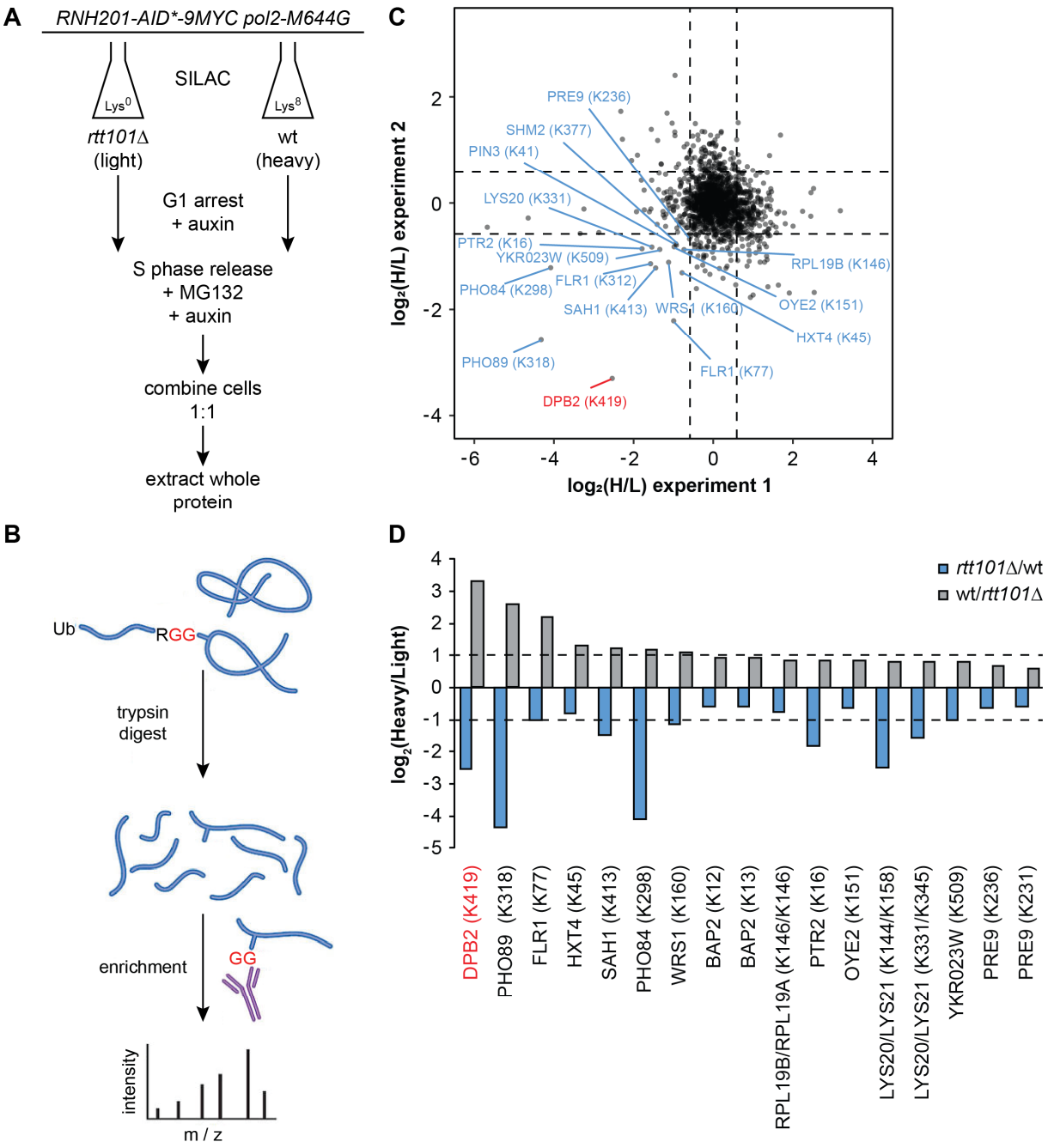

digest, di-glycine IP), measurement and analysis of the data was performed and figures in panel (**C**) and (**D**) were provided by Thomas Juretschke (Petra Beli lab).

Figure 24 Di-glycine remnant profiling identifies putative targets of Rtt101 when rNMPs accumulate. *Figure legend: see previous page.*

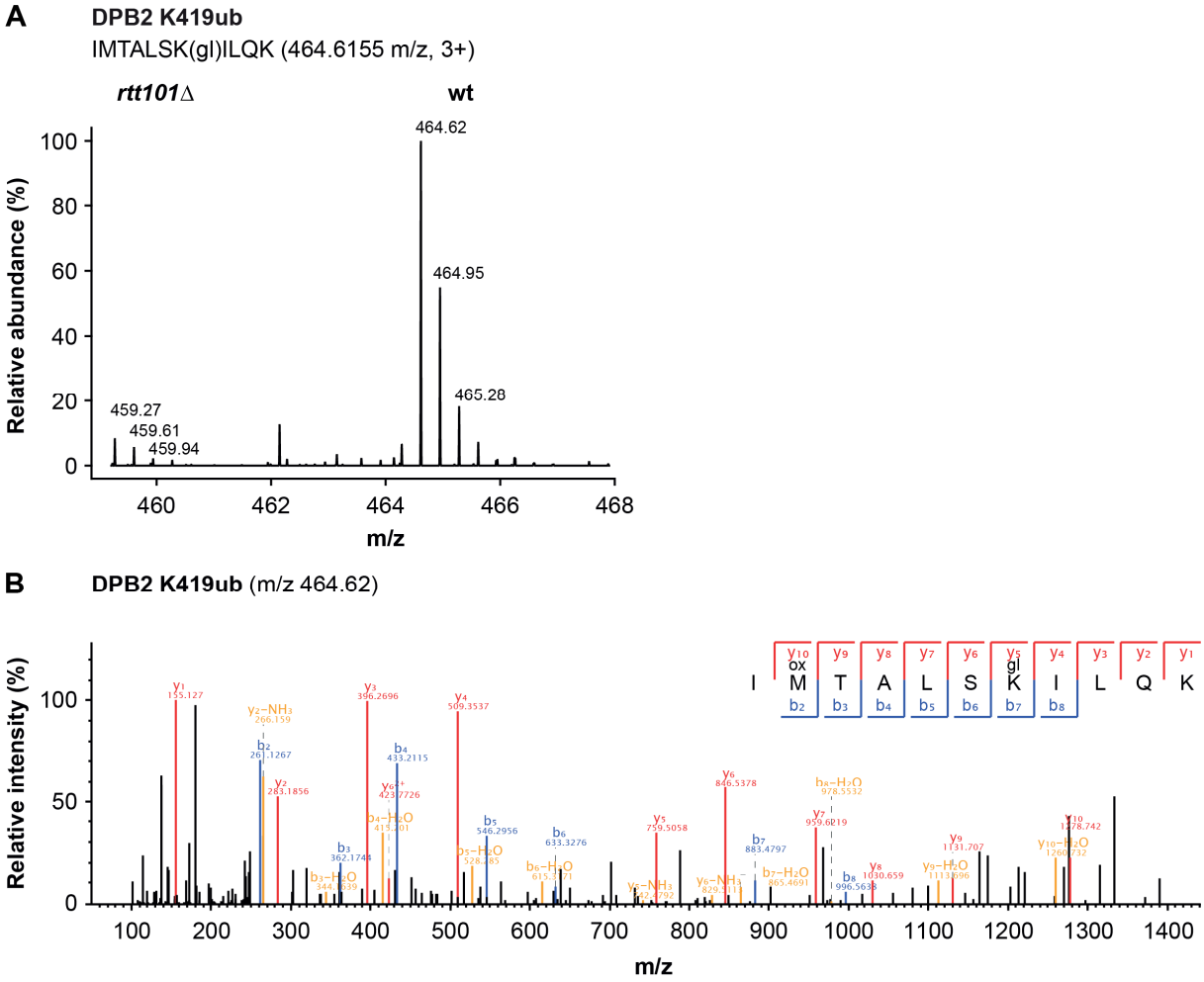

Figure 25. Dpb2 ubiquitylation at lysine 419 is Rtt101-dependent. (**A**) Mass spectrometric parent ion scan of the peptide IMTALSK(di-gly)ILQK corresponding to di-glycine-modified K419 in Dpb2. The SILAC pair shows the relative abundance and mass to charge (m/z) of the di-gly-modified peptide in *rtt101Δ RNH201-AID*-9MYC pol2-M644G* (*rtt101Δ*) and *RNH201-AID*-9MYC pol2-M644G* (wt) cells. (**B**) Fragment spectrum and peptide sequence of the identified di-gly-modified Dpb2 peptide. The di-gly remnant causes a mass shift of approximately 114 Da. Data and figures were provided by Thomas Juretschke (Petra Beli Lab).

Appendix

While investigating why Rtt101 is required when rNMPs accumulate in the genome, we performed additional hypothesis-driven experiments, which turned out to be either negative results or could not be sufficiently interpreted at that time. However, those results might still contribute to the understanding of Rtt101 function and will thus be presented in the following section.

During the initial steps of the project focusing on misincorporated ribonucleotides, we attempted to get a better understanding of the CPT sensitivity in *rtt101*Δ cells, which we originally included into our SGA approach for genetic suppressors (Buser et al., 2016). To be able to determine the contribution of direct Top1-mediated damage in the presence of CPT, we constructed an auxin-inducible *TOP1-AID*-9MYC* allele in analogy to the *RNH201-AID*-9MYC* allele. When expressed, this allele was functional since *rtt101*Δ cells expressing *TOP1-AID*-9MYC* were as sensitive to CPT as *rtt101*Δ cells expressing wildtype *TOP1* (Figure 26A). On the other hand, deletion of *TOP1* fully abolished the CPT sensitivity. In the presence of auxin, the *TOP1-AID*-9MYC* allele behaves as the *TOP1* deletion, confirming that its depletion renders *rtt101*Δ cells resistant to CPT. Using those strains, we tested whether cells lacking Rtt101 would be defective in the recovery from a checkpoint arrest induced by CPT treatment as it is observed upon MMS treatment and induction of DSBs (Diao et al., 2017; Luke et al., 2006; Zaidi et al., 2008). We found that the synchronous release into CPT-containing medium resulted in a phosphorylation of Rad53 in both wildtype and *rtt101*Δ cells, which was maintained in *rtt101*Δ cells, but not in wildtype after drug removal and release into fresh medium (-IAA panel, Figure 26B). We next analysed whether depletion of Top1 at the time when cells are released into damage-free medium would alleviate the checkpoint recovery defect of *rtt101*Δ cells. Surprisingly, the depletion of Top1 during the release of CPT-treated *rtt101*Δ cells did not lead to a dephosphorylation of Rad53 (+IAA panel, Figure 26B), suggesting that persistent Top1 cleavage complexes (Top1cc) are not the cause of a prolonged checkpoint arrest and recovery defect in cells lacking Rtt101.

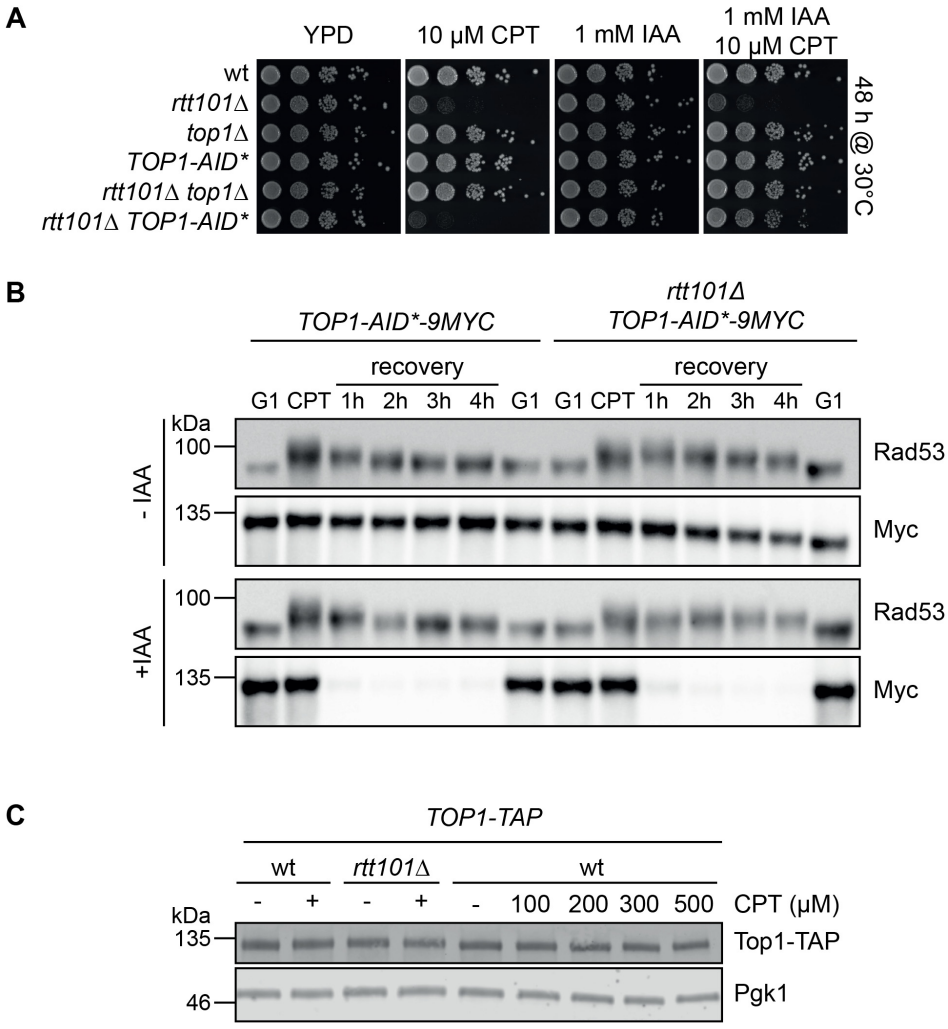

Figure 26. Top1 protein levels are not regulated by Rtt101 and induced degradation of Top1-AID* does not alleviate the checkpoint recovery defect of *rtt101Δ* cells. (**A**) Haploid yeast strains of the indicated genotypes were grown over night in YPD medium in the absence of IAA. Tenfold serial dilutions were spotted onto YPD plates and YPD plates containing 10 µM CPT, 1 mM IAA or both 10 µM CPT and 1 mM IAA. Plates were incubated at 30°C and images were taken after 48 hours. (**B**) Wildtype cells or *rtt101Δ* expressing *TOP1-AID*-9MYC* were synchronized in G1 phase using 1 µM α-factor and synchronously released into fresh YPD medium. After 15 minutes, 50 µM CPT was added and cells were kept at 30°C for 1 hour. Next, CPT was washed out and the cultures were split and either released into YPD (-IAA) or YPD supplemented with 1 mM IAA to induce degradation of Top1-AID* (+IAA). Samples were taken every hour for a total of 4 hours and proteins were extracted. The protein lysates were separated on 7.5 % polyacrylamide gels followed by immunoblotting for Rad53 and Top1-AID*-9Myc protein. Signal was obtained using chemiluminescence. (**C**) *TOP1-TAP*-expressing wildtype or *rtt101Δ* cells were split and either left untreated (-) or were treated with 50 µM CPT (+) for 1 hour at 30°C. Moreover, wildtype cells expressing *TOP1-TAP* were treated with different CPT concentrations ranging from 100 to 500 µM for 1 hour at 30°C. Cell lysates were separated on 7.5 % polyacrylamide gels and subsequently probed with antibodies recognizing Top1-TAP and Pgk1. Signal was obtained using fluorescence.

In human cells, CPT treatment leads to proteasome-dependent degradation of Top1, an important early step in eliciting the DNA damage response (Zhang et al., 2004). We reasoned that Rtt101 might be directly involved in the degradation of Top1 and thus analysed Top1 protein levels in wildtype cells and *rtt101*Δ cells in untreated conditions and upon acute treatment with a high dose of CPT. However, we did not see any difference between treatment conditions (untreated versus treated) or genotypes (wildtype or *rtt101*Δ) (Figure 26C). Since CPT concentrations used in the studies reporting CPT-induced Top1 degradation in human cells were very high, we performed a titration experiment, but even extremely high concentration of 500 µM CPT did not reduce Top1 levels in wildtype yeast cells (Figure 26C).

An additional hypothesis imposed was, that Rtt101 might be required to protect stalled replication forks or to regulate factors directly involved in their remodelling. Therefore, we tested protein levels of two candidates, Exo1 and Rad54. The exonuclease Exo1 has been shown to be degraded upon DNA damage in human cells in response to CPT to limit DNA end resection (Tomimatsu et al., 2017). The Swi2/Snf2 family translocase Rad54 regulates Rad51 displacement from DNA ((Shah et al., 2010) and section 1.4.5).

Strains expressing TAP-tagged *EXO1* or *RAD54* were grown to mid-log phase and either mock-treated or treated with 0.03 % MMS or 50 µM CPT for 90 minutes. Exo1-TAP protein levels were not affected by any treatment or in the absence of Rtt101. Rad54-TAP levels were slightly elevated in the absence of Rtt101 in all conditions, however, in wildtype cells only MMS treatment increased Rad54-TAP levels (Figure 27). Especially the treatment of cells with MMS seems to induce *RAD54* expression, indicating an increased need for this protein. This preliminary result therefore suggests that Rtt101 might be involved in regulating Rad54 protein levels, possibly also upon MMS-induced DNA damage.

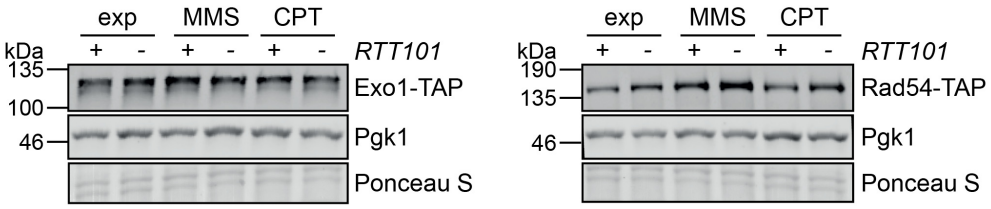

Figure 27. Loss of Rtt101 has no effect on Exo1 levels but might modulate Rad54 levels. Exponentially growing wildtype or *rtt101Δ* cells expressing either EXO1-TAP or RAD54-TAP were split and either left untreated (exp) or were treated with 0.03 % MMS (MMS) or 50 µM CPT (CPT) for 1 hour at 30°C. Cell lysates were separated on 10 % polyacrylamide gels followed by immunoblotting for TAP-tagged proteins and Pgk1. Signal was detected using fluorescence.

To understand why an accumulation of genomic ribonucleotides is toxic in cells lacking a functional Rtt101 E3 ubiquitin ligase, we sought to test the requirement of several DNA damage repair or tolerance pathways. We reasoned that a replication fork encountering unrepaired rNMPs might stall and undergo replication fork reversal to be able to replicate past the obstacle. In such a scenario, Rtt101 might be required to regulate factors involved in promoting fork reversal, such as Mph1 (Zheng et al., 2011) and Rad5 (Blastyák et al., 2007). Deletion of *MPH1* or *RAD5* alone did not cause toxicity in *RNH201-AID* pol2-M644G* strains, and more importantly, it did not rescue *rtt101*Δ *RNH201-AID* pol2-M644G* cell viability as hypothesized (not shown). This suggests that reducing the frequency of fork reversal does not relieve the toxicity associated with accumulating genomic rNMPs in *rtt101*Δ cells. Next, we analysed whether the deletion of *POL32*, which was identified as a genetic suppressor of the CPT sensitivity of *rtt101*Δ cells (Buser et al., 2016), might confer a genetic rescue of *rtt101*Δ *RNH201-AID* pol2-M644G* cells. Rather than improving viability, the additional deletion of *POL32* in those cells decreased viability even further (Figure 28). When rNMPs accumulate in the genome, the loss of Pol32 impaired cell growth to a similar level as the loss of Rtt101, indicating that Pol32 fulfils an important role when genomic rNMPs accumulate, that is probably independent of Rtt101.

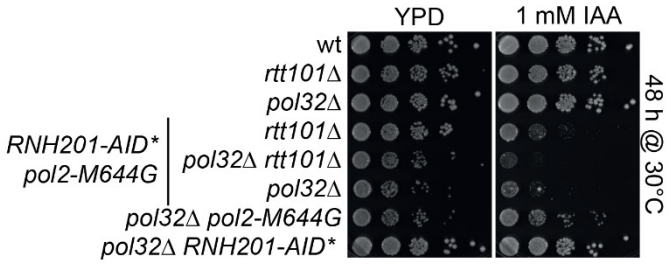

Figure 28. Pol32 is required for viability in a genetic pathway different from Rtt101 when genomic rNMPs accumulate. Haploid yeast strains of the indicated genotypes were grown over night in YPD medium at 30°C. Tenfold serial dilutions were spotted onto YPD plates and YPD plates containing 1 mM IAA. Plates were incubated at 30°C and images were taken after 48 hours.

While performing the SGA screen for genetic suppressors of the CPT and MMS sensitivity of *rtt101*Δ cells during my master thesis, we also scored synthetic interactions of the tested double mutants. As only the list of suppressors was published (Buser et al., 2016), the synthetic genetic interactions are summarized in the following (Table 1).

Table 1. Summary of negative genetic interactions of *rtt101Δ* identified by SGA approach

ARP5	+++	*CTK1*	++	*MRPL20*	++	*PPA2*	++
BUD25	+++	*CTR9*	++	*MRPL22*	++	*RAD6*	++
CCR4	+++	*CWH36*	++	*MRPL23*	++	*RMD9*	++
DBP9	+++	*DIA4*	++	*MRPL25*	++	*RMI1*	++
EMI2	+++	*DLD3*	++	*MRPL32*	++	*RNR4*	++
ICT1	+++	*DOA4*	++	*MRPL35*	++	*RPB9*	++
MRPL15	+++	*DSS1*	++	*MRPL36*	++	*RPL42a*	++
MSE1	+++	*FZO1*	++	*MRPL37*	++	*RPN9*	++
MSM1	+++	*GCD7*	++	*MRPL38*	++	*RPS9b*	++
MST1	+++	*GCN5*	++	*MRPL40*	++	*RRG1*	++
PMC1	+++	*GEP5*	++	*MRPL49*	++	*RSM19*	++
POP2	+++	*GIS2*	++	*MRPL51*	++	*RSM23*	++
RPO41	+++	*GYP6*	++	*MRPL6*	++	*RSM25*	++
RSM18	+++	*HEM14*	++	*MRPL7*	++	*RSM27*	++
RSM23	+++	*HER2*	++	*MRPS12*	++	*RTT101*	++
SMD2	+++	*HFI1*	++	*MRPS16*	++	*RTT105*	++
SOM1	+++	*HSP60*	++	*MRPS18*	++	*SEC22*	++
SPC98	+++	*ILM1*	++	*MRPS5*	++	*SFH1*	++
STE11	+++	*ISM1*	++	*MRPS8*	++	*SHP1*	++
UAF30	+++	*MAP1*	++	*MRX1*	++	*SLS1*	++
VMA16	+++	*MCM5*	++	*MRX14*	++	*SNF7*	++
YGL082W	+++	*MEF1*	++	*MSF1*	++	*SNF8*	++
YGL165C	+++	*MEF2*	++	*MSR1*	++	*SNU66*	++
AIM10	++	*MHR1*	++	*MSW1*	++	*SWS2*	++
AIM22	++	*MIM1*	++	*MSY1*	++	*TAD3*	++
AIM3	++	*MKK1*	++	*MYO1*	++	*TDA5*	++
ANP1	++	*MNN10*	++	*NAT1*	++	*TOP3*	++
ARD1	++	*MRF1*	++	*NPR2*	++	*TUF1*	++
ARG7	++	*MRH4*	++	*OCT1*	++	*UBX6*	++
ATP11	++	*MRP1*	++	*OST4*	++	*ULP2*	++
ATP15	++	*MRP10*	++	*PAF1*	++	*VEL1*	++
AVT2	++	*MRP17*	++	*PDR17*	++	*VID24*	++
BDF1	++	*MRP20*	++	*PEP3*	++	*VMA21*	++
CCM1	++	*MRP21*	++	*PEP5*	++	*VPH2*	++
CCR4	++	*MRP51*	++	*PET112*	++	*VPS16*	++
CDC3	++	*MRP7*	++	*PET123*	++	*VPS20*	++
CDC40	++	*MRPL11*	++	*PET130*	++	*VPS34*	++
CHM7	++	*MRPL19*	++	*POP2*	++	*YCS4*	++

YEF3	++	*CYS4*	+	*IRA1*	+	*NSR1*	+
YEL059W	++	*DAL81*	+	*IRC19*	+	*NUP1*	+
YHC1	++	*DEG1*	+	*ISC1*	+	*NUP120*	+
YJL015C	++	*DFG16*	+	*IWR1*	+	*NUP133*	+
YJL022W	++	*DHH1*	+	*JJJ1*	+	*NUP170*	+
YJL045W	++	*DIG1*	+	*KAR3*	+	*NUP84*	+
YJL047C-A	++	*DST1*	+	*KRE6*	+	*OPI3*	+
YKL118W	++	*EAF1*	+	*KTI11*	+	*PAP2*	+
YLR235C	++	*EAP1*	+	*KTI12*	+	*PCP1*	+
YLR317W	++	*ECM13*	+	*LOA1*	+	*PEP12*	+
YLR338W	++	*EFG1*	+	*LRP1*	+	*PEP7*	+
YML6	++	*ELP3*	+	*LSM6*	+	*PER1*	+
YNL184C	++	*END3*	+	*LSM7*	+	*PFK1*	+
YOR331C	++	*ERI1*	+	*LST4*	+	*PHO85*	+
YPR099C	++	*EXO5*	+	*LST7*	+	*PMR1*	+
ZAP1	++	*FLX1*	+	*LTE1*	+	*POR1*	+
ACL4	+	*FYV5*	+	*LTV1*	+	*PPT2*	+
ADA2	+	*FYV6*	+	*MDL2*	+	*PRE9*	+
ADH3	+	*FYV7*	+	*MDM12*	+	*RAD50*	+
ADO1	+	*GEP3*	+	*MDM20*	+	*RAI1*	+
AFG3	+	*GEP4*	+	*MDM31*	+	*REI1*	+
ARC1	+	*GET1*	+	*MDM32*	+	*RGP1*	+
ARP8	+	*GET2*	+	*MET18*	+	*RIM1*	+
ATP25	+	*GLN3*	+	*MET7*	+	*RIM13*	+
BEM2	+	*GSH1*	+	*MGM1*	+	*RIM20*	+
BFR1	+	*GTF1*	+	*MGM101*	+	*RIM21*	+
BRO1	+	*HBT1*	+	*MIP1*	+	*RIM8*	+
BUB3	+	*HCR1*	+	*MMM1*	+	*RMR1*	+
BUD21	+	*HIT1*	+	*MRM1*	+	*RNR4*	+
BUD26	+	*HMI1*	+	*MRPL27*	+	*RPD3*	+
BUD27	+	*HMO1*	+	*MRS1*	+	*RPL16b*	+
CGI121	+	*HNT3*	+	*MRT4*	+	*RPL19b*	+
CHO2	+	*HOM6*	+	*MSD1*	+	*RPL1b*	+
CIK1	+	*HSL7*	+	*MSL1*	+	*RPL20a*	+
CPR7	+	*HTA1*	+	*MTF2*	+	*RPL20b*	+
CSG2	+	*HTD2*	+	*MTG1*	+	*RPL21a*	+
CST26	+	*HUR1*	+	*MTG2*	+	*RPL23b*	+
CTK2	+	*IKI1*	+	*MTQ2*	+	*RPL2b*	+
CTK3	+	*IMG1*	+	*NAT3*	+	*RPL37b*	+
CYS3	+	*INO4*	+	*NPL3*	+	*RPL42b*	+

RPL43a	+	*SAC6*	+	*TOM5*	+	YDL034W	+
RPL6a	+	*SAM37*	+	*TPS2*	+	YDR417C	+
RPL7a	+	*SEH1*	+	*TPS3*	+	YDR433W	+
RPP2b	+	*SGO1*	+	*TRK1*	+	YDR442W	+
RPS10a	+	*SIC1*	+	*UBI4*	+	*YEF1*	+
RPS16a	+	*SLX5*	+	*UMP1*	+	YGL046W	+
RPS19b	+	*SLX8*	+	*UTR1*	+	YGL088W	+
RPS21b	+	*SNF6*	+	*VMA11*	+	YGL218W	+
RPS23b	+	*SPE1*	+	*VMA13*	+	YGR064W	+
RPS6b	+	*SPE2*	+	*VMA22*	+	YGR122W	+
RPS7a	+	*SPT4*	+	*VMA9*	+	YGR160W	+
RPS9b	+	*SRB5*	+	*VPH1*	+	YJL175W	+
RRF1	+	*SRB8*	+	*VPS24*	+	YLR358C	+
RRG8	+	*SSE1*	+	*VPS25*	+	*YME1*	+
RRM3	+	*SSN2*	+	*VPS27*	+	YMR242W-A	+
RRP6	+	*SSN3*	+	*VPS28*	+	YNL226W	+
RRP8	+	*SSN8*	+	*VPS3*	+	YNL228W	+
RSA1	+	*STB5*	+	*VPS41*	+	YOR200W	+
RSC1	+	*STE50*	+	*VPS61*	+	YOR235W	+
RSM22	+	*SUV3*	+	*VPS69*	+	YOR309C	+
RTC1	+	*SWA2*	+	*XRN1*	+	*YPK1*	+
RTS1	+	*TCO89*	+	*XRS2*	+	YPL205C	+
RVS167	+	*TFB5*	+	YBL071C-B	+	*YRB2*	+
SAC1	+	*THP1*	+	YBR266C	+	*YTA12*	+
SAC3	+	*TIM18*	+	*YDJ1*	+	*YVH1*	+

Genetic interaction of the indicated genes with RTT101 deletion were scored manually for lethality (+++), strong negative interaction (++) and weak negative interaction (+).

Discussion

In this work we have gained insight into the function of the Rtt101 E3 ubiquitin ligase at stalled replication forks. Employing yeast genetics combined with molecular and cell biological approaches, we found that upon DNA damage caused by MMS Rtt101 modulates the replisome component Mrc1. This allows DNA replication to resume *via* a recombination-mediated mechanism presumably as a consequence of altered protein-protein interactions of Mrc1 within the replisome.

We further uncovered a previously unknown role of $Rtt101^{Mms22}$ in the tolerance of misincorporated genomic ribonucleotides. $Rtt101^{Mms22}$ is not involved in the direct removal of rNMPs or in the regulation of an alternative removal pathway. Instead, we suggest that Rtt101 coordinates the remodelling of stalled replication forks presumably through ubiquitylation of the DNA polymerase ε subunit Dpb2 to allow tolerance of rNMPs. Moreover, when rNMPs accumulate, Rtt101-mediated ubiquitylation of histone H3 and the upstream Rtt109-dependent acetylation of H3 on lysine 56 are crucial for cell viability.

4.1 The role of Rtt101 at replication forks stalled by MMS-induced DNA lesions

Several cullin-based E3 ubiquitin ligases are important for processes regulating cell cycle progression, DNA replication and the response to DNA damage (reviewed in (Villa-Hernández et al., 2017)). In line with this, yeast cells lacking the CUL4 ortholog Rtt101 display sensitivity to DNA damaging agents such as MMS and are defective in replication fork restart when DNA lesions accumulate (Luke et al., 2006). This damage sensitivity is shared by cells lacking any member of the Rtt101-Mms1-Mms22 E3 ligase complex and can be offset by the deletion of *MRC1* (Figure 7).

A simplified explanation for this genetic suppression would be that in the absence of Rtt101, Mrc1 protein accumulates and causes toxicity in the presence of DNA damage. Indeed, Mrc1 protein levels are controlled in response to DNA damage by the SCF E3 ligase employing Dia2 as substrate adaptor (Mimura et al., 2009). SCF^{Dia2}-mediated degradation of Mrc1 promotes checkpoint recovery and is required for recombination-mediated fork restart (Chaudhury and Koepp, 2017; Fong et al., 2013). Rtt101 could act in a parallel pathway targeting a different subset of Mrc1 protein or acting upon a different condition. However, in contrast to *dia2Δ* mutants,

cells lacking Rtt101 did not stabilize Mrc1 protein levels (Figure 8) suggesting that Rtt101 does not globally regulate Mrc1 abundance in response to replication stress.

4.1.1 Rtt101 counteracts a replicative function of Mrc1

While Mrc1 is required to transduce S phase checkpoint signalling from the 'sensor' kinase Mec1 to the 'effector' kinase Rad53 (Alcasabas et al., 2001), it is also an integral component of replication forks. Mrc1 is associated with active replisomes during unperturbed S phase (Katou et al., 2003), where it supports replication fork progression independent of its checkpoint function (Szyjka et al., 2005). This function in the regulation of fork progression is likely addressed to the Mrc1-Tof1-Csm3 or fork pausing complex (FPC) (Yeeles et al., 2017). Although Tof1 and Csm3 have been proposed to promote Mrc1 interaction with replisome components (Katou et al., 2003; Nedelcheva et al., 2005), Mrc1 also has a replication-associated role independent of the Tof1-Csm3 complex and is able to interact with replisome components independently of those two factors (Bando et al., 2009; Calzada et al., 2005). Indeed, both the C-terminus and the N-terminus of Mrc1 interact with Pol2, the catalytic subunit of the leading strand polymerase Pol ε (Lou et al., 2008) as well as with Mcm6, a subunit of the MCM helicase (Komata et al., 2009). The fact that in cells lacking Rtt101^{Mms22} the checkpoint-defective *mrc1$_{AQ}$* allele behaved like wildtype Mrc1 (Figure 9) excludes that checkpoint function of Mrc1 is toxic in *rtt101Δ* cells. Moreover, the suppressive effect could not be achieved by disruption of the FPC. Instead, it could be partially phenocopied by the abrogation of Mrc1-Mcm6 interaction. It is thus likely that a replicative function of Mrc1 outside of the FPC is regulated through Rtt101 in response to replication stress.

4.1.2 Modulation of Mrc1 allows restoration of HR

The loss of Rtt101^{Mms22} is associated with decreased sister chromatid recombination in response to DNA damage caused by MMS or CPT (Duro et al., 2008). Consistently, treatment with MMS results in a reduced formation of Rad52 foci in *rtt101Δ* and *mms22Δ* cells (Figure 11C). Interestingly, in unchallenged conditions an increase in Rad52 foci formation is reported in cells lacking Rtt101 or Mms1 (Alvaro et al., 2007). This could mean that those mutants experience more spontaneous DNA damage, or, as the authors prefer, that the resolution of Rad52 foci is impaired so that they are

more persistent, leading to a higher overall number of foci. Consistently, damage-induced degradation of Mms22 in an Rtt101-Mms1-dependent manner is required to limit Rad51 loading onto the ssDNA overhang (Diao et al., 2017) and thus would allow recombination to be completed. Additionally, the concomitant loss of Rtt101 and HR proteins such as Rad52 leads to synthetic lethality or sickness when cells experience mild replication stress (Figure 11A), indicating that HR is crucial when Rtt101 is non-functional. Interestingly, persistent Rad51-bound ssDNA results in a checkpoint recovery defect (Yeung and Durocher, 2011). The recovery from an MMS-induced DNA damage checkpoint is impaired in *rtt101Δ, mms1Δ* and *mms22Δ* cells (Luke et al., 2006; Duro et al., 2008) (Figure 10). The observation that loss of Mrc1 in those cells could alleviate both the defect in Rad52 foci formation and the defective recovery from a checkpoint arrest strongly points to a role for Mrc1 in the initiation or completion of HR. In support of that, the Mrc1-dependent reduction of HR in *mms22Δ* cells was confirmed by a plasmid-based reporter assay (Buser et al., 2016). Indeed, *mrc1Δ* cells exhibit a hyperrecombination phenotype that does not stem from a loss of S phase checkpoint function (Alabert et al., 2009; Xu et al., 2004).

How can the absence of Mrc1 upregulate HR in *rtt101Δ* cells? Mrc1 physically couples the CMG helicase with Pol ε through interactions with Mcm6 and Pol2, respectively (Komata et al., 2009; Lou et al., 2008). Upon replication fork stalling in response to HU, DNA unwinding becomes uncoupled from DNA synthesis in the absence of Mrc1, a process referred to as ‘replisome uncoupling’ (Katou et al., 2003). Similar to the complete loss of Mrc1, a C-terminal truncation mutant of Mrc1 as well as the *mcm6IL* mutant unable to interact with Mrc1 could suppress MMS sensitivity of *rtt101Δ* cells (Figure 12). This strongly suggests that altering interactions between Mrc1 and replisome components is sufficient to rescue Rtt101-deficient cells. Consequently, we suggest a model in which Rtt101-mediated modulation of Mrc1 allows replisome uncoupling, which improves HR-mediated repair or restart of stalled replication forks (Figure 29). Similarly, deletion of *DPB4*, one of the non-essential subunits of Pol ε implicated in mediating structural stability and DNA association of the polymerase (Aksenova et al., 2010; Ohya et al., 2000), might induce a change in inter-replisomal interactions, thus supporting replisome uncoupling when a replication fork encounters a DNA lesion.

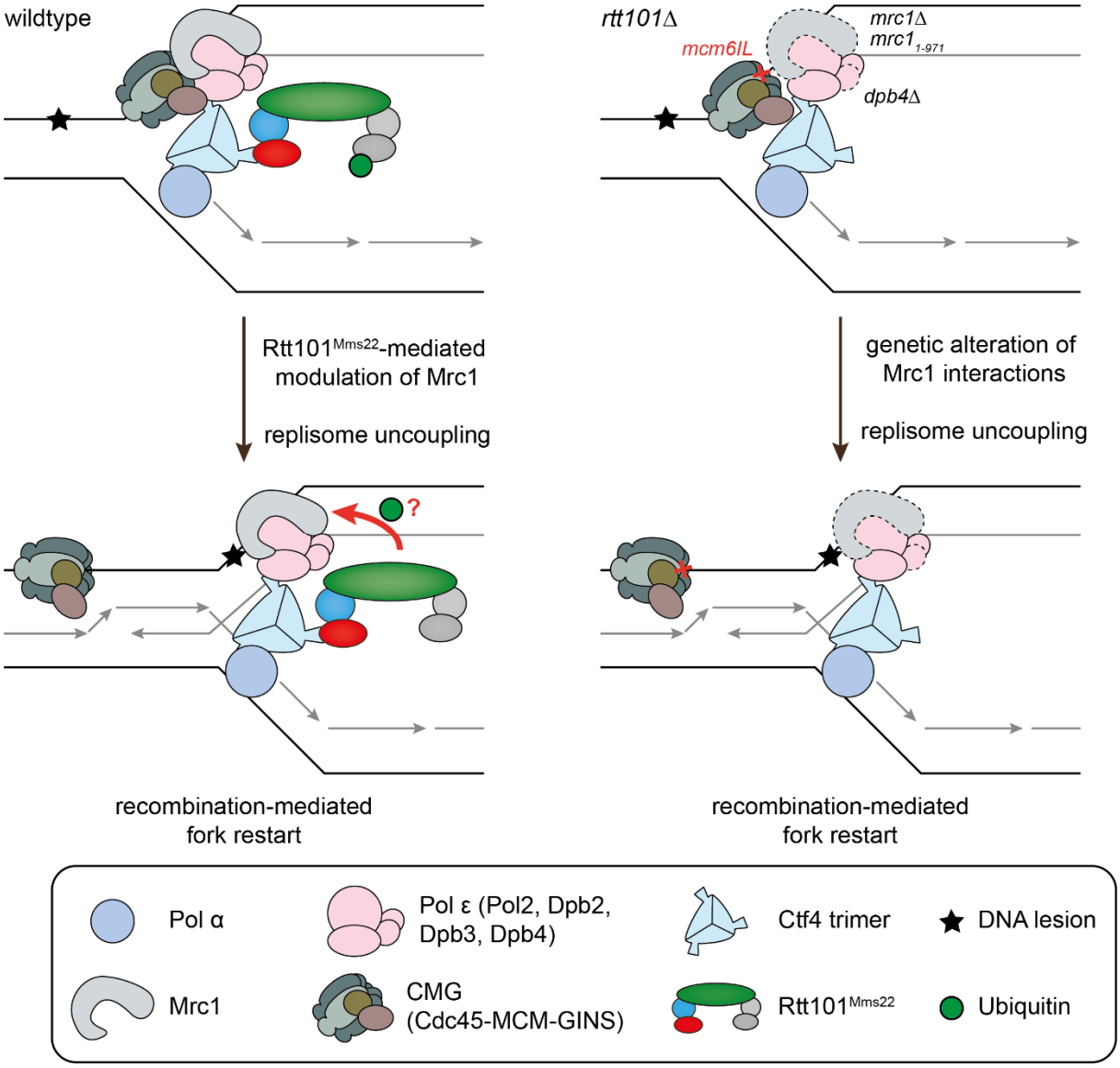

Figure 29. Model of Rtt101 function at stalled replication forks. In wildtype cells, Rtt101 is associated with active replisomes through the Mms22-Ctf4 interaction. At a DNA lesion such as caused by MMS, Rtt101-mediated modulation of Mrc1 leads to uncoupling of the CMG helicase and the DNA polymerases, thus creating ssDNA ahead of the stalled fork that can be used for a recombination-mediated fork restart. We speculate that Mrc1 might be a direct target of Rtt101, however the modulation could also be indirect. In *rtt101Δ* cells, a recombination-mediated fork restart becomes possible when the replisome structure is altered by genetic manipulation through *MRC1* deletion or when the Mrc1 protein is truncated in its C-terminus, when the interaction between Mrc1 and Mcm6 is abrogated, or when the DNA Pol ε subunit *DPB4* is deleted. Each of these modifications might facilitate uncoupling of the CMG helicase from the DNA polymerases and thus allow fork restart.

Intriguingly, the genetic rescue of MMS sensitivity of *rtt101Δ* cells described in this work involves changes in interactions of leading strand components. Leading and lagging strand are coupled by homotrimeric Ctf4, which interacts both with Pol α/Primase on the lagging strand and the CMG on the leading strand (Gambus et

al., 2009). Loss of Ctf4 is epistatic with the loss of Rtt101 with respect to MMS sensitivity, consistent with Ctf4 being the recruitment platform for Rtt101 *via* the interaction with Mms22 (Mimura et al., 2010; Buser et al., 2016). Strikingly, deletion of *MRC1* in *ctf4Δ* cells results in lethality due to loss of the interaction between Ctf4 and the CMG (Villa et al., 2016; Warren et al., 2004). This could mean that both Mrc1 and Ctf4 are important components of the replisome that coordinate the coupling between DNA unwinding and leading strand synthesis in the case of Mrc1 and between leading and lagging strand synthesis in the case of Ctf4. $Rtt101^{Mms22}$ might therefore regulate the Mrc1-dependent, leading strand-specific, pathway of replisome uncoupling in response to DNA lesions.

4.2 Unrepaired genomic ribonucleotides induce replication stress

One major threat for genome integrity coming from an endogenous source of damage are ribonucleotides that are mistakenly incorporated into nascent DNA during replication. Both human and yeast cells incorporate high numbers of ribonucleoside monophosphates (rNMPs) into their genome with every round of replication (Clausen et al., 2013b; Nick McElhinny et al., 2010a). The dedicated ribonucleotide excision repair (RER) pathway mediated by the RNase H2 enzyme ensures that most of those erroneously incorporated rNMPs are removed to prevent their accumulation (reviewed in (Cerritelli and Crouch, 2009)). The biochemical properties of rNMPs *per se* are interfering with DNA replication as the main replicative polymerases are less efficiently replicating across a single rNMP and are almost completely blocked when three or more consecutive rNMPs are present in the template DNA (Clausen et al., 2013b; Göksenin et al., 2012; Watt et al., 2011). Moreover, rNMPs alter the structure of DNA molecules and can thus have notable consequences on processes involving DNA-interacting proteins (Chiu et al., 2014; Derose et al., 2012; Jaishree et al., 1993; Rychlik et al., 2010; Tumbale et al., 2014). Besides their structural impact, faulty rNMP processing can occur in different modes. First, spontaneous hydrolysis at rNMPs induces single-stranded breaks (SSBs) that will become harmful in a subsequent S phase (Li and Breaker, 1999). Second, in an attempt to repair a misinserted rNMP, Top1 can either be trapped as a Top1 cleavage complex (Top1cc) after incising the DNA, or it can create DSBs (Huang et al., 2016; Sparks and Burgers, 2015). Third, if RNase H2 incises an rNMP in an unscheduled manner, abortive ligation results in

adenylate groups that are covalently linked to 5'-phosphate termini of those nicks and require aprataxin (or the yeast homolog Hnt3) to be removed (Ahel et al., 2006; Rass et al., 2007). Thus, the presence of rNMPs in the genome leads to replication stress by different means. Consequently, RER has to be tightly regulated.

4.2.1 Rtt101 becomes crucial in the absence of RNase H2

The unexpected finding that Rtt101 becomes vital for cells, in which RER is impaired (Figure 13) raises the question of what type of damage accumulates that requires Rtt101-dependent salvation. As overall rNMP levels in genomic DNA were not affected by the absence of Rtt101 or Mms22 (Figure 16), it is unlikely that the E3 ligase complex is actively involved in a removal process. We could further rule out that the alternative Top1-dependent repair pathway that is active in the absence of canonical RER causes the observed toxicity in *rtt101*Δ cells (Figure 17). This is particularly intriguing since cells lacking Rtt101 are extremely sensitive to the Top1 poison CPT (Luke et al., 2006), suggesting that damage arising from covalently DNA-bound Top1ccs requires Rtt101 to be tolerated. Although in RER-deficient cells in terms of mutagenesis and chromosome rearrangements Top1 has been pointed out as the underlying cause (Kim et al., 2011; Williams et al., 2017), we speculate that a yet to be defined source of damage other than Top1cc requires Rtt101 to be tolerated.

4.2.2 HR is vital when rNMPs accumulate and *MRC1* deletion reduces toxicity

Huang and colleagues showed in the *pol2-M644G* strain background that the combined loss of RNase H2 and Rad52 is lethal, and cells lacking both RNase H2 and Rad51 grow poorly (Huang et al., 2016). They further showed that this is due to Top1-dependent generation of DSBs that require HR to be repaired. Consequently, deletion of *TOP1* could offset this negative genetic interaction. Although we excluded Top1-mediated processes as the source of damage in *rtt101Δ* cells, the fact that viability of *rtt101Δ* cells facing MMS-induced damage also depends on HR (Figure 11) led us to investigate the effect of HR deficiency in *rtt101Δ* cells accumulating genomic rNMPs. The observed additive effect can be explained by Rtt101 functioning in a genetic pathway independent of HR, or by a requirement for HR when rNMPs accumulate in the absence of Rtt101 (Figure 18A). It would be interesting to see whether the deletion of *TOP1* in *RNH201-AID* pol2-M644G* cells lacking both Rtt101 and Rad51 restores

viability to a level of the *rtt101Δ RNH201-AID* pol2-M644G* mutant, or whether the concomitant loss of Rad51 and Rtt101 exhibits Top1-independent additivity.

MRC1 deletion confers a rescue of *rtt101Δ* cells that accumulate genomic rNMPs (Figure 18). This opens the possibility that, in analogy to MMS-induced lesions, Rtt101 might modulate Mrc1 also at misincorporated rNMPs to allow replisome uncoupling. Indeed, by employing the checkpoint-defective *mrc1$_{AQ}$* allele this rescue could not be achieved, strongly indicating that the loss of a replicative Mrc1 function leads to increased viability. We like to point out that this rescue is only partial: the deletion of *MRC1* does not restore viability to a level comparable to wildtype growth as we have previously seen for growth of *rtt101Δ mrc1*Δ cells on MMS (Figure 7). The loss of Mrc1 in *RNH201-AID* pol2-M644G* mutants does not result in any visible growth impairment, thus it is likely that the accumulation of rNMPs in the absence of Rtt101 might have additional consequences on viability other than inducing fork stalling. Moreover, based on their spontaneous DNA damage checkpoint activation and G2/M arrest, *rtt101Δ mrc1Δ RNH201-AID* pol2-M644G* cells seem to accumulate even more unresolved damage than if either Rtt101 or Mrc1 is present. Thus, even though fork restart at sites of rNMP-induced stalling might be enhanced by the loss of Mrc1, this does not completely abolish the threat posed by accumulating rNMPs in the absence of Rtt101.

4.2.3 RER might be cell cycle regulated

While the mechanism of ribonucleotide excision repair is well studied (Sparks et al., 2012), little is known about the timing of this repair. The Rnh202 subunit of the RNase H2 complex harbours a PCNA-interacting peptide (PIP) (Chon et al., 2013), and in human cells this PIP box supports localization of RNase H2 to sites of replication and PCNA-dependent repair (Bubeck et al., 2011). However, a yeast RNase H2 mutant lacking this PIP box does not exhibit a phenotype different from the wildtype enzyme both in the presence and absence of Rtt101 (not shown), and its *in vitro* activity is indistinguishable from wildtype RNase H2 (Chon et al., 2013). Whether RNase H2 is recruited to active replication forks by other means than its interaction with PCNA remains to be discovered. Based on the results we obtained using cell cycle-restricted alleles of *RNH202* (Figure 20), we conclude that allowing expression of *RNH202* and thus activity of the RNase H2 complex only in late S phase or G2 phase by using the *G2-RNH202-TAP* allele is sufficient to circumvent the need for Rtt101. Strikingly, we

observed that expressing *RNH202* only throughout S phase causes an even bigger load of replication stress in *rtt101*Δ cells than the deletion of *RNH202*. This could mean that if RNase H2 is active in S phase, a second RNase H2-dependent reaction is required at a later point to process intermediate repair products. If those repair products accumulate in the absence of Rtt101, viability of cells decreases, and the DNA damage checkpoint is activated. Alternatively, RNase H2-dependent incision at rNMPs might normally be prevented during S phase. Indeed, unscheduled rNMP incision can lead to abortive ligation events during which the 5'OH group at the resulting nick is adenylated, resulting in a 5'-AMP (reviewed in (Schellenberg et al., 2015)). This bulky lesion needs to be removed by the action of aprataxin (Hnt3 in yeast). When rNMPs accumulate as they do in a *pol2-M644G* mutant, loss of Hnt3 is lethal for cells. The lethality can be rescued by the additional inactivation of RNase H2, suggesting that RNase H2-mediated processing of rNMPs requires Hnt3 activity (Tumbale et al., 2014). Interestingly, we identified *HNT3* in a synthetic interaction screen as a negative genetic interactor of *RTT101* (see Appendix, Table 1). This suggests that an accumulation of 5'-AMP is less well tolerated in the absence of Rtt101. Consequently, unscheduled RER in S phase could lead to the increased formation of 5'AMPs, which induce replication stress in *rtt101*Δ cells. We favour this explanation over a possible two-step mechanism of RER since the G2-restricted *RNH202* allele did not show any negative effect on viability, indicating that the presence of RER activity throughout G2 phase is sufficient for repair.

4.3 Mass spectrometric approach to identify Rtt101-dependent ubiquitylation when genomic rNMPs accumulate

The identification of target proteins that are ubiquitylated by a certain E3 ligase is a challenge. A hypothesis-driven analysis might reveal the stabilization of a candidate substrate in the absence of the E3 enzyme, however especially non-degrading ubiquitylation would be missed with biased assays such as cycloheximide chase or promoter shut-off experiments. The ongoing improvement of mass spectrometric approaches allowed to identify many ubiquitylation targets in mammals and yeast in an unbiased manner, with most of those methods relying on the mass shift of a peptide induced by the covalent post-translational modification with ubiquitin (reviewed in (Xu and Jaffrey, 2013)). The ubiquitin or di-glycine remnant profiling makes use of a small

ubiquitin-derived di-glycine peptide (di-gly) that after trypsinization remains covalently linked to the previously ubiquitylated lysine in a target protein, resulting in a mass shift of 114.1 Dalton (Da) compared to the unmodified peptide (Peng et al., 2003). An enrichment step for those di-gly-modified peptides using a monoclonal antibody (Xu et al., 2010) improves the identification of site-specific ubiquitylation of target proteins. Combined with SILAC (Ong et al., 2002), di-gly remnant profiling directly compares the abundance of a ubiquitylation site in the presence and absence of the E3 ligase investigated. Trypsin cleaves C-terminally after arginine (R) and lysine (K) residues. However, the modified lysine is usually excluded from trypsin digest due to sterical hindrance, thus remaining situated internally within a peptide or at its N-terminus (Olsen et al., 2004; Peng et al., 2003). The very C-terminal RGG sequence of ubiquitin is shared with the closely related NEDD8 (Rub1 in yeast). Thus, the method does not allow a discrimination between ubiquitylation and neddylation. However, the main targets of neddylation are cullins (Rabut et al., 2011), so it is relatively unlikely that any of the identified modifications would represent a neddylated site on a different type of protein. SUMO, another small protein modifier closely related to ubiquitin, is also attached through its C-terminal glycine residue followed by a second glycine (reviewed in (Müller et al., 2001)). The identification of SUMOylated peptides however can be excluded in the analysis of ubiquitin remnant profiling as the tryptic digest leaves a longer peptide on a SUMOylated lysine (Impens et al., 2014).

The use of di-glycine remnant profiling enabled us to identify potential target proteins of the Rtt101 E3 ligase during an S phase in which RNase H2 is non-functional and the incorporation of rNMPs into genomic DNA is increased (Figure 24). We identified a list of candidate targets of Rtt101-mediated ubiquitylation encompassing different transmembrane transporters, metabolic enzymes and a proteasome subunit. One of the strongest candidates, Dpb2, is directly involved in DNA replication and might thus be a critical target in a situation where replication is impaired by the accumulation of genomic rNMPs.

4.3.1 Dpb2 is an important structural component of the replisome

DNA Polymerase B subunit 2 (Dpb2) is the second largest subunit of DNA polymerase ε and essential for viability of yeast cells (Araki et al., 1991). Besides Dpb2, Pol ε further comprises the biggest subunit Pol2 harbouring a polymerase and a 3'-5' proofreading activity in its N-terminal domain (Pol2N), while the C-terminal domain (Pol2C) is important for the structure of the polymerase complex (reviewed in (Hogg and Johansson, 2012)). Moreover, the small non-essential subunits Dpb3 and Dpb4 stabilize Pol ε association with DNA (Ohya et al., 2000; Tsubota et al., 2003; Aksenova et al., 2010). Strikingly, while a Pol2 mutant lacking the N-terminal catalytic domain is still viable and cells are able to replicate and repair DNA, loss of the C-terminal domain implicated in S phase checkpoint activation is lethal (Navas et al., 1995; Kesti et al., 1999).

Dpb2 interacts with a region of Pol2C that harbours two zinc finger (ZnF) motives. This interaction is important for S phase checkpoint activation as a mutation within the ZnF domain impairs checkpoint activation (Dua et al., 1998, 1999). Within Dpb2, the six most C-terminal amino acids have been indicated to be responsible for Pol2 interaction, and their mutation leads to cell death (Isoz et al., 2012). The assembly of Pol ε is regulated by Cdc28 (CDK1)-mediated phosphorylation of Dpb2 in late G1 phase (Kesti et al., 2004). While the Dpb2 C-terminus mediates interaction with Pol2, its N-terminal region directly interacts with Psf1, a subunit of the GINS complex of the CMG helicase (Sengupta et al., 2013). This interaction is essential for replication initiation and is thought to tether Pol ε to the replisome during DNA synthesis. Moreover, the CMG-Dpb2 interaction restricts Pol ε to the leading strand (Georgescu et al., 2014; Langston et al., 2014). In addition, a Ctf4-interacting motif in the Dpb2 N-terminus (residues 83-92) as well as a weak interaction with the Mrc1 central domain further enhance replisome tethering of Dpb2 and presumably the whole Pol ε complex (Lou et al., 2008; Villa et al., 2016). Of note, Dpb2 was further identified as an interaction partner of Mms22 during S phase (Buser et al., 2016), which would be required for $Rtt101^{Mms22}$-mediated ubiquitylation of Dpb2.

4.3.2 Possible consequences of Rtt101-mediated ubiquitylation of Dpb2

The identified Rtt101-dependent ubiquitylation of Dpb2 is situated at K419, which according to literature does not precisely match to any of the determined regions required for interaction with GINS, Ctf4, Mrc1 or Pol2, although it might be within or close to the portion of Dpb2 that contacts Pol2. The ubiquitin remnant profiling approach does not allow an identification of ubiquitin chain types. Thus, it remains to be determined whether K419 (i) is indeed an Rtt101-dependent ubiquitylation site, (ii) is modified with a monoubiquitin or a polyubiquitin chain, and (iii) whether ubiquitylation might directly interfere with one of the known interactions.

Once Rtt101 has been clearly identified as the E3 ligase modifying Dpb2, the circumstances of this modification will have to be determined. Originally detected in a scenario where rNMPs accumulate in the absence of RER, it will be interesting to see whether this modification of Dpb2 also occurs in unperturbed S phase or in the presence of MMS, CPT or HU. Moreover, the shared phenotype of *rtt101*Δ cells with cells lacking Mms1 or Mms22 suggests that the $Rtt101^{Mms22}$ E3 ligase becomes crucial for viability when genomic rNMPs accumulate. Therefore, ubiquitylation of Dpb2 might also depend on the presence of Mms1 and Mms22, which has to be experimentally confirmed. Further, a point mutant of Dpb2 in which K419 is replaced with an arginine (Dpb2-K419R) should phenocopy *rtt101*Δ cells and, more importantly, when combined with deletion of *RTT101* should be epistatic. Finally, identifying the linkage type of possible polyubiquitin chains attached to Dpb2 *via* the use of linkage specific antibodies or ubiquitin binding domains, or by employing ubiquitin mutants unable to form a specific type of linkage (K48R, K63R, etc.), will allow us to draw conclusions about the consequence of Dpb2 ubiquitylation.

If Dpb2 is indeed a true substrate of Rtt101 under conditions in which rNMPs are misincorporated, different consequences of such a modification are imaginable that do not have to be mutually exclusive. Considering that *MRC1* deletion through a checkpoint-independent function, improves viability of *rtt101*Δ *RNH201-AID* pol2-M644G* cells (Figure 18), it is tempting to speculate that Dpb2 ubiquitylation might act through the same mechanism. Mrc1 and Dpb2 directly interact with one another, moreover they both are in physical contact with the C-terminus of Pol2 (Dua et al., 1998, 1999; Isoz et al., 2012; Lou et al., 2008). In addition, Mrc1 contacts the Mcm6 subunit of the MCM helicase, while Dpb2 interacts with the GINS subunit Psf1 (Komata et al., 2009; Sengupta et al., 2013). Thus, the CMG complex and Pol ε are connected

through both Mrc1 and Dpb2 (Figure 30). According to the 'replisome uncoupling' model, a replication fork that encounters a ribonucleotide on the leading strand would stall and pause leading strand synthesis. Subsequently, the CMG helicase would have to lose contact with the rest of the replisome to continue unwinding of the parental duplex DNA beyond the lesion. We speculate that this uncoupling is facilitated in the absence of Mrc1 due to a partial loss of interaction between CMG and Pol ε (Figure 29). Similarly, ubiquitylation of Dpb2 could either interfere with the interaction of Dpb2 and the CMG, or with that of Dpb2 and Pol2. Both options are consistent with a monoubiquitylation event as well as with the attachment of a polyubiquitin chain other than K48-linked. Nevertheless, degradation of Dpb2 as a consequence of K48-linked polyubiquitylation could result in a similar outcome: the complete removal of Dpb2 would also weaken the interaction of Pol ε with the CMG and probably lead to its release from the replisome. In either way, recombination-mediated fork restart would be enabled to allow replication bypass of the misincorporated rNMP (Figure 30). This model could also be applied when considering SSBs as the main type of rNMP-induced DNA damage.

Selective degradation of DNA polymerase subunits has been reported in budding yeast, fission yeast and human cells. In budding yeast, the Pol δ subunit Pol3 is degraded upon UV irradiation, while the accessory subunits Pol31 and Pol32 remain intact (Daraba et al., 2014). This allows the association of Pol31 and Pol32 with TLS polymerases such as Rev1 or the Pol ζ complex Rev3-Rev7 (Daraba et al., 2014; Johnson et al., 2012). Fission yeast mutants lacking Swi1, the homolog of *S. cerevisiae* Tof1 and human Timeless, exhibit unstable forks at which Pol2, Pol3 and MCM subunits are ubiquitylated by SCF^{Pof3} (SCF^{Dia2} in budding yeast) and degraded through the ubiquitin proteasome system to prevent abnormal DNA replication (Roseaulin et al., 2013). Finally, in human cells the smallest subunit of Pol δ, p12, has to be degraded upon UV irradiation to prevent fork progression through damaged templates and to ensure viability (Terai et al., 2013). Of note, the Rtt101 ortholog CUL4 in complex with Cdt2 ($CRL4^{Cdt2}$) is responsible for p12 ubiquitylation, but p12 is not conserved in budding yeast. Taken together, several lines of evidence suggest that targeted degradation of DNA polymerase subunits in response to replication stress helps to prevent replication through damaged DNA or allow the employment of TLS polymerases that continue replication at the cost of increased mutation rates. Thus, another possible consequence of Rtt101-mediated ubiquitylation of Dpb2 could be that

it causes the removal of Pol ε from the site of fork stalling to subsequently replace Pol ε with a TLS polymerase that can replicate across the unrepaired rNMP. Intriguingly, *dpb2* mutants that show a reduced affinity to Pol2 displayed increased mutation rates (Jaszczur et al., 2008). The frequency of mutagenesis correlated with the degree of defective Dpb2-Pol2 interaction, and mutations were assigned to a more frequent participation of the TLS polymerase Pol ζ, strongly suggesting that destabilization of the Pol ε complex increases postreplicative repair events (Jaszczur et al., 2009; Kraszewska et al., 2012).

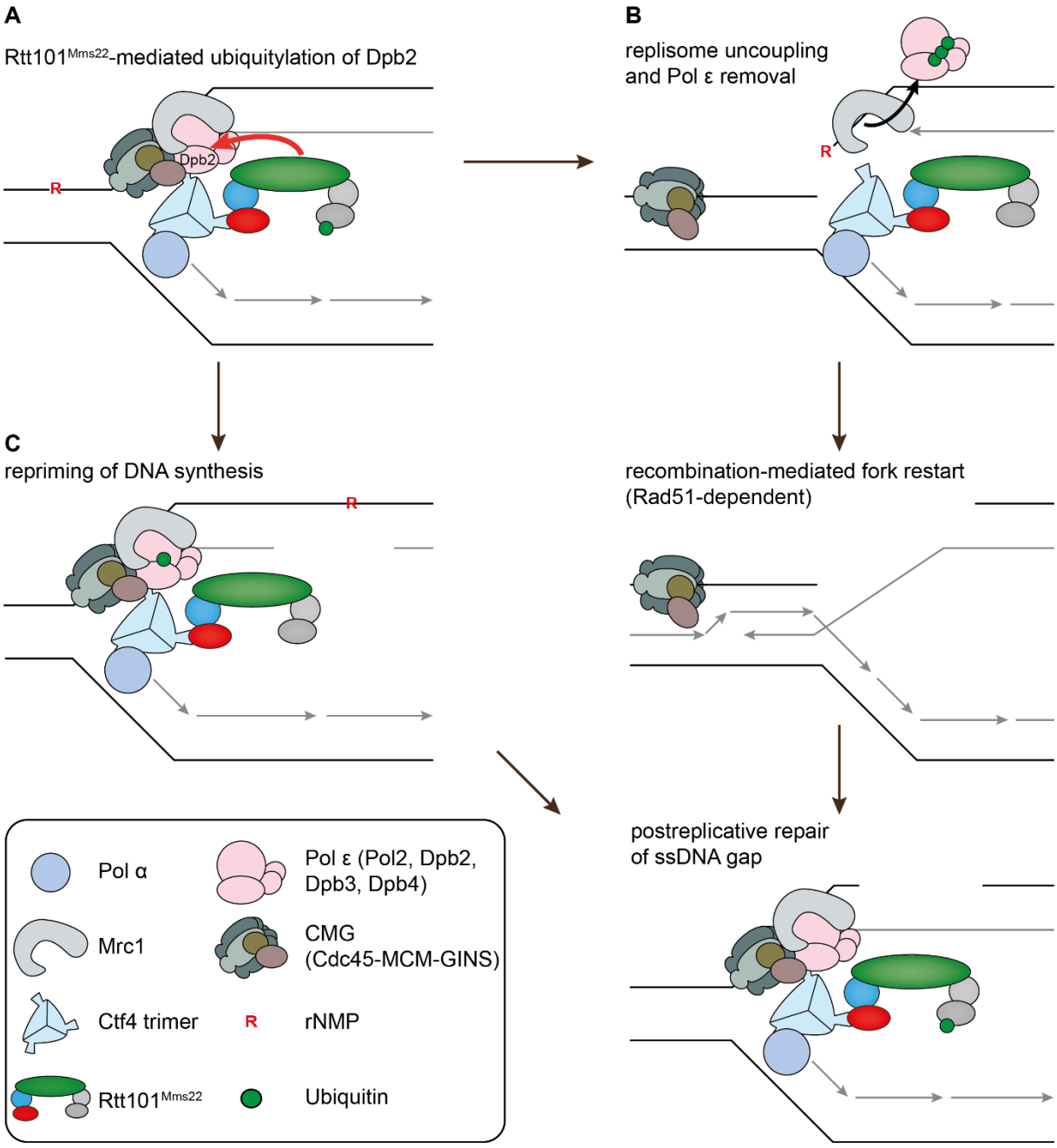

Figure 30. Rtt101 targets Dpb2 at misincorporated rNMPs. *Figure legend: see next page.*

Figure 30. Rtt101 targets Dpb2 at misincorporated rNMPs. (**A**) At a ribonucleotide incorporated into genomic DNA replication forks stall. Rtt101 targets the Pol ε subunit Dpb2 and ubiquitylates it at lysine 419. Depending on the type of DNA lesion caused by the rNMP, at least two different scenarios are possible. (**B**) If the rNMP previously underwent spontaneous hydrolysis, a single-stranded break will be present. We suggest that Rtt101-mediated ubiquitylation of Dpb2 leads to the extraction of Pol ε from the leading strand. Subsequently, resection of the free end and Rad51-mediated strand invasion into the sister chromatid allows recombination-mediated fork restart. A functional replisome is restored, and the remaining ssDNA gap can be repaired by postreplicative repair (TS or TLS).

4.4 H3K56Ac and H3 ubiquitylation

During DNA replication, parental histones that are temporally displaced ahead of replication forks subsequently are deposited on both DNA daughter strands. To maintain histone occupancy on both copies of the chromosome, *de novo* nucleosome assembly is directly coupled to replication fork progression (reviewed in (Prado and Maya, 2017)). Perturbation of this pathway renders cells sensitive to genotoxic agents (Clemente-Ruiz et al., 2011; Masumoto et al., 2005; Schneider et al., 2006). This is true for mutants defective for the upstream event of H3K56 acetylation (*rtt109Δ*, *asf1Δ and H3K56R)* as well as for double mutants defective for the redundant factors involved in downstream deposition of the modified H3-H4 dimers onto nascent DNA (CAF-1 mutants and *rtt106Δ*) (Clemente-Ruiz et al., 2011). However, H3K56Ac is critical for genome integrity beyond replication-coupled chromatin assembly. During normal cell cycle, the acetylation is removed in late S phase by Hst3 and Hst4 (Maas et al., 2006; Masumoto et al., 2005), but upon activation of the DNA damage checkpoint it is maintained at the site of damage (Thaminy et al., 2007), implicating a role for H3K56Ac in response to DNA damage. Rtt101 promotes H3K56Ac deposition onto newly replicated DNA through ubiquitylation of H3, and the lack of Rtt101-mediated H3 ubiquitylation interferes with nucleosome assembly (Han et al., 2013). On the other hand, an accumulation of rNMPs influences the interaction of DNA with proteins, the most frequent of those interactions would be represented by nucleosomes (Dunn and Griffith, 1980; Hovatter and Martinson, 1987). Thus, the toxicity observed in *rtt101*Δ *RNH201-AID* pol2-M644G* cells could be the additive effect of reduced *de novo* nucleosome assembly on nascent DNA and a general destabilization of nucleosome binding to rNMP-containing DNA.

4.4.1 H3 ubiquitylation becomes crucial when genomic ribonucleotides accumulate

Indeed, the loss of Rtt109 or Asf1, which leads to a complete absence of H3K56Ac (Figure 22A), has a severe impact on viability of *RNH201-AID* pol2-M644G* cells in the presence of auxin. Compared to *RTT101* deletion, the negative effect exerted by *RTT109* and *ASF1* deletion was even stronger since viability was compromised when Rnh201-AID* was depleted in *rtt109Δ* or *asf1Δ* cells expressing wildtype *POL2* instead of the *pol2-M644G* allele (Figure 21). This observation could be phenocopied by histone point mutants that cannot be acetylated by Rtt109 (*H3K56R*) or ubiquitylated by Rtt101 (*H3-3KR*), implicating that both histone marks become important when genomic rNMPs accumulate.

Measuring nucleosome occupancy by H3 ChIP experiments, as well as measuring the deposition of newly synthesized H3-H4 dimers by H3K56Ac ChIP experiments did not reveal any significant defect in nucleosome assembly when cells accumulate rNMPs (Figure 22, Figure 23). We assume that the ChIP method offers a readout sensitive enough to detect defects in nucleosome deposition as in both *rtt109Δ* and *asf1Δ* mutants H3K56Ac levels were highly reduced. Thus, we conclude that rNMPs incorporated into genomic DNA do not change nucleosome occupation or deposition efficiency. However, we cannot exclude that the interaction between nucleosomes and DNA is altered in a way that changes the chromatin structure and might impede fork progression or stability, which we are not able to detect using ChIP. This possibility will be addressed in the future by DNA combing experiments that are frequently used to quantify DNA replication dynamics and fork stalling and restart events (García-Rodríguez et al., 2018; Luke et al., 2006).

We would like to point out that in our hands *rtt101Δ* cells did not show a defect in H3K56Ac deposition as previously described at the tested loci (Han et al., 2013). To exclude possible secondary mutations in the strain used for the ChIP assay, we supplemented those *rtt101Δ* cells with either an empty control plasmid or a plasmid expressing wildtype Rtt101 and tested the MMS and CPT sensitivity of the resulting strains. As expected, the *rtt101Δ* cells containing the control plasmid were sensitive to both drugs, while expression of plasmid-born Rtt101 completely rescued drug sensitivity (data not shown). Thus, the inconsistent ChIP result is most likely not due to a faulty strain. Recently, several labs reported significant differences in specificity of different commercially available antibodies against H3K56Ac and cross-reactivity with

other acetylated lysines in H3 (Drogaris et al., 2012; Pal et al., 2016). For our experiments, the antibody was purchased by Active motif, which is among those antibodies displaying an imperfect specificity for H3K56Ac. The supplier of the antibody used in the ChIP experiments by Han and colleagues is not explicitly named (Han et al., 2013), thus their use of a different antibody could be a possible reason for the deviating results.

Comparing the loss of viability in *RNH201-AID* pol2-M644G* cells expressing either the non-acetylatable *H3K56R* or the non-ubiquitylatable *H3-3KR* mutant, lack of H3 acetylation is more detrimental than lack of ubiquitylation. This might reflect additional functions of H3K56Ac, while H3 ubiquitylation might be exclusively important during nucleosome assembly in the transfer of the H3-H4 dimer from Asf1 to the downstream histone chaperones Rtt106 or CAF-1. Indeed, H3K56Ac, like Rtt101^{Mms22}, is implicated in promoting sister chromatid recombination (Endo et al., 2010). Moreover, the acetylation is proposed to ensure that the preferred repair template after a replication-born DSB is the replicated sister chromatid (Muñoz-Galván et al., 2013). Loss of H3K56Ac delays replication completion in the presence of CPT or MMS, and cells enter mitosis with persistent Rad51 and Rad52 foci (Wurtele et al., 2012). A further indication for an Rtt101-independent function of H3K56Ac is the fact that the deletion of *HST3* and *HST4* inhibits BIR due to inhibition of long gap repair synthesis, a defect that could be rescued by deletion of *RTT109* or *ASF1*, but not *MMS22* (Che et al., 2015). This is consistent with a requirement for Hst3 in the faithful maintenance of an artificial chromosome III with longer than average inter-origin distances (Irene et al., 2016).

Rtt101 association with chromatin in response to MMS treatment as measured by chromatin spreads has been shown to depend on Rtt109 (Roberts et al., 2007). Although we recently published that Rtt101 associates with active replisomes during unperturbed S phase through the Mms22-Ctf4 interaction (Buser et al., 2016), Rtt109-mediated H3K56Ac might further stabilizes Rtt101 at stalled forks. This is reminiscent of recruitment of the MMS22L-TONSL complex in human cells, which recognizes unmethylated H4K20, a histone mark associated with newly synthesized histones in human cells (Saredi et al., 2016).

To our knowledge, the results presented in this thesis are the first to demonstrate a requirement for the H3K56Ac pathway implicated in replication-coupled nucleosome assembly when genomic rNMPs accumulate.

4.4.2 Newly synthesized H3-H4 might recruit DNA repair factors

The laboratory of Jessica Tyler has recently proposed a model in which newly synthesized histones are deposited onto resected ssDNA at an induced DSB (Huang et al., 2018). They argue that damage-induced phosphorylation of the histone chaperone ASF1A in human cells triggers the deposition of newly synthesized H3-H4 dimers carrying the H4K20me0 mark (Huang et al., 2018), which in turn recruits the MMS22L-TONSL complex (Saredi et al., 2016). Thus, the transient deposition of histones on ssDNA would help to coordinate repair factors, and in case of MMS22L to promote RAD51 loading (Piwko et al., 2016). While a direct proof of this model in human cells was not possible due to technical difficulties, an HO-induced DSB in a yeast strain lacking donor sequences for repair allowed them to monitor resection kinetics by real-time PCR at the site flanking the DSB (Huang et al., 2018). Measuring histone occupancy by H3 ChIP over time, they could observe a retention of histones at already resected and thus single-stranded DNA. The idea of histones occupying ssDNA is not new: early electron microscopy-based studies reconstituted nucleosome structures on ssDNA that were morphologically indistinguishable from those reconstituted on dsDNA (Palter et al., 1979). Moreover, a recently published *in vitro* study revealed that resection can take place on nucleosomal templates without ejecting nucleosomes from the template DNA (Adkins et al., 2017). In this *in vitro* system, ssDNA wrapped around nucleosomes was preferentially recognized by the chromatin remodelling enzyme Fun30 over double-stranded nucleosomal DNA, and the interaction promoted Fun30 ATPase activity. Intriguingly, Fun30 is recruited to a DSB in an Exo1- and Sgs1-dependent manner, where it is important for efficient RPA and Rad51 loading (Chen et al., 2012). Therefore, histone deposition on ssDNA might exert a functional role in coordinating repair processes. Rtt101-mediated ubiquitylation of H3 has been described as an intermediate step throughout *de novo* nucleosome assembly (Han et al., 2013). Whether this modification has any further consequence once nucleosomes are assembled on DNA, whether it is removed in a regulated way and whether it might offer a recruitment platform for other proteins remains to be investigated. It would be interesting to dissect why H3 ubiquitylation becomes crucial when cells accumulate rNMPs (Figure 21C). Although we do not have any indication for an increase in two-ended DSBs in this scenario as they would appear upon an HO endonuclease cut, stalled or collapsed replication forks also exhibit stretches of ssDNA and upon breakage need to be resected to allow fork restart. Thus, also at replication

forks nucleosomes might be transiently deposited on ssDNA and might promote repair functions, possibly through modifications such as H3K56Ac and H3 ubiquitylation.

4.4.3 The role of Rtt101 in nucleosome assembly and fork stability might be interdependent

The requirement for Rtt101-dependent H3 ubiquitylation in the presence of accumulating rNMPs might reflect a general need for functional replication-coupled nucleosome assembly in this situation mediated by the acetylation and ubiquitylation marks. This would not have to be directly coupled to the fork but could present an additional repair-supporting pathway. However, there are some indications that there could be a direct relation between fork problems and nucleosome assembly. First, the deletion of *MRC1* is able to rescue the MMS sensitivity of nucleosome assembly mutants *rtt109*Δ, *H3K56R* and *asf1*Δ (Hang et al., 2015; Luciano et al., 2015). Consistent with our observations in *rtt101*Δ cells, the checkpoint-deficient $mrc1_{AQ}$ allele does not confer this genetic rescue, while a C-terminal truncation of the Mrc1 protein does (Luciano et al., 2015). This suggests that the H3K56Ac pathway functionally interacts with replisomes in the presence of replication stress. Moreover, the *asf1*Δ mutant when combined with deletion of the helicase *RRM3* is inviable due to mitotic catastrophe (Luciano et al., 2015). This lethality could be offset by genetically uncoupling Ctf4 and GINS using a C-terminal truncation mutant of Ctf4. Interestingly, an N-terminal truncation mutant of Ctf4 that is unable to bind to Mms22 (Mimura et al., 2010) conferred lethality when expressed in *asf1*Δ *rrm3*Δ mutants (Luciano et al., 2015). The authors speculate that H3K56Ac modulates replisomes when challenged by DNA damage through the Mms22-Ctf4 interaction to promote uncoupling. The hypothesis that H3K56Ac is required for Mms22 function at stalled replisomes is consistent with a report showing that Rtt101 recruitment to chromatin is promoted by Rtt109 and H3K56Ac (Roberts et al., 2007). Together these findings propose a model (Figure 31) in which H3K56Ac helps to recruit the Rtt101 protein probably accompanied by Mms1 to DNA where it acts as the $Rtt101^{Mms22}$ E3 ligase to promote uncoupling of replisomes in the presence of DNA damage. As Mms22 does not seem to be involved in H3 ubiquitylation (Han et al., 2013), the nucleosome deposition pathway might bring Rtt101 and Mms1 to active replisomes, while Mms22 is recruited through Ctf4. Together, they function as the $Rtt101^{Mms22}$ E3 ubiquitin ligase to ensure faithful replication through damaged DNA templates.

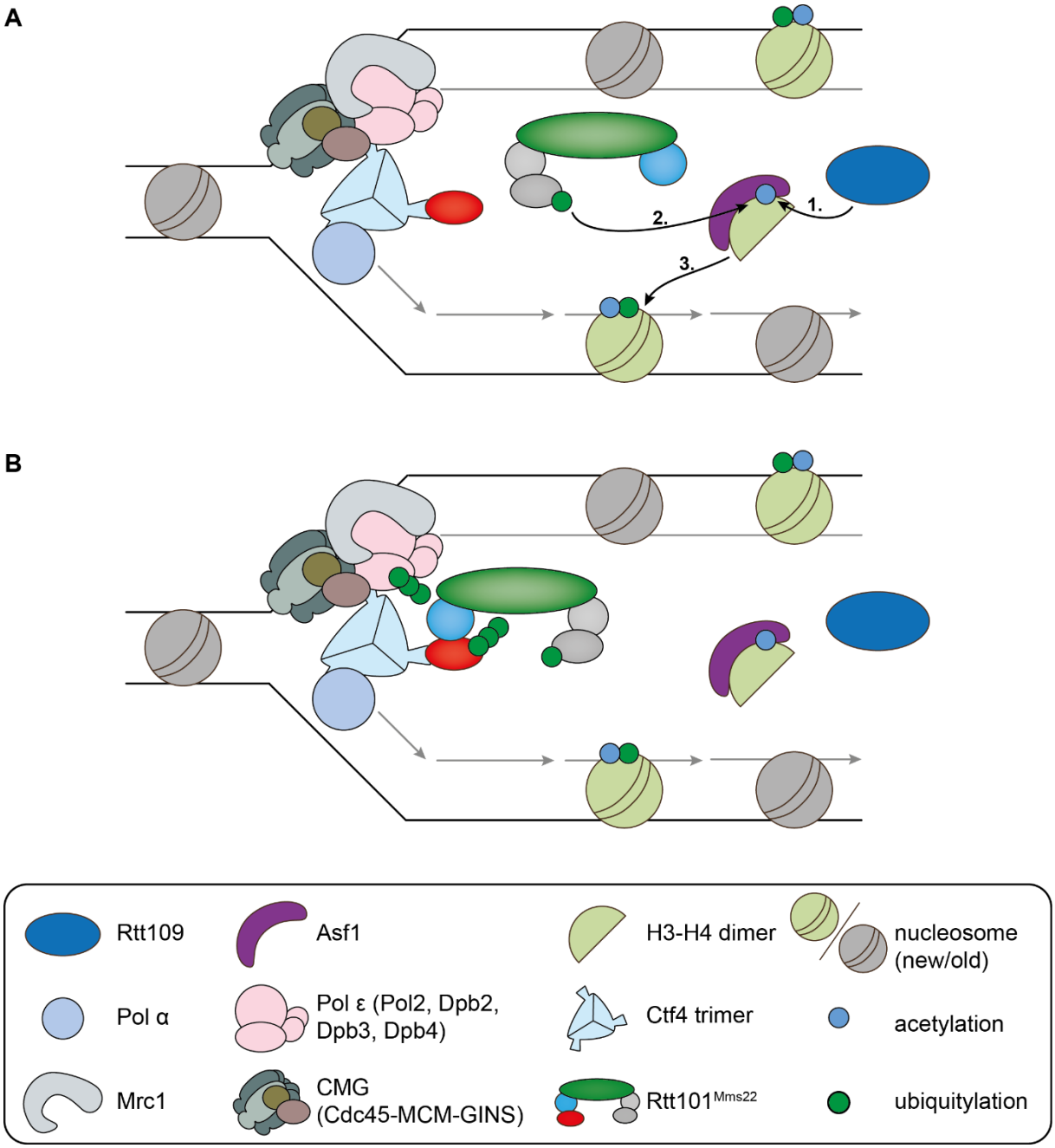

Figure 31. *De novo* nucleosome assembly could enhance association of Rtt101 with replisomes. (**A**) Mms22 is tethered to active replisomes *via* its interaction with Ctf4. In the wake of the replication fork the H3K56Ac pathway regulates *de novo* nucleosome assembly: The H3-H4 dimer bound by Asf1 is acetylated on lysine 56 by Rtt109 (1.). Subsequently, $Rtt101^{Mms1}$ ubiquitylates H3 on lysine 121, 122 and 125 (2.), thereby leading to a release of the H3-H4 dimer and its deposition on nascent DNA by the action of histone chaperones such as CAF-1 and Rtt106 (3.). Since nucleosome assembly is coupled to replication forks, this brings $Rtt101^{Mms1}$ close to Mms22 and the replisome. (**B**) When replication encounters a DNA lesion, the active $Rtt101^{Mms22}$ is ready to ubiquitylate Dpb2 and other potential targets, one of those being Mms22 itself. This could free $Rtt101^{Mms1}$ and might allow to participate in nucleosome assembly again.

4.5 Rtt101-dependent lesions might have common features

As Rtt101 is associated with replisomes during unperturbed S phase as well as when forks encounter DNA lesions (Buser et al., 2016), it is conceivable that Rtt101 function is not restricted to a single target in a certain situation. Indeed, the loss of Rtt101 function might impair more than one step within a pathway, and it will be challenging to dissect distinct pathways regulated by Rtt101-mediated ubiquitylation. While cells lacking $Rtt101^{Mms22}$ are highly sensitive to CPT, MMS and as presented in this thesis also to an accumulation of genomic rNMPs, their viability is barely affected in the presence of HU (Chang et al., 2002; Hryciw et al., 2001; Luke et al., 2006) or when R-loops accumulate (data not shown). This implies that some stalled or damaged replication forks must exhibit certain features to provoke a requirement for $Rtt101^{Mms22}$, which are dependent on the origin of damage.

4.5.1 MMS-induced lesions and rNMPs

Treatment with MMS causes a heterogeneous mix of DNA lesions (reviewed in (Shrivastav et al., 2009)). Moreover, during faulty processing of MMS-induced lesions *via* base excision repair, AP sites can accumulate (Glassner et al., 1998; Xiao and Samson, 1993). Although MMS-induced lesions are in general able to induce DSBs due to the general susceptibility of stalled forks for nucleolytic processing or due to spontaneous hydrolysis of AP sites (Groth et al., 2010; Nikolova et al., 2010), the MMS concentrations used in this thesis rather induce the accumulation of ssDNA gaps that are repaired post-replicatively in a Rad51- and Rad52-dependent manner (González-Prieto et al., 2013). The accumulation of single-stranded gaps in replicated DNA suggests that DNA synthesis has reinitiated downstream of the lesion. DNA synthesis repriming involves two critical steps: First, the MCM helicase has to translocate downstream of the lesion to continue unwinding of the template DNA since it is exclusively loaded onto DNA during G1 phase (reviewed in (Blow and Dutta, 2005)). Second, DNA synthesis has to be initiated and a functional replisome has to be re-established. Helicase translocation might be facilitated by its physical uncoupling from the replisome. While in human cells the activity of the PrimPol enzyme, a DNA polymerase with both TLS and primase activity, is capable of performing origin-independent DNA replication initiation (García-Gómez et al., 2013; Mourón et al., 2013), in yeast such a specialized enzyme is not described. Budding yeast Pol ε is

unable to reinitiate synthesis downstream of a lesion (Sabouri and Johansson, 2009). Instead, Pol α/primase-dependent priming downstream of the lesion is required to favour gap repair over fork remodelling that would lead to reversed forks (Fumasoni et al., 2015). DNA synthesis can then be continued by Pol δ, which would dissociate once it catches up with the MCM helicase to allow Pol ε-dependent replication of the leading strand to resume. The resulting ssDNA gap can then be repaired by error-free TS (reviewed in (Marians, 2018)).

How exactly misincorporated ribonucleotides cause fork stalling has not been extensively studied yet. It is likely that through spontaneous hydrolysis of the phosphate-sugar backbone at rNMPs a number of single-stranded breaks might accumulate. Thus, in the absence of RER the most frequent lesion cells would have to cope with in an Rtt101-dependent manner would be SSBs, which could be transformed into one-ended DSBs when a replication fork approaches one of them. Ubiquitin remnant profiling identified the Pol ε subunit Dpb2 as a potential target of the E3 ligase activity of Rtt101 (Figure 24). While the Pol δ subunits Pol31 and Pol32 can associate with TLS polymerases (Daraba et al., 2014; Johnson et al., 2012), subunits of the Pol ε polymerase complex have not been shown to participate in TLS. Thus, it is more likely that ubiquitylation of Dpb2 leads to the removal or remodelling of the whole Pol ε complex rather than affecting only single subunits. Indeed, Pol ε is tethered to the CMG helicase via Dpb2, and interfering with the interaction between Pol2 and Dpb2 leads to increased substitution of Pol ε with the more error-prone Pol δ or TLS polymerases (Garbacz et al., 2015; Sengupta et al., 2013). Intriguingly, using *Xenopus laevis* egg extracts as a model system, a mechanism for the recombination-mediated restart of broken forks corresponding to one-ended DSBs was proposed (Hashimoto et al., 2012). When the replisome encountered a SSB, the MCM helicase and Cdc45 remained associated with chromatin, while Pol ε and the GINS complex were lost. Subsequently, MRE11-dependent processing of the DNA end and RAD51-mediated strand invasion was followed by DNA extension employing the TLS polymerase Pol η. Only then Pol ε and GINS were reloaded, and a functional replisome was re-established. A mechanism for how Pol ε and GINS are removed and what creates the signal for their return is not known.

It is conceivable that a temporal removal of Pol ε prior to recombination-mediated fork restart is conserved in budding yeast. This removal process might depend on the Cdc48/p97 segregase, a ubiquitin-recognizing AAA ATPase that can extract

ubiquitylated proteins from larger complexes such as the replisome and is involved in DNA replication initiation, termination and several DNA repair pathways (reviewed in (Ramadan et al., 2017)). If this holds true, Rtt101 could specifically mark Dpb2 to induce the extraction of Pol ε from a broken replication fork to allow recombination-mediated fork restart (Figure 30).

In line with this, mutational signatures of cells lacking the only nonessential Pol ε subunits Dpb3 and Dpb4 suggest that their loss leads to a higher occurrence of ssDNA gaps, which are a consequence of DNA repriming events (Aksenova et al., 2010). As Dpb3 and Dpb4 are further thought to stabilize Pol ε interaction with DNA (Ohya et al., 2000; Tsubota et al., 2003), this implies that the removal of Pol ε from DNA is an important step of DNA synthesis repriming. Thus, targeting Dpb2 to promote the removal of Pol ε from DNA might happen and be required in a similar fashion at MMS-induced lesions as at a nick in the DNA. We therefore propose that Rtt101 fulfils the same function both at MMS-induced DNA lesions and at sites of misincorporated rNMPs that underwent spontaneous hydrolysis.

4.5.2 Other types of DNA damage

The above presented model for a role of Rtt101^{Mms22} at DNA lesions caused by alkylating damage or misincorporated rNMPs suggests that Rtt101 is important at sites where DNA synthesis must be continued downstream of a lesion. Mechanistically, this could be achieved by skipping the lesion to reinitiate DNA replication as we propose for MMS-induced damage, or by a recombinational fork restart as it might be required at hydrolysed rNMPs. Cells lacking functional Rtt101^{Mms22} are further hypersensitive towards the Top1 poison CPT (Chang et al., 2002; Hryciw et al., 2001; Luke et al., 2006). This drug leads to an accumulation of Top1ccs, which consist of covalently bound Top1 to a single strand nick on DNA and require ongoing replication to create toxicity. Thus, the resulting fork structure would be a nick that is converted into a one-sided DSB due to replication runoff when Top1cc is situated at the leading strand (Strumberg et al., 2000). Alternatively, in human cells the structure-specific endonuclease MUS81 has been shown to target replication forks that stall at a Top1cc to facilitate replication restart (Regairaz et al., 2011). By doing so, MUS81 creates one-sided DSBs. Therefore, CPT lesions might require the same type of repair as a hydrolysed rNMP. We can exclude that in the absence of Rtt101 the removal of a

Top1cc is impaired since Top1 levels are unchanged in CPT-treated wildtype and *rtt101*Δ cells. Moreover, the auxin-induced degradation of Top1-AID* did not alleviate the checkpoint recovery defect of *rtt101*Δ cells, suggesting that Top1cc *per se* and its removal is not causing this defect (Figure 26). Deletion of *MRC1* is sufficient to restore viability of *rtt101*Δ cells in the presence of CPT (Buser et al., 2016), indicating that also at CPT lesions, Rtt101^{Mms22} is required for efficient fork restart. Of note, in the same SGA screen for suppressors several genes such as *POL32* and *RAD27* were identified, that only confer a rescue of the CPT sensitivity, but do not affect MMS sensitivity. This could be explained by different possibilities of how CPT-induced Top1ccs can be processed, or by the genomic context in which Top1 is trapped. The fact that deletion of those genes does not rescue the growth defect of *rtt101*Δ *RNH201-AID*-9MYC pol2-M644G* cells, but instead decrease viability when combined with the *RNH201-AID*-9MYC pol2-M644G* mutant background might be explained by a difference between the Top1-induced nick associated with a bulky Top1cc and the 'clean' SSB created by spontaneous hydrolysis of the rNMP. At the same time this observation further underscores that Top1 is likely not the main source of toxicity in *rtt101*Δ *RNH201-AID*-9MYC pol2-M644G* cells, supporting our observation that *TOP1* deletion does not relieve toxicity in those cells.

A DSB such as induced by HO endonuclease does not affect viability of *rtt101*Δ cells and is repaired with wildtype-like kinetics (Luke et al., 2006). Considering the model discussed in this thesis, this is comprehensible as we propose that Rtt101 functions within the context of active replication forks.

The HU sensitivity of *rtt101*Δ cells is only moderate (Luke et al., 2006). Consistently, replication fork stalling induced by HU does not require a restart or repriming of DNA synthesis due to the nature of HU-induced replication stress: the inhibition of ribonucleotide reductase causes a depletion of the intracellular dNTP pool, which slows down replication and ultimately arrests forks (reviewed in (Singh and Xu, 2016)). In this situation, a repriming event or recombination-mediated fork restart is not feasible since the lack of dNTPs would not allow replication to continue.

Finally, we could show that the growth defect of *rtt101*Δ cells lacking RNase H2 does not stem from an accumulation of R-loops (Figure 13). Moreover, the concomitant loss of Rtt101 and factors that prevent R-loop formation, such as subunits of the THO/TREX complex (Gómez-González et al., 2011), did not show an additive effect on viability of

the double mutants (data not shown). Thus, we conclude that Rtt101 is not required to handle R-loop-induced replication stress. R-loops lead to conflicts between the replication and transcription machinery, and their collision can result in DSBs (reviewed in (Hamperl and Cimprich, 2014)). Additionally, the displaced ssDNA strand within the R-loop is susceptible to cleavage and thus the creation of SSBs. However, the removal of the R-loop would have to precede the restart of a broken or stalled fork in either case. It is thus likely, that replication forks at R-loops might not be reprimed or restarted for this reason.

4.6 Implications on human disease: DNA replication defects underlie symptoms of AGS patients

Aicardi-Goutières syndrome (AGS) is a severe neurological and autoinflammatory disease associated with mutations in the genes encoding for any of the three human RNase H2 subunits (Crow et al., 2006; Rice et al., 2007). While the mutations are precisely mapped, their direct consequence is less well understood. A faulty localization of the mutated RNase H2 complex is proposed to be the underlying cause of an increased accumulation of genomic rNMPs in AGS patient cells (Günther et al., 2015; Kind et al., 2014). Intriguingly, the cause of autoimmunity has been recently identified to be an accumulation of micronuclei in the cytoplasm of AGS patient cells. Micronuclei can activate the DNA-sensing cGAS-STING pathway when they undergo spontaneous nuclear envelope breakdown, which drives the inflammatory response (Bartsch et al., 2017; Mackenzie et al., 2016; MacKenzie et al., 2017; Pokatayev et al., 2016). Micronuclei are formed when cells attempt to undergo mitosis in the presence of under-replicated DNA, entangled sister chromatids as caused by recombination intermediates or dicentric chromosomes (reviewed in (Gelot et al., 2015)). Lagging chromosomes that cannot be properly segregated are refractory to breakage and will eventually accumulate in a micronucleus separated from the main nucleus. Thus, micronuclei are a result of increased replication stress and incomplete chromosome duplication and segregation.

In budding yeast, micronuclei have not been observed. However, it is expected that rNMPs cause the same type of replication stress in yeast as they do in the mammalian genome due to their biochemistry. Understanding the type of damage caused by

rNMPs that requires Rtt101^{Mms22} to be tolerated will give valuable insight into the damage underlying AGS.

4.7 Future perspectives

In this thesis we could shed light on how the Rtt101^{Mms22} E3 ubiquitin ligase promotes DNA replication in the presence of alkylating DNA damage. We further unravelled a key role for Rtt101^{Mms22} for several aspects of faulty RER. When ribonucleotides are misincorporated into genomic DNA and cannot be removed by RER, Rtt101^{Mms22} ensures viability presumably through ubiquitylation of the Pol ε subunit Dpb2. Moreover, timely deregulated RER that might cause abortive ligation of nicked rNMPs also relies on the presence of Rtt101. Finally, Rtt101-mediated ubiquitylation of histone H3 seems to be an important step in the tolerance of genomic rNMPs. Together, our data indicates a direct connection of the function of Rtt101^{Mms22} both in the presence of MMS and when rNMPs accumulate.

The results provided in this study predict that Rtt101^{Mms22} is required for replication fork restart or repriming events that allow lesion skipping during S phase to ensure the completion of chromosome duplication. Single-stranded gaps could then be repaired by postreplicative repair pathways such as template switch or translesion synthesis. This interpretation becomes particularly interesting considering a study performed in *rnh1Δ rnh201Δ* mutant cells (Lazzaro et al., 2012). The authors claim that both arms of the DDT pathway, TS and TLS, are essential when rNMPs accumulate. It would be interesting to see whether also in an *rnh201Δ* single mutant, or in the *RNH201-RED* expressing cells, DDT is crucial for viability. If so, this would strongly support a role for Rtt101^{Mms22} in DNA damage tolerance when genomic rNMPs accumulate, but not when the frequency of R-loops increases.

In future experiments we will confirm and test our proposed model in more detail: Once Dpb2 can be confirmed as a *bona fide* Rtt101 ubiquitylation target when genomic rNMPs accumulate, the consequences of this modification need to be tested. It is crucial to determine the fate of Dpb2 and the whole Pol ε complex which could range from altered interactions within the replisome to removal and possibly degradation of Pol ε. Further, it should be tested whether Dpb2 is targeted by Rtt101 also in the presence of MMS and CPT, or during an unperturbed S phase. If this is indeed the case, it would strongly support our model that suggests a general role for Rtt101^{Mms22}

at a certain type of stalled or collapsed DNA replication forks. In case Dpb2 is not ubiquitylated in the presence of MMS, ubiquitin remnant profiling could be employed to identify the critical Rtt101-dependent ubiquitylation targets when alkylating damage accumulates.

Another interesting field to investigate is the requirement of H3 ubiquitylation and H3K56 acetylation when rNMPs accumulate. We observed that a complete loss of either of those modifications impairs viability of RER-defective cells. We currently do not have any evidence on the reason for this loss of viability as nucleosome occupancy does not seem to be affected.

Finally, an important question to address is the conservation of faulty RER in human cells. The Rtt101 ortholog, CUL4, has not been connected to an accumulation of rNMPs or the pathology of AGS, so it will be conclusive to see whether CUL4 is required for the viability of AGS patient-derived cells. Although it is now known that the occurrence of micronuclei connect DNA replication problems with the cGAS-STING-mediated immune response (Bartsch et al., 2017; Mackenzie et al., 2016; MacKenzie et al., 2017; Pokatayev et al., 2016), the source of those DNA replication problems remains to be characterized. It will thus be particularly interesting to understand the type of damage inflicted by misincorporated rNMPs both in yeast and in human cells. A possible requirement for certain types of histone modifications such as H3K56Ac would, if conserved in human cells, encourage the exploration of drugs inhibiting histone modifiers such as histone deacetylases (HDAC inhibitors) as a treatment for AGS and similar diseases caused by replication stress.

Materials and Methods

5.1 Materials

5.1.1 Yeast strains

All yeast strains used in this study are derivatives of BY4741 (MATa *his3Δ1 leu2Δ0 met15Δ0 ura3Δ0*) (Winston et al., 1995). For spotting experiments shown in Figures 11-28 one representative replicate is shown and the diploid from which those strains were derived is listed. For strains used to transform with a plasmid, only the parental strain is given if not indicated otherwise.

Alias	Genotype	Figures	Source
yMD1458	*MATa*	7A, 9B, 9D	Buser et al. 2016
yMD1459	*MATa rtt101::NAT*	7A, 9B, 9D	Buser et al. 2016
yMD1460	*MATalpha mrc1::KAN*	7A	Buser et al. 2016
yMD1461	*MATalpha rtt101::NAT mrc1::KAN*	7A, 9B, 9D	Buser et al. 2016
yVK278	*MATa*	7B	Buser et al. 2016
yVK279	*MATalpha mms1::NAT*	7B	Buser et al. 2016
yVK280	*MATa mrc1::KAN*	7B	Buser et al. 2016
yVK281	*MATa mms1::NAT mrc1::KAN*	7B	Buser et al. 2016
yMD1478	*MATa*	7B	Buser et al. 2016
yMD1479	*MATalpha mms22::NAT*	7B	Buser et al. 2016
yMD1480	*MATalpha mrc1::KAN*	7B	Buser et al. 2016
yMD1481	*MATa mms22::NAT mrc1::KAN*	7B	Buser et al. 2016
yVK174	*MATa bar1::HIS3 NAT-pGAL1-3HA-MRC1*	8B, 8C	Buser et al. 2016
yVK175	*MATa bar1::HIS3 NAT-pGAL1-3HA-MRC1 rtt101::KAN*	8B, 8C	Buser et al. 2016
yVK168	*MATa bar1::HIS3 NAT-pGAL1-3HA-MRC1 dia2::HYG*	8B, 8C	Buser et al. 2016
yVK242	*MATalpha*	8B, 8C	Buser et al. 2016
yVK244	*MATa rtt101::NAT*	9A	Buser et al. 2016
yVK246	*MATa rtt101::NAT csm3::HYG*	9A	Buser et al. 2016
yVK248	*MATalpha rtt101::NAT tof1::KAN*	9A	Buser et al. 2016
yVK250	*MATa rtt101::NAT csm3::HYG tof1::KAN*	9A	Buser et al. 2016
yVK252	*MATalpha csm3::HYG*	9A	Buser et al. 2016
yVK254	*MATalpha tof1::KAN*	9A	Buser et al. 2016
yVK256	*MATalpha csm3::HYG tof1::KAN*	9A	Buser et al. 2016
yVK396	*MATa bar1::KAN sml1::KAN mrc1::NAT rad9::HYG*	9C	Buser et al. 2016
yVK69	*MATa bar1::HIS3*	10A, 10B	Buser et al. 2016
yVK70	*MATa bar1::HIS3 rtt101::NAT*	10A, 10B	Buser et al. 2016
yVK71	*MATa bar1::HIS3 rtt101::NAT mrc1::KAN*	10A, 10B	Buser et al. 2016
yVK72	*MATa bar1::HIS3 mrc1::KAN*	10A, 10B	Buser et al. 2016
yVK79	*MATa bar1::HIS3 mms22::NAT*	10A, 10B	Buser et al. 2016
yVK80	*MATa bar1::HIS3 mms22::NAT mrc1::KAN*	10A, 10B	Buser et al. 2016
yVK91	*MATa/MATalpha RTT101/rtt101::HYG RAD52/rad52::NAT MRC1/mrc1::KAN*	11A	Buser et al. 2016

Alias	Genotype	Figures	Source
yVK300	*MATa bar1::HIS3 RAD52-mCherry-NAT*	11B, 11C	Buser et al. 2016
yVK303	*MATa bar1::HIS3 RAD52-mCherry-NAT rtt101::HYG*	11B, 11C	Buser et al. 2016
yVK306	*MATa bar1::HIS3 RAD52-mCherry-NAT mms22::HYG*	11B, 11C	Buser et al. 2016
yVK308	*MATa bar1::HIS3 RAD52-mCherry-NAT mms22::HYG mrc1::KAN*	11B, 11C	Buser et al. 2016
yRS214	*MATa/MATalpha RTT101/rtt101::NAT MRC1/mrc1::KAN MCM6/mcm6IL-LEU2*	12A	Buser et al. 2016
yRS215	*MATa/MATalpha RTT101/rtt101::NAT MRC1/mrc1::HYG DPB4/dpb4::KAN*	12B	Buser et al. 2016
yVK485	*MATa/MATalpha RTT101/rtt101::NAT RNH1/rnh1::HIS3 RNH201/rnh201::HYG*	13A	This study
yVK587	*MATa, transformed with pBL97*	13B	This study
yVK458	*MATa rtt101::NAT*	13B, 15C	This study
yVK464	*MATa rtt101::NAT rnh201::HYG*	13B, 13C, 15C	This study
yVK1171	*MATa*	14B	This study
yVK1173	*MATa rnh1::KAN*	14B	This study
yBL435	*MATa rnh201::KAN*	14B	B. Luke
yAM197	*MATa rnh1::KAN rnh201::HYG*	14B	A. Maicher
yVK1175	*MATa RNH201-AID*-9MYC-HIS3 leu2::PromGPD-AFB2-LEU2*	14B	This study
yVK1177	*MATa RNH201-AID*-9MYC-HIS3 leu2::PromGPD-AFB2-LEU2 rnh1::KAN*	14B	This study
yVK1086	*MATa RNH201-AID*-9MYC-HIS3 leu2::PromGPD-AFB2-LEU2*	14C	This study
yVK1087	*MATa RNH201-AID*-9MYC-HIS3 leu2::PromGPD-AFB2-LEU2 rtt101::KAN*	14C	This study
yVK1179	*MATa/MATalpha RNH201/ RNH201-AID*-9MYC-HIS3 LEU2/ leu2::PromGPD-AFB2-LEU2 POL2/pol2-M644G-NAT RTT101/rtt101::KAN*	14D	This study
yVK1194	*MATa RNH201-AID*-9MYC-HIS3 leu2::PromGPD-AFB2-LEU2 rtt101::KAN pol2::pol2-M644G-NAT*	14D	This study
yVK1296	*MATa/MATalpha RNH201/ RNH201-AID*-9MYC-HIS3 LEU2/ leu2::PromGPD-AFB2-LEU2 POL2/pol2-M644G-NAT MMS1/mms1::KAN*	15A	This study
yVK1313	*MATa/MATalpha RNH201/ RNH201-AID*-9MYC-HIS3 LEU2/ leu2::PromGPD-AFB2-LEU2 POL2/pol2-M644G-NAT MMS22/mms22::KAN*	15B	This study
yBL7	*MATa*	15C, 20B, 21C, 22, 23, 26A	Euroscarf
yVK460	*MATalpha rnh201::HYG*	15C	This study
yVK735	*MATa*	16A, 16B	This study
yVK739	*MATa pol2::pol2-M644G-NAT*	16A, 16B	This study
yVK737	*MATa rnh201::HYG*	16A, 16B	This study
yVK741	*MATa pol2::pol2-M644G-NAT rnh201::HYG*	16A, 16B	This study
yVK743	*MATa mms22::KAN*	16A, 16B	This study
yVK747	*MATa pol2::pol2-M644G-NAT mms22::KAN*	16A, 16B	This study
yVK745	*MATa mms22::KAN rnh201::HYG*	16A, 16B	This study
yVK749	*MATa pol2::pol2-M644G-NAT mms22::KAN rnh201::HYG*	16A, 16B	This study

Alias	Genotype	Figures	Source
yVK843	*MATalpha rtt101::KAN*	16A, 16B	This study
yVK845	*MATa rtt101::KAN rnh201::HYG*	16A, 16B	This study
yVK849	*MATalpha rtt101::KAN pol2::pol2-M644G-NAT rnh201::HYG*	16A, 16B	This study
yVK1528	*MATa/MATalpha RNH201/ RNH201-AID*-9MYC-HIS3 LEU2/ leu2::PromGPD-AFB2-LEU2 POL2/pol2-M644G-NAT RTT101/rtt101::KAN TOP1/top1::HYG*	17A	This study
yVK1540	*MATa/MATalpha RNH201/ RNH201-AID*-9MYC-HIS3 LEU2/ leu2::PromGPD-AFB2-LEU2 POL2/pol2-M644G-NAT MMS1/mms1::KAN TOP1/top1::HYG*	17B	This study
yVK1552	*MATa/MATalpha RNH201/ RNH201-AID*-9MYC-HIS3 LEU2/ leu2::PromGPD-AFB2-LEU2 POL2/pol2-M644G-NAT MMS22/mms22::KAN TOP1/top1::HYG*	17C	This study
yVK1381	*MATa/MATalpha RNH201/ RNH201-AID*-9MYC-HIS3 LEU2/ leu2::PromGPD-AFB2-LEU2 POL2/pol2-M644G-NAT RTT101/rtt101::KAN RAD51/rad51::HYG*	18A	This study
yVK1651	*MATa*	18B, 18C, 18D	This study
yVK1652	*MATalpha mrc1::URA3*	18B	This study
yVK1653	*MATa RNH201-AID*-9MYC-HIS3 leu2::PromGPD-AFB2-LEU2 mrc1::URA3*	18B	This study
yVK1654	*MATa mrc1::URA3 pol2::pol2-M644G-NAT*	18B	This study
yVK1655	*MATalpha RNH201-AID*-9MYC-HIS3 leu2::PromGPD-AFB2-LEU2 mrc1::URA3 pol2::pol2-M644G-NAT*	18B, 18C, 18D	This study
yVK1656	*MATalpha RNH201-AID*-9MYC-HIS3 leu2::PromGPD-AFB2-LEU2 rtt101::KAN pol2::pol2-M644G-NAT*	18B, 18C, 18D	This study
yVK1657	*MATalpha RNH201-AID*-9MYC-HIS3 leu2::PromGPD-AFB2-LEU2 rtt101::KAN mrc1::URA3 pol2::pol2-M644G-NAT*	18B, 18C, 18D	This study
yVK1745	*MATa*	18E	This study
yVK1747	*MATa RNH201-AID*-9MYC-HIS3 leu2::PromGPD-AFB2-LEU2 rtt101::KAN pol2::pol2-M644G-NAT*	18E	This study
yVK1749	*MATa RNH201-AID*-9MYC-HIS3 leu2::PromGPD-AFB2-LEU2 rtt101::KAN pol2::pol2-M644G-NAT mrc1::URA3*	18E	This study
yVK1751	*MATa RNH201-AID*-9MYC-HIS3 leu2::PromGPD-AFB2-LEU2 pol2::pol2-M644G-NAT mrc1::URA3*	18E	This study
yAL350	*MATa RNH202-TAP-HIS3*	19A, 19B, 19C	Open Biosystems
yVK1669	*MATa NAT-S-RNH202-TAP-HIS3*	19A, 19B, 19C, 20B	A. Lockhart
yVK1649	*MATa NAT-G2-RNH202-TAP-HIS3*	19A, 19B, 19C	This study
yVK1579	*MATa/MATalpha RTT101/rtt101::KAN RNH202/rnh202::HIS3*	20A	This study
yVK1580	*MATa/MATalpha RTT101/rtt101::KAN RNH202/rnh202::NAT-S-RNH202-TAP-HIS3*	20A	This study
yVK1672	*MATa/MATalpha RTT101/rtt101::KAN RNH202/rnh202::NAT-G2-RNH202-TAP-HIS3*	20A	This study
yVK1027	*MATalpha rtt101::KAN*	20B	This study
yVK1634	*MATa rnh202::HIS3*	20B	This study
yVK1684	*MATa NAT-G2-RNH202-TAP-HIS3*	20B	This study
yVK1636	*MATa rnh202::HIS3 rtt101::KAN*	20B	This study
yVK1670	*MATa rnh202:: NAT-S-RNH202-TAP-HIS3 rtt101::KAN*	20B	This study

Alias	Genotype	Figures	Source
yVK1685	*MATa rnh202:: NAT-G2-RNH202-TAP-HIS3 rtt101::KAN*	20B	This study
yVK1697	*MATa/MATalpha RNH201/ RNH201-AID*-9MYC-HIS3 LEU2/ leu2::PromGPD-AFB2-LEU2 POL2/pol2-M644G-NAT RTT109/rtt109::KAN*	21A	This study
yVK1696	*MATa/MATalpha RNH201/ RNH201-AID*-9MYC-HIS3 LEU2/ leu2::PromGPD-AFB2-LEU2 POL2/pol2-M644G-NAT ASF1/asf1::KAN*	21B	This study
yVK1754	*MATa/MATalpha HHT1/hht1::URA3 HHT2/hht2::KAN POL2/pol2::pol2-M644G-NAT RNH201/ RNH201-AID*-9MYC-HIS3 LEU2/ leu2::PromGPD-AFB2-LEU2 transformed with pBL509*	21C	This study
yVK1756	*MATa/MATalpha HHT1/hht1::URA3 HHT2/hht2::KAN POL2/pol2::pol2-M644G-NAT RNH201/ RNH201-AID*-9MYC-HIS3 LEU2/ leu2::PromGPD-AFB2-LEU2 transformed with pBL510*	21C	This study
yVK1758	*MATa/MATalpha HHT1/hht1::URA3 HHT2/hht2::KAN POL2/pol2::pol2-M644G-NAT RNH201/ RNH201-AID*-9MYC-HIS3 LEU2/ leu2::PromGPD-AFB2-LEU2 transformed with pBL511*	21C	This study
yVK1026	*MATa rtt101::KAN*	22, 23, 26A	This study
yTW59	*MATa asf1::KAN*	22	T. Wagner
ySLG600	*MATa rtt109::KAN*	22, 23	S. Luke-Glaser
yVK1192	*MATa RNH201-AID*-9MYC-HIS3 leu2::PromGPD-AFB2-LEU2 pol2::pol2-M644G-NAT*	22, 23	This study
yVK1715	*MATa RNH201-AID*-9MYC-HIS3 leu2::PromGPD-AFB2-LEU2 pol2::pol2-M644G-NAT rtt109::KAN*	23	This study
yVK1707	*MATa RNH201-AID*-9MYC-HIS3 leu2::PromGPD-AFB2-LEU2 pol2::pol2-M644G-NAT lys1::HYG*	24, 25	This study
yVK1708	*MATa RNH201-AID*-9MYC-HIS3 leu2::PromGPD-AFB2-LEU2 pol2::pol2-M644G-NAT lys1::HYG*	24, 25	This study
yVK1710	*MATa rtt101::KAN RNH201-AID*-9MYC-HIS3 leu2::PromGPD-AFB2-LEU2 pol2::pol2-M644G-NAT lys1::HYG*	24, 25	This study
yVK1711	*MATa rtt101::KAN RNH201-AID*-9MYC-HIS3 leu2::PromGPD-AFB2-LEU2 pol2::pol2-M644G-NAT lys1::HYG*	24, 25	This study
yVK1224	*MATalpha top1::HYG*	26A	This study
yVK1422	*MATa bar1::NAT TOP1-AID*-9MYC-HIS3 leu2::PromGPD-AFB2-LEU2*	26A, 26B	This study
yVK1412	*MATalpha rtt101::KAN*	26A	This study
yVK1423	*MATa bar1::NAT TOP1-AID*-9MYC-HIS3 leu2::PromGPD-AFB2-LEU2 rtt101::KAN*	26A, 26B	This study
yMD1590	*MATa TOP1-TAP-HIS3 bar1::NAT*	26C	M. Dees
yMD1594	*MATa TOP1-TAP-HIS3 bar1::NAT rtt101::KAN*	26C	M. Dees
yJK162	*MATa EXO1-TAP-HIS3*	27	J. Klermund
yVK1673	*MATa rtt101::KAN EXO1-TAP-HIS3*	27	This study
yVK1664	*MATa RAD54-TAP-HIS3*	27	Open Biosystems
yVK1674	*MATa rtt101::KAN RAD54-TAP-HIS3*	27	This study
yVK1575	*MATa/MATalpha RNH201/ RNH201-AID*-9MYC-HIS3 LEU2/ leu2::PromGPD-AFB2-LEU2 POL2/pol2-M644G-NAT RTT101/rtt101::KAN POL32/pol32::HYG*	28	This study

5.1.2 Plasmids

Name	Description	Figure	Source
pBL187	pRS423 *pADH*, 2µ, *HIS3*	9B	M. Peter
pBL372	pRDK1780 pRS426, *MRC1-AQ-HIS*3, 2µ, *URA3*	9B, 18E	R. Kolodner
pBL428	*HIS3*	9C	M. Peter
pBL433	*MRC1*, *HIS3*	9C, 18E	M. Peter
pBL380	pCMF013 pRS415 *MRC1*$_{1-971,}$ CEN*, LEU2*	9D	D. Koepp
pBL374	pRS415 CEN, *LEU2*	9D	D. Koepp
pBL377	pCMF001 pRS415 *MRC1,* CEN*, LEU2*	9D	D. Koepp
pBL189	pRS426 pGPD, 2µ, URA3	13B	Balk et al. 2013
pBB39	pRS426 pGPD-RNH1-HA, 2µ, URA3	13B	Balk et al. 2013
pBL97	pRS316, CEN, *URA3*	13C, 14D	M. Peter
pBL399	pRS316, *RNH201-P45D-Y219A*, CEN, *URA3*	13C, 14D	A.Lockhart
pBL401	pRS316, *RNH201*, CEN, *URA3*	13C, 14D	A.Lockhart
pBL425	pGR95, *HIS3*	15C	M. Peter
pBL427	pGR82-*RTT101*, *HIS3*	15C	M. Peter
pBL426	pGR83-*RTT101-K791R*, *HIS3*	15C	M. Peter
pBL197	pRS413, CEN, *HIS3*	18E	M. Peter
pBL508	#820 pRS313, CEN, *HIS3*	21C	Z.Zhang
pBL509	#724 pRS313 *yH3-H4*, CEN, *HIS3*	21C	Z.Zhang
pBL510	#1075 pRS313 *yH3K56R-H4*, CEN, *HIS3*	21C	Z.Zhang
pBL511	#1087 pRS313 *yH3K121.122.125R-H4*, CEN, *HIS3*	21C	Z.Zhang

Plasmids used for strain generation (knockout/tagging)		
Name	**Description**	**Source**
pBL438	pFA6-hphNT1, contains *HYG* cassette	Euroscarf
pBL440	pFA6-natNT2, contains *NAT* cassette	Euroscarf
pBL488	pHIS-AID*-9 MYC, contains *AID*-9MYC-HIS3* cassette	H. Ulrich
pBL492	pGIK43 contains *NAT-G2* cassette	Karras and Jentsch, 2010
pBL439	pFA6 -hphNT1, contains *HYG* cassette	Euroscarf
pBL403	pFA6-KanMX4, contains *KAN* cassette	M. Knop
pBL325	pYM-N24, contains *NAT-GAL1-3HA* cassette	M. Knop

5.1.3 Oligonucleotides

List of oligonucleotides used for: knockout (KO), tagging (tag), confirmation of knockout or tagging (test), qRT-PCR after ChIP (qRT-PCR), and probe for Southern Blot (probe). Forward (fw) and reverse (rev) oligonucleotides are listed in 5' to 3' direction. More details on the use of the oligonucleotides can be found in the Methods section.

Name	Sequence (5'→ 3')	Used for
oVK11	AGGAAGTTCGTTATTCGCTTTTGAACTTATCACCAAATATT TTAGTGATGCGTACGCTGCAGGTCGAC	*GAL1-3HA* tag *MRC1* fw
oVK12	GTAGTTCTCTTCTTTGCAGTCAACGAGGACAAAGCATGCA AGGCATCATCCATCGATGAATTCTCTGTCG	*GAL1-3HA* tag *MRC1* rev
oHP2	CATGAAGCTTGACGTTAAAGTATAGAGGTATATT	*GAL1* test fw
oVK14	GGCGATCCTTTTCGGTAGAC	*MRC1* test rev
#352	AGAAACGCCATAGAAAAGAGCATAGTGAGAAAATCTTCAA CATCAGGGCTCGTACGCTGCAGGTCGAC	*RAD9* KO fw
#353	TATTTAATCGTCCCTTTCTATCAATTATGAGTTTATATATTT TTATAATTATCGATGAATTCGAGCTCG	*RAD9* KO rev
#779	CTAAGGAAGTTCGTTATTCGCTTTTGAACTTATCACCAAAT ATTTTAGTGCGTACGCTGCAGGTCGAC	*MRC1* KO fw
#780	ACAGCTTCTGGAGTTCAATCAACTTCTTCGGAAAAGATAAA AAACCACTAATCGATGAATTCGAGCTCG	*MRC1* KO rev
#1053	ACCTCAAGGGGAAGTGTCAG	*RAD9* KO test fw
oBL29	CTGCAGCGAGGAGCCGTAAT	KO/tag test rev
#781	CCTTATCCTTCTTCGACGCG	*MRC1* KO test fw
oVK67	CTAAGCCTGTTAGAAGGAAGAGGCTGAGAACCCTAGATA ATTGGTACCGGCGTACGCTGCAGGTCGAC	*RNH201* tag fw
oVK70	GACATATGTAGTATTACATGAAGATATATAGTATGTGCAA ACTGGAGGTGAATCGATGAATTCGAGCTCG	*RNH201* tag rev
oVK69	CTGAAGCGCAACCAGACAAG	*RNH201* tag test fw
oVK78	GAGAAAAATTCAAATGGGCCATAGAATCGGTAGATGAAA ATTGGAGGTTTCGTACGCTGCAGGTCGAC	*TOP1* tag fw
oVK87	ACTTGATGCGTGAATGTATTTGCTTCTCCCCTATGCTGCG TTTCTTTGCGATCGATGAATTCGAGCTCG	*TOP1* tag rev
oVK80	ATGGTTGGAGAAAGTCGACGAA	*TOP1* tag test fw
oAL61	TCTGTCGCAATAGTTGACTTTCTTTTCTGGCCTCTCGAAC AAAAAGCATGCGTACGCTGCAGGTCGAC	*RNH202* tag fw
oAL63	TCGTCTGGTAAAATTATTAGTCGTTCTTCCCCCCCAATGT TGGAAACGGTATCAGTTTCACTTTCGGTATTTCT	*RNH202* tag rev
oAL64	CAAGTTTGTCAAAAGCACG	*RNH202* tag test fw
oAL65	GCTCGATACGAGGTTTGG	*RNH202* tag test rev
#2850	ATACCATAAGATAACAACGAAAACGCTTTATTTTTCACAC AACCGCAAAACGTACGCTGCAGGTCGAC	*LYS1* KO fw
#2851	TAAACTTGTAAATGTCAGCGTAACGATAATGTATATACTT TAAATGTAAAATCGATGAATTCGAGCTCG	*LYS1* KO rev

Name	Sequence (5'→ 3')	Used for
#2853	CAAATTGGCCCTTCATGGTA	*LYS1* KO test fw
oVK44	CCAATCTTTTTTACTGGTATAAATTCTCGTACGGGTTCA CAGGAACAATGCGTACGCTGCAGGTCGAC	*RTT101* KO fw
oBL334	TACATACGTGAGCTCGGAGA	*RTT101* KO test fw
AGP1-F	CTTCTGTGCTGCATCTCCCAAGG	probe
AGP1-R	TCCCTATATTCTTCGTCTTCTTGC	probe
oBL292	CCCAGGTATTGCCGAAAGAATGC	qRT-PCR *ACT1* fw
oBL293	TTTGTTGGAAGGTAGTCAAAGAAGCC	qRT-PCR *ACT1* rev
oAL33	TTGTGCCCGAATCCAGTGA	qRT-PCR *GCN4* fw
oAL34	TGGCGGCTTCAGTGTTTCTA	qRT-PCR *GCN4* rev
oAL76	CCTTGATACGAGCGTAACCATCA	qRT-PCR *PDC1* fw
oAL78	GAAGGTATGAGATGGGCTGGTAA	qRT-PCR *PDC1* rev
oVK103	CGGCTCGTGCATTAAGCTTG	qRT-PCR ARS607 fw
oVK104	TGCCGCACGCCAAACATTGC	qRT-PCR ARS607 rev
oVK105	CGGCTGTCATGCCAAGATGC	qRT-PCR ARS607 + 14 kB fw
oVK106	CTCTTCATCACTGGAGTCCT	qRT-PCR ARS607 + 14 kB rev

5.1.4 Liquid media

Medium	Composition
Lysogeny broth (LB) medium	
	1 % (w/v) NaCl
	1 % (w/v) Bacto tryptone
	0.5 % (w/v) Bacto yeast extract
	100 µg/mL carbenicillin
Yeast peptone (YP) medium 2.5x	
	4.4 % (w/v) peptone
	2.2 % (w/v) Bacto yeast extract
	add 2 % (w/v) glucose and H_2O to obtain 1x YPD
YPRaf (1 % raffinose)	
	2 % (w/v) peptone
	1 % (w/v) yeast extract
	1.18 % (w/v) Raffinose x 5 H_2O

Medium	Composition
YPGal/Raf (2 % galactose/1 % raffinose)	
	2 % (w/v) peptone
	1 % (w/v) Bacto yeast extract
	1.18 % (w/v) raffinose x 5 H_2O
	2 % (w/v) galactose
Synthetic complete (SC) medium w/o amino acid	
	0.192 % (w/v) yeast synthetic dropout medium without desired amino acid
	0.67 % (w/v) yeast nitrogen base without amino acids
	2 % (w/v) glucose
Sporulation (SPO) medium	
	0.005 % zinc acetate
	1 % potassium acetate
SILAC medium (SC-Lys with Lys-0 or Lys-8)	
	add 30 mg/L Lys-0 (light) or Lys-8 (heavy) to SC-Lys medium

5.1.5 Agar plates

Antibiotics or drugs were added after autoclaving when the medium was cooled down to approximately 50°C.

Plate	Composition
LB plates	
	1 % (w/v) tryptone
	0.5 % (w/v) Bacto yeast extract
	1 % (w/v) NaCl
	1.5 % (w/v) agar
	100 µg/mL carbenicillin
SC plates without amino acid	
	0.192 % (w/v) yeast synthetic dropout medium w/o amino acid
	0.67 % (w/v) yeast nitrogen base without amino acids
	2 % (w/v) glucose
	2.4 % (w/v) agar

Plate	Composition
YPD plates	
	6.5 % (w/v) YPD agar
Presporulation plates	
	3 % (w/v) standard nutrient broth
	1 % (w/v) Bacto yeast extract
	2 % (w/v) agar
	5 % (w/v) glucose

Antibiotics (single or multiple) were used in the following concentrations:	
Nourseothricin-dihydrogen sulfate (ClonNaT)	100 µg/mL
Hygromycin B	300 µg/mL
G418 disulfate solution (Kanamycin)	250 µg/mL

5.1.6 Buffers and solutions

Buffer/Solution	Composition
LiAc mix	
	0.1 M lithium acetate, 1 x TE, ddH_2O at final volume
PEG mix	
	40 % (w/v) PEG 400, dissolved in LiAc mix, autoclaved
Urea buffer	
	120 mM Tris-HCl pH 6.8, 5 % glycerol, 8 M urea, 143 mM β-mercaptoethanol, 8 % SDS, bromophenol blue
10 x SDS running buffer	
	25 mM Tris, 192 mM glycine, 0.1 % SDS, adjusted to pH 8.3, autoclaved
10 x blotting buffer	
	25 mM Tris, 192 mM glycine, , 0.45 µm filter-sterilized
10 x PBS	
	1.37 M NaCl, 0.03 M KCl, 0.08 M Na_2HPO_4 x 2 H_2O, 0.02 M KH_2PO_4, adjusted to pH 7.4 with HCl, autoclaved
1 x PBST	
	1 x PBS (diluted in ddH_2O), 0.1 % Tween-20
blocking buffer	
	5 % (w/v) skim milk powder in 1 x PBST

Buffer/Solution	Composition
FA lysis buffer - SOD	
	50 mM HEPES pH 7.5, 140 mM NaCl, 1 mM EDTA pH 8.0, 1 % Triton X-100
FA lysis buffer + SOD	
	50 mM HEPES pH 7.5, 140 mM NaCl, 1 mM EDTA pH 8.0, 1 % Triton X-100, 0.1 % sodium deoxycholate (SOD)
FA lysis buffer 500	
	50 mM HEPES pH 7.5, 0.5 M NaCl, 1 mM EDTA pH 8.0, 1 % Triton X-100, 0.1 % sodium deoxycholate (SOD)
Buffer III	
	10 mM Tris-HCl pH 8.0, 1 mM EDTA pH 8.0, 250 mM LiCl, 1 % NP-40, 1 % sodium deoxycholate (SOD)
10 x TE	
	0.1 M Tris-HCl pH 7.5, 10 mM EDTA pH 8.0
Elution buffer B	
	50 mM Tris-HCl pH 7.5, 1 % SDS, 10 mM EDTA pH 8.0
10 x TBE	
	0.89 M Tris base, 0.89 M boric acid, 0.02 M EDTA pH 8.0, autoclaved
6 x DNA loading buffer	
	15 % Ficoll, 10 mM EDTA pH 8.0, Orange G
EDTA pH 8.0	
	0.5 M disodium EDTA x $2H_2O$, adjusted to pH 7.5 or 8.0 with NaOH

If indicated, buffers and solutions were autoclaved for 20 minutes at 121°C.

5.1.7 Antibodies

Antibodies were used for western blot (WB) diluted in blocking buffer as indicated. For chromatin immunoprecipitation (ChIP), the amount of antibody *per* reaction is indicated.

Antibody	Use/Dilution	Source
mouse anti-HA	WB/1:2000	Covance, #MMS-101P, monoclonal
mouse anti-PGK1	WB/1:200000	Invitrogen, #459250, monoclonal
mouse anti-Rad53	WB/1:1000	Abcam, #ab166859, clone EI7.E1
mouse anti-Myc	WB/1:1000	Cell Signaling/NEB, #2276S, clone 9B11
rabbit anti-Rnr3	WB/1:1000	Agrisera, #AS09 574, polyclonal
rabbit peroxidase anti-peroxidase (PAP)	WB/1:1000	Sigma Aldrich, #P1291, monoclonal

Antibody	Use/Dilution	Source
rabbit anti-Sic1	WB/1:2000	Santa Cruz, #sc-50441, polyclonal
rabbit anti-Clb2	WB/1:1000	Santa Cruz, #y-180, polyclonal
rabbit anti-H3	WB/1:2000 ChIP/2 µL	Abcam, #ab1791, polyclonal
rabbit anti-H3K56Ac	WB/1:3000 ChIP/2 µL	Active Motif, #39281, polyclonal
goat anti-mouse (HRP conjugate)	WB/1:3000	BioRad, #170-5047
goat anti-rabbit (HRP conjugate)	WB/1:3000	BioRad, #170-5046
Goat-anti-mouse IgG IRDye 680RD	WB/1:10000	LI-COR, #926-68070
Goat-anti-rabbit IgG IRDye 680RD	WB/1:10000	LI-COR, #926-68071
Goat-anti-mouse IgG IRDye 800CW	WB/1:10000	LI-COR, #926-32210
Goat-anti-rabbit IgG IRDye 800CW	WB/1:10000	LI-COR, #926-32211

5.1.8 Enzymes, reagents and commercially available kits

Enzyme	Supplier
2x Phusion HF Mastermix GC buffer	New England Biolabs
2x Taq Mastermix	New England Biolabs
lyticase	Sigma-Aldrich
Proteinase K	Qiagen
RNase A	Thermo Scientific
Reagent	**Supplier**
0.5 mm silica beads	Roth
1 kB DNA ladder	New England Biolabs
100 bp DNA ladder	New England Biolabs
3-Indoleacetic acid (auxin)	Sigma-Aldrich
Agar	Sigma-Aldrich
Agarose	Sigma-Aldrich
alpha factor	Zymo Research
Bacto Yeast	BD Biosciences
Bovine Serum Albumin (BSA), acetylated	Promega
Bradford Solution	AppliChem

Reagent	Supplier
Bromphenol blue	Sigma-Aldrich
Camptothecin (CPT)	Sigma-Aldrich
cOmplete Mini EDTA-free Protease Inhibitor Cocktail Tablets	Roche
Concanavalin A	Sigma-Aldrich
Dimethyl sulfoxide (DMSO)	Sigma-Aldric
Ethanol, absolite	Sigma-Aldrich
Formaldehyde 37 %	AppliChem
G418 disulfate solution (Kanamycin)	AppliChem
Glucose (D+)	AppliChem, Merck Millipore
Glycerol	Grüssing
Glycine	AppliChem
HEPES buffer pH 7.5	AppliChem
hydroxyurea (HU)	Sigma-Aldrich
Hygromycin B	InvivoGen
methylmethane sulfonate (MMS)	Sigma-Aldrich
MG-132	Sigma-Aldrich
Mini-Protean TGX stain free precast gels (7.5/10/4-15 %)	BioRad
N-Ethylmaleimide (NEM)	Sigma-Aldrich
Nitrocellulose membrane	GE Healthcare Amersham
Nonidet P 40 (NP-40)	AppliChem
Nourseothricin-dihydrogen sulfate (ClonNaT)	WERNER BioAgents
Peptone	Sigma-Aldrich
PhosSTOP Tablets	Roche
Poly(ethylenglycol) 400 (PEG)	Sigma-Aldrich
Ponceau S	Sigma-Aldrich
Potassium chloride (KCl)	Sigma-Aldrich
Potassium Phosphate monobasic (KH_2PO_4)	Sigma-Aldrich
Prestained Protein Marker, Broad range (11-190 kDa)	New England Biolabs
Prestained Protein Marker, Broad range (7-175 kDa)	New England Biolabs
Protein G Sepharose 4 Fast Flow	GE Healthcare
Raffinose x 5 H_2O (D+)	AppliChem
RedSafe Nucleic Acid Stain	iNtRON
Skim milk powder	Sigma-Aldrich
Sodium acetate (NaAc)	Sigma-Aldrich
Sodium chloride (NaCl)	Sigma-Aldrich
Sodium deoxycholate (SOD)	Sigma-Aldrich

Reagent	Supplier
Sodium dodecyl sulfate (SDS)	AppliChem
Sodium hydroxide (NaOH)	Sigma-Aldrich
Sodium phosphate dibasic (Na_2HPO_4 x 2 H_2O)	Sigma-Aldrich
Sodium thiosulfate ($Na_2S_2O_3$)	Sigma-Aldrich
SuperSignal West Dura Extended Duration Substrate	Thermo Scientific
SuperSignal West Pico Chemiluminescent Substrate	Thermo Scientific
Sytox Green	Thermo Scientific
Trichloroacetic acid (TCA)	Sigma-Aldrich
Tris (Trizma base)	Sigma-Aldrich
Triton-X 100	Sigma-Aldrich
Tween-20	Sigma-Aldrich
Urea	Sigma-Aldrich
Yeast nitrogen base without amino acids	Sigma-Aldrich
Yeast synthetic dropout medium supplement without amino acid (SC or SD)	MP Biomedicals
Yeastmarker carrier DNA	Clontech
β-Mercaptoethanol	Sigma-Aldrich
Kit	**Supplier**
DyNAmo Flash SYBR Green qRT-PCR Kit	Thermo Scientific
QIAprep Spin Miniprep Kit	Qiagen
QIAquick PCR Purification Kit	Qiagen

5.1.9 Electronic devices and software

Electronic device	Supplier
BD FACSVerse	Becton Dickinson
BioRuptor Pico	Diagenode
BioRuptor Water Cooler Minichiller	Diagenode
ChemiDoc Touch Imaging System	BioRad
Dissection Microscope MSM 400	Singer Instruments
FastPrep-25	MP Biomedicals
Leica DM1000 LED	Leica
NanoDrop 2000	Thermo Scientific
Real Time PCD Detection System CFX384 Touch	BioRad
Sonifier 450	Branson
Spectrophotometer Ultrospec 2100 pro	Biochrom

Electronic device	Supplier
Thermal Cycler C1000 Touch	BioRad
Western blot equipment and PowerPac Basic	BioRad
Widefield microscope AF7000	Leica
Software	**Supplier**
Excel 2013	Microsoft
FACSuite 1.0.5	Becton Dickinson
Fiji 1.51d	ImageJ
FileMaker Pro 10	FileMaker Inc
Illustrator CC 2017 and CS5	Adobe
ImageLab 5.2	BioRad
ImageStudio	LI-COR
Leica Application Suite X	Leica
Mendeley Desktop	Elsevier
Prism 7.02	GraphPad
Word 2013	Microsoft

5.1.10 Additional materials

Material	Supplier
Nunc LabTek coverglass	Thermo Scientific
Replica plater for 96 well plate	Sigma-Aldrich
15 ml Bioruptor Pico Tubes & sonication beads	Diagenode
Lysing Matrix C tubes	MP Biomedicals

5.2 Methods

5.2.1 Yeast strains and culture

All yeast strains in this study are derived from the *Saccharomyces cerevisiae* parental strain BY4741 (MATa *his3Δ1 leu2Δ0 met15Δ0 ura3Δ0*) (Winston et al., 1995) which in turn is derived from the S288C laboratory strain (Mortimer and Johnston, 1986). For strain creation, standard yeast genetics procedures were applied (Guthrie and Fink, 1991). Alternative approaches will be described in the following.

To obtain yeast strains by tetrad dissection, diploid strains heterozygous for the desired gene knockouts or constructs were grown in a patch on presporulation plates over night at 30°C, then most of those cells were transferred into 3 mL of sporulation medium (SPO medium). The resulting SPO cultures were incubated at 23°C until a sufficient amount of sporulated tetrads was detectable. A small volume of SPO culture (usually 10-15 µL) was mixed with the same volume of lyticase and incubated at room temperature for 15 min. Then cells were seeded onto a YPD plate, or in case of diploids containing a plasmid onto plates with the appropriate selection to maintain the plasmid. Tetrads were picked and separated by micromanipulation. Spores were allowed to form colonies for 3 days at the appropriate temperature and the genotypes were determined.

The *mrc1Δ rad9 Δ sml1Δ* strain was created by sequential PCR-based knockout of *RAD9* followed by *MRC1* in the *sml1Δ bar1Δ* strain according to (Janke et al., 2004). Oligonucleotides were kindly provided by Helle Ulrich. In detail, the following plasmids and oligonucleotides were used: pBL438 (pFA6-hphNT2) with #352 and #353 for *RAD9* and pBL440 (pFA6-NatNT2) with #779 and #780 for *MRC1*. 100 ng plasmid DNA, 0.32 µL of the respective 10 µM oligonucleotides, 25 µL Phusion HF 2x Mastermix and water to a final volume of 50 µL were subjected to the following PCR protocol: 3 min at 95°C; 10 cycles of 30 sec at 95°C, 30 sec at 54°C, 2 min 40 sec at 72°C; followed by 20 cycles of 30 sec at 95°C, 30 sec at 54°C and 2 min 40 sec at 72°C with increasing this time for 20 sec with every cycle. For the reaction containing pBL440, the steps at 95°C were performed at 97°C and elongation time was raised from 30 sec to 1 min. The correct size of the PCR product was verified on an agarose gel, and competent yeast cells were transformed with 5 µL of the PCR mix. Colonies were allowed to form on YPD plates containing the appropriate drugs and the knockout was confirmed by colony PCR using oligonucleotide oBL29 with either #1053 (*RAD9*

knockout) or #781 (*MRC1* knockout) by boiling cells from half a single colony in 10 µL 0.02 N NaOH at 100°C, and subjecting 2 µL of this lysate to a PCR reaction containing in addition 10 µL Taq 2x Mastermix, 1 µL of each 10 µM oligo and water up to 20 µL. The PCR protocol was as follows: 3 min at 98°C; followed by 34 cycles of 10 sec at 98°C, 30 sec at 58°C, 45 sec at 68°C; and a final 5 min at 68°C.

The endogenous construct to express *3HA-MRC1* under control of the *GAL1* promoter was created by amplification of the *NAT-3HA-GAL1* cassette from pBL325 (pYM-N24) using oligos oVK11 and oVK12. The PCR reaction was set up and performed as described above for the *MRC1* knockout. Transformed yeast cells were plated on YPD + NAT plates and growing colonies were tested for the presence of the cassette in the *MRC1* locus by colony PCR using oligos oHP2 and oVK14 as described above.

The *RNH201-AID*-9MYC* and *TOP1-AID*-9MYC* strains were created as previously described (Morawska and Ulrich, 2013). The *AID*-9MYC-HIS* cassette was amplified by PCR using oligos oVK67 and oVK70 (for *RNH201*) or oVK78 and oVK87 (for *TOP1*) designed in accordance to (Morawska and Ulrich, 2013) from the plasmid pBL488 by setting up a reaction of 100 ng plasmid DNA, 0.32 µL of each 10 µM oligonucleotide, 25 µL Phusion HF 2x Mastermix and water to a final volume of 50 µL. The following PCR protocol was used: 3 min at 95°C; 10 cycles of 30 sec at 95°C, 30 sec at 54°C, 2 min 40 sec at 72°C; followed by 20 cycles of 30 sec at 95°C, 30 sec at 54°C and 2 min 40 sec at 72°C with increasing this time for 20 sec with every cycle. The production of a PCR fragment of the desired length was confirmed by agarose gel electrophoresis and subsequently 5 µL of the PCR product were transformed into yKB244, a strain expressing *Arabidopsis thaliana* F-box protein AFB2 under control of the GPD promoter. Selection was performed by growing transformed cells on SC-His plates. Integration of the PCR cassette at the desired locus was tested by colony PCR using oVK67 + oBL29 (for *RNH201*) or oVK80 + oBL29 (for *TOP1*) as described above. Positive clones were grown to log phase, proteins were extracted before and after treatment with auxin (IAA) and levels of the *AID*-9MYC* tagged proteins as well as auxin-induced degradation were checked by western blot.

The G2-restricted *RNH202* allele was created by amplifying the G2 cassette comprising the *CLB2* promoter, the first 543 bp of the *CLB2* coding sequence with a point mutation changing lysine 26 to alanine to ensure nuclear retention of the resulting fusion protein, and the *NAT* resistance cassette from the plasmid pBL492 using

oligonucleotides oAL61 and oAL63. PCR reactions contained 100 ng plasmid DNA, 0.64 µL of each oligonucleotide diluted to 5 µM, 25 µL Phusion HF 2x Mastermix and water to a final volume of 50 µL. The PCR reaction was performed as follows: 3 min at 97°C; 10 cycles of 1 min at 97°C, 30 sec at 54°C, 2 min 40 sec at 72°C; followed by 20 cycles of 1 min at 97°C, 30 sec at 54°C and 2 min 40 sec at 72°C with increasing this time for 20 sec with every cycle. The correct size of the PCR product was confirmed on an agarose gel and 10 µL of the PCR reaction were transformed into yAL350 (*RNH202-TAP-HIS*). Cells were grown on YPD + NAT plates and positive transformants were confirmed by colony PCR (as described above for the AID*-tagged strains) using oAL64 and oBL29, and in a second PCR reaction using oAL64 and oAL65. Verified clones were tested for cell cycle specific expression of the created *G2-RNH202-TAP* allele.

The yeast strains that were used for the SILAC/di-glycine pulldown experiment had to be deleted for *LYS1*. The PCR-based knockout cassette replacing *LYS1* with NAT was created using oligonucleotides #2850 and #2851 (kindly provided by Helle Ulrich) and pBL439 as a template. The PCR reaction was set up as described for the *RNH201-AID*-9MYC* allele. Heterozygous diploid *RTT101/rtt101 RNH201/RNH201-AID*-9MYC POL2/pol2-M644G* cells were transformed with 5 µL PCR product and positive transformants were subjected to colony PCR as described previously using oligonucleotides #2853 and oBL29. Confirmed transformants were then sporulated and tetrads were dissected as described above. The desired *lys1*Δ haploid mutants were chosen from the dissected spores.

RTT101 was knocked out in strains expressing *EXO1-TAP* or *RAD54-TAP* as described for the knockout of *RAD9* using oligonucleotides oVK44 and oVK45 and the plasmid pBL403 as a template. The knockout was confirmed using oligonucleotides oBL334 and oBL29.

5.2.2 Yeast transformation

Competent yeast cells were created by centrifuging exponentially growing cells from a 25 mL culture grown at 30°C (OD_{600}<1) for 3 min at 3,000 rpm at RT and washing them once with 5 mL LiAc-mix. After another centrifugation step, the cell pellets were resuspended in 250 µL LiAc-mix and aliquoted. 100 µL of competent yeast cells were either used directly for transformation or supplemented with 7 µL DMSO and stored at

-80°C until use. The transformation reaction was set up using 100 µL of competent yeast cells, 10 µL Yeast Marker Carrier DNA, 100-200 ng of plasmid and 700 µL PEG-mix. In case of an integration, 5 µL PCR product or 1 µg of purified PCR product was used instead of the plasmid DNA. The transformation reaction was incubated for 30 min at RT on a rotating wheel and subsequently heat shocked for 15 min at 42°C. Cells were then harvested by centrifugation (3 min at 3,000 rpm) and resuspended in 300 µL of YPD medium. After a recovery time of 30 min (plasmids) or up to 5 hours (integration), cells were plated onto selective media and incubated at 30°C until colonies formed.

5.2.3 Bacterial transformation

To propagate and store plasmids, competent DH5α *E. coli* cells were mixed with 1 µL of plasmid DNA and incubated on ice for 30 min. After a heat shock for 1 min at 42°C the transformation reaction was returned to ice for another minute. Then 300 µL of LB medium was added and cells were allowed to recover for 30 min at 37°C before they were plated on LB-Amp plates and incubated overnight at 37°C.

5.2.4 Protein extraction and western blot

A number of cells equalling 2 OD_{600} units were harvested by centrifugation (2 min at 13,000 rpm at 4°C) and resuspended in 200 µL of 20 % TCA on ice. The resuspended cells were transferred into a 1.5 mL tube containing approximately 200 µL of silica beads and either processed immediately or stored at -20°C. The protein extraction was performed on ice and centrifuges were cooled down to 4°C. Cells were vortexed for 10 min at 4°C and the lysate was recovered by first collecting the supernatant, and second washing the beads briefly with 600 µL 5 % TCA, the supernatant of which was combined with the supernatant of the first step. The extract was centrifuged for 5 min at 9000 rpm at 4°C and the supernatant was discarded. The resulting pellet was resuspended in 100 µL urea buffer and, if necessary, supplemented with 1-5 µL 1M Tris-Cl pH 7.5 to achieve a blue colour of the buffer. Lysates were either stored at -20°C or directly prepared for loading onto a polyacrylamide gel.

Before loading, samples were boiled at 75°C for 5 min and centrifuged for 1 min at 8,000 rpm at RT. 4-8 µL of the samples were loaded onto Mini Protean TGX Precast gels (7.5 %, 10 % or 4-15 % gradients – indicated in the Figure legends) and run in

1x SDS running buffer for 5 min at 150 V, then the voltage was decreased to 80-100 V for 1-3 hours.

Gels were blotted onto nitrocellulose membranes by wet blot in 1x blotting buffer at 4°C at constant voltage (120 V) for 1 hour or in case of blots that should detect Rad53 phosphoshift or other large proteins for 2 hours.

The membrane was stained with Ponceau solution to monitor the transfer efficiency and loading, then unspecific binding was blocked by incubating the membrane in blocking buffer for 1 hour at RT. The primary antibody diluted in blocking buffer was added and membranes were incubated overnight at 4°C while shaking gently. The following day, membranes were washed 4 times in 1x PBS-T, followed by incubation with the secondary antibody diluted in blocking buffer. In case of fluorescently labelled antibodies, the membranes were kept dark from this point on. After 1 hour at RT, membranes were washed 3 times with 1x PBS-T and once with 1x PBS and signals were detected either by chemiluminescence or fluorescence and imaged with the ChemiDoc™ Touch Imaging System (BioRad) and the Odyssey Clx 9140 (LI-COR Biosciences), respectively.

5.2.5 Cell cycle synchronization and release

In order to synchronize yeast cells in the cell cycle, exponentially growing MATa cultures (OD_{600} of 0.3-0.6) were supplemented with 2.4 µM (4 µg/mL) α-factor and cells were incubated at 30°C for 2-2.5 hours. The efficiency of the arrest was determined qualitatively by looking at cell morphology (pear-shaped shmoo formation in >95 % of cells) and confirmed by flow cytometry. For cells in which *BAR1* was deleted, the amount of α-factor was reduced to 2 µM (3.3 µg/mL).

For the synchronous release of cells from a G1 arrest, cultures were pelleted for 3 min at 3,000 rpm at 30°C and washed twice in sterile H_2O prewarmed to 30°C. After the last centrifugation step, cells were resuspended in prewarmed medium and put back to the appropriate temperature. The release was monitored by flow cytometry at the respective timepoints.

5.2.6 Flow cytometry to measure DNA content

Culture samples corresponding to 0.68 OD_{600} units of exponentially growing cells were centrifuged for 5 min at 3,000 rpm at RT, then washed with 1 mL H_2O before repeating the centrifugation. The pellet was then resuspended in 500 µL of 50 mM Tris-CL pH 8.0, supplemented with 10 µL RNase A (10 mg/mL) and incubated for 3 hours at 37°C. The buffer was removed after centrifugation for 5 min at 3,000 rpm at RT, and cells were resuspended in 500 µL of 50 mM Tris-CL pH 7.5 that contained 1 mg/mL Proteinase K. Following an incubation of 45 min at 50°C, samples were centrifuged again for 5 min at 3,000 rpm at RT and resuspended in 500 µL of 50 mM Tris-CL pH 7.5. The processed cells were then either stored at 4°C or directly prepared for measuring. To this end, 100 µL of samples were subjected to sonification using the BioRuptor Pico for 3 x 5 sec with 30 sec in between runs. Half of the sonified sample was transferred into FACS test tubes (Falcon), to which subsequently 1 mL of 50 mM Tris-CL pH 7.5 supplied with 1 µM SytoxGreen was added. Tubes were kept in the dark and measured immediately using the FACSVerse flow cytometer (BD) and analysed with the FACS Suite software (BD).

5.2.7 Spotting assay

Overnight cultures were inoculated from single colonies in 3 mL of the appropriate medium and grown at 30°C. The overnight cultures were diluted to an OD_{600} of 0.5 in 200 µL sterile water. From this diluted culture tenfold serial dilutions were prepared and approximately 3-4 µL were transferred onto appropriate agar plates with or without drugs using a replica plater (Sigma). Cells were incubated for 3-4 days, and plates were imaged every 24 hours using the ChemiDoc™ Touch Imaging System (BioRad).

5.2.8 Galactose-shutoff

Cells were grown overnight in 4 mL YP medium containing 1 % raffinose (YPRaf (1 %)) at 23°C and diluted back the next morning to OD_{600} of 0.2 in 25 mL YPRaf (1 %) and shifted to 30°C. Cultures were allowed to reach an OD_{600} of 0.6-0.8, then *3HA-MRC1* expression was induced *via* the addition of 2.5 mL galactose to 22.5 mL of culture (final concentration is 2 %) and cell cycle synchronization initiated by adding 2 µM of α-factor. After 2 h 30 min, samples for flow cytometry and protein extraction were taken, the remaining culture was centrifuged for 3 min at 3,000 rpm and 30°C, then washed

twice with prewarmed YPRaf (1 %) containing 2 % galactose (YPGal/Raf (2 %/1 %)), then released into 30 mL of pre-warmed YPGal/Raf for 15 min at 30°C. A 5 mL aliquot was taken from the culture to collect samples for flow cytometry and protein extraction (time point 0 min). To the remaining culture, 0.03 % MMS and 2 % glucose were added to induce damage and stop transcription of *3HA-MRC1*. Cultures were placed back to 30°C and samples for flow cytometry and protein extraction were taken every 15 min over a total time course of 150 min.

5.2.9 Checkpoint recovery

Cultures were inoculated in 20 mL YPD at a very low OD_{600} (0.0003-0.001) and grown at 30°C to achieve an overnight OD_{600} of approximately 0.4-0.6. All cultures were brought to the OD_{600} of the culture with the lowest cell density in 20 mL YPD and 2 µM α-factor was added. G1 arrest was confirmed microscopically after 2 h 15 min, and an aliquot of the cultures was harvested for flow cytometry and protein extraction (sample G1). The remaining culture was centrifuged for 3 min at 3,000 rpm and 30°C, then washed twice with sterile water prewarmed to 30°C. Subsequently, the culture was released into 20 mL YPD medium containing 0.01 % MMS and incubated for one hour at 30°C. After removal of an aliquot for flow cytometry and protein extraction (sample MMS), the culture was centrifuged for 3 min at 3,000 rpm and 30°C and resuspended in YPD containing 2.5 % (w/v) sodium thiosulfate ($Na_2S_2O_3$) to quench MMS. After an additional centrifugation step, cultures were released into fresh YPD medium and allowed to recover at 30°C. Every hour a 5-8 mL aliquot was removed and used to collect samples for flow cytometry and protein extraction (samples 1 h - 4 h recovery), the same volume of YPD medium as was removed before was added to keep cultures in exponential growth throughout the time course.

5.2.10 Microscopy of Rad52-mCherry foci

15 mL YPD medium was inoculated at a very low OD_{600} to obtain an exponentially growing culture the next morning. Once cultures reached an OD_{600} of approximately 0.5, they were arrested in G1 using 1 µM α-factor for 2 h 15 min at 30°C. Samples for flow cytometry were taken, and the remaining culture was centrifuged (3 min at 3,000 rpm at 30°C) and washed twice with H_2O. Cells were then released into YPD or YPD containing 0.03 % MMS and grown for one hour at 30°C. After collecting an

aliquot for flow cytometry, culture volumes corresponding to 0.08 OD_{600} units were centrifuged for 2 min at 3,000 rpm at RT, resuspended in 300 µL SC-Trp medium containing 0.03 % MMS, and transferred into one chamber of an 8 chamber Nunc Lab-Tek® coverglass (Thermo Fisher Scientific) coated with 2 mg/mL Concanavalin A (Sigma Aldrich). Samples were immediately taken to the Leica AF7000 widefield microscope and imaged using a 63x/1.4 oil objective. Fluorescent and brightfield images were recorded along the z-axis. Rad52-mCherry foci were manually counted in all focal planes of the z-stack for at least 400–600 cells per strain.

5.2.11 Growth assay

Cultures were inoculated in 5 mL YPD medium and grown overnight at 30°C. The next morning, cultures were diluted back to an OD_{600} of 0.1 in 8 mL YPD medium. Cell density of the culture was determined every hour for a total period of 8 hours. The measured optical density was plotted against time. Doubling times (PD) were derived from measurements taken throughout exponential growth phase (between 4 and 5 hour measurements) and calculated using the following formulas:

$$PD = t \div n$$

$$n = 3.32 \times \log(\frac{ODend}{ODstart})$$

In this calculation, t is the time between two measurements in minutes, n is the number of population doublings within the time interval t, and OD_{end} and OD_{start} the measured optical densities of the cell cultures at the time points 5 hours and 4 hours, respectively. PD values were calculated separately for each of the three biological replicates per genotype, then the average and standard deviation was calculated.

5.2.12 Alkaline hydrolysis, alkaline gel and southern blot

The experiment was performed by Jessica Williams in the laboratory of Thomas Kunkel as described (Nick McElhinny et al., 2010b; Williams et al., 2013) using strains generated by Vanessa Kellner. Cells were grown in 5 mL YPD medium throughout the day and diluted in 50 mL YPD medium using 1-2 mL of the preculture. Cultures were incubated over night at 30°C. The next day, genomic DNA was extracted using the MasterPure™ Yeast DNA purification kit (epicentre). Subsequently, 5 µg DNA was

precipitated in a total volume of 200 µL using 20 µL sodium acetate (NaOAc), then 500 µL of 100 % ethanol were added and samples were incubated over night at -20°C. After centrifugation, the pellet was dried over night at room temperature. Finally, the DNA was resuspended in 14 µL water and treated with 0.3 M KOH by addition of 6 µL 1 M KOH. Alkaline hydrolysis was performed for 2 hours at 55°C, then 4 µL 6x alkaline loading buffer (300 mM KOH, 6 mM EDTA, 18 % (w/v) Ficoll (Type 400), 0.15 % (w/v) bromocresol green, 0.25 % (w/v) xylene cyanol) was added to the samples. DNA was subjected to alkaline gel electrophoresis on a 1 % alkaline agarose gel (50 mM NaOH, 1 mM EDTA) in alkaline electrophoresis buffer (50 mM NaOH, 1 mM EDTA) for 20 hours at 1 V cm^{-1}. The gel was neutralized twice for 45 minutes in 1 M Tris HCl, pH 8.0, 1.5 M NaCl and stained with 25 µL SyBr Gold (Invitrogen) in 250 mL H_2O for 2 hours.

The alkaline-treated DNA was transferred to a nylon membrane (Hybond N+) by capillary transfer over night in alkaline transfer buffer (0.4 N NaOH, 1 M NaCl). Strand-specific radiolabelled ssDNA probes were designed and created by amplification of a 400 bp fragment within the *AGP1* locus adjacent to ARS306 as described (Miyabe et al., 2011). Oligos AGP1-F and AGP1-R were used.

5.2.13 Chromatin immunoprecipitation (ChIP) and qPCR

Cells were grown in 10 mL YPD medium overnight at 30°C and rediluted the following morning to an OD_{600} of 0.1. If the ChIP was performed with exponentially growing cells, a culture volume of 155 mL was grown at 30°C until it reached an OD_{600} of approximately 0.8. Depletion of Rnh201-AID* was initiated by the addition of 1 mM IAA at the time of dilution. All cultures were diluted to the exactly same OD_{600} in a total volume of 150 mL and crosslinked with 1.2 % formaldehyde for 10 min followed by quenching with 360 mM glycine for 5 min and subsequent incubation on ice for at least 10 min.

If the ChIP was performed on cultures released into HU from a G1 cell cycle arrest, the overnight culture was diluted in a volume of 130 mL YPD. When the culture reached an OD_{600} of approximately 0.3, 2.4 µM α-factor was added to120 mL of the culture. From the remaining 10 mL, samples for flow cytometry and protein extraction were harvested (sample ‘asynchronous’). After 90 min at 30°C 1 µM IAA was added to all cultures to deplete Rnh201-AID* prior to release into S phase. Cells were kept for an

additional 45-60 min to ensure arrest in G1, which was confirmed microscopically. Cell density of the arrested cultures was measured and culture volumes corresponding to 110 mL of the culture with the lowest OD_{600} were centrifuged for 3 min at 3,000 rpm at 30°C. From the remaining cultures samples for flow cytometry and protein extraction were taken (sample 'G1'). The pelleted cells were washed twice with pre-warmed H_2O and released into 125 ml YPD containing 0.2 M HU and 1 mM IAA. After 45 min incubation at 25°C (water bath) 5 mL of the cultures were put aside on ice to take samples for flow cytometry and protein extraction (sample 'HU'). The remaining 120 mL of cultures were crosslinked with 1.2 % formaldehyde for 10 min, then quenched with 360 mM glycine for 5 min and subsequently incubated on ice for at least 10 min.

The crosslinked and chilled cultures were pelleted for 4 min at 3,000 rpm at 4°C and washed twice with cold 1x PBS. The supernatant was removed completely, and cells were stored at -80°C.

Frozen cell pellets were thawed on ice and resuspended in 200 µL FA lysis buffer – SOD supplemented with protease inhibitor. Cell lysis was performed using the FastPrep24 device (settings: twice 6.5 M/ s for 30 sec interrupted by a 1 min break on ice in between runs) and extracts were recovered by the addition of 800 µL FA lysis buffer + SOD + protease inhibitor. The lysed cells were centrifuged for 7 min at 13,000 rpm at 4°C and the pellet was resuspended in 1.5 mL FA lysis buffer + SOD + protease inhibitor and supplemented with 20 µL of 20 % SDS. Each sample was split in half and transferred into sonication tubes containing 0.4 g sonication beads, in which chromatin was sheared using the BioRuptor pico (Diagenode) and the following settings: 5 times 30 sec on/30 sec off. The sonicated samples were recovered and centrifuged for 15 min at 13,000 rpm at 4°C and the resulting supernatant, the ChIP extract, was transferred into a new tube. If not further processed immediately, the ChIP extract was frozen at -80°C.

100 µL of ChIP extract was used to control for sonication efficiency. The aliquot was mixed with 100 µL elution buffer B and incubated while shaking at 65°C overnight. Then 7.5 µL of 20 mg/mL Proteinase K was added and incubated at 37°C for 2 hours. The DNA was subsequently purified using the QIAquick PCR purification kit (Qiagen) and eluted in 20 µL H_2O. After treatment of the DNA with 1 µL RNase A at 37°C for

30 min, the DNA was mixed with 6x DNA loading buffer and separated on a 1.5 % agarose gel. The fragmented DNA reached a size distribution of 300-500 bp.

The protein concentration of the ChIP extract was determined using Bradford: 2.5 µL of the extract (or FA lysis buffer + SOD as blank) was added to 97.5 µL of H_2O, then 1 mL of Bradford solution was added. The absorption at 595 nm was determined for two technical replicates.

The ChIP extract was diluted to 1 mg/mL in FA lysis buffer + SOD supplemented with protease inhibitor. 50 µL of this diluted ChIP extract was saved as 'input', and 3 aliquots of 1 mL each were used for the no antibody control ('-AB'), the IP for histone 3 ('H3 IP') and the IP for histone 3 acetylated at lysine 56 ('H3K56Ac IP'). The extracts were pre-cleared with 30 µL of washed and equilibrated beads (blocked for 1 hour at 4°C with 5 % BSA) for 30 min on the rotating wheel at 4°C. After centrifugation for 2 min at 2,000 rpm at 4°C the pre-cleared extracts were transferred into new tubes and incubated with the respective antibody (or kept on ice in case of the '-AB' sample) for 2 hours at 4°C rotating. Then 50 µL of washed and equilibrated beads was added to each sample and the IP was kept rotating overnight at 4°C.

The following day the beads were washed: upon centrifugation for 2 min at 3,000 rpm at 4°C and removal of the supernatant, 1 mL of the respective cooled wash buffer was added, incubated for 5 min at 4°C while rotating, and centrifuged again. The IP was washed with FA lysis buffer + SOD, FA 500 buffer, Buffer III and 1x TE. After the last wash beads were incubated for 8 min at 65°C with 100 µL elution buffer B, then centrifuged at 13,300 rpm at RT. The supernatant was collected in a new tube and the elution was repeated. The pooled eluate was incubated overnight with 7.5 µL Proteinase K (20 mg/mL) at 65°C. At this time 150 µL elution buffer B was added to the 50 µL 'input' samples, which were from now on processed side by side with the IP samples. The following day, the DNA was purified using the QIAquick PCR purification kit (Qiagen) and eluted in 50 µL H_2O.

qRT-PCR was performed on 'input', '-AB' and 'IP' samples using the CFX384 Touch Real-Time PCR Detection System. In 10 µL reactions 2x DyNAmo Flash SYBR Green master mix was used with 2 µL of DNA and oligonucleotides at a final concentration of 0.5 µM. For each sample a technical replicate was included. The settings for the PCR reaction were as follows: 95°C – 10 min; 95°C – 15 sec followed by 60°C – 1 min (repeated 40 times); 95°C – 5 min; 65°C – 1 min; 65°C to 97°C – 5 sec with an increase

of 0.5°C/cycle to determine the melting temperature of the amplicons. The measured cq values were normalized to input values. The oligonucleotides used are specified in section 5.1.3.

5.2.14 SILAC, di-glycine pulldown and mass spectrometry

The respective *lys1Δ* strains +/- *RTT101* were inoculated in 10 mL SC-Lys medium supplemented with 30 mg/L of either lysine-0 (light) or lysine-8 (heavy) and grown for 24 hours at 30°C. For the biological replicates, the SILAC labels were switched resulting in each genotype growing once in light and once in heavy medium. The 24 hours pre-cultures were diluted to an OD_{600} of 0.05 in 50 mL of the same medium and grown overnight at 30°C. The following morning, cultures were diluted to an OD_{600} of 0.1 in 505 mL of heavy or light SC-Lys medium (maintaining the supplemented type of lysine). When these cultures reached an OD_{600} of 0.4-0.5, samples for flow cytometry and protein extraction were taken and in the remaining culture the G1 arrest was induced by adding 2.4 µM α-factor. After 2 hours at 30°C, 1 mM IAA was added for an additional 1 hour 20 min to deplete Rnh201-AID*. Samples for flow cytometry and protein extraction were kept. The same number of cells were centrifuged for wildtype *RTT101* and *rtt101Δ* culture pairs (heavy/light and light/heavy) for 3 min at 3,000 rpm at RT and washed twice with pre-warmed H_2O. Each culture was released into 500 mL of light or heavy SILAC medium (again maintaining the same type of lysine isotope) containing 75 µM MG132 and 1 mM IAA. After 60 min at 25°C, aliquots for flow cytometry and protein extraction were taken and the *RTT101*/*rtt101Δ* culture pairs were mixed, resulting in a 1:1 ratio between wildtype *RTT101* and *rtt101Δ* cells. Cells were pelleted by centrifugation for 4 min at 3,000 rpm at 4°C and washed twice with ice-cold 1x PBS. Each *RTT101*/*rtt101Δ* pair was distributed to 5 falcon tubes in order to process them side by side. Pellets were frozen at -80°C.

Frozen cell pellets were thawed on ice and resuspended in 200 µL FA lysis buffer – SOD supplemented with protease inhibitor (cOmplete), phosphatase inhibitor (PhosStop) and 1x N-ethylmaleimide (NEM). Cell lysis was performed using the FastPrep24 device (settings: twice 6.5 M/ s for 30 sec interrupted by a 1 min break on ice in between runs) and extracts were recovered by the addition of 800 µL FA lysis buffer + SOD + protease inhibitor (cOmplete), phosphatase inhibitor (PhosStop) and 1x NEM. The lysed cells were centrifuged for 15 min at 13,000 rpm at 4°C. The

supernatant from the 5 identical samples was pooled and kept on ice, while the pellet was resuspended in 1.5 mL FA lysis buffer + SOD + protease inhibitor, phosphatase inhibitor and 1x NEM and supplemented with 20 µL of 20 % SDS. The samples were centrifuged again for 15 min at 13,000 rpm at 4°C, the supernatant collected, combined from the five aliquots of each *RTT101*/*rtt101Δ* pair and pooled with the supernatant from the previous step. The pellets were resuspended in 450 µL FA lysis buffer + SOD + protease inhibitor, phosphatase inhibitor and 1x NEM and NaCl was added to a final concentration of 1 M. Samples were sonified with a 3 mm sonification tip using the Sonifier 450 (Branson) with the following settings: 3 times 30 sec, 'constant' mode, output level 1 at 4°C. In between sonification cycles, samples were kept on ice. After a final centrifugation for 15 min at 13,000 rpm at 4°C and pooling of the supernatants belonging to the same *RTT101*/*rtt101Δ* pair, the collected supernatants of all steps were mixed, and protein concentration was determined by Bradford: 97.5 µL H_2O was mixed with 2.5 µL of the extract, then 1 mL of Bradford solution was added. Technical triplicates were measured, and the absorption was determined at 595 nm. The cell lysate was added to 4 volumes of ice-cold acetone and kept at -20°C for several days to allow precipitation of proteins. Each *RTT101*/*rtt101Δ* pair was subjected to two separate di-glycine lysine immunoprecipitations and measured separately in the mass spectrometer. Thus, from each biological replicate with switched labelling two technical replicates were measured. The samples were handed over to Thomas Juretschke in the lab of Petra Beli for further processing as described (Heidelberger et al., 2018).

Precipitated proteins were dissolved in denaturation buffer, followed by reduction of cysteines using 1 mM dithiothreitol and alkylation using 5.5 mM chloroacetamide. Subsequently, proteins were proteolytically digested with endoproteinase Lys-C (Wako) and sequencing grade modified trypsin (Sigma). The digestion reaction was stopped by adding trifluoroacetic acid to a final amount of 0.5 % and the extract was cleared by centrifugation. From the resulting supernatant, the peptides were purified on a reversed-phase Sep-Pak C18 cartridge (Waters) and eluted with 50 % acetonitrile. For the di-glycine IP, 20 mg eluted peptide was resuspended in immunoprecipitation buffer, which was cleared by centrifugation once before being subjected to IP. Ubiquitin remnant peptides were enriched using 40 µL of di-glycine-lysine antibody resin (Cell Signaling Technology) for 4 hours at 4°C under constant rotation. The IP was washed three times with ice-cold immunoprecipitation buffer, followed by three washes in water. Subsequently, peptides binding to the beads were

eluted with 0.15 % trifluoroacetic acid. Next, the eluate was fractionated into six fractions by micro-column-based strong cation exchange chromatography (SCX) and finally desalted using reversed-phase C18 StageTips.

MS analysis was performed using a quadrupole Orbitrap mass spectrometer (Q Exactive Plus, Thermo Scientific) equipped with an Ultra High Performance Liquid Chromatography (UHPLC) system (EASY-nLC 1000, Thermo Scientific). Peptides were eluted from C18 reversed-phase columns (15 cm length, 75 µM inner diameter, 1.9 µM bead size) over 2 hours in a linear 8-40 % acetonitrile gradient supplemented with 0.1 % formic acid. Operation of the mass spectrometer was in data-dependent mode, automatically alternating between MS and MS^2 acquisition. In the Orbitrap, survey full scan MS spectra (m/z 300-1700) were measured. After their isolation, the 10 most intense ions were fragmented by higher energy C-trap dissociation (HCD) using an ion selection threshold of 5000, and the resulting fragment spectra were acquired in the Orbitrap mass analyser. Peptides with unassigned charge states or charge states < +2 were excluded from fragmentation.

Analysis of raw data files was performed using MaxQuant (development version 1.5.2.8). The Andromeda search engine was applied to search parent ion and MS^2 spectra against a database containing 6749 yeast protein sequences obtained from UniProtKB released in May 2016. Search parameters were a mass tolerance of 6 ppm in MS mode/20 ppm in HCD MS^2 mode, strict trypsin specificity and up to two miscleavages allowed. Protein N-terminal acetylation, methionine oxidation, N-ethylmaleimide modification of cysteines (mass difference to cysteine carbamidomethylation), and di-glycine- lysine were searched as variable modifications, whereas cysteine carbamidomethylation was searched as a fixed modification. Using the PTM scoring algorithm in MaxQuant, site localization probabilities were calculated. Based on posterior error probability (PEP), the dataset was filtered using a target-decoy approach to reach a false discovery rate of below 1 % estimated. Peptides with a di-glycine lysine of a minimum score of 40 and a minimum delta score of 6 are used for the analysis.

From this analysis we extracted the strong hits falling into the following category: the normalized H/L ratio should be > 1.5 (when *rtt101Δ* cells are labelled light) and < 0.66 (when *rtt101Δ* cells are labelled heavy) in both measurements. Moreover, the intensity should have reached a value > 10^6 in addition to a minimum score of 80 and a low

PEP. In some cases, hits that slightly differed only in the normalized H/L (*rtt101Δ* cells labelled heavy) were manually added to the list if all other criteria were fulfilled.

References

Abbas, T., and Dutta, A. (2009). P21 in cancer: Intricate networks and multiple activities. Nat. Rev. Cancer *9*, 400–414.

Abbas, T., Sivaprasad, U., Terai, K., Amador, V., Pagano, M., and Dutta, A. (2008). PCNA-dependent regulation of p21 ubiquitylation and degradation via the CRL4Cdt2 ubiquitin ligase complex. Genes Dev. *22*, 2496–2506.

Abbas, T., Shibata, E., Park, J., Jha, S., Karnani, N., and Dutta, A. (2010). CRL4Cdt2 regulates cell proliferation and histone gene expression by targeting PR-Set7/Set8 for degradation. Mol. Cell *40*, 9–21.

Adkins, N.L., Swygert, S.G., Kaur, P., Niu, H., Grigoryev, S.A., Sung, P., Wang, H., and Peterson, C.L. (2017). Nucleosome-like, single-stranded DNA (ssDNA)-histone octamer complexes and the implication for DNA double strand break repair. J. Biol. Chem. *292*, 5271–5281.

Aguilera, A., and García-Muse, T. (2012). R Loops: From Transcription Byproducts to Threats to Genome Stability. Mol. Cell *46*, 115–124.

Ahel, I., Rass, U., El-Khamisy, S.F., Katyal, S., Clements, P.M., McKinnon, P.J., Caldecott, K.W., and West, S.C. (2006). The neurodegenerative disease protein aprataxin resolves abortive DNA ligation intermediates. Nature *443*, 713–716.

Aksenova, A., Volkov, K., Maceluch, J., Pursell, Z.F., Rogozin, I.B., Kunkel, T.A., Pavlov, Y.I., and Johansson, E. (2010). Mismatch repair-independent increase in spontaneous mutagenesis in yeast lacking non-essential subunits of DNA polymerase ε. PLoS Genet. *6*.

Alabert, C., Bianco, J.N., and Pasero, P. (2009). Differential regulation of homologous recombination at DNA breaks and replication forks by the Mrc1 branch of the S-phase checkpoint. EMBO J. *28*, 1131–1141.

Alcasabas, A.A., Osborn, A.J., Bachant, J., Hu, F., Werler, P.J.H., Bousset, K., Furuya, K., Diffley, J.F.X., Carr, A.M., and Elledge, S.J. (2001). Mrc1 transduces signals of DNA replication stress to activate Rad53. Nat. Cell Biol. *3*, 958–965.

Allen-Soltero, S., Martinez, S.L., Putnam, C.D., and Kolodner, R.D. (2014). A Saccharomyces cerevisiae RNase H2 Interaction Network Functions To Suppress Genome Instability. Mol. Cell. Biol. *34*, 1521–1534.

Alvaro, D., Lisby, M., and Rothstein, R. (2007). Genome-wide analysis of Rad52 foci reveals diverse mechanisms impacting recombination. PLoS Genet. *3*, 2439–2449.

Araki, H., Hamatake, R.K., Johnston, L.H., and Sugino, a (1991). DPB2, the gene encoding DNA polymerase II subunit B, is required for chromosome replication in Saccharomyces cerevisiae. Proc. Natl. Acad. Sci. U. S. A. *88*, 4601–4605.

Arudchandran, A., Cerritelli, S.M., Narimatsu, S.K., Itaya, M., Shin, D.Y., Shimada, Y., and Crouch, R.J. (2000). The absence of ribonuclease H1 or H2 alters the sensitivity of Saccharomyces cerevisiae to hydroxyurea, caffeine and ethyl methanesulphonate: Implications for roles of RNases H in DNA replication and repair. Genes to Cells *5*, 789–802.

Balk, B., Maicher, A., Dees, M., Klermund, J., Luke-Glaser, S., Bender, K., and Luke, B. (2013). Telomeric RNA-DNA hybrids affect telomere-length dynamics and senescence. Nat. Struct. Mol. Biol. *20*, 1199–1206.

Ban, C., Ramakrishnan, B., and Sundaralingam, M. (1994). Crystal structure of the highly distorted chimeric decamer r(C)d(CGGCGCCG)r(G) spermine complex - spermine binding to phosphate only and minor groove tertiary base-pairing. Nucleic Acids Res. *22*, 5466–5476.

Bando, M., Katou, Y., Komata, M., Tanaka, H., Itoh, T., Sutani, T., and Shirahige, K. (2009). Csm3, Tof1, and Mrc1 form a heterotrimeric mediator complex that associates with DNA replication forks. J. Biol. Chem. *284*, 34355–34365.

Bartsch, K., Knittler, K., Borowski, C., Rudnik, S., Damme, M., Aden, K., Spehlmann, M.E., Frey, N., Saftig, P., Chalaris, A., et al. (2017). Absence of RNase H2 triggers generation of immunogenic micronuclei removed by autophagy. Hum. Mol. Genet. *26*, 3960–3972.

Bärtsch, S., Kang, L.E., and Symington, L.S. (2000). RAD51 is required for the repair of

plasmid double-stranded DNA gaps from either plasmid or chromosomal templates. Mol. Cell. Biol. *20*, 1194–1205.
Baumann, P., Benson, F.E., and West, S.C. (1996). Human Rad51 protein promotes ATP-dependent homologous pairing and strand transfer reactions in vitro. Cell *87*, 757–766.
Bell, S.P., and Labib, K. (2016). Chromosome duplication in Saccharomyces cerevisiae. Genetics *203*, 1027–1067.
Ben-Aroya, S., Agmon, N., Yuen, K., Kwok, T., McManus, K., Kupiec, M., and Hieter, P. (2010). Proteasome nuclear activity affects chromosome stability by controlling the turnover of Mms22, a protein important for DNA repair. PLoS Genet. *6*.
Benson, F.E., Baumann, P., and West, S.C. (1998). Synergistic actions of Rad51 and Rad52 in recombination and DNA repair. Nature *391*, 401–404.
Beranek, D.T. (1990). Distribution of methyl and ethyl adducts following alkylation with monofunctional alkylating agents. Mutat. Res. - Fundam. Mol. Mech. Mutagen. *231*, 11–30.
Berens, T.J., and Toczyski, D.P. (2012). Colocalization of Mec1 and Mrc1 is sufficient for Rad53 phosphorylation in vivo. Mol. Biol. Cell *23*, 1058–1067.
Bermejo, R., Capra, T., Jossen, R., Colosio, A., Frattini, C., Carotenuto, W., Cocito, A., Doksani, Y., Klein, H., Gómez-González, B., et al. (2011). The replication checkpoint protects fork stability by releasing transcribed genes from nuclear pores. Cell *146*, 233–246.
Berti, M., Chaudhuri, A.R., Thangavel, S., Gomathinayagam, S., Kenig, S., Vujanovic, M., Odreman, F., Glatter, T., Graziano, S., Mendoza-Maldonado, R., et al. (2013). Human RECQ1 promotes restart of replication forks reversed by DNA topoisomerase I inhibition. Nat. Struct. Mol. Biol. *20*, 347–354.
Bienko, M., Green, C.M., Crosetto, N., Rudolf, F., Zapart, G., Coull, B., Kannouche, P., Wider, G., Peter, M., Lehmann, A.R., et al. (2005). Ubiquitin-binding domains in translesion synthesis polymerases. Science (80-.). *310*, 1821–1824.
Blastyák, A., Pintér, L., Unk, I., Prakash, L., Prakash, S., and Haracska, L. (2007). Yeast Rad5 Protein Required for Postreplication Repair Has a DNA Helicase Activity Specific for Replication Fork Regression. Mol. Cell *28*, 167–175.
Blow, J.J., and Dutta, A. (2005). Preventing re-replication of chromosomal DNA. Nat. Rev. Mol. Cell Biol. *6*, 476–486.
Brown, J.A., and Suo, Z. (2011). Unlocking the sugar “steric gate” of DNA polymerases. Biochemistry *50*, 1135–1142.
Brown, J.S., and Jackson, S.P. (2015). Ubiquitylation, neddylation and the DNA damage response. Open Biol. *5*, 150018–150018.
Bubeck, D., Reijns, M.A.M., Graham, S.C., Astell, K.R., Jones, E.Y., and Jackson, A.P. (2011). PCNA directs type 2 RNase H activity on DNA replication and repair substrates. Nucleic Acids Res. *39*, 3652–3666.
Bugreev, D. V., Rossi, M.J., and Mazin, A. V. (2011). Cooperation of RAD51 and RAD54 in regression of a model replication fork. Nucleic Acids Res. *39*, 2153–2164.
Buisson, R., Boisvert, J.L., Benes, C.H., and Zou, L. (2015). Distinct but Concerted Roles of ATR, DNA-PK, and Chk1 in Countering Replication Stress during S Phase. Mol. Cell *59*, 1011–1024.
Buser, R., Kellner, V., Melnik, A., Wilson-Zbinden, C., Schellhaas, R., Kastner, L., Piwko, W., Dees, M., Picotti, P., Maric, M., et al. (2016). The Replisome-Coupled E3 Ubiquitin Ligase Rtt101Mms22 Counteracts Mrc1 Function to Tolerate Genotoxic Stress. PLoS Genet.
Cai, Y., Geacintov, N.E., and Broyde, S. (2014). Ribonucleotides as nucleotide excision repair substrates. DNA Repair (Amst). *13*, 55–60.
Calzada, A., Hodgson, B., Kanemaki, M., Bueno, A., and Labib, K. (2005). Molecular anatomy and regulation of a stable replisome eukaryotic DNA at a paused replication fork. Genes Dev. *19*, 1905–1919.
Cejka, P., Plank, J.L., Bachrati, C.Z., Hickson, I.D., and Kowalczykowski, S.C. (2010). Rmi1 stimulates decatenation of double Holliday junctions during dissolution by Sgs1-Top3. Nat. Struct. Mol. Biol. *17*, 1377–1382.
Celic, I., Masumoto, H., Griffith, W.P., Meluh, P., Cotter, R.J., Boeke, J.D., and Verreault, A. (2006). The Sirtuins Hst3 and Hst4p Preserve Genome Integrity by Controlling Histone H3 Lysine 56 Deacetylation. Curr. Biol. *16*, 1280–1289.

Centore, R.C., Havens, C.G., Manning, A.L., Li, J.M., Flynn, R.L., Tse, A., Jin, J., Dyson, N.J., Walter, J.C., and Zou, L. (2010). CRL4Cdt2-mediated destruction of the histone methyltransferase Set8 prevents premature chromatin compaction in S phase. Mol. Cell *40*, 22–33.

Cerritelli, S.M., and Crouch, R.J. (2009). Ribonuclease H: The enzymes in eukaryotes. FEBS J. *276*, 1494–1505.

Chang, M., Bellaoui, M., Boone, C., and Brown, G.W. (2002). A genome-wide screen for methyl methanesulfonate-sensitive mutants reveals genes required for S phase progression in the presence of DNA damage. Proc. Natl. Acad. Sci. U. S. A. *99*, 16934–16939.

Chau, V., Tobias, J.W., Bachmair, A., Marriotr, D., Ecker, D.J., Gonda, D.K., and Varshavsky, A. (1989). A Multiubiquitin Chain Is Confined to Specific Lysine in a Targeted Short-Lived Protein. Science (80-.). *243*, 1576–1583.

Chaudhury, I., and Koepp, D.M. (2017). Degradation of Mrc1 promotes recombination-mediated restart of stalled replication forks. Nucleic Acids Res. *45*, 2558–2570.

Che, J., Smith, S., Kim, Y.J., Shim, E.Y., Myung, K., and Lee, S.E. (2015). Hyper-Acetylation of Histone H3K56 Limits Break-Induced Replication by Inhibiting Extensive Repair Synthesis. PLoS Genet. *11*, 1–24.

Chen, C.C., Carson, J.J., Feser, J., Tamburini, B., Zabaronick, S., Linger, J., and Tyler, J.K. (2008). Acetylated Lysine 56 on Histone H3 Drives Chromatin Assembly after Repair and Signals for the Completion of Repair. Cell *134*, 231–243.

Chen, J.Z., Qiu, J., Shen, B., and Holmquist, G.P. (2000). Mutational spectrum analysis of RNase H(35) deficient Saccharomyces cerevisiae using fluorescence-based directed termination PCR. Nucleic Acids Res. *28*, 3649–3656.

Chen, L.-C., Manjeshwar, S., Lu, Y., Moore, D., Ljung, B.-M., Kuo, W.-L., Dairkee, S.H., Wernick, M., Collins, C., and Smith, H.S. (1998). The Human Homologue for the Caenorhabditis elegans cul-4 Gene Is Amplified and Overexpressed in Primary Breast Cancers. Cancer Res. *58*, 3677 LP-3683.

Chen, X., Zhang, Y., Douglas, L., and Zhou, P. (2001). UV-damaged DNA-binding Proteins Are Targets of CUL-4A-mediated Ubiquitination and Degradation. J. Biol. Chem. *276*, 48175–48182.

Chen, X., Cui, D., Papusha, A., Zhang, X., Chu, C.D., Tang, J., Chen, K., Pan, X., and Ira, G. (2012). The Fun30 nucleosome remodeller promotes resection of DNA double-strand break ends. Nature *489*, 576–580.

Chiu, H.-C., Koh, K.D., Evich, M., Lesiak, A.L., Germann, M.W., Bongiorno, A., Riedo, E., and Storici, F. (2014). RNA intrusions change DNA elastic properties and structure. Nanoscale *6*, 10009–10017.

Cho, J.E., Kim, N., and Jinks-Robertson, S. (2015). Topoisomerase 1-dependent deletions initiated by incision at ribonucleotides are biased to the non-transcribed strand of a highly activated reporter. Nucleic Acids Res. *43*, 9306–9313.

Chon, H., Sparks, J.L., Rychlik, M., Nowotny, M., Burgers, P.M., Crouch, R.J., and Cerritelli, S.M. (2013). RNase H2 roles in genome integrity revealed by unlinking its activities. Nucleic Acids Res. *41*, 3130–3143.

Ciosk, R., Zachariae, W., Michaelis, C., Shevchenko, A., Mann, M., and Nasmyth, K. (1998). An ESP1/PDS1 complex regulates loss of sister chromatid cohesion at the metaphase to anaphase transition in yeast. Cell *93*, 1067–1076.

Clausen, A.R., Murray, M.S., Passer, A.R., Pedersen, L.C., and Kunkel, T.A. (2013a). Structure-function analysis of ribonucleotide bypass by B family DNA replicases. Proc. Natl. Acad. Sci. *110*, 16802–16807.

Clausen, A.R., Zhang, S., Burgers, P.M., Lee, M.Y., and Kunkel, T.A. (2013b). Ribonucleotide incorporation, proofreading and bypass by human DNA polymerase δ. DNA Repair (Amst). *12*, 121–127.

Clemente-Ruiz, M., Gonzále-Prieto, R., and Prado, F. (2011). Histone H3K56 Acetylation, CAF1, and Rtt106 Coordinate Nucleosome Assembly and Stability of Advancing Replication Forks. PLoS Genet. *7*.

Cobb, J.A., Bjergbaek, L., Shimada, K., Frei, C., and Gasser, S.M. (2003). DNA polymerase stabilization at stalled replication forks requires Mec1 and the RecQ helicase Sgs1. EMBO

J. *22*, 4325–4336.
Collins, S.R., Miller, K.M., Maas, N.L., Roguev, A., Fillingham, J., Chu, C.S., Schuldiner, M., Gebbia, M., Recht, J., Shales, M., et al. (2007). Functional dissection of protein complexes involved in yeast chromosome biology using a genetic interaction map. Nature *446*, 806–810.
Conover, H.N., Lujan, S.A., Chapman, M.J., Cornelio, D.A., Sharif, R., Williams, J.S., Clark, A.B., Camilo, F., Kunkel, T.A., and Argueso, J.L. (2015). Stimulation of chromosomal rearrangements by ribonucleotides. Genetics *201*, 951–961.
Costes, A., and Lambert, S.A.E. (2013). Homologous recombination as a replication fork escort: Fork-protection and recovery. Biomolecules *3*, 39–71.
Crow, Y.J., and Manel, N. (2015). Aicardi-Goutières syndrome and the type I interferonopathies. Nat. Rev. Immunol. *15*, 429–440.
Crow, Y.J., Leitch, A., Hayward, B.E., Garner, A., Parmar, R., Griffith, E., Ali, M., Semple, C., Aicardi, J., Babul-Hirji, R., et al. (2006). Mutations in genes encoding ribonuclease H2 subunits cause Aicardi-Goutières syndrome and mimic congenital viral brain infection. Nat. Genet. *38*, 910–916.
Daigaku, Y., Davies, A.A., and Ulrich, H.D. (2010). Ubiquitin-dependent DNA damage bypass is separable from genome replication. Nature *465*, 951–955.
Daraba, A., Gali, V.K., Halmai, M., Haracska, L., and Unk, I. (2014). Def1 Promotes the Degradation of Pol3 for Polymerase Exchange to Occur During DNA-Damage-Induced Mutagenesis in Saccharomyces cerevisiae. PLoS Biol. *12*.
Davies, A.A., Huttner, D., Daigaku, Y., Chen, S., and Ulrich, H.D. (2008). Activation of Ubiquitin-Dependent DNA Damage Bypass Is Mediated by Replication Protein A. Mol. Cell *29*, 625–636.
Deem, A., Keszthelyi, A., Blackgrove, T., Vayl, A., Coffey, B., Mathur, R., Chabes, A., and Malkova, A. (2011). Break-induced replication is highly inaccurate. PLoS Biol. *9*.
Degrassi, F., De Salvia, R., Tanzarella, C., and Palitti, F. (1989). Induction of chromosomal aberrations and SCE by camptothecin, and inhibitor of mammalian topoisomerase I. Mutat. Res. - Fundam. Mol. Mech. Mutagen. *211*, 125–130.
Derose, E.F., Perera, L., Murray, M.S., Kunkel, T.A., and London, R.E. (2012). Solution structure of the Dickerson DNA dodecamer containing a single ribonucleotide. Biochemistry *51*, 2407–2416.
Dhanwani, R., Takahashi, M., and Sharma, S. (2018). Cytosolic sensing of immuno-stimulatory DNA, the enemy within. Curr. Opin. Immunol. *50*, 82–87.
Diao, L., Chen, C., Dennehey, B., Pal, S., Wang, P., Shen, Z., Deem, A., and Tyler, J.K. (2017). Delineation of the role of chromatin assembly and the Rtt101 Mms1 E3 ubiquitin ligase in DNA damage checkpoint recovery in budding yeast. PLoS One *12*, 1–22.
Donnianni, R.A., and Symington, L.S. (2013). Break-induced replication occurs by conservative DNA synthesis. Proc. Natl. Acad. Sci. *110*, 13475–13480.
Downs, J.A. (2008). Histone H3 K56 acetylation, chromatin assembly, and the DNA damage checkpoint. DNA Repair (Amst). *7*, 2020–2024.
Drogaris, P., Villeneuve, V., Pomiès, C., Lee, E.H., Bourdeau, V., Bonneil, É., Ferbeyre, G., Verreault, A., and Thibault, P. (2012). Histone deacetylase inhibitors globally enhance H3/H4 tail acetylation without affecting H3 lysine 56 acetylation. Sci. Rep. *2*, 1–12.
Drury, L.S., Perkins, G., and Diffley, J.F.X. (1997). The Cdc4/34/53 pathway targets Cdc6p for proteolysis in budding yeast. EMBO J. *16*, 5966–5976.
Dua, R., Levy, D.L., and Campbell, J.L. (1998). Role of the putative zinc finger domain of Saccharomyces cerevisiae DNA polymerase ε in DNA replication and the S/M checkpoint pathway. J. Biol. Chem. *273*, 30046–30055.
Dua, R., Levy, D.L., and Campbell, J.L. (1999). Analysis of the essential functions of the C-terminal protein/protein interaction domain of Saccharomyces cerevisiae pol ?? and its unexpected ability to support growth in the absence of the DNA polymerase domain. J. Biol. Chem. *274*, 22283–22288.
Dungrawala, H., Rose, K.L., Bhat, K.P., Mohni, K.N., Glick, G.G., Couch, F.B., and Cortez, D. (2015). The Replication Checkpoint Prevents Two Types of Fork Collapse without Regulating Replisome Stability. Mol. Cell *59*, 998–1010.

Dunn, K., and Griffith, J.D. (1980). The presence of RNA in a double helix inhibits its interaction with histone protein. Nucleic Acids Res. *8*, 555–566.

Duro, E., Vaisica, J.A., Brown, G.W., and Rouse, J. (2008). Budding yeast Mms22 and Mms1 regulate homologous recombination induced by replisome blockage. DNA Repair (Amst). *7*, 811–818.

Duro, E., Lundin, C., Ask, K., Sanchez-Pulido, L., MacArtney, T.J., Toth, R., Ponting, C.P., Groth, A., Helleday, T., and Rouse, J. (2010). Identification of the MMS22L-TONSL Complex that promotes homologous recombination. Mol. Cell *40*, 632–644.

Eder, P.S., Walder, R.Y., and Walder, J.A. (1993). Substrate specificity of human RNase H1 and its role in excision repair of ribose residues misincorporated in DNA. Biochimie *75*, 123–126.

Eggler, A.L., Inman, R.B., and Cox, M.M. (2002). The Rad51-dependent pairing of long DNA substrates is stabilized by replication protein A. J. Biol. Chem. *277*, 39280–39288.

Egli, M., Usman, N., and Rich, A. (1993). Conformational Influence of the Ribose 2′-Hydroxyl Group: Crystal Structures of DNA-RNA Chimeric Duplexess. Biochemistry *32*, 3221–3237.

Emili, A., Schieltz, D.M., Iii, J.R.Y., and Hartwell, L.H. (2001). Dynamic Interaction of DNA Damage Checkpoint Protein Rad53 with Chromatin Assembly Factor Asf1. *7*, 13–20.

Endo, H., Kawashima, S., Sato, L., Lai, M.S., Enomoto, T., Seki, M., and Horikoshi, M. (2010). Chromatin dynamics mediated by histone modifiers and histone chaperones in postreplicative recombination. Genes to Cells *15*, 945–958.

Fasching, C.L., Cejka, P., Kowalczykowski, S.C., and Heyer, W.D. (2015). Top3-Rmi1 dissolve Rad51-mediated D loops by a topoisomerase-based mechanism. Mol. Cell *57*, 595–606.

Feldman, R.M.R., Correll, C.C., Kaplan, K.B., and Deshaies, R.J. (1997). A complex of Cdc4p, Skp1p, and Cdc53p/cullin catalyzes ubiquitination of the phosphorylated CDK inhibitor Sic1p. Cell *91*, 221–230.

Finley, D., Ulrich, H.D., Sommer, T., and Kaiser, P. (2012). The ubiquitin-proteasome system of Saccharomyces cerevisiae. Genetics *192*, 319–360.

Fisher, R.I., Bernstein, S.H., Kahl, B.S., Djulbegovic, B., Robertson, M.J., De Vos, S., Epner, E., Krishnan, A., Leonard, J.P., Lonial, S., et al. (2006). Multicenter phase II study of bortezomib in patients with relapsed or refractory mantle cell lymphoma. J. Clin. Oncol. *24*, 4867–4874.

Fong, C.M., Arumugam, A., and Koepp, D.M. (2013). The saccharomyces cerevisiae F-Box Protein Dia2 is a mediator of S-Phase checkpoint recovery from DNA damage. Genetics *193*, 483–499.

Fotedar, R., Bendjennat, M., and Fotedar, A. (2004). Role of p21 WAF1 in the Cellular Response to UV. Cell Cycle *3*, 134–137.

Fu, Y., and Xiao, W. (2006). Identification and characterization of CRT10 as a novel regulator of Saccharomyces cerevisiae ribonucleotide reductase genes. Nucleic Acids Res. *34*, 1876–1883.

Fujii, K., Kitabatake, M., Sakata, T., Miyata, A., and Ohno, M. (2009). A role for ubiquitin in the clearance of nonfunctional rRNAs. Genes Dev. *23*, 963–974.

Fujiwara, Y., and Tatsumi, M. (1976). Replicative bypass repair of ultraviolet damage to DNA of mammalian cells: Caffeine sensitive and caffeine resistant mechanisms. Mutat. Res. *37*, 91–109.

Fumasoni, M., Zwicky, K., Vanoli, F., Lopes, M., and Branzei, D. (2015). Error-Free DNA Damage Tolerance and Sister Chromatid Proximity during DNA Replication Rely on the Polα/Primase/Ctf4 Complex. Mol. Cell *57*, 812–823.

Gadaleta, M.C., and Noguchi, E. (2017). Regulation of DNA replication through natural impediments in the eukaryotic genome. Genes (Basel). *8*.

Gaines, W.A., Godin, S.K., Kabbinavar, F.F., Rao, T., VanDemark, A.P., Sung, P., and Bernstein, K.A. (2015). Promotion of presynaptic filament assembly by the ensemble of S. cerevisiae Rad51 paralogues with Rad52. Nat. Commun. *6*.

Gambus, A., Jones, R.C., Sanchez-Diaz, A., Kanemaki, M., van Deursen, F., Edmondson, R.D., and Labib, K. (2006). GINS maintains association of Cdc45 with MCM in replisome progression complexes at eukaryotic DNA replication forks. Nat. Cell Biol. *8*, 358–366.

Gambus, A., Van Deursen, F., Polychronopoulos, D., Foltman, M., Jones, R.C., Edmondson,

R.D., Calzada, A., and Labib, K. (2009). A key role for Ctf4 in coupling the MCM2-7 helicase to DNA polymerase α within the eukaryotic replisome. EMBO J. *28*, 2992–3004.

Gan, H., Yu, C., Devbhandari, S., Sharma, S., Han, J., Chabes, A., Remus, D., and Zhang, Z. (2017). Checkpoint Kinase Rad53 Couples Leading- and Lagging-Strand DNA Synthesis under Replication Stress. Mol. Cell *68*, 446–455.e3.

Garbacz, M., Araki, H., Flis, K., Bebenek, A., Zawada, A.E., Jonczyk, P., Makiela-Dzbenska, K., and Fijalkowska, I.J. (2015). Fidelity consequences of the impaired interaction between DNA polymerase epsilon and the GINS complex. DNA Repair (Amst). *29*, 23–35.

García-Gómez, S., Reyes, A., Martínez-Jiménez, M.I., Chocrón, E.S., Mourón, S., Terrados, G., Powell, C., Salido, E., Méndez, J., Holt, I.J., et al. (2013). PrimPol, an Archaic Primase/Polymerase Operating in Human Cells. Mol. Cell *52*, 541–553.

García-Rodríguez, N., Morawska, M., Wong, R.P., Daigaku, Y., and Ulrich, H.D. (2018). Spatial separation between replisome- and template-induced replication stress signaling. EMBO J. e98369.

Garg, P., and Burgers, P.M. (2005). Ubiquitinated proliferating cell nuclear antigen activates translesion DNA polymerases eta and REV1. Proc. Natl. Acad. Sci. U. S. A. *102*, 18361–18366.

Gari, K., Decaillet, C., Delannoy, M., Wu, L., and Constantinou, A. (2008). Remodeling of DNA replication structures by the branch point translocase FANCM. Proc. Natl. Acad. Sci. *105*, 16107–16112.

Gelot, C., Magdalou, I., and Lopez, B.S. (2015). Replication stress in mammalian cells and its consequences for mitosis. Genes (Basel). *6*, 267–298.

Georgescu, R.E., Langston, L., Yao, N.Y., Yurieva, O., Zhang, D., Finkelstein, J., Agarwal, T., and O'Donnell, M.E. (2014). Mechanism of asymmetric polymerase assembly at the eukaryotic replication fork. Nat. Struct. Mol. Biol. *21*, 664–670.

Glassner, B.J., Rasmussen, L.J., Najarian, M.T., Posnick, L.M., and Samson, L.D. (1998). Generation of a strong mutator phenotype in yeast by imbalanced base excision repair. Proc. Natl. Acad. Sci. U. S. A. *95*, 9997–10002.

Göksenin, A.Y., Zahurancik, W., LeCompte, K.G., Taggart, D.J., Suo, Z., and Pursell, Z.F. (2012). Human DNA polymerase ε is able to efficiently extend from multiple consecutive ribonucleotides. J. Biol. Chem. *287*, 42675–42684.

Gómez-González, B., García-Rubio, M., Bermejo, R., Gaillard, H., Shirahige, K., Marín, A., Foiani, M., and Aguilera, A. (2011). Genome-wide function of THO/TREX in active genes prevents R-loop-dependent replication obstacles. EMBO J. *30*, 3106–3119.

González-Prieto, R., Muñoz-Cabello, A.M., Cabello-Lobato, M.J., and Prado, F. (2013). Rad51 replication fork recruitment is required for DNA damage tolerance. EMBO J. *32*, 1307–1321.

Gravel, S., Chapman, J.R., Magill, C., and Jackson, S.P. (2008). DNA helicases Sgs1 and BLM promote DNA double-strand break resection. Genes Dev. *22*, 2767–2772.

Groisman, R., Polanowska, J., Kuraoka, I., Sawada, J.I., Saijo, M., Drapkin, R., Kisselev, A.F., Tanaka, K., and Nakatani, Y. (2003). The ubiquitin ligase activity in the DDB2 and CSA complexes is differentially regulated by the COP9 signalosome in response to DNA damage. Cell *113*, 357–367.

Groth, P., Ausländer, S., Majumder, M.M., Schultz, N., Johansson, F., Petermann, E., and Helleday, T. (2010). Methylated DNA Causes a Physical Block to Replication Forks Independently of Damage Signalling, O6-Methylguanine or DNA Single-Strand Breaks and Results in DNA Damage. J. Mol. Biol. *402*, 70–82.

Günther, C., Kind, B., Reijns, M.A.M., Berndt, N., Martinez-bueno, M., Wolf, C., Tüngler, V., Chara, O., Lee, Y.A., Hübner, N., et al. (2015). Defective removal of ribonucleotides from DNA promotes systemic autoimmunity. J. Clin. Invest. *125*, 413–424.

Guo, C., Tang, T.-S., Bienko, M., Parker, J.L., Bielen, A.B., Sonoda, E., Takeda, S., Ulrich, H.D., Dikic, I., and Friedberg, E.C. (2006). Ubiquitin-Binding Motifs in REV1 Protein Are Required for Its Role in the Tolerance of DNA Damage. Mol. Cell. Biol. *26*, 8892–8900.

Guthrie, C., and Fink, G.R. (1991). Guide to Yeast Genetics and Molecular Biology (San Diego: Academic Press).

Hamatake, R.K., Hasegawa, H., Clark, A.B., Bebenek, K., Kunkel, T.A., and A, S. (1990). Purification and characterization of DNA polymerase II from the yeast Saccharomyces

cerevisiae. J. Biol. Chem. *265*, 4072–4088.
Hamperl, S., and Cimprich, K.A. (2014). The contribution of co-transcriptional RNA:DNA hybrid structures to DNA damage and genome instability. DNA Repair (Amst). *19*, 84–94.
Han, J., Zhou, H., Horazdovsky, B., Zhang, K., Xu, R., and Zhang, Z. (2007a). Rtt109 Acetylates Histone H3 Lysine 56 and Functions in DNA Replication. Science (80-.). *3*, 653–656.
Han, J., Zhou, H., Li, Z., Xu, R., and Zhang, Z. (2007b). The Rtt109-Vps75 Histone Acetyltransferase Complex Acetylates Non-nucleosomal Histone H3. J. Biol. Chem. *282*, 14158–14164.
Han, J., Li, Q., McCullough, L., Kettelkamp, C., Formosa, T., and Zhang, Z. (2010). Ubiquitylation of FACT by the Cullin-E3 ligase Rtt101 connects FACT to DNA replication. Genes Dev. *24*, 1485–1490.
Han, J., Zhang, H., Zhang, H., Wang, Z., Zhou, H., and Zhang, Z. (2013). A Cul4 E3 ubiquitin ligase regulates histone hand-off during nucleosome assembly. Cell *155*, 817–829.
Hanada, K., Budzowska, M., Davies, S.L., Van Drunen, E., Onizawa, H., Beverloo, H.B., Maas, A., Essers, J., Hickson, I.D., and Kanaar, R. (2007). The structure-specific endonuclease Mus81 contributes to replication restart by generating double-strand DNA breaks. Nat. Struct. Mol. Biol. *14*, 1096–1104.
Hang, L.E., Peng, J., Tan, W., Szakal, B., Menolfi, D., Sheng, Z., Lobachev, K., Branzei, D., Feng, W., and Zhao, X. (2015). Rtt107 Is a Multi-functional Scaffold Supporting Replication Progression with Partner SUMO and Ubiquitin Ligases. Mol. Cell *60*, 268–279.
Hannah, J., and Zhou, P. (2015). Distinct and overlapping functions of the cullin E3 ligase scaffolding proteins CUL4A and CUL4B. Gene *573*, 33–45.
Hashimoto, Y., Puddu, F., and Costanzo, V. (2012). RAD51-and MRE11-dependent reassembly of uncoupled CMG helicase complex at collapsed replication forks. Nat. Struct. Mol. Biol. *19*, 17–25.
Heidelberger, J.B., Wagner, S.A., and Beli, P. (2016). Mass spectrometry-based proteomics forinvestigating DNA damage-associated protein ubiquitylation. Front. Genet. *7*, 1–7.
Heidelberger, J.B., Voigt, A., Borisova, M.E., Petrosino, G., Ruf, S., Wagner, S.A., and Beli, P. (2018). Proteomic profiling of VCP substrates links VCP to K6-linked ubiquitylation and c-Myc function. EMBO Rep. e44754.
Hicks, W.M., Kim, M., and Haber, J.E. (2010). Increased mutagenesis and unique mutation signature associated with mitotic gene conversion. Science (80-.). *329*, 82–85.
Higa, L.A.A., Mihaylov, I.S., Banks, D.P., Zheng, J., and Zhang, H. (2003). Radiation-mediated proteolysis of CDT1 by CUL4-ROC1 and CSN complexes constitutes a new checkpoint. Nat. Cell Biol. *5*, 1008–1015.
Higgins, N.P., Kato, K., and Strauss, B. (1976). A model for replication repair in mammalian cells. J. Mol. Biol. *101*, 417–425.
Hiller, B., Achleitner, M., Glage, S., Naumann, R., Behrendt, R., and Roers, A. (2012). Mammalian RNase H2 removes ribonucleotides from DNA to maintain genome integrity. J. Exp. Med. *209*, 1419–1426.
Hodgson, B., Calzada, A., and Labib, K. (2007). Mrc1 and Tof1 Regulate DNA Replication Forks in Different Ways during Normal S Phase. Mol. Biol. Cell *18*, 3894–3902.
Hoege, C., Pfander, B., Moldovan, G.L., Pyrowolakis, G., and Jentsch, S. (2002). RAD6-dependent DNA repair is linked to modification of PCNA by ubiquitin and SUMO. Nature *419*, 135–141.
Hogg, M., and Johansson, E. (2012). DNA Polymerase ε. In The Eukaryotic Replisome: A Guide to Protein Structure and Function, pp. 237–257.
Hombauer, H., Srivatsan, A., Putnam, C.D., and Kolodner, R.D. (2011). Mismatch Repair, But Not Heteroduplex Rejection, Is Temporally Coupled to DNA Replication. Science (80-.). 1713–1716.
Hovatter, K.R., and Martinson, H.G. (1987). Ribonucleotide-induced helical alteration in DNA prevents nucleosome formation. Proc. Natl. Acad. Sci. *84*, 1162–1166.
Hryciw, T., Tang, M., Fontanie, T., and Xiao, W. (2001). MMS1 protects against replication-dependent DNA damage in saccharomyces cerevisiae. Mol. Genet. Genomics *266*, 848–857.

Hu, F., Alcasabas, A.A., and Elledge, S.J. (2001). Asf1 links Rad53 to control of chromatin assembly. Genes Dev. *15*, 1061–1066.

Hu, J., McCall, C.M., Ohta, T., and Xiong, Y. (2004). Targeted ubiquitination of CDT1 by the DDB1-CUL4A-ROC1 ligase in response to DNA damage. Nat. Cell Biol. *6*, 1003–1009.

Huang, S.N., Williams, J.S., Arana, M.E., Kunkel, T.A., and Pommier, Y. (2017). Topoisomerase I-mediated cleavage at unrepaired ribonucleotides generates DNA double-strand breaks. EMBO J. *36*, 361–373.

Huang, S.Y.N., Ghosh, S., and Pommier, Y. (2015). Topoisomerase I alone is sufficient to produce short DNA deletions and can also reverse nicks at ribonucleotide sites. J. Biol. Chem. *290*, 14068–14076.

Huang, S.Y.N., Williams, S.K., Arana, M.E., Kunkel, T.A., and Pommier, Y. (2016). Topoisomerase I-mediated cleavage at unrepaired ribonucleotides generates DNA double-strand breaks. EMBO J.

Huang, T.-H., Fowler, F., Chen, C.-C., Shen, Z.-J., Sleckman, B., and Tyler, J.K. (2018). The Histone Chaperones ASF1 and CAF-1 Promote MMS22L-TONSL-Mediated Rad51 Loading onto ssDNA during Homologous Recombination in Human Cells. Mol. Cell 1–14.

Huertas, P., and Aguilera, A. (2003). Cotranscriptionally formed DNA:RNA hybrids mediate transcription elongation impairment and transcription-associated recombination. Mol. Cell *12*, 711–721.

Ii, M., Ii, T., Mironova, L.I., and Brill, S.J. (2011). Epistasis analysis between homologous recombination genes in Saccharomyces cerevisiae identifies multiple repair pathways for Sgs1, Mus81-Mms4 and RNase H2. Mutat. Res. - Fundam. Mol. Mech. Mutagen. *714*, 33–43.

Impens, F., Radoshevich, L., Cossart, P., and Ribet, D. (2014). Mapping of SUMO sites and analysis of SUMOylation changes induced by external stimuli. Proc. Natl. Acad. Sci. *111*, 12432–12437.

Ira, G., Satory, D., and Haber, J.E. (2006). Conservative Inheritance of Newly Synthesized DNA in Double-Strand Break-Induced Gene Conversion. Mol. Cell. Biol. *26*, 9424–9429.

Irene, C., Theis, J.F., Gresham, D., Soteropoulos, P., and Newlon, C.S. (2016). Hst3p, a histone deacetylase, promotes maintenance of Saccharomyces cerevisiae chromosome III lacking efficient replication origins. Mol. Genet. Genomics *291*, 271–283.

Isoz, I., Persson, U., Volkov, K., and Johansson, E. (2012). The C-terminus of Dpb2 is required for interaction with Pol2 and for cell viability. Nucleic Acids Res. *40*, 11545–11553.

Jain, S., Sugawara, N., Lydeard, J., Vaze, M., Gac, N.T. Le, and Haber, J.E. (2009). A recombination execution checkpoint regulates the choice of homologous recombination pathway during DNA double-strand break repair. Genes Dev. *23*, 291–303.

Jaishree, T.N., Wang, A.H.J., van der Marel, G.A., and van Boom, J.H. (1993). Structural Influence of RNA Incorporation in DNA: Quantitative Nuclear Magnetic Resonance Refinement of d(CG)r(CG)d(CG) and d(CG)r(C)d(TAGCG). Biochemistry *32*, 4903–4911.

Jang, S.-M., Redon, C.E., and Aladjem, M.I. (2018). Chromatin-Bound Cullin-Ring Ligases: Regulatory Roles in DNA Replication and Potential Targeting for Cancer Therapy. Front. Mol. Biosci. *5*.

Janke, C., Magiera, M.M., Rathfelder, N., Taxis, C., Reber, S., Maekawa, H., Moreno-Borchart, A., Doenges, G., Schwob, E., Schiebel, E., et al. (2004). A versatile toolbox for PCR-based tagging of yeast genes: New fluorescent proteins, more markers and promoter substitution cassettes. Yeast *21*, 947–962.

Jaszczur, M., Flis, K., Rudzka, J., Kraszewska, J., Budd, M.E., Polaczek, P., Campbell, J.L., Jonczyk, P., and Fijalkowska, I.J. (2008). Dpb2p, a noncatalytic subunit of DNA polymerase ε, contributes to the fidelity of DNA replication in Saccharomyces cerevisiae. Genetics *178*, 633–647.

Jaszczur, M., Rudzka, J., Kraszewska, J., Flis, K., Polaczek, P., Campbell, J.L., Fijalkowska, I.J., and Jonczyk, P. (2009). Defective interaction between Pol2p and Dpb2p, subunits of DNA polymerase epsilon, contributes to a mutator phenotype in Saccharomyces cerevisiae. Mutat. Res. - Fundam. Mol. Mech. Mutagen. *669*, 27–35.

Jeong, H.S., Backlund, P.S., Chen, H.C., Karavanov, A.A., and Crouch, R.J. (2004). RNase H2 of Saccharomyces cerevisiae is a complex of three proteins. Nucleic Acids Res. *32*,

407–414.
Johnson, R.E., Prakash, L., and Prakash, S. (2012). Pol31 and Pol32 subunits of yeast DNA polymerase are also essential subunits of DNA polymerase . Proc. Natl. Acad. Sci. *109*, 12455–12460.
Karras, G.I., and Jentsch, S. (2010). The RAD6 DNA damage tolerance pathway operates uncoupled from the replication fork and is functional beyond S phase. Cell *141*, 255–267.
Katou, Y., Kanoh, Y., Bando, M., Noguchi, H., Tanaka, H., Ashikari, T., Sugimoto, K., and Shirahige, K. (2003). S-phase checkpoint proteins Tof1 and Mrc1 form a stable replication-pausing complex. Nature *424*, 1078–1083.
Katyal, S., El-Khamisy, S.F., Russell, H.R., Li, Y., Ju, L., Caldecott, K.W., and McKinnon, P.J. (2007). TDP1 facilitates chromosomal single-strand break repair in neurons and is neuroprotective in vivo. EMBO J. *26*, 4720–4731.
Katyal, S., Lee, Y., Nitiss, K.C., Downing, S.M., Li, Y., Shimada, M., Zhao, J., Russell, H.R., Petrini, J.H.J., Nitiss, J.L., et al. (2014). Aberrant topoisomerase-1 DNA lesions are pathogenic in neurodegenerative genome instability syndromes. Nat. Neurosci. *17*, 813–821.
Kaur, M., Khan, M.M., Kar, A., Sharma, A., and Saxena, S. (2012). CRL4-DDB1-VPRBP ubiquitin ligase mediates the stress triggered proteolysis of Mcm10. Nucleic Acids Res. *40*, 7332–7346.
Kellner, V. (2014). Understanding the function of the Rtt101 ubiquitin ligase in response to DNA damage and telomere dysfunction in Saccharomyces Cerevisiae. 1–72.
Kerzendorfer, C., Whibley, A., Carpenter, G., Outwin, E., Chiang, S.C., Turner, G., Schwartz, C., El-Khamisy, S., Raymond, F.L., and O'Driscoll, M. (2010). Mutations in Cullin 4B result in a human syndrome associated with increased camptothecin-induced topoisomerase I-dependent DNA breaks. Hum. Mol. Genet. *19*, 1324–1334.
Kesti, T., Flick, K., Keränen, S., Syväoja, J.E., and Wittenberg, C. (1999). DNA polymerase epsilon catalytic domains are dispensable for DNA replication, DNA repair, and cell viability. Mol. Cell *3*, 679–685.
Kesti, T., McDonald, W.H., Yates, J.R., and Wittenberg, C. (2004). Cell Cycle-dependent Phosphorylation of the DNA Polymerase Epsilon Subunit, Dpb2, by the Cdc28 Cyclin-dependent Protein Kinase. J. Biol. Chem. *279*, 14245–14255.
Kim, N., Huang, S.Y.N., Williams, J.S., Li, Y.C., Clark, A.B., Cho, J.E., Kunkel, T.A., Pommier, Y., and Jinks-Robertson, S. (2011). Mutagenic processing of ribonucleotides in DNA by yeast topoisomerase I. Science (80-.). *332*, 1561–1564.
Kim, Y., Starostina, N.G., and Kipreos, E.T. (2008). The CRL4 Cdt2 ubiquitin ligase targets the degradation of p21 Cip1 to control replication licensing. Genes Dev. *22*, 2507–2519.
Kind, B., Muster, B., Staroske, W., Herce, H.D., Sachse, R., Rapp, A., Schmidt, F., Koss, S., Cardoso, M.C., and Lee-Kirsch, M.A. (2014). Altered spatio-temporal dynamics of RNase H2 complex assembly at replication and repair sites in Aicardi-Goutières syndrome. Hum. Mol. Genet. *23*, 5950–5960.
Kirisako, T., Kamei, K., Murata, S., Kato, M., Fukumoto, H., Kanie, M., Sano, S., Tokunaga, F., Tanaka, K., and Iwai, K. (2006). A ubiquitin ligase complex assembles linear polyubiquitin chains. EMBO J. *25*, 4877–4887.
Kobayashi, T. (2003). The replication fork barrier site forms a unique structure with Fob1p and inhibits the replication fork. Mol. Cell. Biol. *23*, 9178–9188.
Kobayashi, T., and Horiuchi, T. (1996). A yeast gene product, Fob1 protein, required for both replication fork blocking and recombinational hotspot activities. Genes Cells *1*, 465–474.
Kolinjivadi, A.M., Sannino, V., De Antoni, A., Zadorozhny, K., Kilkenny, M., Técher, H., Baldi, G., Shen, R., Ciccia, A., Pellegrini, L., et al. (2017). Smarcal1-Mediated Fork Reversal Triggers Mre11-Dependent Degradation of Nascent DNA in the Absence of Brca2 and Stable Rad51 Nucleofilaments. Mol. Cell *67*, 867–881.e7.
Komander, D., and Rape, M. (2012). The Ubiquitin Code. Annu. Rev. Biochem. *81*, 203–229.
Komata, M., Bando, M., Araki, H., and Shirahige, K. (2009). The Direct Binding of Mrc1, a Checkpoint Mediator, to Mcm6, a Replication Helicase, Is Essential for the Replication Checkpoint against Methyl Methanesulfonate-Induced Stress. Mol. Cell. Biol. *29*, 5008–5019.

Kondo, T., Matsumoto, K., and Sugimoto, K. (1999). Role of a complex containing Rad17, Mec3, and Ddc1 in the yeast DNA damage checkpoint pathway. Mol Cell Biol *19*, 1136–1143.

Krakoff, I.H., Brown, N.C., and Reichard, P. (1968). Inhibition Reductase of Ribonucleoside by Hydroxyurea1 Diphosphate. Proteins 1559–1565.

Kraszewska, J., Garbacz, M., Jonczyk, P., Fijalkowska, I.J., and Jaszczur, M. (2012). Defect of Dpb2p, a noncatalytic subunit of DNA polymerase e{open}, promotes error prone replication of undamaged chromosomal DNA in Saccharomyces cerevisiae. Mutat. Res. - Fundam. Mol. Mech. Mutagen. *737*, 34–42.

Kravtsova-Ivantsiv, Y., and Ciechanover, A. (2012). Non-canonical ubiquitin-based signals for proteasomal degradation. J. Cell Sci. *125*, 539–548.

Krejci, L., Van Komen, S., Li, Y., Villemain, J., Reddy, M.S., Klein, H.L., Ellenberger, T., and Sung, P. (2003). DNA helicase Srs2 disrupts the Rad51 presynaptic filament. Nature *423*, 305–309.

Langston, L.D., Zhang, D., Yurieva, O., Georgescu, R.E., Finkelstein, J., Yao, N.Y., Indiani, C., and O'Donnell, M.E. (2014). CMG helicase and DNA polymerase form a functional 15-subunit holoenzyme for eukaryotic leading-strand DNA replication. Proc. Natl. Acad. Sci. *111*, 15390–15395.

Laplaza, J., Bostick, M., Scholes, D., CURCIO, M., and Callis, J. (2004). Saccharomyces cerevisiae ubiquitin-like protein Rub1 conjugates to cullin proteins Rtt101 and Cul3 in vivo. Biochem. J. *377*, 459–467.

LaRiviere, F.J., Cole, S.E., Ferullo, D.J., and Moore, M.J. (2006). A late-acting quality control process for mature eukaryotic rRNAs. Mol. Cell *24*, 619–626.

Lazzaro, F., Novarina, D., Amara, F., Watt, D.L., Stone, J.E., Costanzo, V., Burgers, P.M., Kunkel, T.A., Plevani, P., and Muzi-Falconi, M. (2012). RNase H and postreplication repair protect cells from ribonucleotides incorporated in DNA. Mol. Cell *45*, 99–110.

Lemaçon, D., Jackson, J., Quinet, A., Brickner, J.R., Li, S., Yazinski, S., You, Z., Ira, G., Zou, L., Mosammaparast, N., et al. (2017). MRE11 and EXO1 nucleases degrade reversed forks and elicit MUS81-dependent fork rescue in BRCA2-deficient cells. Nat. Commun. *8*.

Lesher, D.-T.T., Pommier, Y., Stewart, L., and Redinbo, M.R. (2002). 8-oxoguanine rearranges the active site of human topoisomerase I. Proc. Natl. Acad. Sci. U. S. A. *99*, 12102–12107.

Van Leung-Pineda, Huh, J., and Piwnica-Worms, H. (2009). DDB1 targets Chk1 to the Cul4 E3 ligase complex in normal cycling cells and in cells experiencing replication stress. Cancer Res. *69*, 2630–2637.

Li, Y., and Breaker, R.R. (1999). Kinetics of RNA degradation by specific base catalysis of transesterification involving the 2'-hydroxyl group. J. Am. Chem. Soc. *121*, 5364–5372.

Li, Q., Zhou, H., Wurtele, H., Davies, B., Horazdovsky, B., Verreault, A., and Zhang, Z. (2008). Acetylation of Histone H3 Lysine 56 Regulates Replication-Coupled Nucleosome Assembly. Cell *134*, 244–255.

Li, Q., Burgess, R., and Zhang, Z. (2012). All roads lead to chromatin: Multiple pathways for histone deposition. Biochim. Biophys. Acta - Gene Regul. Mech. *1819*, 238–246.

Li, X., Stith, C.M., Burgers, P.M., and Heyer, W.D. (2009). PCNA Is Required for Initiation of Recombination-Associated DNA Synthesis by DNA Polymerase δ. Mol. Cell *36*, 704–713.

Liakopoulos, D., Doenges, G., Matuschewski, K., and Jentsch, S. (1998). A novel protein modification pathway related to the ubiquitin system. EMBO J. *17*, 2208–2214.

Liang, F., and Wang, Y. (2007). DNA Damage Checkpoints Inhibit Mitotic Exit by Two Different Mechanisms. Mol. Cell. Biol. *27*, 5067–5078.

Lin, C.P., Ban, Y., Lyu, Y.L., Desai, S.D., and Liu, L.F. (2008). A ubiquitin-proteasome pathway for the repair of topoisomerase I-DNA covalent complexes. J. Biol. Chem. *283*, 21074–21083.

Lin, C.P., Ban, Y., Lyu, Y.L., and Liu, L.F. (2009). Proteasome-dependent processing of topoisomerase I-DNA adducts into DNA double strand breaks at arrested replication forks. J. Biol. Chem. *284*, 28084–28092.

Lindsey-Boltz, L.A., Kemp, M.G., Hu, J., and Sancar, A. (2015). Analysis of ribonucleotide removal from DNA by human nucleotide excision repair. J. Biol. Chem. *290*, 29801–29807.

Lisby, M., Rothstein, R., and Mortensen, U.H. (2001). Rad52 forms DNA repair and

recombination centers during S phase. Proc. Natl. Acad. Sci. *98*, 8276–8282.
Liu, J., Renault, L., Veaute, X., Fabre, F., Stahlberg, H., and Heyer, W.D. (2011). Rad51 paralogues Rad55-Rad57 balance the antirecombinase Srs2 in Rad51 filament formation. Nature *479*, 245–248.
Liu, L., Lee, S., Zhang, J., Peters, S.B., Hannah, J., Zhang, Y., Yin, Y., Koff, A., Ma, L., and Zhou, P. (2009). CUL4A Abrogation Augments DNA Damage Response and Protection against Skin Carcinogenesis. Mol. Cell *34*, 451–460.
Lopes, M., Cotta-Ramusino, C., Pellicioli, A., Liberi, G., Plevani, P., Muzi-Falconi, M., Newlon, C.S., and Foiani, M. (2001). The DNA replication checkpoint response stabilizes stalled replication forks. Nature *412*, 557–561.
Lopes, M., Foiani, M., and Sogo, J.M. (2006). Multiple mechanisms control chromosome integrity after replication fork uncoupling and restart at irreparable UV lesions. Mol. Cell *21*, 15–27.
Lopez-Mosqueda, J., Maas, N.L., Jonsson, Z.O., Defazio-Eli, L.G., Wohlschlegel, J., and Toczyski, D.P. (2010). Damage-induced phosphorylation of Sld3 is important to block late origin firing. Nature *467*, 479–483.
Lou, H., Komata, M., Katou, Y., Guan, Z., Reis, C.C., Budd, M., Shirahige, K., and Campbell, J.L. (2008). Mrc1 and DNA Polymerase ε Function Together in Linking DNA Replication and the S Phase Checkpoint. Mol. Cell *32*, 106–117.
Luciano, P., Dehé, P.M., Audebert, S., Géli, V., and Corda, Y. (2015). Replisome function during replicative stress is modulated by histone H3 lysine 56 acetylation through Ctf4. Genetics *199*, 1047–1063.
Lujan, S.A., Williams, J.S., Pursell, Z.F., Abdulovic-Cui, A.A., Clark, A.B., Nick McElhinny, S.A., and Kunkel, T.A. (2012). Mismatch Repair Balances Leading and Lagging Strand DNA Replication Fidelity. PLoS Genet. *8*.
Lujan, S.A., Williams, J.S., Clausen, A.R., Clark, A.B., and Kunkel, T.A. (2013). Ribonucleotides are signals for mismatch repair of leading-strand replication errors. Mol. Cell *50*, 437–443.
Luke, B., Versini, G., Jaquenoud, M., Zaidi, I.W., Kurz, T., Pintard, L., Pasero, P., and Peter, M. (2006). The Cullin Rtt101p Promotes Replication Fork Progression through Damaged DNA and Natural Pause Sites. Curr. Biol. *16*, 786–792.
Lydeard, J.R., Jain, S., Yamaguchi, M., and Haber, J.E. (2007). Break-induced replication and telomerase-independent telomere maintenance require Pol32. Nature *448*, 820–823.
Lydeard, J.R., Lipkin-Moore, Z., Sheu, Y.J., Stillman, B., Burgers, P.M., and Haber, J.E. (2010). Break-induced replication requires all essential DNA replication factors except those specific for pre-RC assembly. Genes Dev. *24*, 1133–1144.
Maas, N.L., Miller, K.M., and Toczyski, D.P. (2006). Taking it off: Regulation of H3 K56 acetylation by Hst3 and Hst4. Cell Cycle *5*, 2561–2565.
Mackenzie, K.J., Carroll, P., Lettice, L., Tarnauskaitė, Ž., Reddy, K., Dix, F., Revuelta, A., Abbondati, E., Rigby, R.E., Rabe, B., et al. (2016). Ribonuclease H2 mutations induce a cGAS/STING-dependent innate immune response. EMBO J. *35*, 831–844.
MacKenzie, K.J., Carroll, P., Martin, C.A., Murina, O., Fluteau, A., Simpson, D.J., Olova, N., Sutcliffe, H., Rainger, J.K., Leitch, A., et al. (2017). CGAS surveillance of micronuclei links genome instability to innate immunity. Nature *548*, 461–465.
Maculins, T., Nkosi, P.J., Nishikawa, H., and Labib, K. (2015). Tethering of SCF^{Dia2} to the Replisome Promotes Efficient Ubiquitylation and Disassembly of the CMG Helicase. Curr. Biol. *25*, 2254–2259.
Majka, J., Binz, S.K., Wold, M.S., and Burgers, P.M.J. (2006). Replication protein a directs loading of the DNA damage checkpoint clamp to 5'-DNA junctions. J. Biol. Chem. *281*, 27855–27861.
Malkova, A., Ivanov, E.L., and Haber, J.E. (1996). Double-strand break repair in the absence of RAD51 in yeast: a possible role for break-induced DNA replication. Proc. Natl. Acad. Sci. U. S. A. *93*, 7131–7136.
Malkova, A., Naylor, M.L., Yamaguchi, M., Ira, G., and Haber, J.E. (2005). Replication Differs in Kinetics and Checkpoint Responses from RAD51 -Mediated Gene Conversion. Mol. Cell. Biol. *25*, 933–944.

Marians, K.J. (2018). Lesion Bypass and the Reactivation of Stalled Replication Forks. Annu. Rev. Biochem. 1–22.

Maric, M., Maculins, T., De Piccoli, G., and Labib, K. (2014). Cdc48 and a ubiquitin ligase drive disassembly of the CMG helicase at the end of DNA replication. Science (80-.). *346*.

Masumoto, H., Hawke, D., Kobayashi, R., and Verreault, A. (2005). A role for cell-cycle-regulated histone H3 lysine 56 acetylation in the DNA damage response. Nature *436*, 294–298.

Mehta, A., Beach, A., and Haber, J.E. (2017). Homology Requirements and Competition between Gene Conversion and Break-Induced Replication during Double-Strand Break Repair. Mol. Cell *65*, 515–526.e3.

Mevissen, T.E.T., and Komander, D. (2017). Mechanisms of Deubiquitinase Specificity and Regulation. Annu. Rev. Biochem. *86*, 159–192.

Miao, Z.H., Agama, K., Sordet, O., Povirk, L., Kohn, K.W., and Pommier, Y. (2006). Hereditary ataxia SCAN1 cells are defective for the repair of transcription-dependent topoisomerase I cleavage complexes. DNA Repair (Amst). *5*, 1489–1494.

Michel, J.J., McCarville, J.F., and Xiong, Y. (2003). A role for Saccharomyces cerevisiae Cul8 ubiquitin ligase in proper anaphase progression. J. Biol. Chem. *278*, 22828–22837.

Mimitou, E.P., and Symington, L.S. (2008). Sae2, Exo1 and Sgs1 collaborate in DNA double-strand break processing. Nature *455*, 770–774.

Mimura, S., Komata, M., Kishi, T., Shirahige, K., and Kamura, T. (2009). SCF(Dia2) regulates DNA replication forks during S-phase in budding yeast. EMBO J. *28*, 3693–3705.

Mimura, S., Yamaguchi, T., Ishii, S., Noro, E., Katsura, T., Obuse, C., and Kamura, T. (2010). Cul8/Rtt101 forms a variety of protein complexes that regulate DNA damage response and transcriptional silencing. J. Biol. Chem. *285*, 9858–9867.

Miyabe, I., Kunkel, T.A., and Carr, A.M. (2011). The major roles of DNA polymerases epsilon and delta at the eukaryotic replication fork are evolutionarily conserved. PLoS Genet. *7*.

Morawska, M., and Ulrich, H. (2013). An expanded tool kit for the auxin-inducible degron system in budding yeast. Yeast *30*, 341–351.

Mortimer, R.K., and Johnston, J.R. (1986). Genealogy of principal strains of the yeast genetic stock center. Genetics *113*, 35–43.

Mourón, S., Rodriguez-Acebes, S., Martínez-Jiménez, M.I., García-Gómez, S., Chocrón, S., Blanco, L., and Méndez, J. (2013). Repriming of DNA synthesis at stalled replication forks by human PrimPol. Nat. Struct. Mol. Biol. *20*, 1383–1389.

Müller, S., Hoege, C., Pyrowolakis, G., and Jentsch, S. (2001). Sumo, ubiquitin's mysterious cousin. Nat. Rev. Mol. Cell Biol. *2*, 202–210.

Muñoz-Galván, S., Jimeno, S., Rothstein, R., and Aguilera, A. (2013). Histone H3K56 Acetylation, Rad52, and Non-DNA Repair Factors Control Double-Strand Break Repair Choice with the Sister Chromatid. PLoS Genet. *9*, 1–12.

Navas, T.A., Zhou, Z., and Elledge, S.J. (1995). DNA polymerase ε links the DNA replication machinery to the S phase checkpoint. Cell *80*, 29–39.

Naylor, M.L., Li, J., Osborn, A.J., and Elledge, S.J. (2009). Mrc1 phosphorylation in response to DNA replication stress is required for Mec1 accumulation at the stalled fork. Proc. Natl. Acad. Sci. U. S. A. *106*, 12765–12770.

Nedelcheva, M.N., Roguev, A., Dolapchiev, L.B., Shevchenko, A., Taskov, H.B., Shevchenko, A., Stewart, A.F., and Stoynov, S.S. (2005). Uncoupling of unwinding from DNA synthesis implies regulation of MCM helicase by Tof1/Mrc1/Csm3 checkpoint complex. J. Mol. Biol. *347*, 509–521.

Neelsen, K.J., and Lopes, M. (2015). Replication fork reversal in eukaryotes: From dead end to dynamic response. Nat. Rev. Mol. Cell Biol. *16*, 207–220.

Nick McElhinny, S.A., Watts, B.E., Kumar, D., Watt, D.L., Lundstrom, E.-B., Burgers, P.M.J., Johansson, E., Chabes, A., and Kunkel, T.A. (2010a). Abundant ribonucleotide incorporation into DNA by yeast replicative polymerases. Proc. Natl. Acad. Sci. *107*, 4949–4954.

Nick McElhinny, S.A., Kumar, D., Clark, A.B., Watt, D.L., Watts, B.E., Lundström, E.B., Johansson, E., Chabes, A., and Kunkel, T.A. (2010b). Genome instability due to ribonucleotide incorporation into DNA. Nat. Chem. Biol. *6*, 774–781.

Nikolova, T., Ensminger, M., Löbrich, M., and Kaina, B. (2010). Homologous recombination protects mammalian cells from replication-associated DNA double-strand breaks arising in response to methyl methanesulfonate. DNA Repair (Amst). *9*, 1050–1063.

Nimonkar, A. V., Sica, R.A., and Kowalczykowski, S.C. (2009). Rad52 promotes second-end DNA capture in double-stranded break repair to form complement-stabilized joint molecules. Proc. Natl. Acad. Sci. *106*, 3077–3082.

Nishitani, H., Shiomi, Y., Iida, H., Michishita, M., Takami, T., and Tsurimoto, T. (2008). CDK Inhibitor p21 Is Degraded by a Proliferating Cell Nuclear Antigen-coupled Cul4-DDB1 ^{Cdt2} Pathway during S Phase and after UV Irradiation. J. Biol. Chem. *283*, 29045–29052.

Nouspikel, T. (2009). Nucleotide excision repair: Variations on versatility. Cell. Mol. Life Sci. *66*, 994–1009.

O'Donnell, L., Panier, S., Wildenhain, J., Tkach, J.M., Al-Hakim, A., Landry, M.C., Escribano-Diaz, C., Szilard, R.K., Young, J.T.F., Munro, M., et al. (2010). The MMS22L-TONSL complex mediates recovery from replication stress and homologous recombination. Mol. Cell *40*, 619–631.

Oda, H., Hübner, M.R., Beck, D.B., Vermeulen, M., Hurwitz, J., Spector, D.L., and Reinberg, D. (2010). Regulation of the Histone H4 Monomethylase PR-Set7 by CRL4Cdt2-Mediated PCNA-Dependent Degradation during DNA Damage. Mol. Cell *40*, 364–376.

Ohya, T., Maki, S., Kawasaki, Y., and Sugino, A. (2000). Structure and function of the fourth subunit (Dpb4p) of DNA polymerase epsilon in Saccharomyces cerevisiae. Nucleic Acids Res *28*, 3846–3852.

Olsen, J. V., Ong, S.-E., and Mann, M. (2004). Trypsin Cleaves Exclusively C-terminal to Arginine and Lysine Residues. Mol. Cell. Proteomics *3*, 608–614.

Ong, S.-E., Blagoev, B., Kratchmarova, I., Kristensen, D.B., Steen, H., Pandey, A., and Mann, M. (2002). Stable Isotope Labeling by Amino Acids in Cell Culture, SILAC, as a Simple and Accurate Approach to Expression Proteomics. Mol. Cell. Proteomics *1*, 376–386.

Orphanides, G., LeRoy, G., Chang, C.H., Luse, D.S., and Reinberg, D. (1998). FACT, a factor that facilitates transcript elongation through nucleosomes. Cell *92*, 105–116.

Orthwein, A., Noordermeer, S.M., Wilson, M.D., Landry, S., Enchev, R.I., Sherker, A., Munro, M., Pinder, J., Salsman, J., Dellaire, G., et al. (2015). A mechanism for the suppression of homologous recombination in G1 cells. Nature *528*, 422–426.

Osborn, A.J., and Elledge, S.J. (2003). Mrc1 is a replication fork component whose phosphorylation in response to DNA replication stress activates Rad53. Genes Dev. *17*, 1755–1767.

Pal, S., Graves, H., Ohsawa, R., Huang, T.H., Wang, P., Harmacek, L., and Tyler, J. (2016). The commercial antibodies widely used to measure H3 K56 acetylation are non-specific in human and drosophila cells. PLoS One *11*, 1–20.

Palter, K.B., Foe, V.E., and Alberts, B.M. (1979). Evidence for the formation of nucleosome-like histone complexes on single-stranded dna. Cell *18*, 451–467.

Papouli, E., Chen, S., Davies, A.A., Huttner, D., Krejci, L., Sung, P., and Ulrich, H.D. (2005). Crosstalk between SUMO and ubiquitin on PCNA is mediated by recruitment of the helicase Srs2p. Mol. Cell *19*, 123–133.

Parker, J.L., Bielen, A.B., Dikic, I., and Ulrich, H.D. (2007). Contributions of ubiquitin- and PCNA-binding domains to the activity of Polymerase η in Saccharomyces cerevisiae. Nucleic Acids Res. *35*, 881–889.

Paulovich, A.G., and Hartwell, L.H. (1995). A checkpoint regulates the rate of progression through S phase in S. cerevisiae in Response to DNA damage. Cell *82*, 841–847.

Peng, J., Schwartz, D., Elias, J.E., Thoreen, C.C., Cheng, D., Marsischky, G., Roelofs, J., Finley, D., and Gygi, S.P. (2003). A proteomics approach to understanding protein ubiquitination. Nat. Biotechnol. *21*, 921–926.

Perrino, F.W., Harvey, S., Shaban, N.M., and Hollis, T. (2009). RNaseH2 mutants that cause Aicardi-Goutieres syndrome are active nucleases. J. Mol. Med. *87*, 25–30.

Petermann, E., Orta, M.L., Issaeva, N., Schultz, N., and Helleday, T. (2010). Hydroxyurea-Stalled Replication Forks Become Progressively Inactivated and Require Two Different RAD51-Mediated Pathways for Restart and Repair. Mol. Cell *37*, 492–502.

Pfander, B., Moldovan, G.L., Sacher, M., Hoege, C., and Jentsch, S. (2005). SUMO-modified

PCNA recruits Srs2 to prevent recombination during S phase. Nature *436*, 428–433.

De Piccoli, G., Katou, Y., Itoh, T., Nakato, R., Shirahige, K., and Labib, K. (2012). Replisome Stability at Defective DNA Replication Forks Is Independent of S Phase Checkpoint Kinases. Mol. Cell *45*, 696–704.

Piwko, W., Olma, M.H., Held, M., Bianco, J.N., Pedrioli, P.G.A., Hofmann, K., Pasero, P., Gerlich, D.W., and Peter, M. (2010). RNAi-based screening identifies the Mms22L–Nfkbil2 complex as a novel regulator of DNA replication in human cells. EMBO J. *29*, 4210–4222.

Piwko, W., Mlejnkova, L.J., Mutreja, K., Ranjha, L., Stafa, D., Smirnov, A., Brodersen, M.M.L., Zellweger, R., Sturzenegger, A., Janscak, P., et al. (2016). The MMS22L – TONSL heterodimer directly promotes RAD51-dependent recombination upon replication stress. EMBO J. *35*, 1–18.

Pizzi, S., Sertic, S., Orcesi, S., Cereda, C., Bianchi, M., Jackson, A.P., Lazzaro, F., Plevani, P., and Muzi-Falconi, M. (2015). Reduction of hRNase H2 activity in Aicardi-Goutières syndrome cells leads to replication stress and genome instability. Hum. Mol. Genet. *24*, 649–658.

Pokatayev, V., Hasin, N., Chon, H., Cerritelli, S.M., Sakhuja, K., Ward, J.M., Morris, H.D., Yan, N., and Crouch, R.J. (2016). RNase H2 catalytic core Aicardi-Goutières syndrome–related mutant invokes cGAS–STING innate immune-sensing pathway in mice. J. Exp. Med. *213*, 329–336.

Pommier, Y., Barcelo, J.M., Rao, V.A., Sordet, O., Jobson, A.G., Thibaut, L., Miao, Z.H., Seiler, J.A., Zhang, H., Marchand, C., et al. (2006). Repair of Topoisomerase I-Mediated DNA Damage. Prog. Nucleic Acid Res. Mol. Biol. *81*, 179–229.

Pommier, Y., Sun, Y., Huang, S.Y.N., and Nitiss, J.L. (2016). Roles of eukaryotic topoisomerases in transcription, replication and genomic stability. Nat. Rev. Mol. Cell Biol. *17*, 703–721.

Potenski, C.J., Niu, H., Sung, P., and Klein, H.L. (2014). Avoidance of ribonucleotide-induced mutations by RNase H2 and Srs2-Exo1 mechanisms. Nature *511*, 251–254.

Pourquier, P., Ueng, L.M., Kohlhagen, G., Mazumder, A., Gupta, M., Kohn, K.W., and Pommier, Y. (1997a). Effects of uracil incorporation, DNA mismatches, and abasic sites on cleavage and religation activities of mammalian topoisomerase I. J. Biol. Chem. *272*, 7792–7796.

Pourquier, P., Pilon, A.A., Kohlhagen, G., Mazumder, A., Sharma, A., and Pommier, Y. (1997b). Trapping of mammalian topoisomerase I and recombinations induced by damaged DNA containing nicks or gaps. Importance of DNA end phosphorylation and camptothecin effects. J. Biol. Chem. *272*, 26441–26447.

Pourquier, P., Ueng, L.M., Fertala, J., Wang, D., Park, H.J., Essigmann, J.M., Bjornsti, M.A., and Pommier, Y. (1999). Induction of reversible complexes between eukaryotic DNA topoisomerase I and DNA-containing oxidative base damages: 7,8-dihydro-8-oxoguanine and 5- hydroxycytosine. J. Biol. Chem. *274*, 8516–8523.

Prado, F., and Maya, D. (2017). Regulation of replication fork advance and stability by nucleosome assembly. Genes (Basel). *8*.

Prindle, M.J., and Loeb, L.A. (2012). DNA Polymerase Delta in DNA Replication and Genome Maintenance. Environ. Mol. Mutagen. *53*, 666–682.

Puddu, F., Piergiovanni, G., Plevani, P., and Muzi-Falconi, M. (2011). Sensing of replication stress and Mec1 activation act through two independent pathways involving the 9-1-1 complex and DNA polymerase epsilon. PLoS Genet. *7*.

Pursell, Z.F., Isoz, I., Lundström, E.B., Johannson, E., and Kunkel, T.A. (2007). Yeast DNA Polymerase ε Participates in Leading-Strand DNA Replication. Science (80-.). *317*, 127–130.

Qiu, J., Qian, Y., Frank, P., Wintersberger, U., and Shen, B. (1999). Saccharomyces cerevisiae RNase H(35) Functions in RNA Primer Removal during Lagging-Strand DNA Synthesis, Most Efficiently in Cooperation with Rad27 Nuclease. Mol. Cell. Biol. *19*, 8361–8371.

Rabut, G., Le Dez, G., Verma, R., Makhnevych, T., Knebel, A., Kurz, T., Boone, C., Deshaies, R.J., and Peter, M. (2011). The TFIIH Subunit Tfb3 Regulates Cullin Neddylation. Mol. Cell *43*, 488–495.

Ramadan, K., Halder, S., Wiseman, K., and Vaz, B. (2017). Strategic role of the ubiquitin-

dependent segregase p97 (VCP or Cdc48) in DNA replication. Chromosoma *126*, 17–32.
Ranjha, L., Howard, S.M., and Cejka, P. (2018). Main steps in DNA double-strand break repair: an introduction to homologous recombination and related processes. Chromosoma 1–28.
Rass, U., Ahel, I., and West, S.C. (2007). Actions of aprataxin in multiple DNA repair pathways. J. Biol. Chem. *282*, 9469–9474.
Ray Chaudhuri, A., Hashimoto, Y., Herrador, R., Neelsen, K.J., Fachinetti, D., Bermejo, R., Cocito, A., Costanzo, V., and Lopes, M. (2012). Topoisomerase i poisoning results in PARP-mediated replication fork reversal. Nat. Struct. Mol. Biol. *19*, 417–423.
Recht, J., Tsubota, T., Tanny, J.C., Diaz, R.L., Berger, J.M., Zhang, X., Garcia, B.A., Shabanowitz, J., Burlingame, A.L., Hunt, D.F., et al. (2006). Histone chaperone Asf1 is required for histone H3 lysine 56 acetylation, a modification associated with S phase in mitosis and meiosis. Proc. Natl. Acad. Sci. *103*, 6988–6993.
Redon, C., Pilch, D.R., Rogakou, E.P., Orr, A.H., Lowndes, N.F., and Bonner, W.M. (2003). Yeast histone 2A serine 129 is essential for the efficient repair of checkpoint-blind DNA damage. EMBO Rep. *4*, 678–684.
Regairaz, M., Zhang, Y.W., Fu, H., Agama, K.K., Tata, N., Agrawal, S., Aladjem, M.I., and Pommier, Y. (2011). Mus81-mediated DNA cleavage resolves replication forks stalled by topoisomerase I-DNA complexes. J. Cell Biol. *195*, 739–749.
Reijns, M.A.M., Rabe, B., Rigby, R.E., Mill, P., Astell, K.R., Lettice, L.A., Boyle, S., Leitch, A., Keighren, M., Kilanowski, F., et al. (2012). Enzymatic removal of ribonucleotides from DNA is essential for mammalian genome integrity and development. Cell *149*, 1008–1022.
Ribar, B., Prakash, L., and Prakash, S. (2006). Requirement of ELC1 for RNA Polymerase II Polyubiquitylation and Degradation in Response to DNA Damage in Saccharomyces cerevisiae. Mol. Cell. Biol. *26*, 3999–4005.
Ribar, B., Prakash, L., and Prakash, S. (2007). ELA1 and CUL3 Are Required Along with ELC1 for RNA Polymerase II Polyubiquitylation and Degradation in DNA-Damaged Yeast Cells. Mol. Cell. Biol. *27*, 3211–3216.
Rice, G., Patrick, T., Parmar, R., Taylor, C.F., Aeby, A., Aicardi, J., Artuch, R., Montalto, S.A., Bacino, C.A., Barroso, B., et al. (2007). Clinical and Molecular Phenotype of Aicardi-Goutières Syndrome. Am. J. Hum. Genet. *81*, 713–725.
Richardson, P.G., Barlogie, B., Berenson, J., Singhal, S., Jagannath, S., Irwin, D., Rajkumar, S.V., Srkalovic, G., Alsina, M., Alexanian, R., et al. (2003). A Phase 2 Study of Bortezomib in Relapsed, Refractory Myeloma. N. Engl. J. Med. *348*, 2609–2617.
Roberts, T.M., Zaidi, I.W., Vaisica, J.A., Peter, M., and Brown, G.W. (2007). Regulation of Rtt107 Recruitment to Stalled DNA Replication Forks by the Cullin Rtt101 and the Rtt109 Acetyltransferase. Mol. Biol. Cell *19*, 171–180.
Rohman, M.S., Koga, Y., Takano, K., Chon, H., Crouch, R.J., and Kanaya, S. (2008). Effect of the disease-causing mutations identified in human ribonuclease (RNase) H2 on the activities and stabilities of yeast RNase H2 and archaeal RNase HII. FEBS J. *275*, 4836–4849.
Roseaulin, L.C., Noguchi, C., Martinez, E., Ziegler, M.A., Toda, T., and Noguchi, E. (2013). Coordinated Degradation of Replisome Components Ensures Genome Stability upon Replication Stress in the Absence of the Replication Fork Protection Complex. PLoS Genet. *9*, 21–28.
Ruff, P., Donnianni, R.A., Glancy, E., Oh, J., and Symington, L.S. (2016). RPA Stabilization of Single-Stranded DNA Is Critical for Break-Induced Replication. Cell Rep. *17*, 3359–3368.
Rychlik, M.P., Chon, H., Cerritelli, S.M., Klimek, P., Crouch, R.J., and Nowotny, M. (2010). Crystal structures of rnase h2 in complex with nucleic acid reveal the mechanism of RNA-DNA junction recognition and cleavage. Mol. Cell *40*, 658–670.
Rydberg, B., and Game, J. (2002). Excision of misincorporated ribonucleotides in DNA by RNase H (type 2) and FEN-1 in cell-free extracts. Proc. Natl. Acad. Sci. *99*, 16654–16659.
Sabouri, N., and Johansson, E. (2009). Translesion synthesis of abasic sites by yeast DNA polymerase ε. J. Biol. Chem. *284*, 31555–31563.
Sadowski, M., Suryadinata, R., Lai, X., Heierhorst, J., and Sarcevic, B. (2010). Molecular Basis for Lysine Specificity in the Yeast Ubiquitin-Conjugating Enzyme Cdc34. Mol. Cell. Biol. *30*, 2316–2329.

Saeki, Y., Kudo, T., Sone, T., Kikuchi, Y., Yokosawa, H., Toh-e, A., and Tanaka, K. (2009). Lysine 63-linked polyubiquitin chain may serve as a targeting signal for the 26S proteasome. EMBO J. *28*, 359–371.

Saha, A., and Deshaies, R.J. (2008). Multimodal Activation of the Ubiquitin Ligase SCF by Nedd8 Conjugation. Mol. Cell *32*, 21–31.

Saini, N., Ramakrishnan, S., Elango, R., Ayyar, S., Zhang, Y., Deem, A., Ira, G., Haber, J.E., Lobachev, K.S., and Malkova, A. (2013). Migrating bubble during break-induced replication drives conservative DNA synthesis. Nature *502*, 389–392.

Saintigny, Y., Delacôte, F., Varès, G., Petitot, F., Lambert, S., Averbeck, D., and Lopez, B.S. (2001). Characterization of homologous recombination induced by replication inhibition in mammalian cells. EMBO J. *20*, 3861–3870.

Sakata, T., Fujii, K., Ohno, M., and Kitabatake, M. (2015). Crt10 directs the cullin-E3 ligase Rtt101 to nonfunctional 25S rRNA decay. Biochem. Biophys. Res. Commun. *457*, 90–94.

Sang, Y., Yan, F., and Ren, X. (2015). The role and mechanism of CRL4 E3 ubiquitin ligase in cancer and its potential therapy implications. Oncotarget *6*, 42590–42602.

Santocanale, C., and Diffley, J.F.X. (1998). A Mec1-and Rad53-dependent checkpoint controls late-firing origins of DNA replication. Nature *395*, 615–618.

Santos-Pereira, J.M., and Aguilera, A. (2015). R loops: New modulators of genome dynamics and function. Nat. Rev. Genet. *16*, 583–597.

Saredi, G., Huang, H., Hammond, C.M., Alabert, C., Bekker-Jensen, S., Forne, I., Reverón-Gómez, N., Foster, B.M., Mlejnkova, L., Bartke, T., et al. (2016). H4K20me0 marks post-replicative chromatin and recruits the TONSL–MMS22L DNA repair complex. Nature *534*, 714–718.

Schellenberg, M.J., Tumbale, P., and Williams, R.S. (2015). Molecular Underpinnings of Aprataxin RNA/DNA Deadenylase Function and Dysfunction in Neurological Disease. Prog Biophys Mol Biol. *117*, 157–165.

Schlesinger, M.B., and Formosa, T. (2000). POB3 is required for both transcription and replication in the yeast Saccharomyces cerevisiae. Genetics *155*, 1593–1606.

Schneider, J., Bajwa, P., Johnson, F.C., Bhaumik, S.R., and Shilatifard, A. (2006). Rtt109 is required for proper H3K56 acetylation: A chromatin mark associated with the elongating RNA polymerase II. J. Biol. Chem. *281*, 37270–37274.

Scholes, D.T., Banerjee, M., Bowen, B., and Curcio, M.J. (2001). Multiple regulators of Ty1 transposition in Saccharomyces cerevisiae have conserved roles in genome maintenance. Genetics *159*, 1449–1465.

Sekiguchi, J.A., and Shuman, S. (1997). Site-specific ribonuclease activity of eukaryotic DNA topoisomerase I. Mol. Cell *1*, 89–97.

Sengupta, S., Van Deursen, F., De Piccoli, G., and Labib, K. (2013). Dpb2 Integrates the Leading-Strand DNA Polymerase into the Eukaryotic Replisome. Curr. Biol. *23*, 543–552.

Shah, P.P., Zheng, X., Epshtein, A., Carey, J.N., Bishop, D.K., and Klein, H.L. (2010). Swi2/Snf2-related translocases prevent accumulation of toxic Rad51 complexes during mitotic growth. Mol. Cell *39*, 862–872.

Shcherbakova, P. V., Pavlov, Y.I., Chilkova, O., Rogozin, I.B., Johansson, E., and Kunkel, T.A. (2003). Unique Error Signature of the Four-subunit Yeast DNA Polymerase ε. J. Biol. Chem. *278*, 43770–43780.

Shirayama, M., Tóth, A., Gálová, M., and Nasmyth, K. (1999). APC(Cdc20) promotes exit from mitosis by destroying the anaphase inhibitor Pds1 and cyclin Clb5. Nature *402*, 203–207.

Shrivastav, N., Li, D., and Essigmann, J.M. (2009). Chemical biology of mutagenesis and DNA repair: Cellular responses to DNA alkylation. Carcinogenesis *31*, 59–70.

Simon, A.C., Zhou, J.C., Perera, R.L., Van Deursen, F., Evrin, C., Ivanova, M.E., Kilkenny, M.L., Renault, L., Kjaer, S., Matak-Vinkovi, D., et al. (2014). A Ctf4 trimer couples the CMG helicase to DNA polymerase Î± in the eukaryotic replisome. Nature *510*, 293–297.

Simoneau, A., Delgoshaie, N., Celic, I., Dai, J., Abshiru, N., Costantino, S., Thibault, P., Boeke, J.D., Verreault, A., and Wurtele, H. (2015). Interplay between histone H3 lysine 56 deacetylation and chromatin modifiers in response to DNA damage. Genetics *200*, 185–205.

Singh, A., and Xu, Y.J. (2016). The cell killing mechanisms of hydroxyurea. Genes (Basel). *7*.

Siwaszek, A., Ukleja, M., and Dziembowski, A. (2014). Proteins involved in the degradation of cytoplasmic mRNA in the major eukaryotic model systems. RNA Biol. *11*, 1122–1139.

Skowyra, D., Craig, K.L., Tyers, M., Elledge, S.J., and Harper, J.W. (1997). F-box proteins are receptors that recruit phosphorylated substrates to the SCF ubiquitin-ligase complex. Cell *91*, 209–219.

Sogo, J.M., Lopes, M., and Foiani, M. (2002). Fork reversal and ssDNA accumulation at stalled replication forks owing to checkpoint defects. Science (80-.). *297*, 599–602.

Solinger, J.A., Kiianitsa, K., and Heyer, W.D. (2002). Rad54, a Swi2/Snf2-like recombinational repair protein, disassembles Rad51:dsDNA filaments. Mol. Cell *10*, 1175–1188.

Song, B.W., and Sung, P. (2000). Functional interactions among yeast Rad51 recombinase, Rad52 mediator, and replication protein A in DNA strand exchange. J. Biol. Chem. *275*, 15895–15904.

Sonoda, E., Sasaki, M.S., Morrison, C., Yamaguchi-Iwai, Y., Takata, M., and Takeda, S. (1999). Sister chromatid exchanges are mediated by homologous recombination in vertebrate cells. Mol. Cell. Biol. *19*, 5166–5169.

Sordet, O., Redon, C.E., Guirouilh-Barbat, J., Smith, S., Solier, S., Douarre, C., Conti, C., Nakamura, A.J., Das, B.B., Nicolas, E., et al. (2009). Ataxia telangiectasia mutated activation by transcription- and topoisomerase I-induced DNA double-strand breaks. EMBO Rep. *10*, 887–893.

Soucy, T.A., Smith, P.G., Milhollen, M.A., Berger, A.J., Gavin, J.M., Adhikari, S., Brownell, J.E., Burke, K.E., Cardin, D.P., Critchley, S., et al. (2009). An inhibitor of NEDD8-activating enzyme as a new approach to treat cancer. Nature *458*, 732–736.

Sparks, J.L., and Burgers, P.M. (2015). Error-free and mutagenic processing of topoisomerase 1-provoked damage at genomic ribonucleotides. EMBO J. *34*, 1259–1269.

Sparks, J.L., Chon, H., Cerritelli, S.M., Kunkel, T.A., Johansson, E., Crouch, R.J., and Burgers, P.M. (2012). RNase H2-Initiated Ribonucleotide Excision Repair. Mol. Cell *47*, 980–986.

Štafa, A., Donnianni, R.A., Timashev, L.A., Lam, A.F., and Symington, L.S. (2014). Template switching during break-induced replication is promoted by the mph1 helicase in Saccharomyces cerevisiae. Genetics *196*, 1017–1028.

Staker, B.L., Hjerrild, K., Feese, M.D., Behnke, C.A., Burgin, A.B., and Stewart, L. (2002). The mechanism of topoisomerase I poisoning by a camptothecin analog. Proc. Natl. Acad. Sci. U. S. A. *99*, 15387–15392.

Stelter, P., and Ulrich, H.D. (2003). Control of spontaneous and damage-induced mutagenesis by SUMO and ubiquitin conjugation. Nature *425*, 188–191.

Strumberg, D., Pilon, A.A., Smith, M., Hickey, R., Malkas, L., and Pommier, Y. (2000). Conversion of topoisomerase I cleavage complexes on the leading strand of ribosomal DNA into 5'-phosphorylated DNA double-strand breaks by replication runoff. Mol. Cell. Biol. *20*, 3977–3987.

Sugasawa, K., Okuda, Y., Saijo, M., Nishi, R., Matsuda, N., Chu, G., Mori, T., Iwai, S., Tanaka, K., Tanaka, K., et al. (2005). UV-induced ubiquitylation of XPC protein mediated by UV-DDB-ubiquitin ligase complex. Cell *121*, 387–400.

Sugawara, N., Wang, X., and Haber, J.E. (2003). In vivo roles of Rad52, Rad54, and Rad55 proteins in Rad51-mediated recombination. Mol. Cell *12*, 209–219.

Sung, P. (1994). Catalysis of ATP-dependent homologous DNA pairing and strand exchange by yeast RAD51 protein. Science (80-.). *265*, 1241–1243.

Sung, P. (1997). Yeast Rad55 and Rad57 proteins form a heterodimer that functions with replication protein A to promote DNA strand exchange by Rad51 recombinase. Genes Dev. *11*, 1111–1121.

Suter, B., Fetchko, M.J., Imhof, R., Graham, C.I., Stoffel-studer, I., Zbinden, C., Raghavan, M., Lopez, L., Beneti, L., Hort, J., et al. (2007). Examining protein − protein interactions using endogenously tagged yeast arrays : The Cross-and-Capture system. Genome Res. *17*, 1774–1782.

Szyjka, S.J., Viggiani, C.J., and Aparicio, O.M. (2005). Mrc1 is required for normal progression of replication forks throughout chromatin in S. cerevisiae. Mol. Cell *19*, 691–697.

Taglialatela, A., Alvarez, S., Leuzzi, G., Sannino, V., Ranjha, L., Huang, J.W., Madubata, C., Anand, R., Levy, B., Rabadan, R., et al. (2017). Restoration of Replication Fork Stability in

BRCA1- and BRCA2-Deficient Cells by Inactivation of SNF2-Family Fork Remodelers. Mol. Cell *68*, 414–430.e8.

Takashima, H., Boerkoel, C.F., John, J., Saifi, G.M., Salih, M.A.M., Armstrong, D., Mao, Y., Quiocho, F.A., Roa, B.B., Nakagawa, M., et al. (2002). Mutation of TDP1, encoding a topoisomerase I-dependent DNA damage repair enzyme, in spinocerebellar ataxia with axonal neuropathy. Nat. Genet. *32*, 267–272.

Tanaka, H., Katou, Y., Yagura, M., Saitoh, K., Itoh, T., Araki, H., Bando, M., and Shirahige, K. (2009). Ctf4 coordinates the progression of helicase and DNA polymerase a. 807–820.

Tarpey, P.S., Raymond, F.L., O'Meara, S., Edkins, S., Teague, J., Butler, A., Dicks, E., Stevens, C., Tofts, C., Avis, T., et al. (2007). Mutations in CUL4B, Which Encodes a Ubiquitin E3 Ligase Subunit, Cause an X-linked Mental Retardation Syndrome Associated with Aggressive Outbursts, Seizures, Relative Macrocephaly, Central Obesity, Hypogonadism, Pes Cavus, and Tremor. Am. J. Hum. Genet. *80*, 345–352.

Terai, K., Shibata, E., Abbas, T., and Dutta, A. (2013). Degradation of p12 subunit by CRL4Cdt2 E3 ligase inhibits fork progression after DNA damage. J. Biol. Chem. *288*, 30509–30514.

Tercero, J.A., and Diffley, J.F.X. (2001). Regulation of DNA replication fork progression through damaged DNA by the Mec1/Rad53 checkpoint. Nature *412*, 553–557.

Thaminy, S., Newcomb, B., Kim, J., Gatbonton, T., Foss, E., Simon, J., and Bedalov, A. (2007). Hst3 is regulated by Mec1-dependent proteolysis and controls the S phase checkpoint and sister chromatid cohesion by deacetylating histone H3 at lysine 56. J. Biol. Chem. *282*, 37805–37814.

Thangavel, S., Berti, M., Levikova, M., Pinto, C., Gomathinayagam, S., Vujanovic, M., Zellweger, R., Moore, H., Lee, E.H., Hendrickson, E.A., et al. (2015). DNA2 drives processing and restart of reversed replication forks in human cells. J. Cell Biol. *208*, 545–562.

Thrower, J.S., Hoffman, L., Rechsteiner, M., and Pickart, C.M. (2000). Recognition of the polyubiquitin proteolytic signal. EMBO J. *19*, 94–102.

Toledo, L.I., Altmeyer, M., Rask, M.B., Lukas, C., Larsen, D.H., Povlsen, L.K., Bekker-Jensen, S., Mailand, N., Bartek, J., and Lukas, J. (2014). ATR prohibits replication catastrophe by preventing global exhaustion of RPA. Cell *156*, 374.

Tomimatsu, N., Mukherjee, B., Harris, J.L., Boffo, F.L., Hardebeck, M.C., Potts, P.R., Khanna, K.K., and Burma, S. (2017). DNA-damage-induced degradation of EXO1 exonuclease limits DNA end resection to ensure accurate DNA repair. J. Biol. Chem. *292*, 10779–10790.

Tsabar, M., Waterman, D.P., Aguilar, F., Katsnelson, L., Eapen, V. V., Memisoglu, G., and Haber, J.E. (2016). Asf1 facilitates dephosphorylation of Rad53 after DNA double-strand break repair. Genes Dev. *30*, 1211–1223.

Tsubota, T., Maki, S., Kubota, H., Sugino, A., and Maki, H. (2003). Double-stranded DNA binding properties of Saccharomyces cerevisiae DNA polymerase epsilon and of the Dpb3p-Dpb4p subassembly. Genes Cells *8*, 873–888.

Tumbale, P., Williams, J.S., Schellenberg, M.J., Kunkel, T.A., and Williams, R.S. (2014). Aprataxin resolves adenylated RNA-DNA junctions to maintain genome integrity. Nature *506*, 111–115.

Uhlmann, F., Lottspelch, F., and Nasmyth, K. (1999). Sister-chromatid separation at anaphase onset is promoted by cleavage of the cohesin subunit Scc1. Nature *400*, 37–42.

Ui, A., Seki, M., Ogiwara, H., Lai, M.S., Yamamoto, K., Tada, S., and Enomoto, T. (2007). Activation of a novel pathway involving Mms1 and Rad59 in sgs1 cells. Biochem. Biophys. Res. Commun. *356*, 1031–1037.

Ulrich, H.D., and Jentsch, S. (2000). Two RING finger proteins mediate cooperation between ubiquitin-conjugating enzymes in DNA repair. EMBO J. *19*, 3388–3397.

Vaisica, J.A., Baryshnikova, A., Costanzo, M., Boone, C., and Brown, G.W. (2011). Mms1 and Mms22 stabilize the replisome during replication stress. Mol. Biol. Cell *22*, 2396–2408.

Vaisman, A., McDonald, J.P., Huston, D., Kuban, W., Liu, L., Van Houten, B., and Woodgate, R. (2013). Removal of Misincorporated Ribonucleotides from Prokaryotic Genomes: An Unexpected Role for Nucleotide Excision Repair. PLoS Genet. *9*.

Van, C., Yan, S., Michael, W.M., Waga, S., and Cimprich, K.A. (2010). Continued primer

synthesis at stalled replication forks contributes to checkpoint activation. J. Cell Biol. *189*, 233–246.

Villa, F., Simon, A.C., Ortiz Bazan, M.A., Kilkenny, M.L., Wirthensohn, D., Wightman, M., Matak-Vinkovíc, D., Pellegrini, L., and Labib, K. (2016). Ctf4 Is a Hub in the Eukaryotic Replisome that Links Multiple CIP-Box Proteins to the CMG Helicase. Mol. Cell *63*, 385–396.

Villa-Hernández, S., Bueno, A., and Bermejo, R. (2017). The Multiple Roles of Ubiquitylation in Regulating Challenged DNA Replication. 395–419.

Vujanovic, M., Krietsch, J., Raso, M.C., Terraneo, N., Zellweger, R., Schmid, J.A., Taglialatela, A., Huang, J.W., Holland, C.L., Zwicky, K., et al. (2017). Replication Fork Slowing and Reversal upon DNA Damage Require PCNA Polyubiquitination and ZRANB3 DNA Translocase Activity. Mol. Cell *67*, 882–890.e5.

Wang, H., and Elledge, S.J. (1999). DRC1, DNA replication and checkpoint protein 1, functions with DPB11 to control DNA replication and the S-phase checkpoint in Saccharomyces cerevisiae. Proc. Natl. Acad. Sci. U. S. A. *96*, 3824–3829.

Wang, H., Zhai, L., Xu, J., Joo, H.-Y., Jackson, S., Erdjument-Bromage, H., Tempst, P., Xiong, Y., and Zhang, Y. (2006). Histone H3 and H4 Ubiquitylation by the CUL4-DDB-ROC1 Ubiquitin Ligase Facilitates Cellular Response to DNA Damage. Mol. Cell *22*, 383–394.

Warren, C.D., Eckley, D.M., Lee, M.S., Hanna, J.S., Hughes, A., Peyser, B., Chunfa, J., Irizarry, R., and Spencer, F.A. (2004). S-Phase Checkpoint Genes Safeguard High-Fidelity Sister Chromatid Cohesion. Mol. Biol. Cell *15*, 1724–1735.

Watanabe, K., Tateishi, S., Kawasuji, M., Tsurimoto, T., Inoue, H., and Yamaizumi, M. (2004). Rad18 guides polη to replication stalling sites through physical interaction and PCNA monoubiquitination. EMBO J. *23*, 3886–3896.

Watt, D.L., Johansson, E., Burgers, P.M., and Kunkel, T.A. (2011). Replication of ribonucleotide-containing DNA templates by yeast replicative polymerases. DNA Repair (Amst). *10*, 897–902.

Wechsler, T., Newman, S., and West, S.C. (2011). Aberrant chromosome morphology in human cells defective for Holliday junction resolution. Nature *471*, 642–646.

Williams, J.S., and Kunkel, T.A. (2014). Ribonucleotides in DNA: Origins, repair and consequences. DNA Repair (Amst). *19*, 27–37.

Williams, J.S., Clausen, A.R., Nick McElhinny, S.A., Watts, B.E., Johansson, E., and Kunkel, T.A. (2012). Proofreading of ribonucleotides inserted into DNA by yeast DNA polymerase ε. DNA Repair (Amst). *11*, 649–656.

Williams, J.S., Smith, D.J., Marjavaara, L., Lujan, S.A., Chabes, A., and Kunkel, T.A. (2013). Topoisomerase 1-Mediated Removal of Ribonucleotides from Nascent Leading-Strand DNA. Mol. Cell *49*, 1010–1015.

Williams, J.S., Clausen, A.R., Lujan, S.A., Marjavaara, L., Clark, A.B., Burgers, P.M., Chabes, A., and Kunkel, T.A. (2015). Evidence that processing of ribonucleotides in DNA by topoisomerase 1 is leading-strand specific. Nat. Struct. Mol. Biol. *22*, 291–297.

Williams, J.S., Gehle, D.B., and Kunkel, T.A. (2017). The role of RNase H2 in processing ribonucleotides incorporated during DNA replication. DNA Repair (Amst). *53*, 52–58.

Wilson, M.A., Kwon, Y., Xu, Y., Chung, W.H., Chi, P., Niu, H., Mayle, R., Chen, X., Malkova, A., Sung, P., et al. (2013). Pif1 helicase and Polδ promote recombination-coupled DNA synthesis via bubble migration. Nature *502*, 393–396.

Winston, F., Dollard, C., and Ricupero-Hovasse, S.L. (1995). Construction of a set of convenient saccharomyces cerevisiae strains that are isogenic to S288C. Yeast *11*, 53–55.

Wolner, B., Van Komen, S., Sung, P., and Peterson, C.L. (2003). Recruitment of the recombinational repair machinery to a DNA double-strand break in yeast. Mol. Cell *12*, 221–232.

Wurtele, H., Kaiser, G.S., Bacal, J., St-Hilaire, E., Lee, E.-H., Tsao, S., Dorn, J., Maddox, P., Lisby, M., Pasero, P., et al. (2012). Histone H3 Lysine 56 Acetylation and the Response to DNA Replication Fork Damage. Mol. Cell. Biol. *32*, 154–172.

Wyatt, H.D.M., and West, S.C. (2014). Holliday junction resolvases. Cold Spring Harb. Perspect. Biol. *6*, 1–30.

Xiao, W., and Samson, L. (1993). In vivo evidence for endogenous DNA alkylation damage as

a source of spontaneous mutation in eukaryotic cells. Proc. Natl. Acad. Sci. U. S. A. *90*, 2117–2121.

Xu, G., and Jaffrey, S.R. (2011). The new landscape of protein ubiquitination. Nat. Biotechnol. *29*, 1098.

Xu, G., and Jaffrey, S.R. (2013). Proteomic identification of protein ubiquitination events. Biotechnol. Genet. Eng. Rev. *29*, 73–109.

Xu, G., Paige, J.S., and Jaffrey, S.R. (2010). Global analysis of lysine ubiquitination by ubiquitin remnant immunoaffinity profiling. Nat. Biotechnol. *28*, 868–873.

Xu, H., Boone, C., and Klein, H.L. (2004). Mrc1 Is Required for Sister Chromatid Cohesion To Aid in Recombination Repair of Spontaneous Damage. Mol. Cell. Biol. *24*, 7082–7090.

Xu, P., Duong, D.M., Seyfried, N.T., Cheng, D., Xie, Y., Robert, J., Rush, J., Hochstrasser, M., Finley, D., and Peng, J. (2009). Quantitative Proteomics Reveals the Function of Unconventional Ubiquitin Chains in Proteasomal Degradation. Cell *137*, 133–145.

Xu, X., Blackwell, S., Lin, A., Li, F., Qin, Z., and Xiao, W. (2015). Error-free DNA-damage tolerance in Saccharomyces cerevisiae. Mutat. Res. - Rev. Mutat. Res. *764*, 43–50.

Xue, X., Choi, K., Bonner, J., Chiba, T., Kwon, Y., Xu, Y., Sanchez, H., Wyman, C., Niu, H., Zhao, X., et al. (2014). Restriction of replication fork regression activities by a conserved SMC complex. Mol. Cell *56*, 436–445.

Yang, J., Zhang, X., Feng, J., Leng, H., Li, S., Xiao, J., Liu, S., Xu, Z., Xu, J., Li, D., et al. (2016). The Histone Chaperone FACT Contributes to DNA Replication-Coupled Nucleosome Assembly. Cell Rep. *14*, 1128–1141.

Yeeles, J.T.P., and Marians, K.J. (2013). Dynamics of leading-strand lesion skipping by the replisome. Mol. Cell *52*, 855–865.

Yeeles, J.T.P., Janska, A., Early, A., and Diffley, J.F.X. (2017). How the Eukaryotic Replisome Achieves Rapid and Efficient DNA Replication. Mol. Cell *65*, 105–116.

Yeung, M., and Durocher, D. (2011). Srs2 enables checkpoint recovery by promoting disassembly of DNA damage foci from chromatin. DNA Repair (Amst). *10*, 1213–1222.

Yuen, K.W.Y., Warren, C.D., Chen, O., Kwok, T., Hieter, P., and Spencer, F.A. (2007). Systematic genome instability screens in yeast and their potential relevance to cancer. Proc. Natl. Acad. Sci. *104*, 3925–3930.

Zaidi, I.W., Rabut, G., Poveda, A., Hofmann, K., Malmström, J., Ulrich, H., Hofmann, K., Pasero, P., Peter, M., and Luke, B. (2008). Rtt101 and Mms1 in budding yeast form a CUL4DDB1-like ubiquitin ligase that promotes replication through damaged DNA. EMBO Rep. *9*, 1034–1040.

Zegerman, P., and Diffley, J.F.X. (2010). Checkpoint-dependent inhibition of DNA replication initiation by Sld3 and Dbf4 phosphorylation. Nature *467*, 474–478.

Zellweger, R., Dalcher, D., Mutreja, K., Berti, M., Schmid, J.A., Herrador, R., Vindigni, A., and Lopes, M. (2015). Rad51-mediated replication fork reversal is a global response to genotoxic treatments in human cells. J. Cell Biol. *208*, 563–579.

Zhang, H., and Lawrence, C.W. (2005). The error-free component of the RAD6/RAD18 DNA damage tolerance pathway of budding yeast employs sister-strand recombination. Proc. Natl. Acad. Sci. U. S. A. *102*, 15954–15959.

Zhang, H.F., Tomida, A., Koshimizu, R., Ogiso, Y., Lei, S., and Tsuruo, T. (2004). Cullin 3 Promotes Proteasomal Degradation of the Topoisomerase I-DNA Covalent Complex. Cancer Res. *64*, 1114–1121.

Zhang, J., Shi, D., Li, X., Ding, L., Tang, J., Liu, C., Shirahige, K., Cao, Q., and Lou, H. (2017). Rtt101-Mms1-Mms22 coordinates replication-coupled sister chromatid cohesion and nucleosome assembly. EMBO Rep. *18*, 1294–1305.

Zhang, S., Zhao, H., Darzynkiewicz, Z., Zhou, P., Zhang, Z., Lee, E.Y.C., and Lee, M.Y.W.T. (2013). A Novel Function of CRL4 ^{Cdt2}. J. Biol. Chem. *288*, 29550–29561.

Zhang, Y.W., Otterness, D.M., Chiang, G.G., Xie, W., Liu, Y.C., Mercurio, F., and Abraham, R.T. (2005). Genotoxic stress targets human Chk1 for degradation by the ubiquitin-proteasome pathway. Mol. Cell *19*, 607–618.

Zhang, Y.W., Regairaz, M., Seiler, J.A., Agama, K.K., Doroshow, J.H., and Pommier, Y. (2011). Poly(ADP-ribose) polymerase and XPF-ERCC1 participate in distinct pathways for the repair of topoisomerase I-induced DNA damage in mammalian cells. Nucleic Acids Res.

39, 3607–3620.
Zhang, Z.X., Zhang, J., Cao, Q., Campbell, J.L., and Lou, H. (2018). The DNA Pol ϵ stimulatory activity of Mrc1 is modulated by phosphorylation. Cell Cycle *17*, 64–72.
Zhao, X., and Rothstein, R. (2002). The Dun1 checkpoint kinase phosphorylates and regulates the ribonucleotide reductase inhibitor Sml1. Proc. Natl. Acad. Sci. *99*, 3746–3751.
Zhao, X., Muller, E.G.D., and Rothstein, R. (1998). A suppressor of two essential checkpoint genes identifies a novel protein that negatively affects dNTP pools. Mol. Cell *2*, 329–340.
Zheng, L., and Shen, B. (2011). Okazaki fragment maturation: Nucleases take centre stage. J. Mol. Cell Biol. *3*, 23–30.
Zheng, N., and Shabek, N. (2017). Ubiquitin Ligases : Structure , Function , and Regulation.
Zheng, X.F., Prakash, R., Saro, D., Longerich, S., Niu, H., and Sung, P. (2011). Processing of DNA structures via DNA unwinding and branch migration by the S. cerevisiae Mph1 protein. DNA Repair (Amst). *10*, 1034–1043.
Zhu, Q., Wei, S., Sharma, N., Wani, G., He, J., and Wani, A.A. (2017). Human $CRL4^{DDB2}$ubiquitin ligase preferentially regulates postrepair chromatin restoration of H3K56Ac through recruitment of histone chaperon CAF-1. Oncotarget *8*, 104525–104542.
Zhu, Z., Chung, W.H., Shim, E.Y., Lee, S.E., and Ira, G. (2008). Sgs1 Helicase and Two Nucleases Dna2 and Exo1 Resect DNA Double-Strand Break Ends. Cell *134*, 981–994.
Zou, L., and Elledge, S.J. (2003). ATRIP Recognition of RPA-ssDNA. Science (80-.). *300*, 1542–1548.
Zou, L., Liu, D., and Elledge, S.J. (2003). Replication protein A-mediated recruitment and activation of Rad17 complexes. Proc. Natl. Acad. Sci. *100*, 13827–13832.
Zou, Y., Liu, Q., Chen, B., Zhang, X., Guo, C., Zhou, H., Li, J., Gao, G., Guo, Y., Yan, C., et al. (2007). Mutation in CUL4B, Which Encodes a Member of Cullin-RING Ubiquitin Ligase Complex, Causes X-Linked Mental Retardation. Am. J. Hum. Genet. *80*, 561–566.

Acknowledgements

Curriculum Vitae